5-2017

Electroproduction of W Mesons Off Protons In The Third Resonance Region and Beyond

Evan Phelps
University of South Carolina

Follow this and additional works at: https://scholarcommons.sc.edu/etd

Part of the Physics Commons

ELECTROPRODUCTION OF ω MESONS OFF PROTONS

IN THE THIRD RESONANCE REGION AND BEYOND

by

Evan Phelps

Bachelor of Science
Southern Polytechnic State University

Submitted in Partial Fulfillment of the Requirements

for the Degree of Doctor of Philosphy in

Physics

College of Arts and Sciences

University of South Carolina

2017

Accepted by:

Ralf Gothe, Major Professor

Yordanka Ilieva, Committee Member

Fred Myhrer, Committee Member

Victor Mokeev, External Committee Member

Cheryl L. Addy, Vice Provost and Dean of the Graduate School

www.manaraa.com

DEDICATION

I dedicate this work to my wife, Dawn Marie Hunter, whose sacrifices and encouragements fueled the completion of this work, and to my daughter, Darcy Jane Phelps, who bravely made night-time goodbyes less guiltful by telling me to go finish my "Ph.B." and come home.

Acknowledgments

First, and foremost, I would like to thank Ralf Gothe for serving as a mentor and friend in physics and in life. In Ralf, I was able to witness the exceptional ideal of being dedicated passionately to research, teaching, and service in equal measure, inseparably blended by matters of *the person.* I believe that his person-centric way is key to the generational transmission of process and knowledge that forms the strongest strands of human progress.

Second, I want to thank my immediate academic family. Crucially, my dissertation committee – Ralf Gothe, Yordanka Ilieva, Victor Mokeev, and Fred Myhrer – dedicated their time to the review of my dissertation. They raised questions that compelled reflection long after my first answers. But most importantly, I deeply appreciate their authentic expressions of support and investment in the completion of my work. Beyond the committee, I'm especially thankful for my friendship and collaboration with Arjun Trivedi, who I progressed alongside from beginning to end. I, also, would like to thank, in alphabetic order, Gleb Fedotov, Lewis Graham, Gary Hollis, Haiyun Lu, Kijun Park, Iuliia Skorodumina, Ye Tian, and Zhiwen Zhao.

Finally, this work would not have been possible without the CLAS Collaboration, the Jefferson Science Associates Graduate Fellowship Program, and the National Science Foundation. I owe special gratitude to (a) Daniel Carman, Chaden Djalali, and Ralf Gothe for the time and attention they dedicated to recommending me for the JSA Fellowship and (b) Chaden Djalali, Ralf Gothe, Steffen Strauch, Yordanka Ilieva, and David Tedeschi for partial funding of my work from their NSF grants.

Abstract

Exclusive electroproduction of $\omega(782)$ mesons in the reaction $ep \to ep\omega \to ep\pi^+\pi^-\pi^0$ was studied from the production threshold, through the third resonance region, and beyond. With electron beam energies close to 6 GeV, the kinematic range covers $W = [1.72, 2.60)$ GeV and $Q^2 = [1.85, 5.15)$ GeV^2. By combining two sets of data collected by the Thomas Jefferson National Accelerator Facility's wide-acceptance spectrometer (CLAS), the largest set of resonance-region differential cross sections, $\frac{d^2\sigma_h}{d\Omega^*}$, for ω electroproduction have been produced. Response functions $\mathscr{R}_T + \epsilon_L \mathscr{R}_L$, $\mathscr{R}_{TT}$, and $\mathscr{R}_{TL}$ were extracted to provide a view of how the cross sections and interference terms depend on the production angle, which is a requirement of single- and coupled-channel analyses that aim to probe the content and dynamics of hadrons and, by extension, of Quantum Chromodynamics (QCD).

TABLE OF CONTENTS

LIST OF TABLES

List of Figures

CHAPTER 1

OVERVIEW AND BACKGROUND

1.1 MOTIVATION AND OUTCOMES

The non-perturbative strong interaction, which generates ground and excited nucleon states, is very complex and far beyond the scope of the perturbative expansion. Studies of the non-perturbative strong interaction and its relation to the Lagrangian of Quantum Chromodynamics (QCD) are necessary to elucidate the dynamical features of QCD [1]. The information needed to explore the dynamical content of QCD is encoded in the baryon spectrum and the elastic and transition form factors. Photoproduction experiments serve as excellent probes of the excited baryon spectrum, while electroproduction experiments afford access to transition form factors that extend our view of the baryons into the virtual photon domain.

The experimental challenges of accessing this information [1, 2] are mitigated by exclusive measurements and selective production channels, such as $\gamma_v p \to \omega p$, which is discriminating in several ways. First, the isoscalar nature of ω restricts its couplings to isospin-1/2 resonances. Second, ω might couple more strongly than π to states previously undetected due to weak π coupling. For previously detected resonances, this channel allows us to check the available information on $\gamma_v p N^\star$ electrocouplings in an independent analysis of an exclusive process with a different background.

In this analysis, exclusive ω electroproduction off the proton is studied via the three-pion decay channel,

$$ep \to e\omega p \to e\pi^+\pi^-\pi^0 p \,.$$

1

The most important outcome will consist of cross sections and response functions to be included in the combined, dynamical coupled-channels (DCC) analysis of Argonne National Laboratory (ANL) and Osaka University. The ANL-Osaka DCC analysis [3, 4] carries forward the work of the Thomas Jefferson National Accelerator Facility's (JLab's) Excited Baryon Analysis Center (EBAC) [5, 6]. An independent outcome is the decomposition of cross sections and response functions into low-order Legendre moments and exponentials for a qualitative assessment of potential resonant contributions and relative strengths of the s-, t-, and u-channel processes.

1.2 REACTION CHANNEL $\gamma_v p \to \omega p$

Kinematics and Independent Variables

The process of exclusive electroproduction of ω mesons off protons is represented by the reaction expression

$$ep \to ep\omega$$

and the following four-momentum equation with respectively ordered variables:

$$\ell + P = \ell' + P' + V.$$

In ep scattering experiments, the electrons of a prepared beam impinge on the protons of a fixed target material. The twelve kinematic final-state parameters, components of three four-momenta, are constrained by the four conservation equations of energy and momentum, the three known masses, azimuthal symmetry of the scattered electron with respect to the beam, and azimuthal symmetry of the hadronic scattering plane with respect to the leptonic scatter plane; so the reaction kinematics can be fully described by three independent variables (see Table 1.1). Later, a fourth independent dynamical variable will be introduced.

The choice of variables depends on the theoretical context and models in which the observables are being compared or interpreted. Common to most current models

2

Table 1.1   Three independent kinematic variables are required to fully describe the kinematics of ω electroproduction.

	d.o.f.
prepared initial state	0
3 final-state particles	12
E, $\vec{p}$ conservation	-4
m_e, m_ω, M_p	-3
ϕ^{lab} symmetry of scattered e	-1
ϕ^* symmetry of hadronic scattering plane	-1
independent kinematic variables	**3**

is the one-photon-exchange (OPE) approximation, which justifies a factorization of leptonic and hadronic parts of the reaction and leads to a reformulation of the reaction expression:

$$ep \to ep\omega \longrightarrow \gamma_v p \to p\omega,$$

where a virtual photon, γ_v, carries the four-momentum $q = \ell - \ell'$ transferred from the electron to the proton. The four-momentum equation for the OPE-factorized reaction is

$$q + P = P' + V.$$

The OPE approximation elevates the picture of an electromagnetic probe, γ_v, that couples directly to hadrons with a space-time extent corresponding to the four-momentum q according to the uncertainty principle. This picture provides a context in which key variables are defined and interpreted.

For the N^* studies that this work aims to inform, the following four independent variables – in order, three kinematic plus one dynamical – will be used to express cross sections:

- $Q^2 = -q^\mu q_\mu$, where q is the four-momentum of the virtual photon. Q^2 is positive for space-like photons.

3

- $W = \sqrt{s} = \sqrt{(q+P)^\mu (q+P)_\mu} = \sqrt{(P'+V)^\mu (P'+V)_\mu}$, the effective mass of the final-state hadronic system, $p\omega$. $W = \sqrt{2M_p\nu + M_p^2 - Q^2}$ in terms of the lab-frame virtual photon energy ($E_\gamma^{lab} = \nu$), the mass of the proton (M_p), and Q^2.

- $\cos\theta^* = \frac{\vec{q}^* \cdot \vec{V}^*}{|\vec{q}^*||\vec{V}^*|}$ defines θ^* as the ω production angle with respect to the direction of the virtual photon in the hadronic CMS coordinate system,

$$\hat{z} = \frac{\vec{q}^*}{|\vec{q}^*|}, \quad \hat{y} = \frac{\vec{q}^* \times \vec{V}^*}{|\vec{q}^* \times \vec{V}^*|}, \quad \hat{x} = \hat{y} \times \hat{z}.$$

These expressions reflect the general convention of superscripting kinematic variables with stars or asterisks when they are meant to be represented in the hadronic CMS.

- ϕ^* is the azimuthal angle of ω production in the hadronic CMS or, of course, in any other frame boosted in the direction of the virtual photon along the $\hat{z}$-axis. The density of final states would be uniform in ϕ^* if not for the dynamical couplings between the leptonic and hadronic spin components. The resulting ϕ^* dependency of the differential cross sections will be used to extract information on the strength of these couplings.

For discussions of ω electroproduction within the deep inelastic scattering (DIS) context or Vector Meson Dominance (VMD) models [7], other variables may be referenced:

- $\nu = \frac{q^\mu P_\mu}{M_p}$, a Lorentz-invariant that can be interpreted in the fixed-target frame as the energy of the virtual photon, $\nu = E_\gamma^{lab}$. It is the parameter that conventionally determines *hard* and *soft* scattering and in the lab-frame corresponds to the time-extent of the electromagnetic probe.

- $x_b = \frac{Q^2}{2P^\mu q_\mu} = \frac{Q^2}{2M_p\nu}$. The *Bjorken scaling variable* is a measure of inelasticity. The parton model provides an additional interpretation, especially useful

4

in DIS, where x_b represents the fraction of the four-momentum of the proton carried by the struck parton.

- $t = (q - V)^\mu (q - V)_\mu = (P - P')^\mu (P - P')_\mu$, the square of the four-momentum transfer between the initial and final proton. In a *t-channel process*, t represents the square of the four-momentum of a virtual meson exchange particle.

- $t' = |t - t_0|$, where $|t_0|$ is the minimum $|t|$ value that could occur with fixed energies and momentum magnitudes but allowing the angle to change. This is conveniently determined in the CMS frame: $t_0 = (E_\gamma^* - E_\omega^*)^2 - (|\vec{q}^{\,*}| - |\vec{p}_\omega^{\,*}|)^2$. t' is needed to determine the *t-slope* parameter of VMD models.

Cross Sections

Cross sections provide a vital connection to quantum theoretic descriptions of processes by relating directly to the transition probability amplitudes predicted by an effective interaction Hamiltonian combined with the density of final states [8].

The four independent variables W, Q^2, $\cos\theta^*$, and ϕ^* form the parameter space in which reaction yields are to be measured and in which corresponding cross sections are to be expressed in the current analysis. The cross sections can then be decomposed into *response functions* that exclusively contain information about the structure of the hadronic system.

Under the one-photon exchange (OPE) approximation, the measured electron scattering exclusive cross sections are reduced to the $\gamma_v p \to \omega p$ exclusive cross sections, i.e., *hadronic cross sections* (σ_h), as

$$\frac{d^4\sigma}{dW\,dQ^2 d\Omega^*} = \Gamma \frac{d^2\sigma_h}{d\Omega^*}\,, \tag{1.1}$$

where $\Gamma = \Gamma(W, Q^2)$ is the virtual photon flux that normalizes events according to

5

the probability density of producing a virtual photon:

$$\Gamma(W, Q^2) = \frac{\alpha}{4\pi} \cdot \frac{W}{M_p^2 E_o^2} \cdot \frac{W^2 - M_p^2}{Q^2} \cdot \frac{1}{1 - \epsilon}. \tag{1.2}$$

In this equation, ϵ is the polarization parameter derived from the transverse components of the leptonic tensor expressed in terms of the *s-channel* helicity amplitudes in the the hadronic CMS. In this representation, the leptonic tensor encodes the spin properties of the virtual photon and, so, can be considered the virtual photon's spin density matrix. Each of its elements, including those with longitudinal and scalar components, can be expressed in terms of the polarization parameter ϵ. For $Q^2 >> m_e^2$, the polarization parameter reduces to the well-known expression in terms of lab-frame parameters:

$$\epsilon \approx \left(1 + \frac{2\vec{q}^2}{Q^2} \cdot \tan^2 \frac{\Theta_e}{2}\right)^{-1}. \tag{1.3}$$

By leveraging that $Q^2 \approx 4EE' \sin^2(\frac{\Theta_e}{2})$, it is convenient to express ϵ in terms of invariants and the lab-frame constant beam energy $E = E_o$:

$$\epsilon \approx \left(1 + 2\frac{Q^2 + \nu^2}{4E_o(E_o - \nu) - Q^2}\right)^{-1}, \tag{1.4}$$

where $\nu = E_o - E' = \frac{W^2 - M_p^2 + Q^2}{2M_p}$. By constructing the polarization parameter in terms of transverse elements, it is invariant under Lorentz transformations along $\vec{q}$. Furthermore, under the same transformations, the longitudinal and scalar components of the spin density matrix transform into each other and can, therefore, be treated as a single entity. Indeed, imposing current conservation eliminates the scalar component and allows us to express the longitudinal component in terms of the transverse polarization parameter:

$$\epsilon_L = \frac{Q^2}{\nu^2}\epsilon. \tag{1.5}$$

A detailed derivation, starting from the matrix element of the process in the OPE, is provided by Schilling and Wolf [9].

An important effect of the lepton-hadron spin couplings, as represented in the contraction of leptonic and hadronic tensors, is an explicit dependence of the cross section on the azimuthal angle ϕ^* according to the polarization. This effect allows for the extraction of not only the unpolarized cross section σ_o but also the interference terms σ_{TT} and σ_{LT} according to the form of their dependence on ϵ and ϕ^* [10]. In order to compare to results of [7], the unpolarized cross section and interference terms are defined as follows:

$$\frac{d\sigma_h}{d\phi^*} = \frac{1}{2\pi}\left(\sigma_o + \epsilon\,\sigma_{TT}\,cos(2\phi^*) + \sqrt{2\epsilon(1+\epsilon)}\,\sigma_{LT}\,cos(\phi^*)\right).\qquad(1.6)$$

Alternatively, the differential cross sections can be expressed in terms of response functions $\mathscr{R}_i(W,Q^2,\theta^*)$, which relate more directly to the hadronic tensor, using the convention of [11]:

$$\frac{d^2\sigma_h}{d\Omega^*} = \frac{|\vec{p}_\omega^*|}{k_\gamma^*}\left(\mathscr{R}_T + \epsilon_L\,\mathscr{R}_L + \epsilon\,\mathscr{R}_{TT}\,cos(2\phi^*) + \sqrt{2\epsilon_L(1+\epsilon)}\,\mathscr{R}_{TL}\,cos(\phi^*)\right),\quad(1.7)$$

where $|\vec{p}_\omega^*|$ and k_γ^* are the CMS magnitudes of the ω momentum and of the *photon equivalent energy,*[1] respectively:

$$|\vec{p}_\omega^*| = \frac{1}{2W}\sqrt{M_\omega^4 - 2M_\omega^2 M_p^2 - 2M_\omega^2 W^2 + M_p^4 - 2M_p^2 W^2 + W^4}\qquad(1.8)$$

$$k_\gamma^* = \frac{M_p}{W}k_\gamma = \frac{M_p}{W}\left(\frac{W^2 - M_p^2}{2M_p}\right) = \frac{W^2 - M_p^2}{2W}.\qquad(1.9)$$

The hadronic differential cross sections are connected to the binned experimental data according to

$$\left\langle\frac{d^2\sigma_h}{d\Omega^*}\right\rangle_i \simeq \frac{1}{B}\cdot\frac{1}{L\left\langle\Gamma\right\rangle_i}\cdot\frac{1}{\Delta_i W \Delta_i Q^2}\cdot\frac{R_i}{\eta_i}\cdot\frac{N_i}{\Delta_i\Omega^*},\qquad(1.10)$$

where $B = 0.892$ is the branching ratio for ω's three-pion decay [12]; L is the integrated luminosity; i is a label for a bin in the four-dimensional kinematic space;

---

[1]The photon equivalent energy, k_γ^{lab} is the lab-frame energy required for a real photon to excite a hadronic system with CM energy W; k_γ^* is the boosted value of k_γ^{lab}.

7

$\langle \Gamma \rangle_i$ is the average virtual photon flux of bin i; $\Delta_i W$, $\Delta_i Q^2$, and $\Delta_i \Omega^*$ multiply to give the four-dimensional bin volume of bin i; η_i is a generic, ideal correction factor that accounts for all inefficiencies;[2] R_i is a radiative correction factor; and N_i is the background-subtracted yield.

The equation of (1.10) will be revisited and elaborated in Chapter 7 so that cross sections can be extracted. However, first we must answer some basic questions: How are particles detected (Chapter 2)? How are their properties at the interaction vertex determined, and how are corresponding events reconstructed (Chapter 3)? How are relevant ω production events selected (Chapter 4)? The answer to each of these questions will motivate methods of this analysis and will hint at or lead to correction factors. We will find in Chapter 5 that simulations play a central role by absorbing the lion's share of these corrections and in Chapter 6 that momentum and energy loss processes, also, play an important role.

---

[2]The generic acceptance/efficiency factor η_i is the product of several multiplicative factors that account for various sources of detection inefficiencies.

CHAPTER 2

THE EXPERIMENTAL CONFIGURATION

Since the early proton size measurements at Stanford Linear Accelerator (SLAC) in 1955, electron scattering has been used to probe nucleons. Subsequent higher Q^2 electron scattering experiments, primarily *inclusive* measurements, provided ground-breaking insights into the nucleonic substructure and were vital to the development of QCD [13, 14]. However, a more detailed understanding of nucleonic structure is a prerequisite to connecting QCD to the basic properties of nucleons. Toward this end, *exclusive* measurements of multi-particle final states are required to identify spin, parity, and isospin, and large solid-angle acceptance is required to separate azimuthal- and polar-angle-dependent observables. The Continuous Electron Beam Accelerator Facility (CEBAF) [15] at Jefferson Lab delivers a high-precision beam of electrons to the CEBAF Large Acceptance Spectrometer (CLAS) [16], making the facility uniquely well-suited to achieve such measurements.

Detailed descriptions of CEBAF and CLAS are given in [15] and [16], respectively. The rest of this chapter describes, at a high level, the experimental apparatus at the time of run periods E16 and E1F, from which data is used for the current analysis. Chapter 3 will continue to elaborate by detailing reconstruction and particle identification procedures.

2.1 CONTINUOUS ELECTRON BEAM ACCELERATOR FACILITY

CEBAF is dedicated to investigations of hadronic and nuclear structure using electromagnetic probes. A schematic view of the facility at the time of data collection

is show in Figure 2.1. The centerpiece of the facility is the electron accelerator that
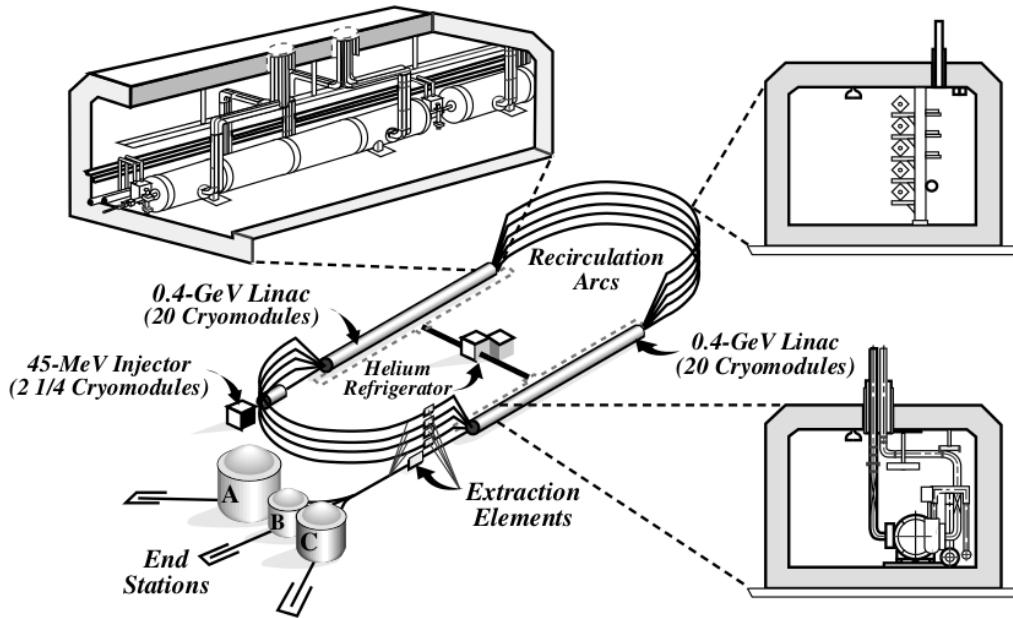
Figure 2.1   Schematic view of Continuous Electron Beam Accelerator Facility, reproduced from [16]. CLAS is housed by Hall B.

is capable of producing a high-current beam of polarized electrons with energies up to 6 GeV and delivering it to three different experimental areas to simultaneously be used in electron scattering or tagged bremsstrahlung experiments.

The 1497-MHz radio-frequency (RF) continuous-wave electron beam comprises three interlaced 499-MHz beams, separated by 667 ps. Each electron bunch has properties that may differ from its nearest neighbors [17, 18]. Every third bunch is *kicked* to a single experimental hall. This characteristic is leveraged to deliver currents that routinely vary by four orders of magnitude [16] between experimental halls. The capability to simultaneously deliver vastly different currents is especially relevant to the CLAS detector, because large acceptance spectrometers are limited by detector occupancies to relatively low luminosities compared to the other detectors serviced by the facility's beam.

2.2 CEBAF Large Acceptance Spectrometer

CLAS consists of electromagnets arranged in a toroidal geometry around the electron beam axis and a layered system of four detector types separated into six sectors that share a common target, trigger, and data acquisition system [16]. Two schematic perspectives of CLAS are shown in Figure 2.2 with the field-generating coils and major detector types indicated. CLAS is capable of detecting and distinguishing
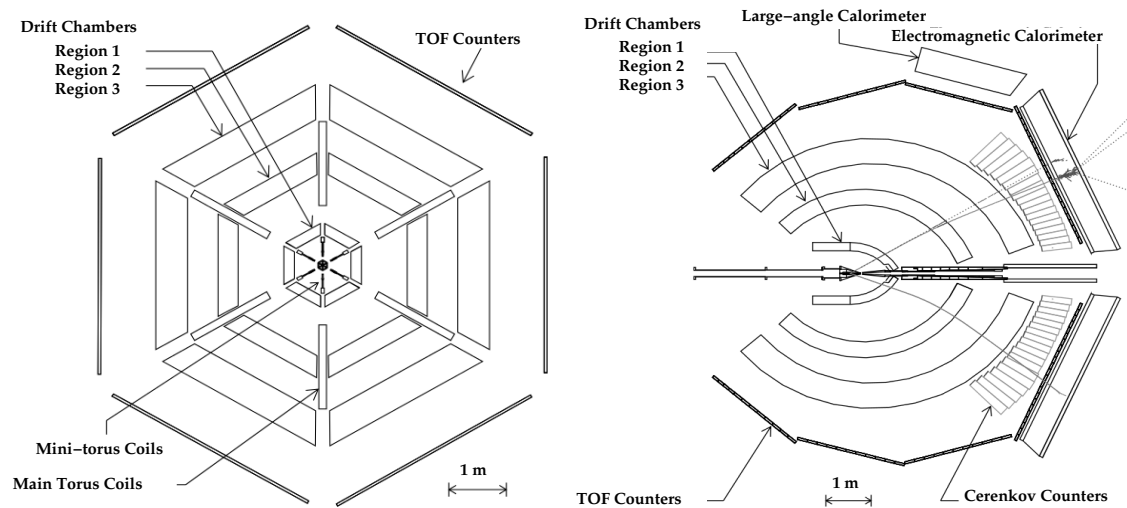
Figure 2.2   Schematic views of CEBAF Large Acceptance Spectrometer.

among both charged and neutral particles. While charged hadrons have historically been the most difficult to distinguish [19], CLAS is highly capable of distinction because of its ability to provide multiple independent measurements of the same particle within a single event.

CLAS employs a toroidal magnetic arrangement to impart curvature to charged particle trajectories, drift chambers (DC) to track particles along their trajectories, time-of-flight (TOF) counters to determine speed, Čerenkov counters (CC) to discriminate electrons from slower negative particles, and electromagnetic calorimeters (EC) to detect photons and to distinguish electrons from other fast negative particles. The most relevant characteristics of each detector subsystem will be briefly described

11

below with references to more detailed technical publications.

Magnetic Field in CLAS

The magnetic field of CLAS discriminately deflects charged particles according to charge and momentum. It is generated by iron-free super-conducting coils situated between the sectors, as seen in Figure 2.2. The resulting field components point mainly along the azimuth, $+\phi$ or $-\phi$ depending on the run configuration. In either case, the field leaves the azimuthal component of velocity unchanged over the course of each particle trajectory. The field strength falls rapidly near the target to accommodate polarization experiments and is stronger in the forward direction than at larger angles so that generally faster-moving forward-scattered particles are subject to a greater path-bending Lorentz force. The maximum coil current of 3860 A produces an integrated field strength, $\oint \vec{B} \cdot d\vec{\ell}$, of about 2.5 Tm in the forward direction and about 0.6 Tm at 90°. Design details and performance characteristics are discussed in [16] and [20].

Drift Chambers (DC)

In tandem with the magnetic field, CLAS's drift chambers (DC) provide the primary means of determining charge and charged particle momentum. As a charged particle travels through the homogeneous magnetic field, the Lorentz force causes the particle to move on a circular-arc path (neglecting energy loss), which is reconstructed from the signals detected in multiple planes of drift chambers. The orientation of curvature determines the particle charge; the radius of curvature determines the momentum.

Before describing some relevant characteristics of the CLAS drift-chamber system, it is helpful to review how a simple drift chamber functions. Drift chambers contain gas and consist of closely spaced wires for producing electric fields and sensing electrons. When a particle passes through the chamber, it ionizes the contained

12

gas thus releasing electrons, which are accelerated toward positive-potential *sensor* wires. Ideally the ionizing particle position in the plane of the wire layer is

$$x = x_{wire} + v_{drift} \cdot (t_{wire} - t_0) \ ,$$

where t_{wire} is the time of the voltage pulse on the sensor wire, t_0 is the independently determined time that the particle crossed the plane, and v_{drift} is the drift velocity of the ionization electrons. Accordingly, $t_{wire} - t_0$ can be called the *drift time*. Mestayer et al. [21] elaborate this simplified concept into its more complex CLAS analog, which relies on simultaneous treatment of many wire layers and detailed field mapping knowledge.

The CLAS drift chamber system supports path reconstruction with 2-mrad angular precision (polar and azimuthal) and $\delta p/p \leq 0.5\%$ momentum resolution. The single-wire resolution accounts for only a small fraction of the effective resolution, which stems primarily from magnetic field uncertainties, chamber misalignments, and multiple scattering. Resolution is improved by measuring trajectories at three different locations along each path with precisions of 100 μm in the bend plane and 1 mm perpendicular to the bend plane and by using the time-of-flight detector (TOF) to correct for drift time. All of the DC system's inactive components are in the shadow of the magnet coils, so the DC does not limit geometric acceptance [21]. On the other hand, an unavoidable cost of using drift chambers for momentum determination is luminosity. Specifically, the occupancy limitations of the Region 1 drift chambers set the limiting luminosity of CLAS experiments as a whole [22].

The DC system is divided into eighteen independent chambers separated into the six CLAS sectors and three regions of increasing radial distance from the target. Region 1 surrounds the target in an area of low magnetic field strength; Region 2 covers the area of maximum field strength between the coils; Region 3 is beyond the coils in radially decreasing field strength. The regions are denoted in the schematic views of Figure 2.2. Each chamber consists of two superlayers – one axial to the

13

magnetic field and one tilted – each with six wire layers.[1] The axial superlayer is critical to bend-plane precision; the tilted superlayer provides azimuthal information. Figure 2.3 shows the *honeycomb* geometry formed by sensor and field wires across two superlayers. The sensor wires are at the center of each hexagonal cell, and the field wires are at the corners.
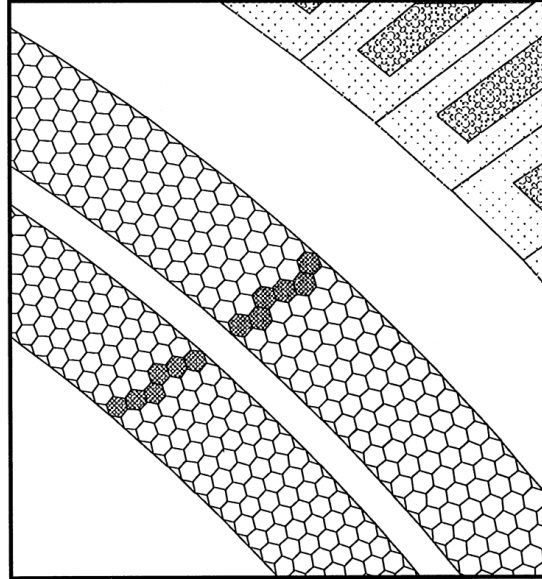
Figure 2.3   Representation of Region 3 of the CLAS drift chamber system, projected onto the sector's mid-plane, reproduced from [21]. This representation emphasizes the *honeycomb* structure by outlining each cell, defined by field wires at the vertices and a sensor wire at the center. Shaded cells represent a charged particle firing cells along its path.

Note that each of the previously mentioned three *location* measurements derives from a fit across the multiple wire layers of one chamber. The three trajectory segments are then linked. Even before drift time corrections, this provides for robust track reconstruction in what is called *hit-based tracking* (HBT). Subsequent *time-based tracking* (TBT) incorporates TOF measurements to correct for drift time and thus further refines the track precision.

---

[1]The tilted superlayer of Region 1 has only four wire layers due to geometric constraints.

Time-of-flight Detector

The time-of-flight detector (TOF) is key to charged particle identification (see Section 3.3). It provides a time measurement t to supplement the DC-determined path length s and momentum p in order to determine the rest mass m according to the well-known relativistic relations $E = \gamma m$ and $\beta = p/E$ (with $c = 1$):

$$m = \frac{E}{\gamma} = \frac{p}{\beta\gamma} = \frac{p\sqrt{1-\beta^2}}{\beta} = \frac{p\sqrt{1-(s/t)^2}}{s/t}, \qquad (2.1)$$

where energy loss along the path is ignored. Velocity and momentum resolutions determine the detector's mass resolution according to ordinary propagation rules for independent Gaussian error sources. The uncertainty in the length of the particle trajectory is insignificant compared to the momentum and time resolution limitations, so the mass resolution can be expressed in terms of only momentum and time:

$$\left(\frac{\delta m}{m}\right)^2 = \left(\frac{\delta p}{p}\right)^2 + \gamma^4 \beta^2 \delta\beta^2 = \left(\frac{\delta p}{p}\right)^2 + \gamma^4 \left(\frac{\delta t}{t}\right)^2. \qquad (2.2)$$

The relative uncertainties in momentum and time are of similar magnitudes, but the γ^4 multiplier makes time resolution the dominant contribution to CLAS mass resolution for large β. TOF is accordingly considered the primary tool for charged hadron identification within CLAS.

Figure 2.4 illustrates the importance of time resolution in differentiating protons and pions. The contour plot represents the number of dual-mass-measurement standard deviations that separates the proton and pion masses for various particle momenta and time resolutions under the assumption of a momentum resolution of 0.5% and a fixed particle path length of 500 cm. Stated differently, for each pair of momentum (p) and time resolution (δt) values, δm is given by (2.2) for an assumed proton or pion mass, δm_p or δm_{π^+}, for a fixed path length. In these terms, the contour represents

$$mass\ separation = \frac{m_p - m_{\pi^+}}{\sqrt{(\delta m_p)^2 + (\delta m_{\pi^+})^2}},$$

15

where the dependence on time resolution and momentum enters through δm_p and δm_{π^+}. The power of distinction can be read directly from the plot. For example, a TOF resolution of 150 ps supports a 3-σ separation of pions from protons at 2 GeV and better than 5σ at 1.5 GeV.
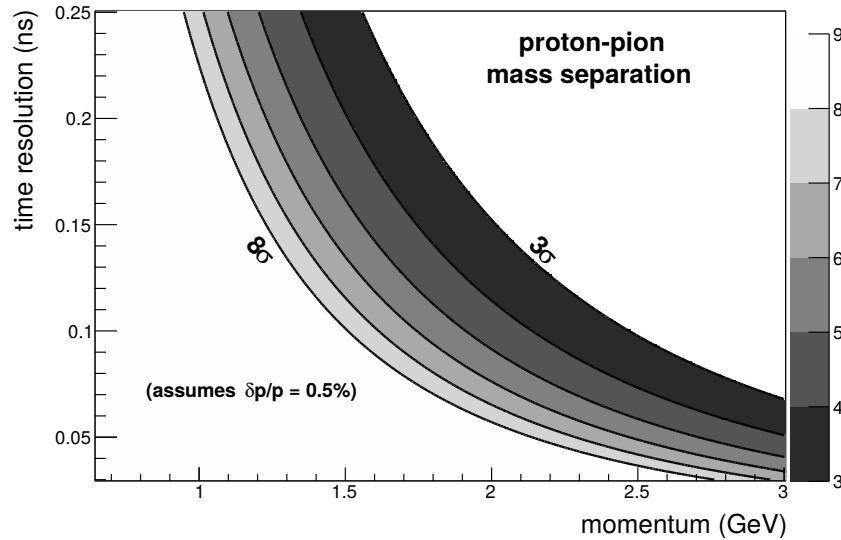
Figure 2.4   TOF resolution, proton-pion mass separation as a function of momentum and time resolution, represented as a contour plot. The TOF resolution (y-scale) required to support any mass separation (z-axis) between 3 and 8 σ at a particular momentum (x-axis) can be read directly from the plot.

TOF, also known as the SC, consists of scintillating counters in planar arrangements of 5-cm thickness in each of the six CLAS sectors. It covers the full active azimuthal range of the detector and from 8° to 142° in the polar angle. Each counter is constructed of a plastic scintillating material with a light guide and photomultiplier tube (PMT) on each end. The resolution is primarily limited by (a) the intrinsic electronic measurement system resolution, (b) the number of photons that reach the photoelectric surface of the PMTs, and (c) light-path variations.

The system is laser-calibrated and time-walk-corrected to time resolutions from 80 ps in the forward direction, where the most energetic particles are detected, to about 160 ps [23]. Figure 2.5, reprinted here from [23], illustrates the time resolution

16

as a function of scintillator length determined from cosmic-ray (left) and laser system (right) data. The resolution degrades with counter length due to attenuation, which reduces the number of photons that reach the PMTs. The shorter scintillators correspond to TOF counters that are positioned in the forward direction. Referring again to Figure 2.4, a typical forward resolution of 100 ps from the cosmic-ray technique would support 5-σ separation of 1.9-GeV protons and pions.
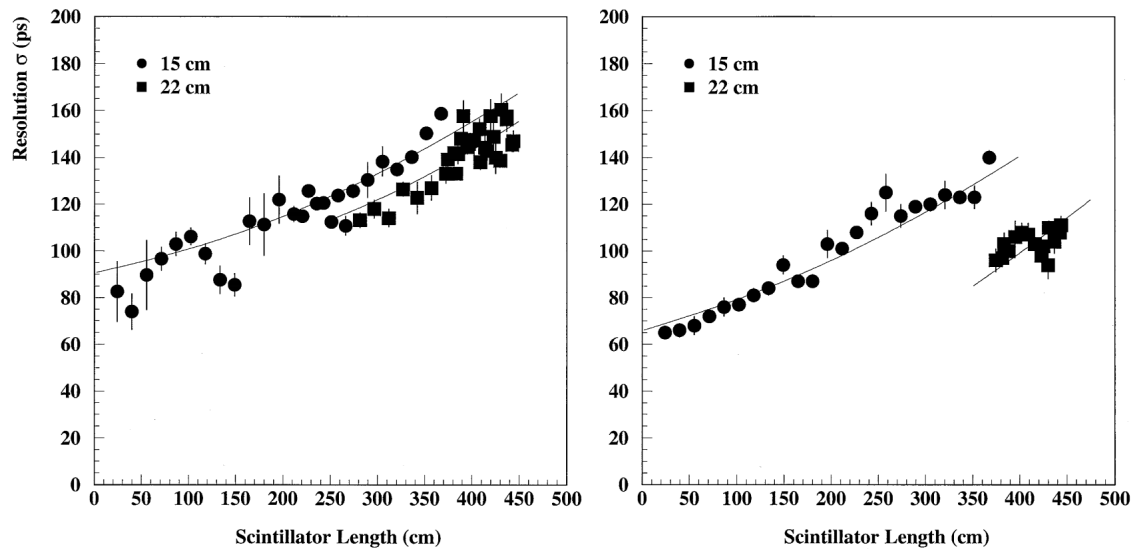
Figure 2.5   Time-of-flight resolutions as measured by cosmic rays (left) and the laser system (right). Circles correspond to 15-cm-wide scintillators with straight light guides, and squares correspond to 22-cm-wide scintillators with bent light guides and larger PMTs.

Čerenkov Counters

The Čerenkov Counter system (CC) is the primary tool for electron discrimination and participates in the two-part level-1 trigger for data acquisition. It operates on the principle of Čerenkov radiation – light is emitted by charged particles that travel through a medium faster than the speed of light in the material. The CC employs a gas (C_4F_{10}, perfluorobutane) with a high refractive index, $n = 1.00153$, that allows

17

for discrimination of electrons from pions up to about 2.5 GeV, which corresponds to the Čerenkov threshold of charged pions according to (2.3).

$$\begin{aligned} \beta &= 1/n &= 0.9985 \\ p_{\pi^-} &= \beta\gamma M_{\pi^-} &= 2.52 \text{ GeV} \end{aligned} \tag{2.3}$$

The CC is designed to detect electrons with better than 99% efficiency within the fiducial volume of CLAS [24].

Each sector contains 18 segments that cover 8° to 42° in the polar angle. Each segment is divided along the sector midline into two modules. Figure 2.6 illustrates one module of the CC with a sample electron track and corresponding Čerenkov light reflecting into the shielded assembly of the light guide and PMT. All inactive components of the CC nominally reside in the shadow of the magnets, but the geometry of the light-collection apparatus limits angular acceptance beyond the intrinsic sector geometry. Specifically, the magnetic shielding can block light reflected off the elliptical mirror in the vicinity of the PMT, which can occur when an electron passes close to the sector edge and to the module-interior side of the PMT assembly. Further toward the sector edge, non-radiating charged particles have a chance of directly activating the PMT, which can lead to falsely identifying negative hadrons as electrons. These issues are addressed in Section 5.2 by restricting the fiducial volume to exclude the exterior edges of each sector.

Electromagnetic Calorimeters

The CLAS electromagnetic calorimeter system (EC) was designed to detect photons and neutrons, which then can be differentiated by time-of-flight measurements, and to supplement the CC in triggering on and identifying electrons [25]. The CC discriminates electrons from pions up to momenta of about 2.5 GeV according to (2.3), but for higher momenta, the particles can be separated according to their distinct energy

18
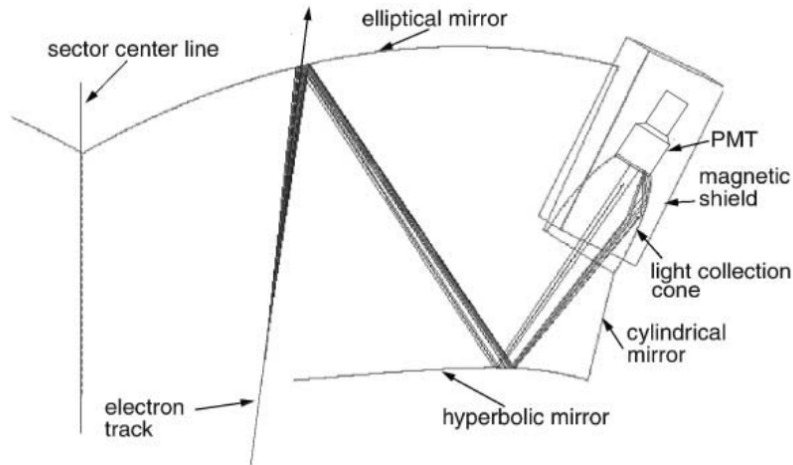
Figure 2.6   Schematic view of Čerenkov chamber from [24]. A sample electron track is shown along with the paths of the corresponding Čerenkov light reflected off the elliptical and hyperbolic mirrors, traveling into the light guide, and striking the photoelectric surface of the shielded PMT.

deposit signatures within the EC. This distinction requires sufficient energy resolution as well as three-dimensional spatial information about the energy deposition pattern.

The EC consists of 39 layers of scintillators interleaved with lead sheets. The scintillator layers are orientated along ternary axes (labeled U, V, and W) defined by the edges of the triangular sector geometry to provide transverse spatial information. Figure 2.7 illustrates this arrangement. The 39 scintillator layers are partitioned into *inner* and *outer* stacks of 15 and 24 sheets, respectively, to record depth of energy deposits. With this arrangement, the system is able to distinguish between three categories of particle interactions: electromagnetic showering, minimum ionizing, and hadronic.

The electron trigger threshold is typically set to a total energy threshold of about twice the minimum ionizing level, which helps mitigate false-positive triggers, especially on very fast pions that trigger the CC. Within a triggered event and above the energy threshold, electromagnetic showers produced by electrons dominate the energy deposition, especially in the inner stack. When one particle satisfies the trigger,
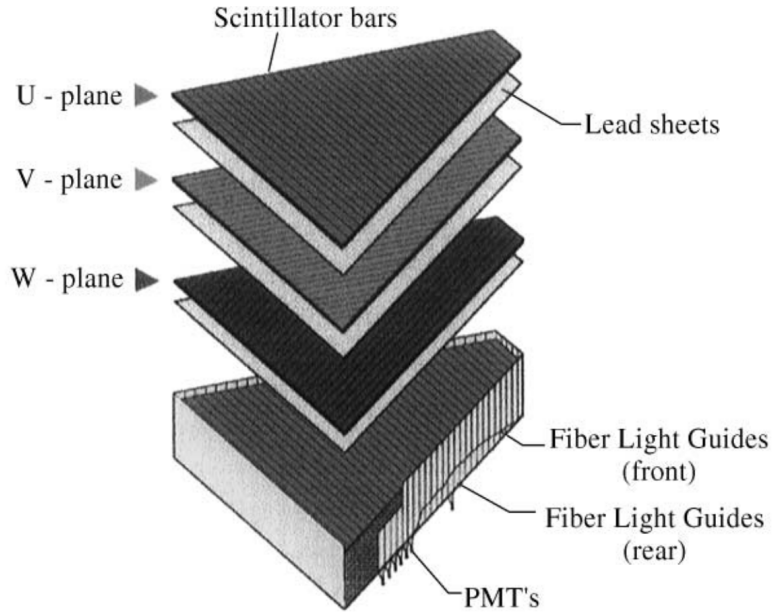
Figure 2.7   Schematic diagram of the CLAS electromagnetic calorimeters from [25].

another can still be registered under the threshold. Of these particles, the minimum-ionizing ones deposit less energy than the threshold level, and hadronically interacting particles deposit less energy per depth but continue depositing energy further into the outer stack. These characterizations are exploited in Section 3.3 to purify the electron sample.

The EC's efficiency of electron detection is nominally greater than 98% [21]. Including an effect of reduced edge efficiency due to electromagnetic shower *leakage*, its geometric acceptance is comparable in angular coverage to that of the CC.

Chapter 3

Reconstruction and Particle Identification

During E1F and E16 run periods, the CLAS detector, as described in Chapter 2, recorded signals from all detector subsystems every time the EC-CC-coincident trigger activated, signifying that an electron candidate emerged from a beam-target collision. The goal of *reconstruction* is to convert the resulting digitized data into particle information and kinematic properties at the *ep* vertex. From this reconstructed particle information per event, the *sample selection*, or *skim*, (see Section 4.1) aims to select the smallest subset of events based on first-pass reconstructed properties without eliminating potential exclusive ω production events.

The general logic to arrive at valid particle information is multi-layered: Event by event, *tracks* that correspond to particle trajectories are reconstructed. A track's extrapolation back to its minimum distance from the beam determines the corresponding particle's momentum direction at the vertex; a track's curvature within the region of well-known magnetic field determines the particle's electric charge and momentum magnitude. From a particle's charge and average momentum with independent timing information over its path, the particle can, in principle, be identified. In practice, energy deposit signatures are used to strengthen the discrimination between same-charge particles when the momentum and time resolutions are insufficient, in particular to distinguish electrons from negative pions. The implementation of this general logic is elaborated in the following sub-sections, without regard to some important deviations of *measured* values from *actual* values to be treated in Chapter 5.

21

3.1 Cooking with RECSIS

The *cooking* process consists of calibration, reconstruction, and data quality checks. Manak and Smith [26] state that the goal of the standard cooking procedure is to provide cooked data files that contain "reconstructed quantities which are deemed by the [CLAS] collaboration to be suitable as input to publishable physics analysis." The infrastructure and steps of the cooking process are well-described in the same document, but specific implementation choices are left up to the user.

Both E1F and E16 experimental data were subjected to detailed calibration and cooking analysis by the collaboration according to the standard cooking procedures. While there is no published CLAS-NOTE that fully documents the efforts, the content can be pieced together from their work product on JLab's `ifarm` computers and from the source code of the cooking software. The final results of the multi-pass calibration and reconstruction efforts are realized by the RECSIS-based program called `user_ana` in tandem with the stored calibration parameters. More specifically, `user_ana` converts digitized data to physically meaningful values modified according to run-level calibration parameters stored in the CLAS calibration database described in [27]. The output of `user_ana` adheres to the Bank Object System (BOS) dynamic memory management system [28, 29, 30]. In the BOS language of *banks* and *data words*,[1] Appendix A lists the relevant `user_ana` data.[2]

The current analysis uses the cooked data in a skeptical mode, trusting only the most basic values along with well-documented derived quantities. Control histograms are produced to verify correctness, and simulations are processed with the same cooking software to derive *acceptance corrections* (see Chapter 5) that absorb reconstruc-

---

[1]Disregarding the memory-centric language of BOS, the terminology can be mapped onto relational terminology for conceptual purposes. A bank corresponds to a table whose columns are data words. The table row entities depend on the bank. For example, in the case of the EVNT bank, each row would be a track, or particle.

[2]Complete BOS bank information is contained within the data definition files available through the JLab SVN at https://jlabsvn.jlab.org/svnroot/clas/trunk/io/bankdefs.

tion inefficiencies and inaccuracies. The most basic information in the cooked data files includes hit positions, energy deposits, and timing information. From these direct measurements, `user_ana` determines particle tracks according to the numerical optimization procedures of [31] and momentum magnitudes and particle charges according to precisely-measured track curvatures within the drift chambers [21]. Starting with this information, independent particle identification and kinematic corrections can be performed.

3.2 Run Quality and Luminosity

Before performing refined particle identification, the data is reduced to events that are associated with good beam and target conditions according to run-time logs and luminosity-normalized event rates. From the golden runs,[3] more restrictive quality constraints are applied at the run level as well as at the luminosity-block[4] level. The preliminary particle identification performed during cooking is used for the run selection process but later verified with refined particle identifications.

Run selection in most analyses involves eliminating an entire run if its trigger count, normalized to live-time-corrected luminosity, deviates from normal values as determined by the full set of runs. Sometimes normalized particle- or event-type counts are additionally used and reveal otherwise undetected anomalies. For example, Gohn [32] describes a case where a run passed the electron count criteria but failed based on pion counts. Going further than run-level statistics by breaking a run into smaller units is rarely performed, as it invalidates the recorded accumulated charge at the end of a run's data, which is often summed over runs to arrive at the integrated

---

[3] *Golden runs* are those without incidents reported in the CLAS Online log entry database (http://clasweb.jlab.org/clasonline/prodlogsearch.html) and without obvious luminosity or detection issues identified during the calibration process.

[4] The accumulated charge in the Faraday cup is recorded approximately every one thousand events. Each of these event groups is called a *luminosity block*.

luminosity of an entire experiment. However, investigating file and luminosity block information can reveal additional issues or allow the inclusion of more data. The integrated luminosity is then the sum of the surviving luminosity blocks.

A file or block analysis is important in the case of E1F. From 606 runs deemed "good" by run-level analysis, 204 are missing at least one file from the reconstructed data due to problems during cooking. The missing files contain about two percent of the golden-run data, and their absence biases the end-of-run luminosity measurements. Without file or block analysis, these runs would be included according to the golden run list or excluded due to low normalized yield, and therefore final cross sections would suffer from an unnecessary source of systematic or statistical error, respectively.

Figure 3.1 illustrates the run quality of the E1F golden runs. All counts are normalized to the charge accumulated in the Faraday cup upstream of the beam dump, which is the only variable quantity entering into the integrated luminosity calculation for each experiment. The first eight rows of Figure 3.1 show block-averaged values, normalized to corresponding Faraday-cup charge. The final row depicts the frequency (z scale, color) of normalized counts per block (y scale), grouped by run (x scale). The dark green and red points identify peaks of the normalized count distributions per run as determined by the means of Gauss fits in the vicinity of the modes. Red points correspond to runs that failed the quality check, which consists of several discriminating filters. First, luminosity blocks with normalized counts that deviate by more than five standard deviations are eliminated before they enter into run-level averages. A run is eliminated if its block-averaged normalized count is an outlier[5] in any of the run-averaged histograms of the figure or if the Gauss fit to its block-level normalized count distribution of N_{pid} has $\sigma < 100\,\mu C^{-1}$, $\sigma > 300\,\mu C^{-1}$,

---

[5]Quantitatively defining *outlier* is problematic and depends strongly on the case-by-case character of data. In this analysis, about 2% of the golden runs clearly deviate from a 98% *bulk*.

24

$\mu < 1550\,\mu C^{-1}$, or $\mu > 2150\,\mu C^{-1}$.

3.3   PARTICLE IDENTIFICATION

CLAS leverages Čerenkov counters and electromagnetic calorimeters to identify electrons; it employs mass spectroscopy techniques to distinguish between charged hadron species. The underlying principles and CLAS-specific hardware implementations are described in Chapter 2. This section describes the *particle identification cuts* used to identify electrons, protons, and charged pions.

The identification of detected particles is imperfect, carrying with it a background of false identification as well as an inefficiency of identifying cuts. The false-identification background is generically compensated by the background subtraction of Chapter 7, and the cut inefficiencies are compensated by the acceptance corrections of Chapter 5, which also account for detection inefficiencies and acceptance gaps. The CC-related photo-electron cut of Section 3.3 is the exception to the standard treatment: CC-related efficiency factors are derived from the experimental data rather than simulation.

Electrons

Electron identification is crucial to the identification of other particles, because the reconstructed time of the electron's extrapolated distance of closest approach (DOCA) to the beam line defines the vertex time, $t = 0$, for the event.[6] This section describes the three cut categories – electron candidate, EC-related, and CC-related – involved in the electron identification process.

---

[6]More specifically, the electron's DOCA time correlates to the high-precision RF time, and the RF time defines the event's vertex time.

25
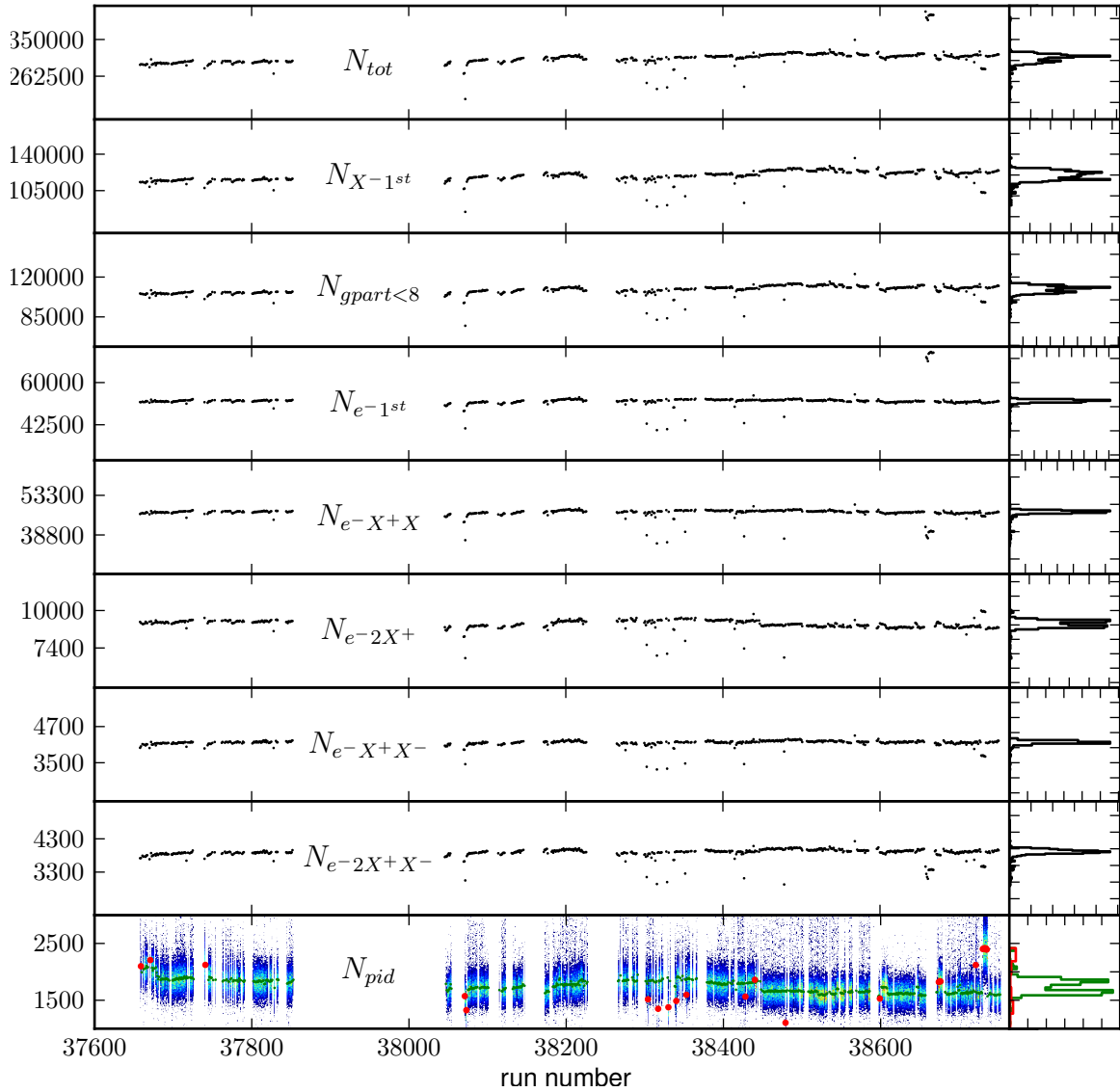
Figure 3.1   Normalized event counts versus run for E1F. From top to bottom, each row illustrates the live-time-corrected, beam-charge-normalized number of events (μC^{-1}) that satisfy successively more restrictive criteria. The first five rows accumulate the following criteria: no restrictions, first particle is negative, less than eight particles are detected, first particle is electron, and at least one positive particle is detected. The next three rows represent mutually exclusive sets according to exact numbers of charged particles detected, not counting the electron: two positive; one positive, one negative; or two positive, one negative. Black points correspond to run-level average counts. The bottom row shows normalized event counts subject to more restrictive particle identification. Events must satisfy all of the first five criteria and contain exactly $ep\pi^+$, $ep\pi^-$, or $ep\pi^+\pi^-$. Green (red) dots correspond to run-level averages of surviving (eliminated) events; the color scale represents the frequency of normalized count values at the luminosity-block level.

26

Candidate e^- cuts

Electron candidate particles are defined by the following detection properties:

- first detected particle of the event,

- negatively charged,

- same-sector, coincident hits in CC, EC, and SC, and

- geometrically consistent, negative-particle track in DC.

The set of electron candidates includes all near-light-speed (Čerenkov-light-producing, as in Section 2.2) negative particles with successfully reconstructed momenta and timing properties, leaving the discrimination of electrons from other fast negative particles to more restrictive criteria described below. In principle, the time of flight, track length, and momentum are sufficient properties to discriminate particles of different masses and thus to reject the non-electrons, which are dominantly negative pions; however, in practice, the detector resolution dominates the difference between these measured candidate properties, as seen in Figure 3.2.

EC-related e^- cuts

The EC provides access to a more practical discriminating property than the time difference of Figure 3.2 – the characteristic energy deposit of an electron's electromagnetic shower in contrast to that of a pion's minimum-ionizing interactions (see Section 2.2). Energy deposited by particles is sampled by the inner (E_{in}) and outer (E_{out}) EC, and the total energy registered by the EC is denoted E_{EC}. Electrons are stopped within the EC, so the corresponding fraction of momentum E_{EC}/p is equal to the EC's *sampling fraction*. On the other hand, minimum-ionizing particles, like charged pions, are not stopped,[7] so the corresponding E_{EC}/p is less than the sampling

---

[7]At least those with momenta relevant to our configuration are not stopped.
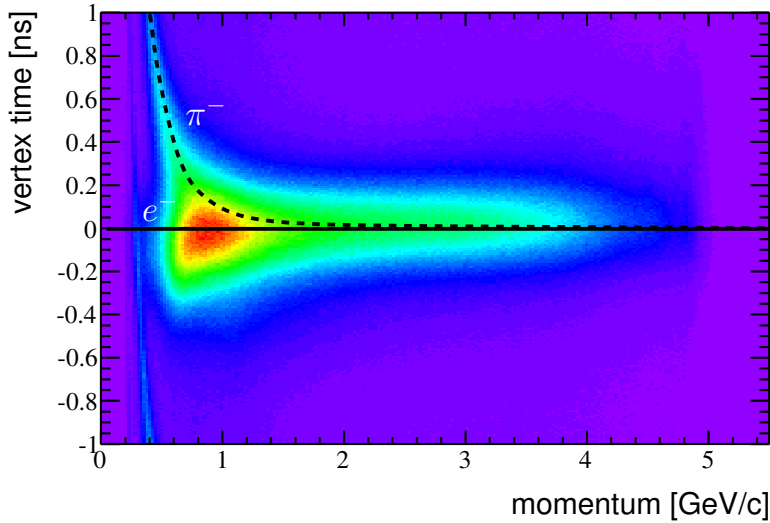
Figure 3.2 The time difference, Δt, between the measured time of flight and the time predicted by the momentum and mass (assumed electron) versus momentum, p, for all electron candidates in the E1F data. The electron assumption leads to an underestimation of predicted time for heavier particles, allowing for separation of particle types by mass, provided sufficient time resolution. The dashed and solid lines correspond to pions and electrons, respectively. In this case, the time resolution is insufficient to reliably separate the two, so other methods of separation must be employed.

fraction and varies with momentum. Furthermore, the minimum-ionizing particles tend to deposit a fixed amount of energy, but since they are primarily hadrons, they have a chance of hadronically producing additional minimum-ionizing particles, especially in the thick lead division between the inner and outer EC layers. In accord with these energy deposit characteristics, two EC-related cuts serve to enrich the electron selection:

- E_{EC}/p must be within 3σ of the EC's sampling fraction, empirically determined and, practically, allowing for some momentum dependence, and

- E_{in} must be greater than the mean energy deposit plus 3σ of the minimum-ionizing particle distribution in the inner EC.

Figure 3.3 illustrates the energy over momentum fraction, E_{EC}/p, versus momen-

tum, p, distribution for E1F electron candidates. In the normalized visualization of the figure's right panel, some notable features are apparent. The electron signature is clearly visible around $E_{EC}/p = SF \approx 0.3$, but it is obfuscated by minimum-ionizing particle contamination and by anomalies at very low and high momenta, which include detection artifacts. However, the anomalies at extreme momenta are below the electron's minimum momentum threshold or above the kinematic reach of electrons within the ωp channel, as illustrated by the overlain momentum distribution of electrons (right panel) in the final exclusive event selection. Within the final electron momentum range, the minimum-ionizing particles are suppressed according to the EC-related cuts on E_{EC}/p and E_{in}.
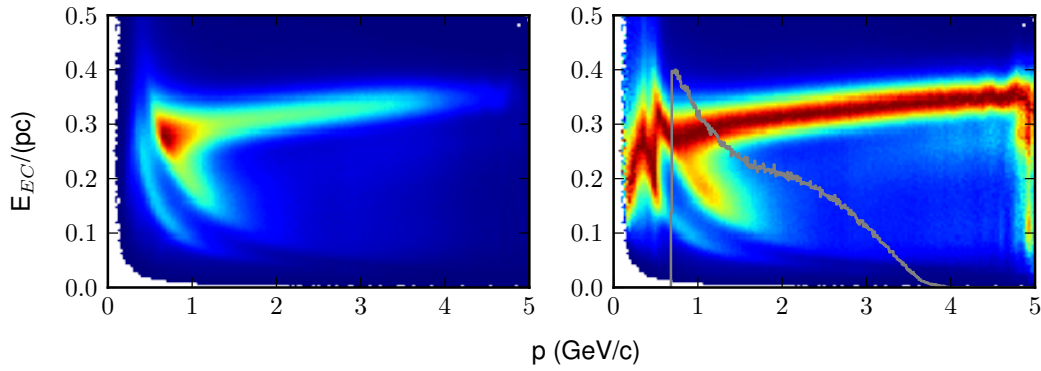
Figure 3.3 E_{EC}/p versus p histogram of electron candidates with linear count (color) scaling (left) and with each momentum slice normalized according to its maximum count (right). The momentum distribution of electrons in the fully exclusive $p\pi^+\pi^-$ detection topology is displayed as an overlay on the right-panel histogram, illustrating that the structures at low and high momentum are irrelevant to the final event selection for the channel under study. The strong, almost horizontal feature at $E_{EC}/p \approx 0.3$ is the manifestation of electrons depositing their full kinetic energy into the sampling EC.

The E_{EC}/p cut parameters are determined from a selection of particles that are very *likely* to be electrons; the E_{in} cut parameters are determined from a selection of particles that are very *unlikely* to be electrons. For the case of determining the E_{in} cut that reduces minimum-ionizing contamination, the following criteria allow only

29

particles that are likely *not* electrons:[8]

- The CC must register a number of photo-electrons in, or lower than, the *noise level* (less than 3 photo-electrons).

- E_{EC}/p must be less than 0.26.

Figure 3.4 illustrates E_{out} versus E_{in} for the corresponding sample of particles. For
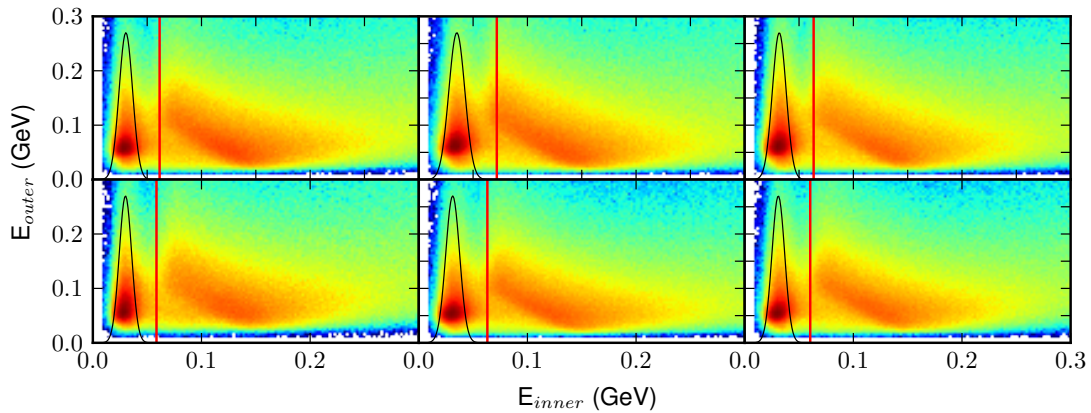
Figure 3.4 E_{out} versus E_{in} for E1F electron candidates with strong enrichment cuts. The Gauss functions at low E_{in} are fits to the one-dimensional E_{in} distributions of the minimum-ioninize particles, including those that hadronically interact to produce more minimum-ioninizing particles, a process that results in the visible tail extending into higher E_{out} values. The solid red lines around 0.06 GeV represent the 3-σ cuts on the Gauss functions, which serve as minimum E_{in} values for electron identification.

each sector (each panel), a Gauss fit to the one-dimensional E_{in} distribution of minimum-ionizing particles, along with a corresponding 3-σ cut, is depicted. The resulting E_{in} cut parameters are denoted in Table 3.1.[9] For the case of determining the momentum-dependent E_{EC}/p cut, Figure 3.5 illustrates the E_{EC}/p versus p distribution for a sample of electrons enriched by requiring all of the following criteria:

---

[8]E_{in} cut parameters consistent with this selection can also be derived by restricting to positive particles, which reduces the electron background under the minimum-ionizing peak.

[9]Simulated data uses similarly determined thresholds of 0.063 GeV.

Table 3.1 E_{in} cut parameters. Electrons must deposit more energy into the inner EC than E_{in}^0. This threshold is set to eliminate 99.7% of the negative hadrons that lose energy by minimum ionization plus hadronic interactions.

Sector	E_{in}^0 (GeV)	
	E1F	E16
1	0.058	0.057
2	0.064	0.062
3	0.060	0.058
4	0.056	0.056
5	0.058	0.060
6	0.056	0.059

- particle is already identified as an electron candidate according to the first three criteria of this section,

- the CC must register a number of photo-electrons above the *noise level* (greater than 3 photo-electrons),

- E_{EC}/p is greater than 0.26,

- E_{EC} is greater than 0.16 GeV, and

- E_{in} is greater than 0.07 GeV.

For each momentum, E_{EC}/p is Gauss-distributed. The means, 3-σ boundaries, and corresponding third-order polynomial cut functions are marked. Electron candidates between the 3-σ boundary functions, determined by fitting the upper and lower boundary points separately, survive the cut,

$$\sum_{i=0}^{3} a_i p^i < \frac{E_{EC}}{p} < \sum_{i=0}^{3} b_i p^i \,. \tag{3.1}$$

Parameters for the polynomial cut lines are tabulated in Table 3.2.

While the EC cuts of (3.1) effectively discriminate electrons from other fast negative particles, they come at the cost of a minimum energy threshold below which the

31
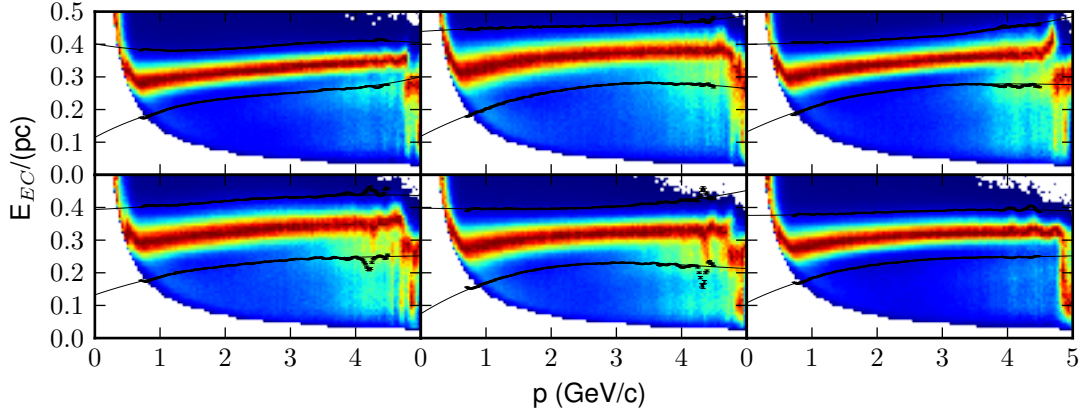
Figure 3.5 E_{EC}/p versus p for E1F electron candidates with strong enrichment cuts to amplify the electron's signature E_{EC}/p distribution for each sector. A Gauss function is fit to the E_{EC}/p distribution of each momentum slice, and the corresponding 3-σ boundaries are marked with black points. The resulting upper and lower bounding points are fit with third-order polynomials represented by the solid lines. Particles with $(p, E_{EC}/p)$ between the bounding functions survive this part of the electron identification process.

Table 3.2   Momentum-dependent function (3.1) parameters for the 3-σ cut around $E_{EC}/p = SF$. Particles with $(p, E_{EC}/p)$ outside of the bounded region are not identified as electrons.

Period	Sector	a_0	a_1	a_2	a_3	b_0	b_1	b_2	b_3
E1F	1	0.13	0.043	-0.008	0.00021	0.31	-0.013	-0.0016	0.00072
	2	0.11	0.065	-0.019	0.0018	0.32	-0.027	0.0053	-0.00039
	3	0.11	0.063	-0.018	0.0017	0.33	-0.035	0.0097	-0.0011
	4	0.13	0.042	-0.0084	0.00036	0.32	-0.019	0.00077	0.00033
	5	0.13	0.042	-0.0078	0.00024	0.32	-0.015	0.00028	0.00037
	6	0.12	0.055	-0.014	0.0012	0.32	-0.018	0.00078	0.00029
E16	1	0.11	0.1	-0.028	0.0026	0.38	-0.032	0.01	-0.00089
	2	0.11	0.098	-0.021	0.0013	0.41	-0.0064	-0.0018	0.00059
	3	0.12	0.099	-0.025	0.002	0.38	-0.018	0.0069	-0.00087
	4	0.12	0.1	-0.029	0.0028	0.38	-0.018	0.0049	-0.00051
	5	0.11	0.1	-0.028	0.0025	0.38	-0.0069	0.00062	0.00025
	6	0.11	0.11	,-0.028	0.0027	0.38	-0.00092	0.00049	-0.00015

EC is unreliable. A safe electron momentum threshold that relates to the 175-mV EC threshold is imposed at 640 MeV. The value was determined according to the empirical formula derived in [33],

$$p_{min} = 214 + 2.47 \times EC_{threshold},$$

where the resulting minimum electron momentum threshold p_{min} is given in MeV/c, and $EC_{threshold}$ is the EC threshold in mV.

CC-related e^- cuts

The final, CC-related electron identification cuts were foreshadowed in the previous section's description of temporary cuts that aided in the determination of EC-related cut parameters. When the CC triggers accidentally or on near-light-speed heavier particles, the electron candidates that survive the EC cuts are contaminated with non-electron negative particles. The contaminating particles correspond dominantly to low photo-electron counts in the CC compared to the photo-electron counts of the Čerenkov light produced by typical electrons.[10] The signature distribution of this low-count *noise* is easily determined by examining the photo-electron count distribution of heavier particles.[11] Combining the noise function with the good-electron signature function, the contaminated distribution of electron candidates can be well described. This allows for both the determination of a reasonable noise cutoff and a corresponding factor to correct for the elimination of some good electrons, as described by the following example.

Figure 3.6 illustrates the distributions and fit functions for three of the 216 CC photomultipliers, selected from low-, medium-, and high-angle CC segments for full

---

[10]Photo-electron counts are determined directly from calibrated ADC measurements of CC PMT output signals.

[11]The photo-electron count distribution produced by positive and negative heavier particles was verified to be equal within the sensitivity of the detector.

signal variety. The noise distributions in the left column are sufficiently described by the convolution of a Gauss and exponential plus a secondary more slowly decaying exponential,

$$Noise(x; A, \mu, \sigma, \lambda, B, \tau) = A\frac{\lambda}{2}e^{\frac{\lambda}{2}(2\mu + \lambda\sigma^2 - 2x)}erfc(\frac{\mu + \lambda\sigma^2 - x}{\sqrt{2}\sigma}) + Be^{-\frac{x}{\tau}}$$

with

$$erfc(x) = 1 - erf(x) = \frac{2}{\pi}\int_x^\infty e^{-t^2}dt,$$

where A and B are amplitudes, μ and σ are the mean and standard deviation of the Gauss function, and λ and $1/\tau$ are decay rates. The vertical dashed lines (all panels) represent potential cutoffs at $x_0 = 3(\sigma + \lambda)$. After using the non-electrons to tightly constrain noise function parameters, a noise plus generalized Poisson function is fit to the contaminated electron sample (middle column),

$$Noise(x; A, \mu, \sigma, \lambda, B, \tau) + F(x; A_p, \mu_p, \sigma_p) = Noise + A_p\frac{\sigma_p\mu_p^x}{\Gamma(\sigma_px - 1)}e^{-\sigma_p\mu_p},$$

where μ_p is the mean and σ_p is a stretching parameter, effectively allowing the variance of the Gamma-generalized Poisson function to differ from the mean. The resulting $F(x)$ (right column) are used to calculate the CC-cut efficiency corrections,

$$\eta_{cc} = \frac{\int_{x_0}^\infty F(x)dx}{\int_0^\infty F(x)dx}.$$

The CC-cut efficiencies for E1F (top) and E16 (bottom) are plotted for each sector as a function of the PMT number in Figure 3.7.

Hadrons

Charged hadron candidates are required to have geometrically consistent tracks in the DC and coincident, same-sector detection in the SC. For these candidates, track reconstruction provides knowledge of particle charge, momentum, and trajectory, as indicated in Section 3.1. In tandem with the trajectory, time-of-flight information

34
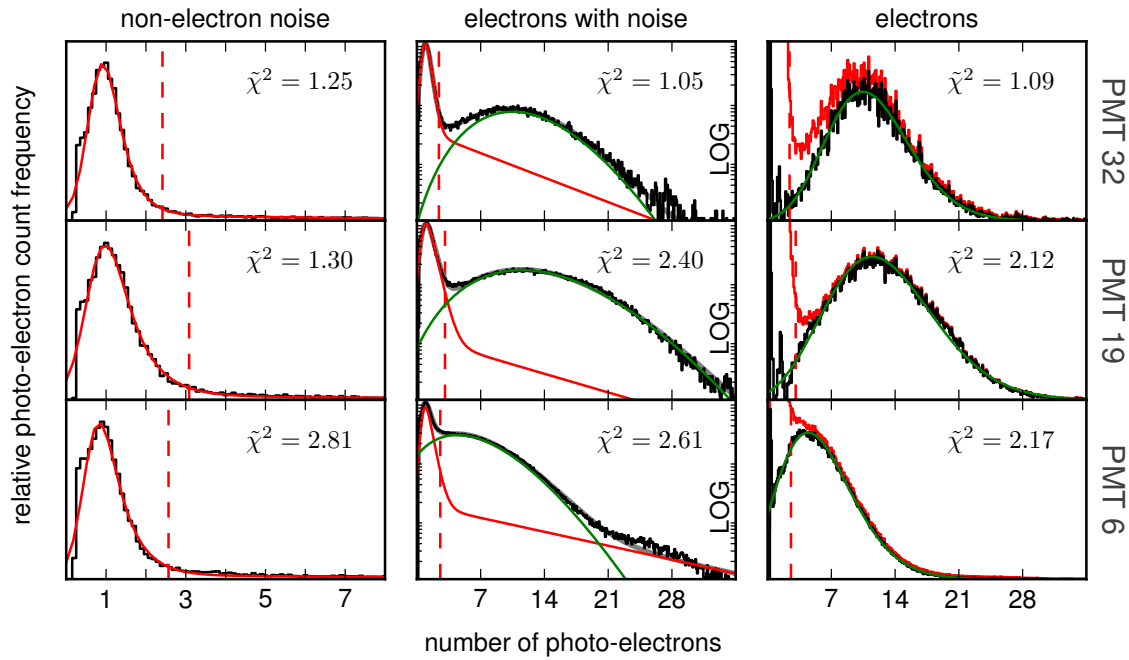
Figure 3.6 CC cut on the number of photo-electrons for electron identification.
Rows correspond to PMTs 6, 19, and 32, which serve as samples over the full signal
variety among the 216 CC PMTs. Column 1 illustrates the positive-particle peak
that provides guidance for fitting the negative-particle noise peak seen in Column 2,
which is plotted with a logarithmic y-scale to emphasize the signature of the
electrons. The noise and electron distributions are together fit with a noise plus
generalized Poisson function. Column 3 superimposes the background-subtracted
electron distribution to illustrate the fit quality. Vertical dotted lines represent the
CC-related e cuts.

affords access to particle velocity, which, for fixed momentum, depends only on the
mass. Accordingly, charged particles of sufficient mass, in this case primarily hadrons,
can be distinguished as illustrated for positive particles of E1F in Figure 3.8.

The mass-dependent relationship (2.1) between velocity and momentum underpins
how the spectroscopic method arrives at the mass to distinguish same-charge particle
types. Practically, however, the relationship is recast in terms of measured and
expected times of flight. The idea is to compare the measured time of flight, t_{TOF}, to
the time predicted by the DC-determined momentum and the mass under different
particle identification assumptions, t_{DC}. In terms of measured and reconstructed
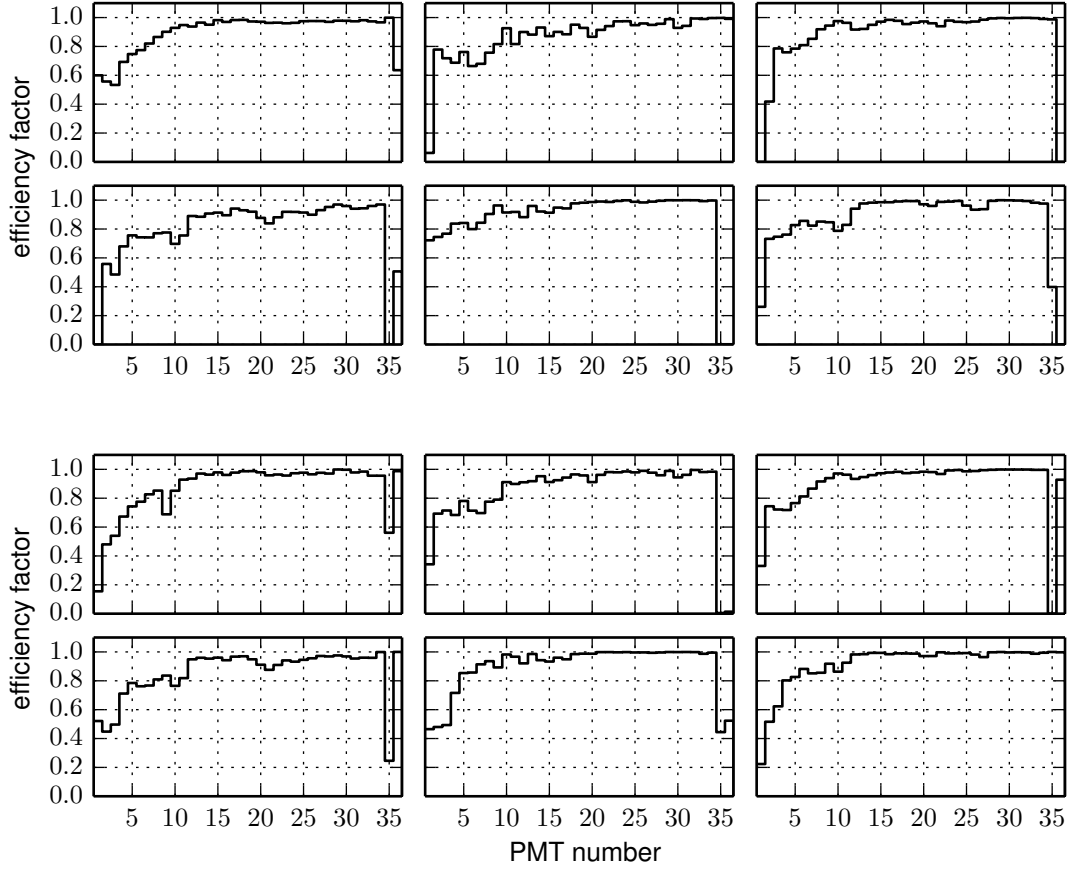
Figure 3.7   CC-cut efficiencies for E1F (top) and E16 (bottom).

values, this time difference, Δt, is expressed as

$$t_{TOF} - t_{DC} = (t_{SC} - t_0) - \frac{d_{DC}}{\tilde{\beta}c},$$

where t_{SC} is the time registered by the time-of-flight detector, t_0 is the event start time, d_{DC} is the distance traveled by the particle between the interaction vertex and the SC plane, and $\tilde{\beta} = \frac{\tilde{v}}{c} = \frac{p}{\sqrt{p^2 + \tilde{m}^2}}$ with $\tilde{m}$ being the mass corresponding to the particle identification assumption. For cases consistent with the mass assumption, the difference is ideally zero and independent of momentum, making the corresponding particle identification cut very simple.

When the electron vertex time is associated with the wrong RF bunch, Δt is offset by a multiple of 2 nanoseconds, the time between bunches delivered to Hall B

36
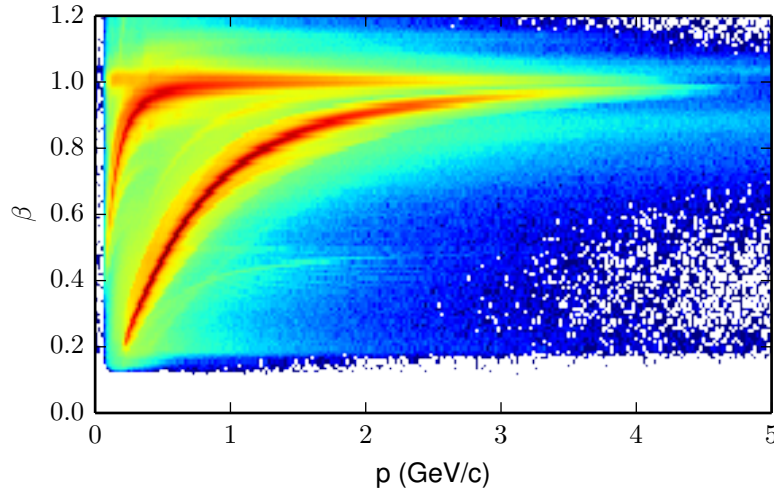
Figure 3.8   Example of β versus momentum for positive particles for E1F on a logarithmic color scale. The proton (lower) and pion (higher) bands are prominent. The pion band reaches close to light speed at low momenta. The proton band is distinguishable to the highest measured momenta. The faint signature of kaons can be seen between proton and pion bands.

(see Section 2.1). If this mis-association occurs consistently within individual runs, it can be corrected even after the cooking procedure. Figure 3.9 illustrates such a case. The first panel shows a proton identification histogram for positive particles passing through one of the 288 TOF paddles. The two distinct loci around zero and two nanoseconds indicate that many of the events are associated with the wrong RF bunch. The second panel represents the offset of the same set of events partitioned by run number and suggests that the vertex times can be corrected by assigning each run a correction factor. Panel three shows the proton identification histogram corrected according to the Panel 2 offsets.

Ultimately, a corrective offset is applied to each of the TOF paddles for each run. After the correction, the Δt distribution of each momentum increment is fit to a Gaussian model to define a 3-σ identifying region around the mean. Kaon contamination is effectively eliminated by the ωp kinematic cuts and background subtraction. The same correction and identification procedure is applied to pions. At

37
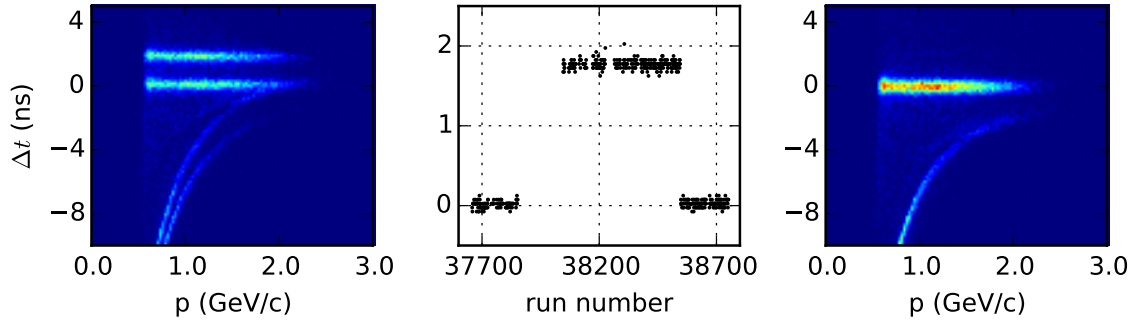
Figure 3.9   Proton identification correction for Sector 3, Paddle 24. Δt (y-axis) is the difference between measured time of flight and the corresponding time predicted by DC-determined momentum with the proton mass assumption. Particles are counted in bins of uncorrected Δt and momentum for positive particles (left). The mean Δt of the *proton locus* (identified based on the horizontal collective character) for each run indicates correctable offsets (middle). The same particles counted in the left histogram are counted in bins of corrected Δt and momentum, presenting a single clear horizontal locus that can be identified to protons.

high momentum, the separation between protons and pions can be less than 3-σ, and so the proton cut will limit the pion identification region. If the simulation accurately reflects the detector resolution, then the acceptance corrections of Section 5.3 absorb this effect. Otherwise, an additional identification efficiency factor must be applied for these events. Within the kinematic region of this study, the effect is insignificant and is, therefore, not separately treated.

CHAPTER 4

DETERMINATION OF YIELD

The key measured value in (1.10) is N_i, the background-subtracted yield of ω events in the four-dimensional bin i. Arriving at N_i requires event selection and background subtraction that eliminate non-ω contributions. Event selection consists of *skimming* a foundational set of events based on the results of Chapter 3 followed by some kinematic cuts to better isolate the ω events while keeping enough events beyond the ω mass region to gain knowledge about the remaining background. The subsequent background subtraction employs a *sideband subtraction* technique that is well-suited to the case when there is not sufficient information to reliably separate the yield into signal and background contributions within each four-dimensional bin independently. The current chapter establishes the skim criteria, kinematic event-selection cuts, and the sideband method of background subtraction.

4.1 FOUNDATIONAL SKIM

A foundational skim of the data is produced during the run quality analysis of Section 3.2. The skim relies primarily on accurate charge determination from cooking (Section 3.1) and electron identification according to parameters derived in Section 3.3 from about 10% of the experimental data. Figure 4.1 and its caption summarize the meaning and impact of each cut and indicate that the cuts based on charged particle counts per event reduce the sample to 5.9% (14.9%) of the E1F (E16) data, thus reducing the frequency of computationally more intensive electron identification refinements, which further reduce the sample to 3.6% (8.5%) of the collected

39

data. While the integrated luminosity of the E16 run is greater than that of E1F, the trigger acceptance is much lower due to the combined effect of higher beam energy, higher magnetic field, and the positioning of the target, resulting in 6.36×10^7 skimmed events in E16 and 1.23×10^8 in E1F.

4.2 KINEMATIC CUTS

Only the missing mass $MM_X(epX)$ is required to determine the exclusive kinematics of ω production, but the foundational skim includes non-ω events that must be separated. In particular, within the spectrum of $MM_X(epX)$, the $\rho^0(770)$ meson overlaps with $\omega(782)$. However, ρ^0 decays primarily into $\pi^+\pi^-$, whereas ω decays primarily into $\pi^+\pi^-\pi^0$, which suggests that they can be separated according to any of the three charged-particle detection configurations: $ep\pi^+\pi^-X$, $ep\pi^-X$, or $ep\pi^+X$. Figure 4.2 illustrates how the ω production events can be effectively separated from ρ^0 and enriched according to the one-pion (top) and two-pion (bottom) detection configurations. The ω events are in the vertical locus at $MM_X(epX) \approx 0.782$ GeV in the top panels and in the spot at $MM_X(epX) \approx 0.782$ GeV and $MM_X(ep\pi^+\pi^-X) \approx 0.140$ GeV in the bottom panels. In all panels, the ρ^0 events are in the horizontal locus below the ω events. The left/right panels represent the events counted before/after the refined electron identification cuts are applied.

In the current analysis, the $ep\pi^+X$ detection configuration was studied, because π^+ has more favorable detection and reconstruction properties than π^-. The unshaded region ($MM_X(ep\pi^+X) \geq 0.300$ GeV) of the top-right panel of Figure 4.2 represents the set of events to which the methods of the subsequent sections apply. The $MM_X(epX)$ range includes ample *sideband* width outside of the ω mass range to provide more information on the shape of the background under the ω mass peak.

In summary, the following selection criteria define the working sample of events.

- Run is good according to golden run list.

40
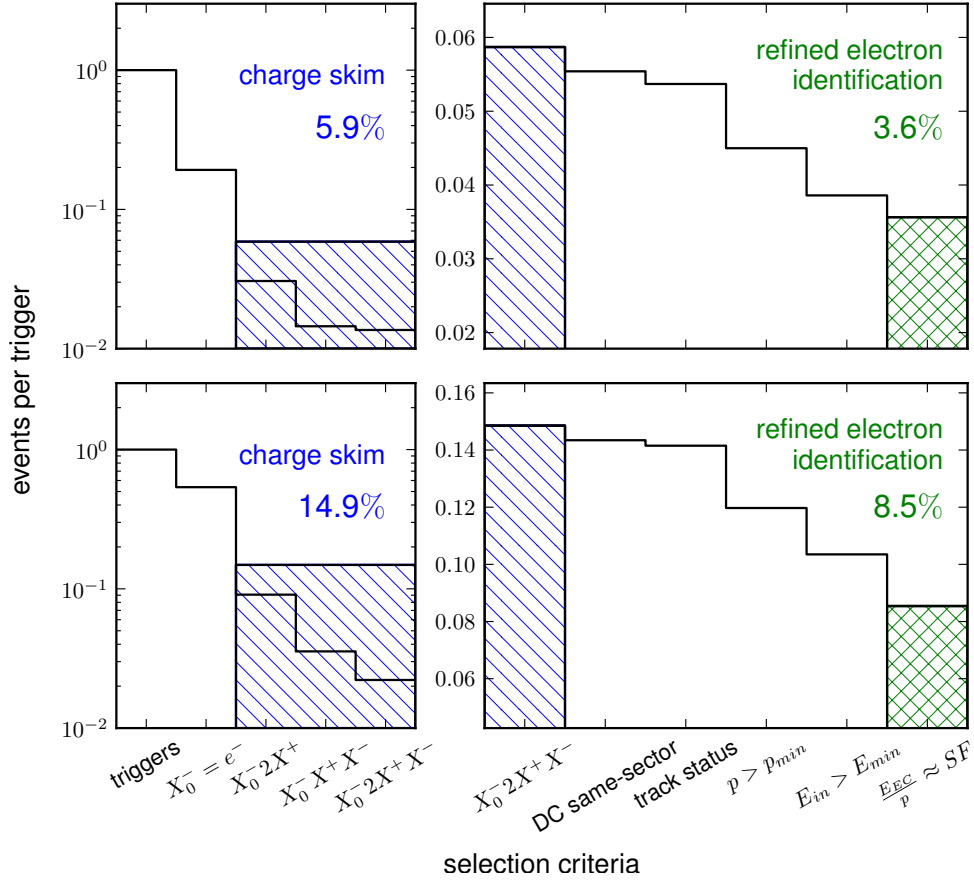
Figure 4.1   Skimmed event count per trigger for E1F on top and E16 on bottom. Diagonal-hatched regions correspond to the number of events that pass the charge skim. The cross-hatched region corresponds to the number of charge-skimmed events that satisfy a refined electron identification. (left) $X_0^- = e^-$ means that the first particle of the event is negative and satisfies very permissive electron candidate criteria; the last three bins of the left histograms are mutually exclusive charged particle counts that correspond to the three detection topologies $e^-p\pi^+$, $e^-p\pi^-$, and $e^-p\pi^+\pi^-$. (right) *DC same-sector* requires the DC hits to be in the same sector as EC, CC, and SC; *track status* must reflect good hit- and time-based tracking results; p_{min} is the momentum associated with the EC threshold; $E_{in} > E_{min}$ eliminates 99.7% of minimum-ionizing particles according to inner EC energy deposit; and $E_{EC}/p \approx SF$ requires the particle's full kinetic energy to be absorbed in the EC.
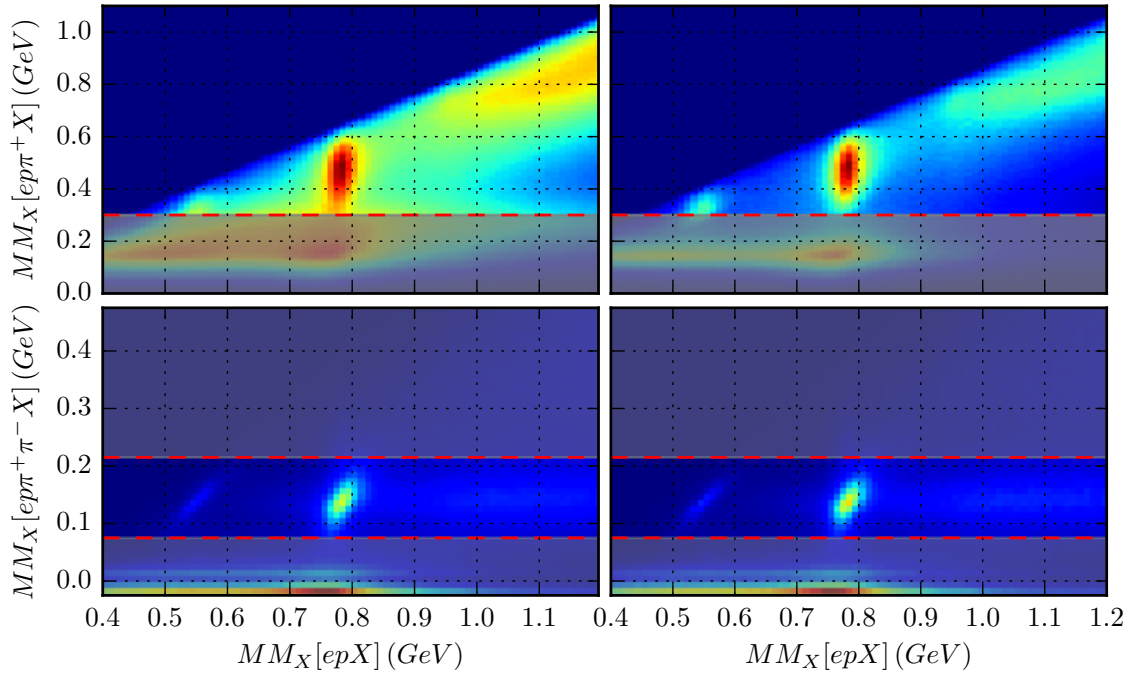
Figure 4.2 E1F event selection by kinematic cuts before (left) and after (right) refined electron identification in two different detection configurations: $ep\pi^+X$ (top) and $ep\pi^+\pi^-X$ (bottom). In the unshaded region of all panels, the ω mass peak is prominent at $MM_X(epX) \approx 0.782$ GeV. The shaded regions are cut away during event selection. Non-ω background among the selected events is subtracted in a later step.

- Luminosity block is good according to Section 3.2.

- First particle is an electron according to the rules of Section 3.3.

- There is exactly 1 proton, exactly 1 positive pion, up to 1 negative pion, and no other charged particles that pass the candidate and identification requirements of Section 3.3.

- $MM_X(epX)$ is in the vicinity of $\omega(782)$, i.e., $MM_X(epX) \in [0.4, 1.2)$ GeV.

- $MM_X(ep\pi^+X)$ is consistent with the three-pion channel, i.e., $MM_X(ep\pi^+X) \geq 0.3$ GeV. Note that this threshold is slightly higher than the minimum, $M_{\pi^-} + M\pi^0 \approx 0.275$ GeV, so that the tail of contaminating ρ^0 events is further reduced.

The corresponding reduction in ω yield will be compensated by the acceptance corrections of Chapter 5.

4.3 Background Subtraction

The event selection procedure of the previous sections provides a sample of events consisting primarily of ω production events and non-interfering background. The bottom panels of Figure 4.2 illustrate that there is not much potentially interfering background – i.e., not much 3-pion background, which would appear in the unshaded region between the dashed lines – under the ω mass peak. Assuming no interference and neglecting asymmetry in the shape of the ω yield distribution, the spectrum of $MM_X(epX)$ is modeled as a linear combination of a Gauss signal peak plus background with a shared phase-space cutoff,

$$f(x; a, b, A, \mu, \sigma, p_0, p_1, p_2) = \left(1 - erf\left(\frac{x-a}{b}\right)\right) \cdot \left(Ae^{-\frac{(x-\mu)^2}{2\sigma^2}} + \sum_{i=0}^{2} p_i x^i\right). \quad (4.1)$$

The parameters are optimized for each W-Q^2 bin in order to arrive at a sideband weight factor in each bin. The factor is then used to normalize the hadronic CMS angular distribution of the sidebands in preparation for subtraction from the angular distribution in the ω mass range. The method is detailed below.

Figure 4.3 illustrates the spectrum with fitted signal, $f^{sig} = f(x; a, b, A, \mu, \sigma, 0, 0, 0)$, plus background, $f^{bg} = f(x; a, b, 0, 0, 0, p_0, p_1, p_2)$, for the $ep\pi^+X$ configuration of E1F for three representative W-Q^2 bins. The shaded regions that surround the unshaded ω signal region represent the background *sidebands*. The angular distribution of the events in the sidebands is assumed to accurately reflect the angular distribution of background events in the ω signal region. Accordingly, for each W-Q^2 cell, the angular distribution of the sideband events, $N_{SB1}^{(2)} + N_{SB2}^{(2)}$, are normalized and subtracted from the angular distribution of the ω region events, $N_{SIG}^{(2)}$, to arrive at the measured

43
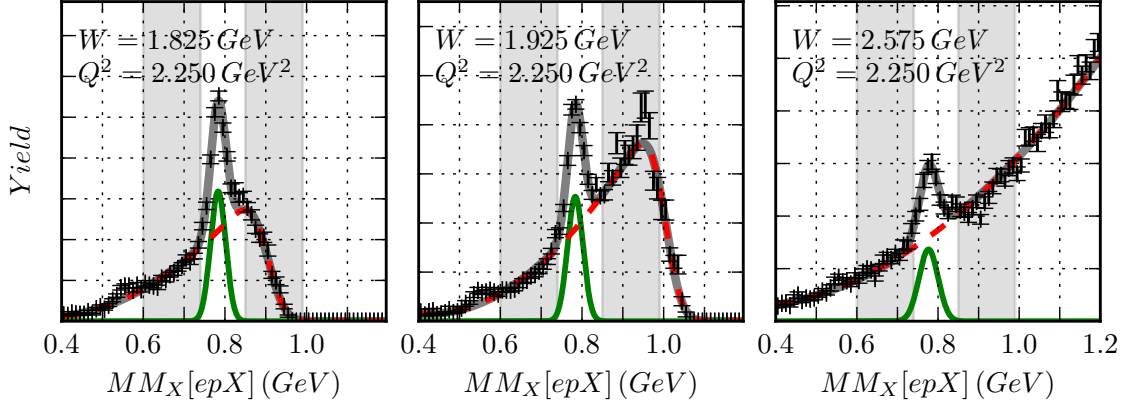
Figure 4.3   Uncorrected spectrum of $MM_X(epX)$ with fitted signal and background for the $ep\pi^+X$ configuration of E1F for three representative W-Q^2 bins. The shaded regions indicate the *sidebands* that serve to estimate the non-ω background in the surrounded signal region.

angular distribution of ω events,

$$N_\omega^{(2)} = N_{SIG}^{(2)} - \left(\frac{\sum\limits_{j \in SIG} f^{bg}(x_j)}{\sum\limits_{\substack{j \in SB1 \\ \cup SB2}} Y_j} \right) \cdot \left(N_{SB1}^{(2)} + N_{SB2}^{(2)} \right) , \qquad (4.2)$$

where the superscript "(2)" indicates a two-dimensional angular distribution for a single W-Q^2 cell, j labels the $MM_X(epX)$ bins in the histograms of Figure 4.3, x_j is the midpoint of the jth $MM_X(epX)$ bin, and Y_j is the yield recorded in the jth $MM_X(epX)$ bin. In concept, the content of each cell of $N_\omega^{(2)}$ corresponds to N_i in (1.10) and, later, in (7.1). All of the $N_\omega^{(2)}$ angular distributions cover all N_i. Ultimately, this correspondence to N_i only applies when the *fiducial cuts* of Section 5.2 additionally restrict the set of events that enter into the above event selection and background subtraction processes.

It is clear from the fits of Figure 4.3, especially from the highest W bin (right panel) where a more significant radiative tail extending above the ω mass would be, that neglecting the asymmetry in the ω signal tends to slightly overestimate the background. However, the main effect of this issue is propagated only through

44

the evaluation of the background function *within* the signal region and typically amounts to less than 3%. The much larger effect of cutting away the radiative tail is compensated through acceptance corrections to be discussed in Section 5.3.

CHAPTER 5

SIMULATIONS AND ACCEPTANCE CORRECTIONS

A major challenge in extracting cross sections is determining the probability of detecting and reconstructing the physics events of interest as a function of the kinematic variables in which the cross sections are expressed. The primary factors that influence this probability are geometric acceptance, detector efficiencies, and reconstruction efficiencies. The principal means of quantifying the impact of these factors involves Monte Carlo simulations of the experiments with the simulated data being subjected to the same reconstruction and event selection as the experimental data. In the limit of infinitely small kinematic binning, these factors depend only on the quality of the detector simulation, not on the thrown event distributions. The probability is also influenced by detector resolution, inaccuracies, and radiative effects that lead to differences between the real and measured kinematic values of the events. These factors can lead to *bin migration*, events being counted in the wrong kinematic bins. The bin migration that results from radiative processes will be treated in Section 6.1. Even in the limit of fine binning, in contrast to the primary factors, the influence of bin migration depends on the thrown event distributions.

In the current analysis, the probabilities of detection and reconstruction were calculated according to simulations that incorporate conditions identical to E16 and E1F data runs. The corresponding *acceptance corrections* and some additional *track reconstruction efficiencies* are described in this chapter. To arrive at the acceptance corrections, which requires a comparison between thrown events and reconstructed simulated events, we must first elucidate details of the simulation and the *fiducial cuts*,

46

which define the well-simulated volume and contribute dominantly to the acceptance corrections.

5.1 Detector Simulation

The cornerstone of our simulations is GSIM,[34] the standard GEANT-based[35] simulation of the CLAS detector. GSIM handles detector geometry, tracking through materials and electromagnetic fields, the physics that govern interactions between particles and the detector, and the detector response. Figure 5.1 illustrates the GSIM simulation of CLAS along with the charged particle tracks of a single simulated event in a cross sectional view. Appendix B includes the contents of the `ffread` files, the
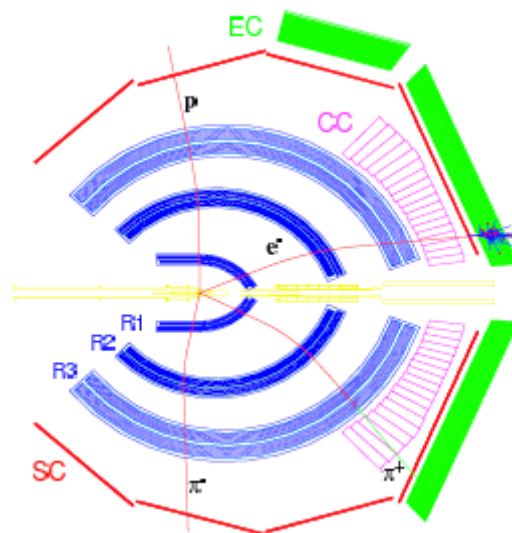
Figure 5.1   Cross sectional view of the CLAS detector as visualized using GEANT-based GSIM. The charged particle tracks of a single event are illustrated. Track curvatures reflect the influence of the magnetic field.

configuration files that drive GSIM, for E1F and E16.

Beyond the idealized GSIM simulation, the GSIM Post-Processor (GPP, a common CLAS software package) smears the simulated detector signals and suppresses detector elements to match the experimental conditions. GPP smears TOF times

47

with consideration to scintillator bar lengths and drift chamber times according to the distance of closest approach to the wires. The degree of GPP smearing is separately tunable for TOF and each of the three regions of the DC. In the current analysis, the three DC regions were required to share a single smearing factor. The parameters were determined by scanning a grid of TOF and DC parameter values to find the pair of parameters that led to the best match between simulation and experiment in terms of (a) electron time resolution and (b) elastic scattering peak width. The GPP parameters used for E1F and E16 appear in Table 5.1. Note that

Table 5.1   GPP parameters for E1F and E16. A single DC smearing parameter value is used for all three regions – `gpp` parameters `a`, `b`, and `c` for regions 1, 2, and 3, respectively – to model spatial resolution. The TOF smearing parameter – `gpp` parameter `f` – was used to model the SC time resolution

.

Parameter	E1F	E16
a/b/c	1.357	1.5
f	1.05	1.35

the GPP parameters determined with this method translate reasonably well to the ω mass peak that is reflected in the missing mass of X in $ep \to epX$, as seen in Figure 5.2. The systematic error introduced by the figure's illustrated difference between background-subtracted experiment and simulation amounts to less than 2% by way of our sideband background subtraction method, as discussed in Section 4.3.

For each experiment, about 250 million $ep \to e\omega p \to e\pi^+\pi^-\pi^0 p$ events, partitioned into Q^2 ranges of 1 GeV^2 width to ensure sufficient statistics at high Q^2, were generated over the full range of W and Q^2 using GENEV, an event generator commonly used in CLAS analyses. GENEV is based on CLAS photoproduction differential cross sections with a dipole function to describe the Q^2 evolution. However, it does not incorporate experimental differential cross sections for ω production. Instead, the ω event model was adapted from more general three-pion data by imposing
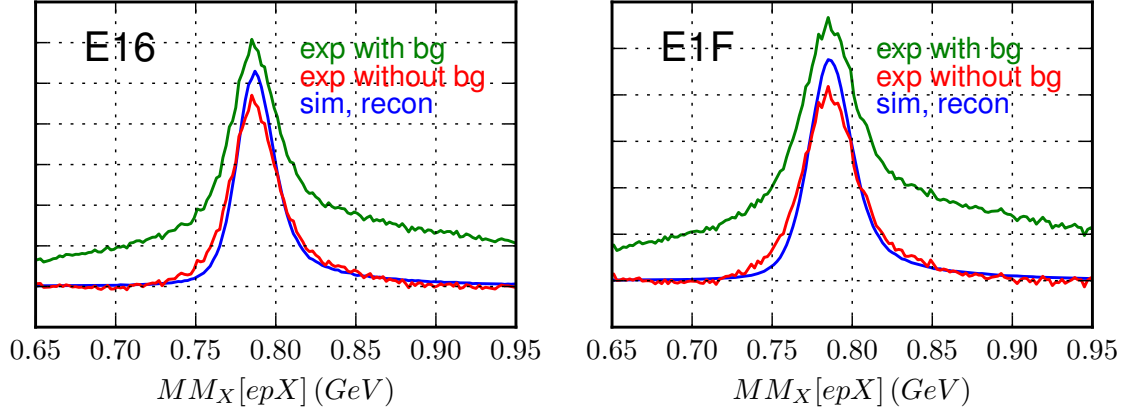
Figure 5.2 Simulated versus experimental distributions of $MM_X(epX)$ for E16 (left) and E1F (right). The highest, green distribution represents experimental data with background from the $ep\pi^+\pi^-$ detection configuration; the red distribution is the background-subtracted experimental data; the smooth blue distribution is the simulated data.

the invariant mass of ω onto the three-pion kinematics. The angular distributions of ω in the hadron CMS (ϕ^* and $\cos\theta^*$ distributions) were forced to be phase-space-like. Additionally, a radiative tail in the invariant mass was simulated according to Mo and Tsai [36] as already implemented in GENEV. The radiative tail contributes to the $MM_X(epX)$ distribution of Figure 5.2, and its effect is treated by the acceptance corrections. The additional impact of the radiative effects in terms of W and Q^2 bin migration is separately treated in Section 6.1.

The level of agreement between simulated and experimental lab-frame particle kinematics is illustrated in Figure 5.3 for E16 and Figure 5.4 for E1F. The experimental distributions include non-ω background, so some differences are expected. There are several notable differences, including between (1) simulated and experimental electron momentum distributions, (2) simulated and experimental proton momentum distributions, and (3) thrown and reconstructed electron distributions in E16. Differences 1 and 2 reflect shortcomings of GENEV's ω event model and represent sources of systematic error that would be improved by a second round of

49
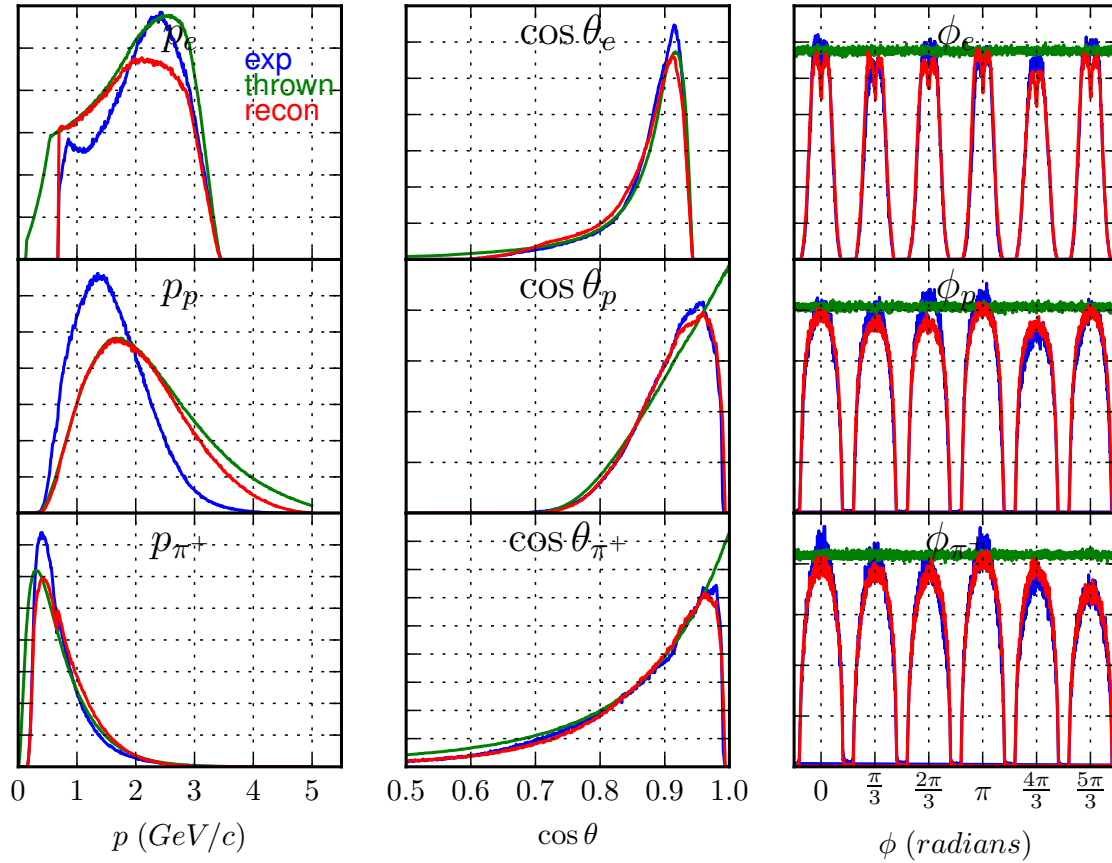
Figure 5.3   Simulated and experimental lab-frame particle kinematics for E16. Lab-frame distributions of momentum magnitude (left), cosine of the polar angle (middle column), and azimuthal angle (right) of particles in the $ep\pi^+$ (top/middle/bottom) detection configuration. Experiment with background appears in blue; and thrown and reconstructed simulated events appear in green and red, respectively.

simulations that are informed by the results of this analysis. These systematic errors have not yet been studied. Difference 3 is an expected feature of E16 and reflects the electron acceptance limitation that motivated the modified target position and magnetic field strength of E1F. The improved electron acceptance is evident by comparing the thrown and reconstructed electron momentum distributions of E1F in the top-left panel of Figure 5.4 (contrasting to the same for E16 in Figure 5.3).

The six-sector geometry of CLAS should be strongly reflected in the acceptance,
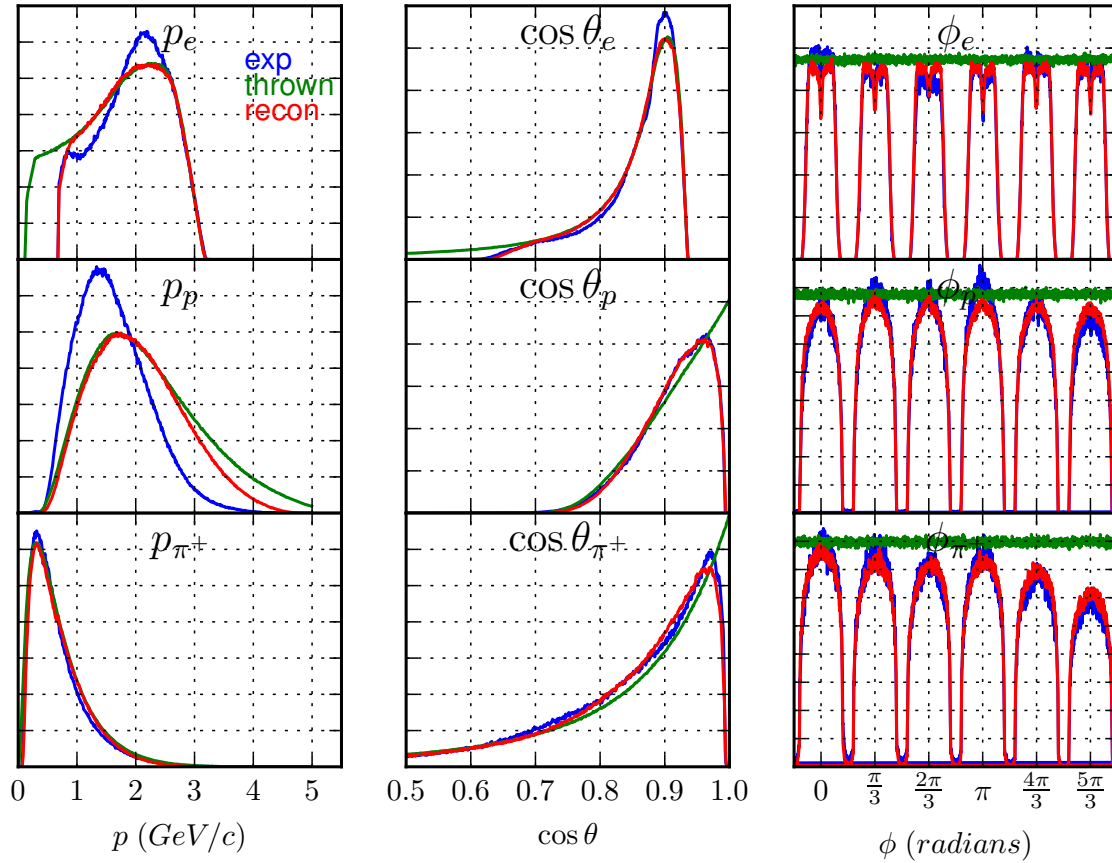
Figure 5.4 Simulated and experimental lab-frame particle kinematics for E1F. Lab-frame distributions of momentum magnitude (left), cosine of the polar angle (middle column), and azimuthal angle (right) of particles in the $ep\pi^+$ (top/middle/bottom) detection configuration. Experiment with background appears in blue; and thrown and reconstructed simulated events appear in green and red, respectively.

so it is important to check that its effect is propagated into the kinematic variables of interest in the simulation as it is in the experiment. The effect manifests as the dominant feature of the hadron CMS $\phi^\star$ distribution. Agreement between simulation and experiment is illustrated in Figure 5.5 for representative W values in E16 (top panels) and E1F (bottom panels).

Ideally, the final cross sections of the current analysis would inform a second round of thrown events, with improved W, Q^2, and angular distributions from which new
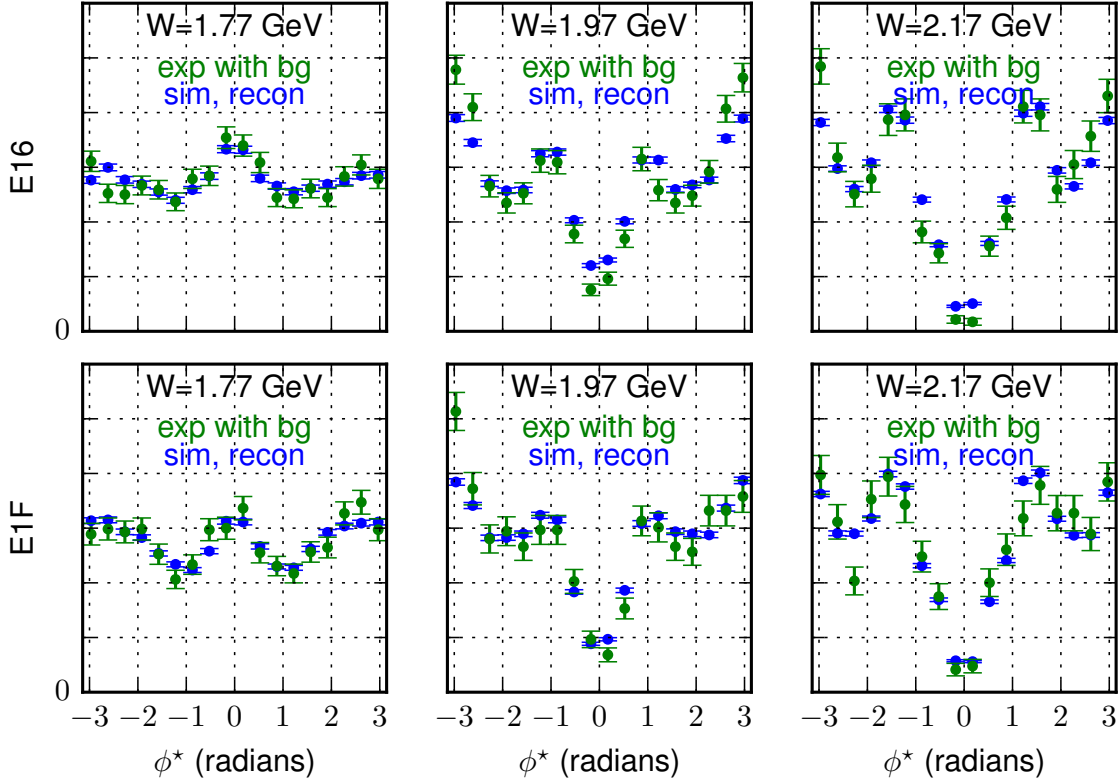
Figure 5.5   Reconstructed simulated (blue) and experimental (green) azimuthal angle distributions of ω in hadronic CMS for E16 (top) and E1F (bottom). Three different W ranges are presented: [1.76,1.78) GeV, [1.96,1.98) GeV, and [2.16,2.18) GeV (from left to right).

acceptance corrections would be obtained. Fortunately, as indicated in the introduction to this chapter, the thrown event distribution is not as influential as the quality of the detector simulation in determining acceptance corrections in our case. Previous studies [7, 37] with coarser binning determined that systematic uncertainties resulting from thrown event model differences were 5-10%. Morand et al. [7] quoted, additionally, much higher uncertainties (up to 20%) in the special cases where a model was used to fill acceptance holes; however, in the current analysis, this hole-filling method was not used.

52

The fiducial volume is defined as the detector-frame p-θ-ϕ volume per particle type in which the geometric acceptance and detector subsystem efficiencies are understood well enough to accurately propagate their effects to the phase space of the final-state particles, where p, θ, and ϕ are the momentum magnitude and direction parameters of the particle at the vertex of interaction. This section describes the determination of fiducial boundaries for both electrons and positive hadrons.

Electrons

There are three main steps, performed on each sector independently, to determine the electron fiducial cuts.

- Remove events in the vicinity of the **Čerenkov Counter flange**.

- Determine the **minimum** θ as a function of momentum,

$$\theta_{min} = \theta(p; A, B, C) = A + \frac{B}{(p + C) * I_{max}/I_B} \, , \tag{5.1}$$

  where I_B is the current driving the magnetic field of the toroidal magnet, and $I_{max} = 3375A$ is the current corresponding to *full* magnetic field strength.

- Determine the ϕ **boundaries** as functions of p and θ,

$$\phi_d = \phi(p, \theta; \{a_i\}, b, A, B, C) = \left(\sum_{i=0}^{3} a_i p^i\right) \left(1 - e^{b(\theta - \theta_0(p; A, B, C))}\right) \, , \tag{5.2}$$

  where θ_0 has the form of (5.1) but is independently parametrized, albeit with a constraint based on θ_{min}.

The final electron fiducial volume is defined by

$$(\theta > \theta_{min}(p) + \delta_\theta) \cap (|\phi| < \phi_d(p, \theta) - \delta_\phi) \, , \tag{5.3}$$

where δ_θ and δ_ϕ are adjustable tightness parameters. Momentum is implicitly bound by kinematics and the detection/selection thresholds described in Section 3.3.

Čerenkov Counter Flange

As described in Section 2.2, the Čerenkov Counters (CC) are a primary tool for electron identification, but the magnetic shielding and PMT housing can block light in the interior-vicinity of the PMT, and the PMT surface is subject to direct activation by non-radiating particles. These features restrict the fiducial volume for electrons to the region interior to the resulting flange, illustrated in Figure 5.6.
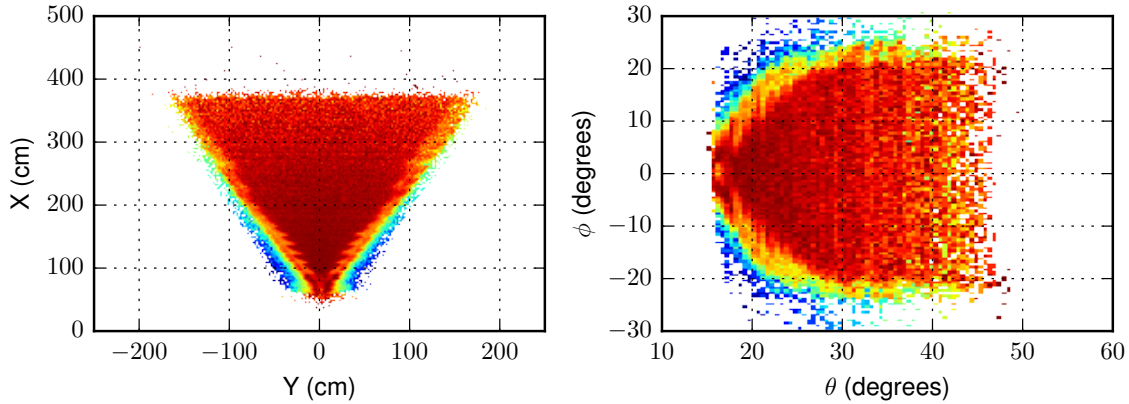
Figure 5.6   Čerenkov Counter edges reflected in electron detection frequency. The CC flange as reflected in the normalized frequency of electrons detected in a reconstructed plane behind one sector's CC plane (left) and in a normalized kinematic angular distribution of electrons of a single 100-MeV momentum slice in the same sector (right).

An efficient way to restrict the p-θ-ϕ fiducial volume to the region interior to the flange is to temporarily cut the flange away based on the tracks' intersections with a coordinate-space plane (left histogram of Figure 5.6) beyond the reach of the high magnetic field that bends the particle paths. By requiring the plane to be beyond the magnetic field, the momentum-dependence of the cuts is removed. These *coordinate flange cuts* are active only during the determination of the p-θ-ϕ surface boundaries described in subsequent subsections, not during the final application of fiducial cuts.

Figure 5.7 illustrates the E1F flange cuts. For each sector, each SC x-slice is

54
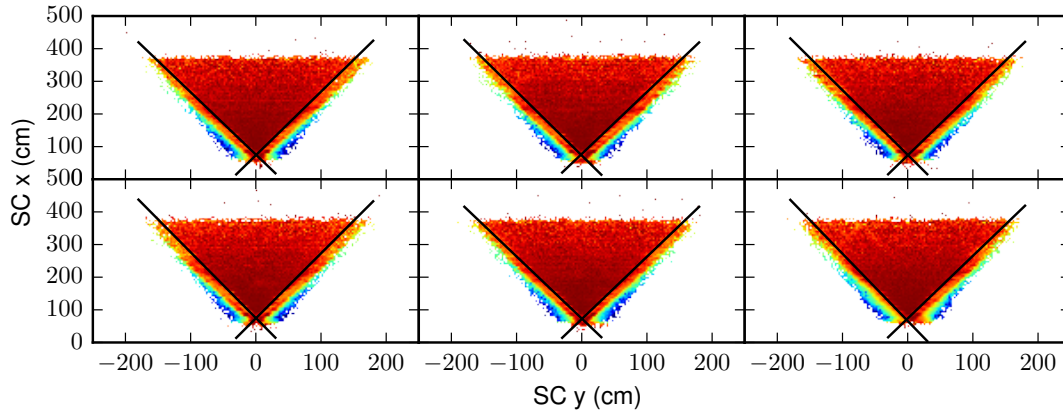
Figure 5.7   Čerenkov Counter flange cuts in coordinate plane for each sector from E1F data.

subjected to an edge-finding process that is tuned to identify the reduced hit frequency that indicates the onset of the flange region. The result is a set of points demarcating the low (negative SC y) and high (positive SC y) edges of the region interior to the flange. First-order polynomials are fit to the data points and used as the linear cut boundaries. Figure 5.8 illustrates the effect of the flange cuts in p-θ-ϕ for one momentum slice in one sector. The cut parameters are tabulated for both E1F and E16 in Table 5.2.

Table 5.2   Coordinate flange cut parameters. Parameters $P0$ and $P1$ are the zeroth and first parameters of a first order polynomial.

| | E1F | | | | E16 | | | |
| | Low | | High | | Low | | High | |
Sector	P0	P1	P0	P1	P0	P1	P0	P1
1	76	-1.909	73	1.950	74	-1.937	73	1.947
2	73	-1.964	78	1.897	70	-2.027	83	1.834
3	75	-1.980	73	1.931	75	-1.943	74	1.861
4	75	-2.013	74	1.991	75	-2.022	73	1.960
5	73	-1.902	72	1.911	72	-1.908	67	1.976
6	66	-2.060	73	1.919	69	-1.993	73	1.894
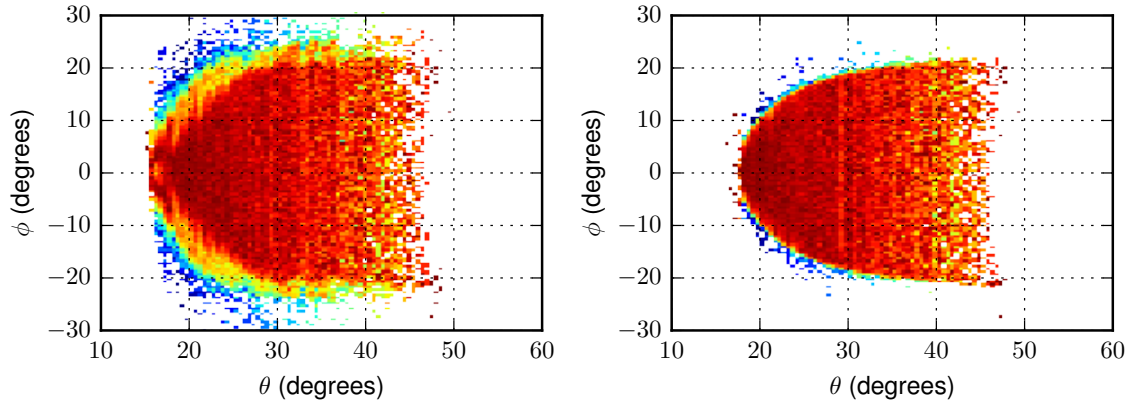
Figure 5.8   Effect of Čerenkov Counter flange cuts that were applied on a coordinate plane. The angular distribution of electrons with p = [1683 MeV, 1783 MeV) in sector 1 of E1F is shown without (left) and with (right) the flange cuts.

Minimum θ

The goal of the minimum theta cut of (5.1) is to remove the areas with rapidly changing efficiencies in the low-scattering-angle area of the detector. From low to high polar angle, the electron yield is expected to fall monotonically, so the contour of the high yield ridges of the θ-p histograms of Figure 5.9 is a reasonable criterion (ridges indicated by white points above black θ_{min} cut lines). However, a looser 50% threshold was chosen as the base θ_{min} – i.e., for each p-slice, the boundary point is set to the θ value at which the yield is 50% of the slice's peak yield. Recall that the tightness parameter δ_θ is a simple translation of θ_{min} and can be tuned separately to more closely align with the highest frequency ridge. For each sector, (5.1) is fit to the θ_{min} boundary points. The E1F results are illustrated in Figure 5.9, and the E1F and E16 parameters are tabulated in Table 5.3.

ϕ Boundaries

Defining a smooth function for the ϕ boundaries requires another edge-finding exercise followed by a multi-pass optimization procedure. With the coordinate flange cut
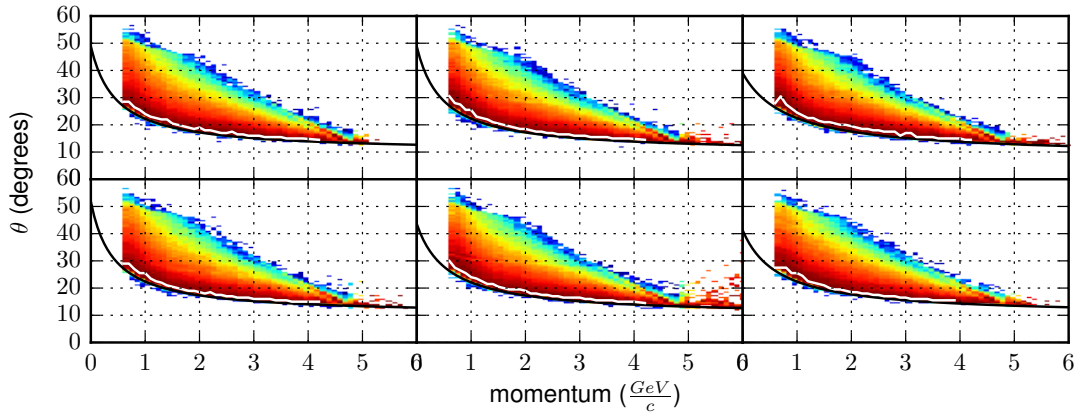
Figure 5.9 Minimum θ cuts for electrons detected in section 1 through 6 (from top left to bottom right) of E1F. The white points mark the highest frequency θ value for each momentum. The black lines represent the result of fitting function (5.1) to the half-maximum on the low θ side of each momentum slice. With a tightness parameter that systematically shifts the values, these function are the basis of the minimum θ cuts.

Table 5.3 Minimum θ boundary parameters. Parameters A, B, and C correspond to the parameters of (5.1).

Sector	E1F			E16		
	A	B	C	A	B	C
1	9.891	27.041	0.463	10.071	28.770	0.659
2	9.658	28.014	0.478	10.788	26.585	0.595
3	8.400	39.080	0.852	9.879	30.107	0.698
4	10.112	26.123	0.418	10.348	27.205	0.572
5	9.633	29.534	0.581	10.128	29.872	0.723
6	9.795	31.501	0.669	9.787	30.775	0.732

still active, the boundary points are determined by finding the edges of the one-dimensional, high-efficiency plateau in the ϕ distribution for every bin of (p,θ). Then, the parameters of (5.2) are optimized to fit these p-θ-ϕ boundary points.

Figure 5.10 illustrates the results of the edge-finding procedure for a single momentum bin of E1F data for sector 1. The left panel shows the angular distribution of electron momenta for one bin of momentum magnitude. Each θ slice is modeled

by a plateau function,

$$P(\phi) = \begin{cases} 0 & \phi < p_2 \\ p_4 \frac{\phi - p_2}{p_0 - p_2} & p_2 \leq \phi < p_0 \\ p_4 & p_0 \leq \phi \leq p_1 \\ p_4 \frac{\phi - p_3}{p_1 - p_3} & p_1 < \phi \leq p_3 \\ 0 & \phi > p_3 \end{cases}, \tag{5.4}$$

where p_0 and p_1 correspond to the low and high ϕ boundary points for the targeted θ bin. The right panel shows the ϕ distribution for $\theta \in [29.75^o, 30.25^o)$ and a fitted plateau function. The ϕ boundaries, p_0 and p_1, are indicated by the two stars and vertical dashed lines, which correspond to the stars in the left panel. The open circles of the left panel indicate similarly determined ϕ boundaries for each θ bin and are fit by (5.2) (dashed green curves) as the result of the multi-pass fitting procedure to be described below. The dashed green vertical line is the independent θ_{min} fiducial boundary. The relationship between the dashed green lines and the fiducial area can be interpreted by (5.3).

The optimization procedure employs multiple passes starting with a two-parameter version of (5.2) that reduces the polynomial function of p and the function θ_0 to scalar parameters. Parameter b is fixed to -0.18, and θ_0 is constrained by $\theta_0 \in [\theta_{min} - 5, \theta_{min} + 2]$. The reduced form eliminates the p dependence and so can be applied independently in each p bin. The algorithm iteratively finds tighter constraints as the p dependence is injected and as the number of parameters are increased, ultimately, to all eight parameters of (5.2). The resulting parameters are tabulated in Table 5.4. Representative results are illustrated in Figure 5.11 for a selection of six momenta ranging from threshold through the kinematic limit for the ω production channel. The same fiducial functions (dashed boundaries) appear in the experimental (top six) and simulated (bottom six) histograms.
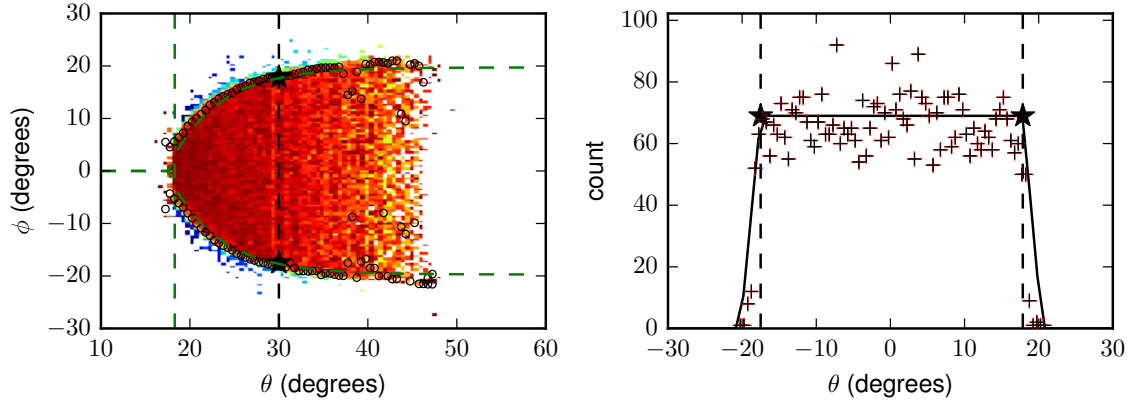
Figure 5.10 Electron ϕ boundary determination, example using E1F, sector 1, and $p \in [1683\ MeV, 1783\ MeV)$. The electron momentum angle distribution (left) is normalized and scaled to emphasize the fiducial area and to diminish internal features. Open circles indicate the ϕ edges as determined by a fitted *plateau* function for every θ slice. The green dashed lines depict the fiducial cut function for this momentum slice. The dashed vertical line at $\theta = 30^o$ marks the slice relevant to the sample ϕ distribution (right). The ϕ distribution of the right panel includes the fitted plateau function from which the boundary ϕ values for $\theta = 30^o$ were taken.

Positive Hadrons

Under the run conditions of E1F and E16, the fiducial boundaries of protons and positive pions (and, indeed, of any heavy positive particle) are common and independent of momentum. Accordingly, the momentum-independent variant of (5.2) is used for both:

$$\phi_d = F \left(1 - e^{b(\theta - \theta_0)} \right). \tag{5.5}$$

The proton and pion fiducial areas are finally specified by $|\phi| < \phi_d(\theta) - \delta_\phi$, analogous to (5.3) for electrons.

In a treatment similar to the determination of the electron fiducial boundaries in ϕ, the parameters F, b, and θ_0 were evaluated independently for each sector and for each momentum. The fitting procedure led to momentum-independent parameters. For each of the experiments, a single set of parameter values, tabulated in Table 5.5, was determined to be within the uncertainty of the fitting procedure for all sectors.
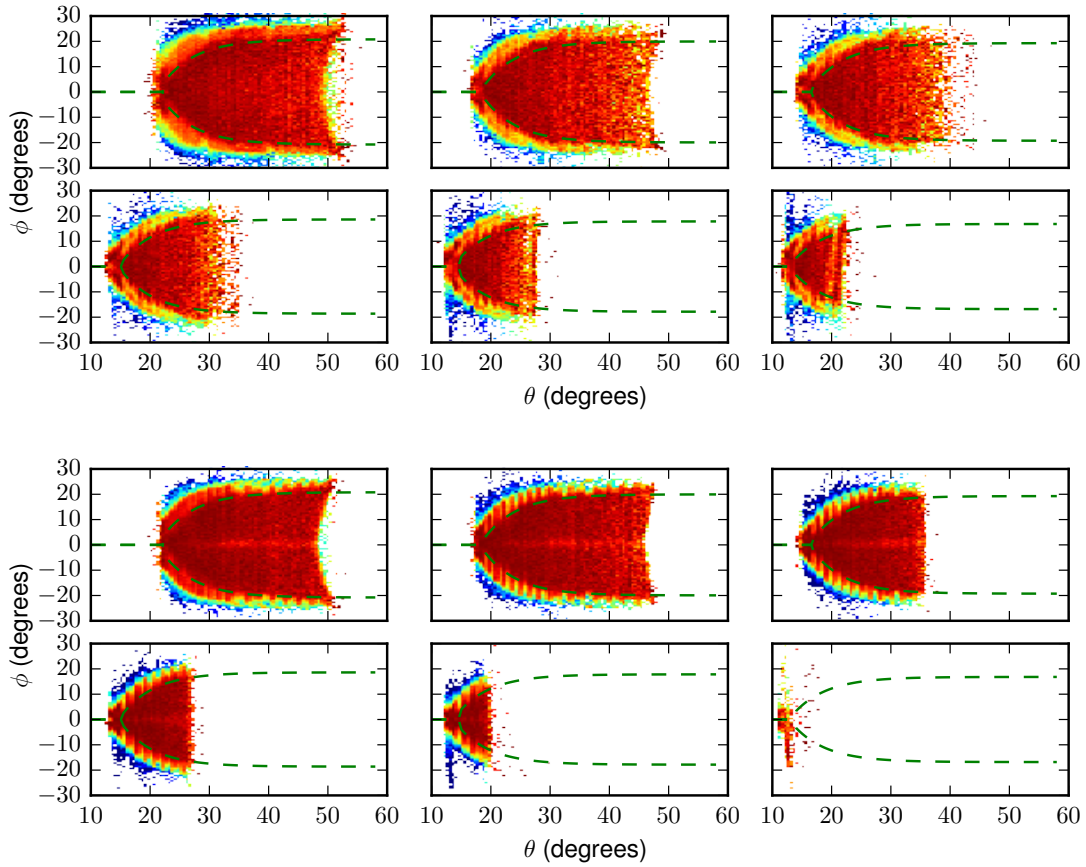
Figure 5.11 E1F's sector-1 electron fiducial volume is illustrated by normalized angular distributions with the fiducial boundaries (dashed curves) for experimental data (top six) and simulation (bottom six). From top-left to bottom-right of each set of six, the panels represent 100-MeV momentum slices centered on 933 MeV, 1.533 GeV, 2.133 GeV, 2.733 GeV, and 3.433 GeV. The differences in the maximum θ at each momentum, most notably at the highest momentum, is due to the experimental data's kinematic range including background that extends beyond the phase space accessible by ω production, unlike the simulated data.

Figure 5.12 illustrates the fiducial area of positive pions and protons for E1F.

5.3 ACCEPTANCE CORRECTIONS

Acceptance corrections are expressed in terms of the physics-frame variables of interest – W, Q^2, $\cos\theta^\star$, and $\phi^\star$. In principle, *geometric* acceptance corrections account for the kinematically accessible volume that is not within the fiducial volume, and

Table 5.4 ϕ boundary parameters for electrons. Parameters correspond to those in (5.2).

	Sector	P0	P1	P2	P3	A	B	C	b
E1F	1	22.842	-2.674	0.702	-0.103	6.284	51.771	1.333	-0.180
	2	24.752	-6.355	2.570	-0.384	6.763	50.465	1.325	-0.180
	3	23.151	-4.193	1.682	-0.272	4.469	74.912	2.047	-0.180
	4	23.470	-4.926	1.840	-0.271	7.304	45.207	1.166	-0.180
	5	24.300	-4.629	1.715	-0.245	6.997	45.839	1.214	-0.180
	6	22.206	-2.621	0.999	-0.173	3.830	79.740	2.185	-0.180
E16	1	25.547	-5.165	1.900	-0.312	6.416	48.614	1.506	-0.180
	2	19.292	5.036	-3.491	0.600	3.937	74.072	2.333	-0.180
	3	26.375	-6.194	2.348	-0.367	5.971	54.593	1.738	-0.180
	4	27.155	-8.160	2.968	-0.423	7.175	42.584	1.248	-0.180
	5	31.381	-16.851	9.564	-1.893	11.216	26.216	0.856	-0.180
	6	26.896	-7.753	3.396	-0.559	3.000	72.870	2.239	-0.180

Table 5.5 ϕ boundary parameters for positive hadrons. Parameters correspond to (5.5).

Experiment	F	b	θ_0
E1F	24	-0.18	6
E16	24	-0.14	6

efficiency corrections account for diminished detection efficiency within the fiducial volume. In practice, acceptance and efficiency effects are treated simultaneously by either simulation or explicitly derived correction factors. In keeping with conventional CLAS nomenclature, I refer to all corrections derived from the difference between thrown and reconstructed, selected (per ω-signal-region event selection criteria of Chapter 4) simulated events as *acceptance corrections*. Thus, acceptance corrections account for not only geometric acceptance but, also, some reconstruction and selection inefficiencies, detector resolution effects, and any other simulated effects, relegating the term *efficiency corrections* to relate to only the inefficiencies that are *not* simulated – e.g., the CC cut efficiencies of Figure 3.7 and the additional track reconstruction efficiencies of Section 5.4.

Figure 5.13 illustrates E1F acceptance factors for 26 representative W-Q^2 values
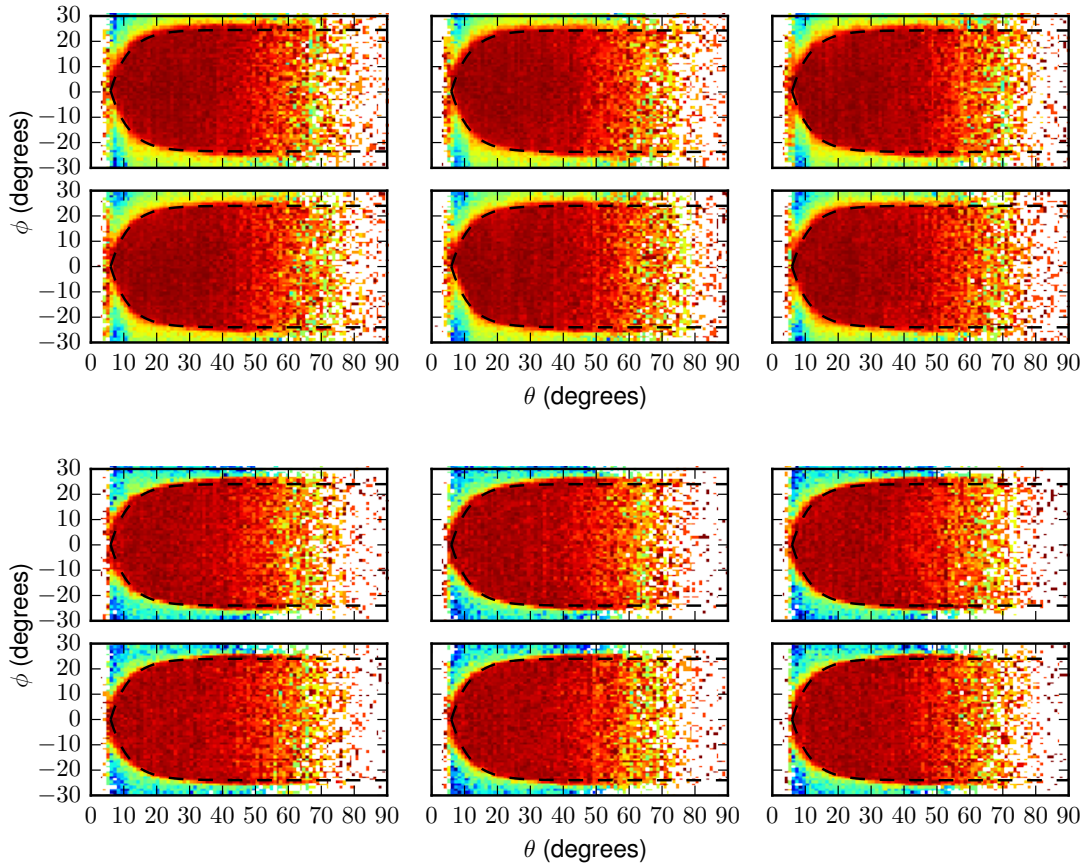
Figure 5.12   Positive hadron fiducial areas. E1F's positive hadron fiducial areas are illustrated by normalized angular distributions with the common fiducial boundaries (dashed curves) in each sector (1-6 from top-left to bottom-right) for experimental data (top six) and simulation (bottom six).

over a wide kinematic range. Each angular distribution is divided into 10 $\cos\theta^*$ bins and 18 ϕ^* bins and represents the events within a W-Q^2 extent of dimensions $\Delta W = 20\,MeV$ and $\Delta Q^2 = 0.3$ GeV^2. Acceptance factors are definable in any bin that has thrown events. In this sample, events were thrown into 3,420 kinematic bins; of those bins, events were reconstructed in 2,628 bins. To get a sense of scale, consider that over the W-Q^2 range spanned by the sample, events were thrown and reconstructed in 82,620 and 67,747 kinematic bins, respectively. The bins that contain thrown but no reconstructed events are called *holes*. It is important to simulate enough events
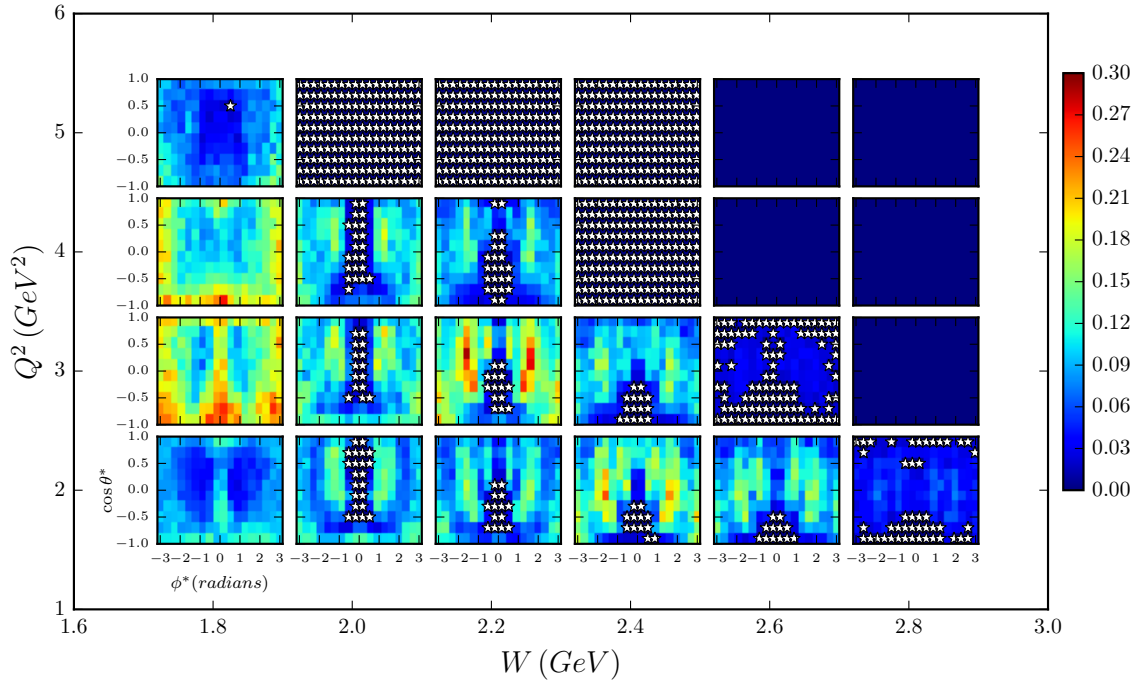
Figure 5.13   E1F hadronic CMS angular acceptance factors for 24 representative W-Q^2 values over a wide range of W. Each 10- by 18-bin angular distribution represents a cell with dimensions $\Delta W = 20\,MeV$ and $\Delta Q^2 = 0.3$ GeV^2. The white stars mark holes where simulated events were thrown but not reconstructed.

to minimize the probability of having holes in kinematic bins that are accessible by detectable events. Figure 5.14 shows the number of kinematic bins filled with reconstructed events as a function of the number of thrown events, cumulatively (left panel) and incrementally (right panel). The curve being very close to the asymptote indicates that most of the accessible bins are already filled. The number of filled bins on the y-axis of the left panel is much higher than the numbers noted with respect to the range of Figure 5.13, because the simulated data supports finer binning than reflected in the sample, which was binned with deference to the lower statistics of the experimental data.

To avoid propagation of excessive error and amplification of differences between experiment and simulation, we remove acceptance factors that are lower than 2% or that carry relative statistical uncertainties greater than 15%. The cuts are illustrated

63
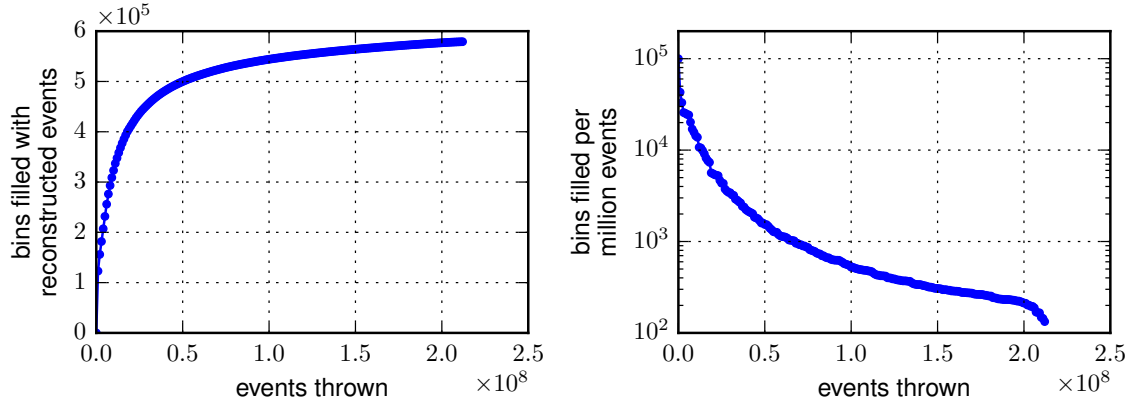
Figure 5.14   Number of kinematic bins filled with reconstructed events as a function of number of events thrown in the simulation of E1F. The left panel shows the cumulative sum of bins filled; the right panel shows the number of new bins filled per increment of thrown events.

in Figure 5.16. Referring back to the sample of Figure 5.13, these restrictions reduce the number of bins with non-zero acceptance from 2,628 to 2,404: the restrictions explicitly create more holes. The combination of naturally occurring and explicitly created holes amounts to 1,016. These holes are indicated by white stars in Figure 5.13. They are compensated when integrated by methods that use information from the experimental data in the kinematic neighborhood of the holes, as will be discussed in Chapter 7. The figure's darkest blue regions that lack white stars are kinematically inaccessible according to the simulation. By zooming into the low-W region, Figure 5.15 uses the same view to provide a higher resolution picture of how the acceptance evolves in smaller W steps.   Figure 5.17, Figure 5.18, and Figure 5.19 illustrate the E16 acceptance factors and cuts in the same way as the E1F figures.

5.4   Track Reconstruction Efficiency

In Section 5.2, the aim was to cut away volumes in the detector-frame p-θ-ϕ space for each particle type so that only the well-simulated volume remained. This was achieved primarily by cutting away the areas that were not highly efficient. However, within
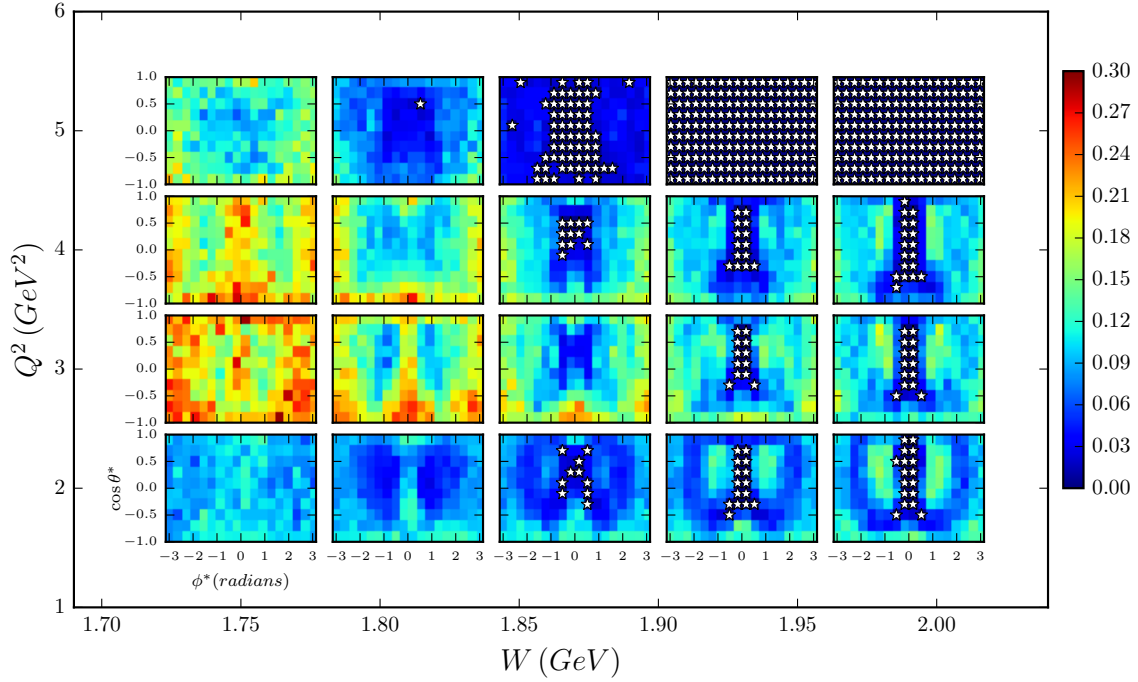
Figure 5.15 E1F hadronic CMS angular acceptance factors for 24 representative W-Q^2 values over a low-W range. Each 10- by 18-bin angular distribution represents a cell with dimensions $\Delta W = 20\,MeV$ and $\Delta Q^2 = 0.3$ GeV^2. The white stars mark holes where simulated events were thrown but not reconstructed.

this high-efficiency volume, there remain track reconstruction inefficiencies that are not captured in the simulation. These reconstruction inefficiencies are primarily attributed to inefficient TOF paddles and DC tracking regions. This effect must be separately treated. To capture these residual track reconstruction inefficiencies, this analysis employs a method described in [37] and [38].

The method was applied to the final ω production event sample to arrive at multiplicative efficiency factors for e, p, and π^+ separately as functions of sector and paddle number. For each particle and paddle, the ratio of the experimental yield to simulated yield is determined. Grouping by paddle number across sectors, the average R_i^{avg} of the highest two ratios is taken as the high-efficiency normalization

65
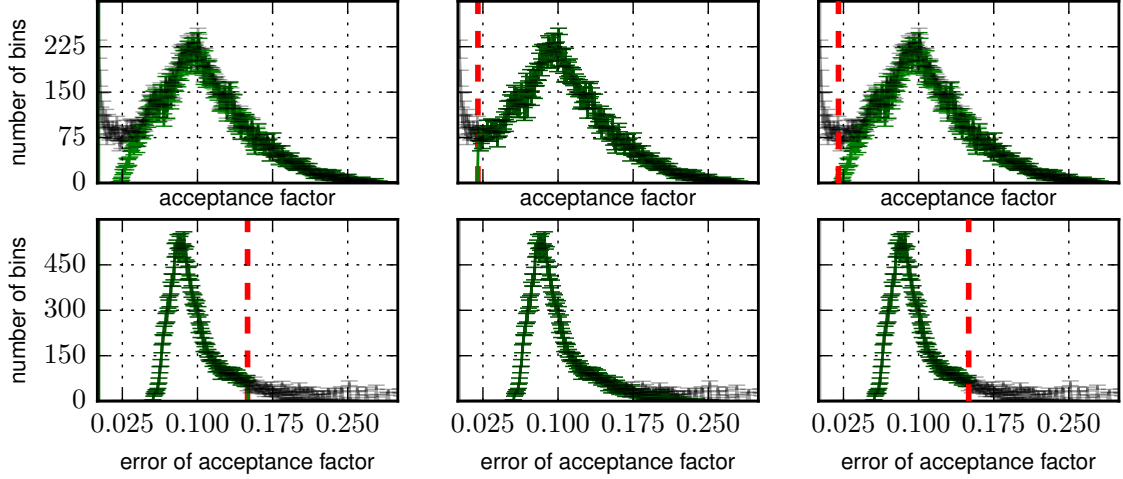
Figure 5.16 E1F frequencies of acceptance factors (top) and their statistical uncertainties (bottom). For each column, the dashed lines represent active cuts for that column – low limit on the acceptance factor and high limit on the factor's uncertainty. The gray distributions represent all values; the green distributions represent only the surviving values. For example, the top-left panel's shows green distribution counts the number of kinematic bins whose acceptance factors have uncertainties of less the 15%, the position of the dashed vertical line in the bottom-left panel.

factor so that the efficiencies for each particle are defined as

$$eff^{ij} = R_{ij}/R_i^{avg} \,, \tag{5.6}$$

where i corresponds to the paddle number and j to the sector. These efficiencies are determined sequentially for each particle type with the previous efficiency factors being already applied. A corresponding overall track reconstruction efficiency is associated to each event,

$$\eta^{TR} = eff_{ij}^e \cdot eff_{kl}^p \cdot eff_{mn}^\pi \,. \tag{5.7}$$

Figure 5.20 illustrates the individual track reconstruction efficiencies (5.6) for E1F (top) and E16 (bottom). Figure 5.21 illustrates the frequencies of event-level efficiencies of (5.7) for E1F and E16.
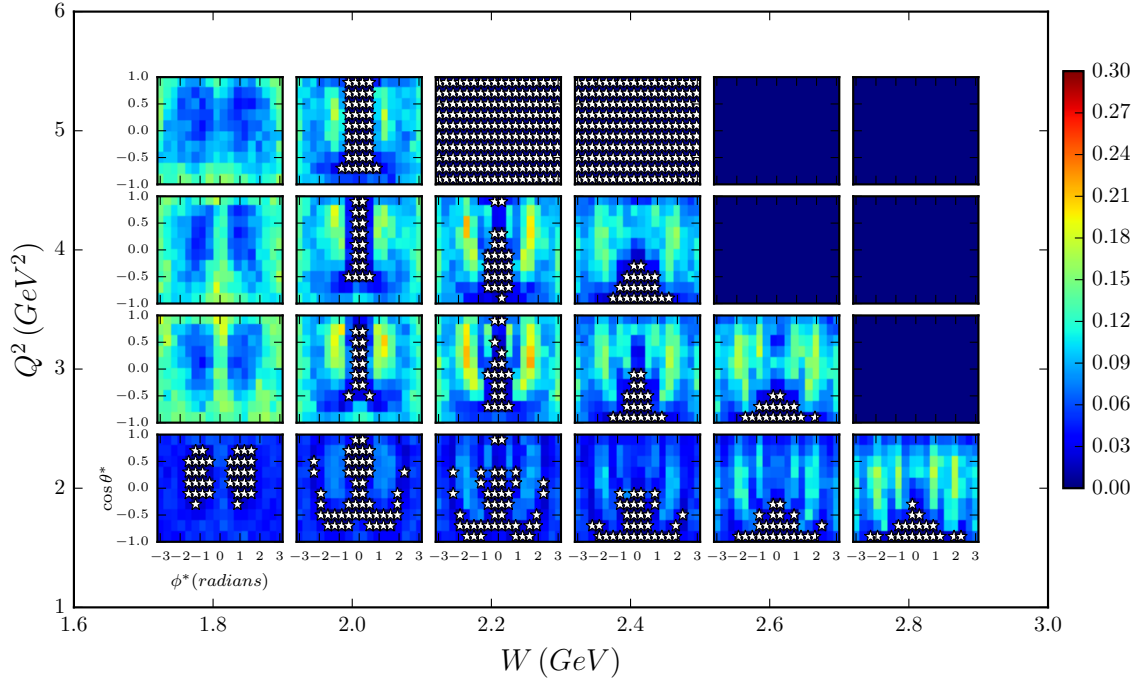
Figure 5.17   E16 hadronic CMS angular acceptance factors for 24 representative W-Q^2 values over a wide range of W. Each 10- by 18-bin angular distribution represents a cell with dimensions $\Delta W = 20\,MeV$ and $\Delta Q^2 = 0.3$ GeV^2. The white stars mark holes where simulated events were thrown but not reconstructed.

Some important features and assumptions are not explicitly stated in previous descriptions[37, 38] of this method. First, the method leverages lab-frame azimuthal symmetry of the scattered particles, and, as a feature, it is insensitive to inaccuracies in the simulated lab-frame polar angle distributions of the detected particles, because the normalization occurs at fixed-polar angles (i.e., by paddle number). Another important feature is that any geometric variation in yield from sector-to-sector is already accounted for by using ratios of experimental to simulated yields that are already subjected to identical fiducial cuts. An underlying assumption of the approach is that the best performing TOF paddles and DC tracking regions are 100% efficient. To the precision of the track reconstruction efficiencies, the assumption is reasonable. The scintillating detectors of TOF are capable of achieving greater than 99% efficiency over the full-length of well-calibrated paddles.[23] The DC is slightly less efficient,
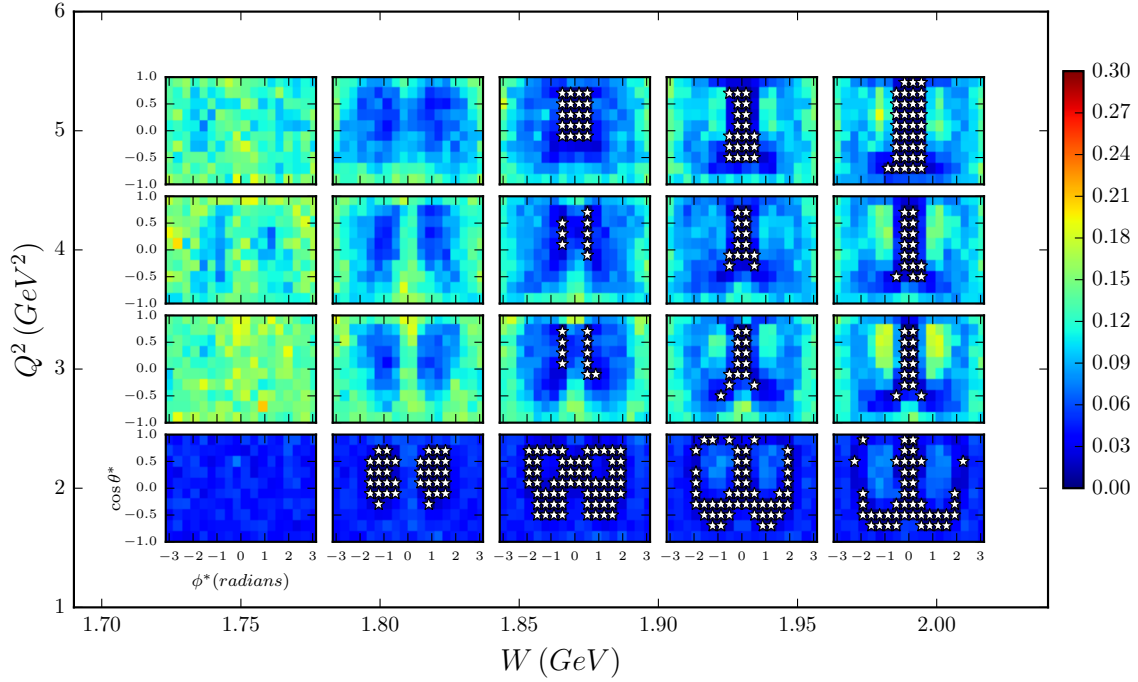
Figure 5.18   E16 hadronic CMS angular acceptance factors for 24 representative W-Q^2 values over a low-W range. Each 10- by 18-bin angular distribution represents a cell with dimensions $\Delta W = 20\,MeV$ and $\Delta Q^2 = 0.3$ GeV^2. The white stars mark holes where simulated events were thrown but not reconstructed.

especially when the hit occupancy rises above 4%; however, the average hit occupancy is well below 4%, where the average efficiency is around 98%.[21]

5.5   Inequivalence of E1F Experimental Reconstruction

As previously discussed, deriving efficiency and acceptance corrections from simulations requires the simulated data to be treated identically to experimental data. One step in verifying that the data is indeed being treated identically is to reproduce the previously cooked[1] experimental data from raw data. Specifically, if we process a raw experimental data file with user_ana (introduced in Section 3.1), we should reproduce events identical to the originally reconstructed output. In the case

---

[1]E16 data was cooked in 2003; E1F was last cooked in 2008.
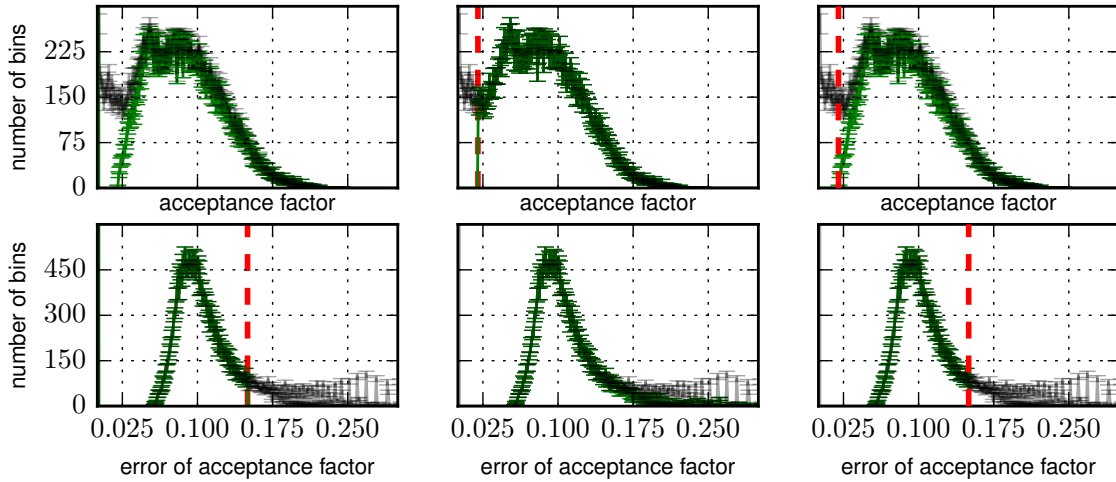
Figure 5.19   E16 frequencies of acceptance factors (top) and their statistical uncertainties (bottom). For each column, the dashed lines represent active cuts for that column – low limit on the acceptance factor and high limit on the factor's uncertainty. The gray distributions represent all values; the green distributions represent only the surviving values. For example, the top-left panel's shows green distribution counts the number of kinematic bins whose acceptance factors have uncertainties of less the 15%, the position of the dashed vertical line in the bottom-left panel.

of E1F, the documented run conditions and archived source code failed to reproduce the reconstructed body of data.

Recalibrating and recooking the experimental data is beyond the scope of this analysis, so the inequivalence is treated as an additional efficiency factor derived by recooking a small subset of raw data and comparing to the original reconstruction. Run 38121 was recooked and subjected to particle identification, fiducial cuts, and event selection. The number of events in the ω signal region were compared to the same in the original reconstruction across the full W and Q^2 ranges of the current analysis. These results are consistent with a systematic efficiency factor $\epsilon_{abs} = 0.7$, independent of W and Q^2, applied to the E1F data. The same exercise on Run 30583 of E16 resulted in an efficiency factor of $\epsilon_{abs} = 1$.

69
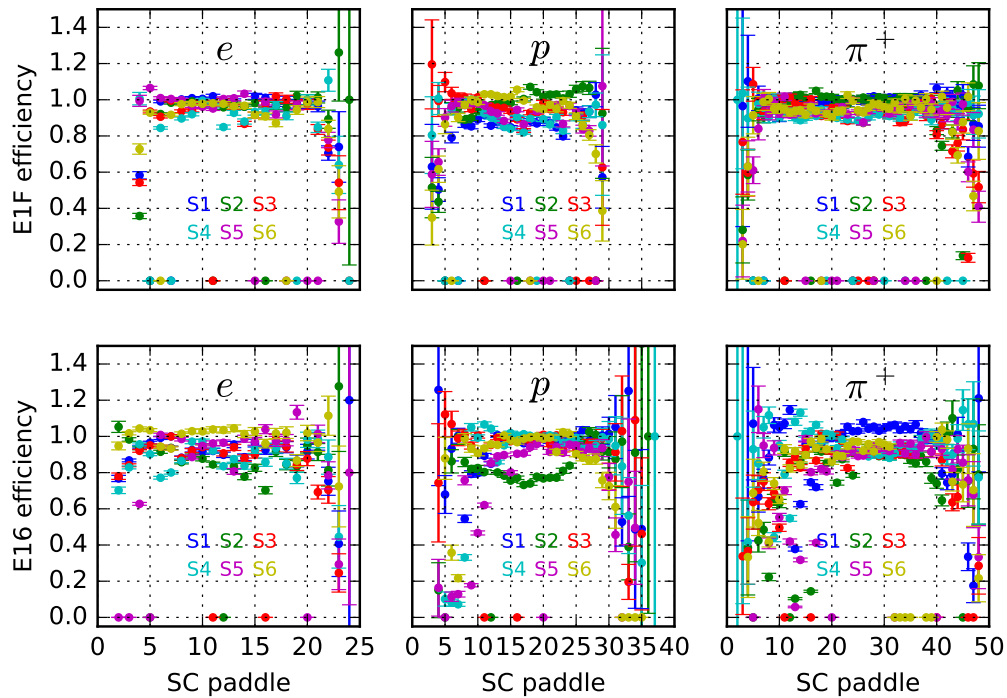
Figure 5.20   Track reconstruction efficiencies for electrons (left), protons (middle), and positive pions (right) for E1F (top) and E16 (bottom), based on ω-selected events with background. The efficiencies are presented with respect to the SC paddle hit by the particle. Each panel shows all six sectors as indicated by the color legend with labels S1-S6. Paddles with efficiency of zero had already been identified as bad paddles.
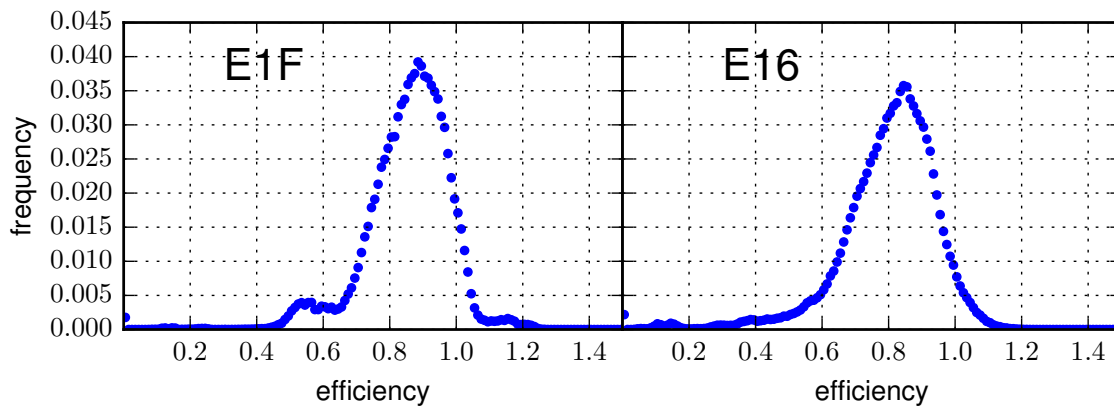
Figure 5.21   Event frequency of overall track reconstruction efficiencies for E1F (left) and E16 (right).

70

CHAPTER 6

MOMENTUM AND ENERGY CORRECTIONS

6.1 RADIATIVE CORRECTIONS

Charged particles, like electrons, lose energy and change course as they interact with constituents of the materials through which they pass. They can interact with atomic (or molecular) electron clouds, thus exciting the material's atoms in an energy loss process described by the well-known Bethe-Bloch equation; or they can radiate photons when *breaking* in the electromagnetic fields of nuclei in a process called *bremsstrahlung* [19].

These radiative effects are prominent in the spectrum of inclusive inelastic *ep* scattering, as can be seen in Figure 6.1, and must be well accounted for in order to extract meaningful hadronic cross sections. In exclusive channels the illustrated effect is greatly diminished by tightly constrained event selection and background subtraction. However, the radiative effects still modify the $W, Q^2, cos(\theta^*), \phi^*$ kinematics of our finally selected events significantly.

For electrons, energy loss through bremsstrahlung becomes more important than ionization at a critical energy of approximately 600 MeV and progressively dominates as the energy increases [12]. Accordingly, at the almost 6-GeV beam energies of E16 and E1F, the effect of ionization within the target is negligible.

The remaining energy loss effects of bremsstrahlung occur in two distinct and separately treated ways: they occur before/after the *ep* interaction vertex of interest – external, or *straggling* – as well as within the primary *ep* interaction itself – internal

71
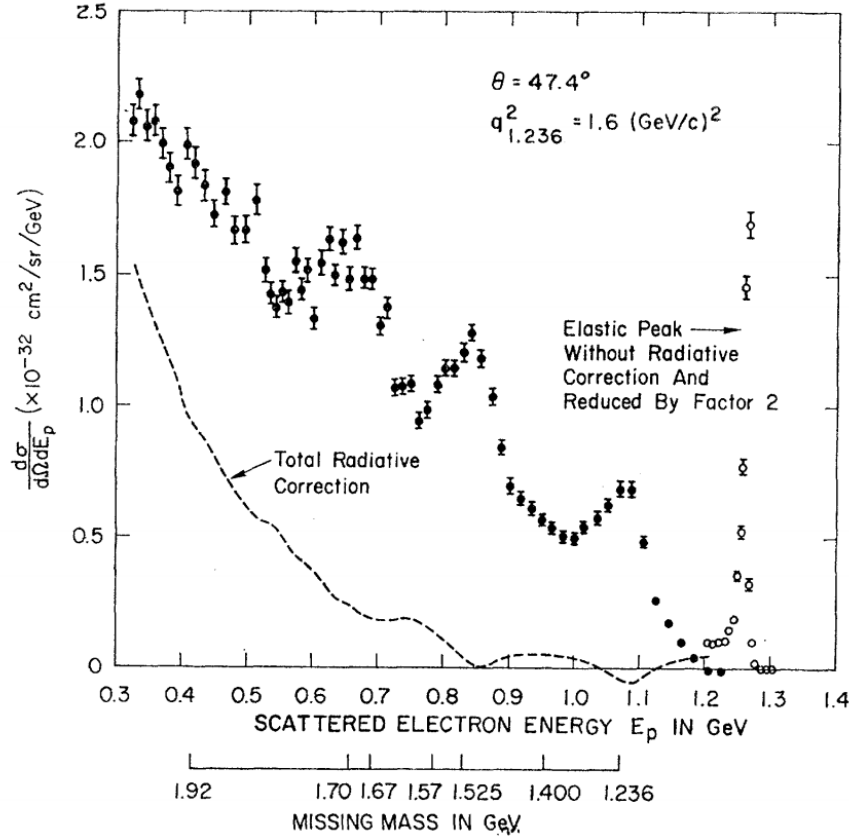
Figure 6.1   Radiative effects in a typical spectrum of inelastic *ep* scattering, taken from [36] with copyright permission.

[39]. The relative strength of external bremsstrahlung increases with target width. To estimate the effect, consider that internal bremsstrahlung is roughly equivalent to the effect of two external radiators straddling the interaction vertex, each with a thickness of $t = \frac{3}{4}(\alpha/\phi)[ln(Q^2/m^2) - 1]$ radiation lengths [36]. The hydrogen targets of E1F and E16 have a density of about $0.0708\,\mathrm{g/cm^3}$ and are five centimeters long, or only 0.00562 radiation lengths, making external radiative effects much smaller than internal radiative effects.

The GSIM detector simulation employed in this analysis accounts for various energy loss mechanisms within the materials of the detectors and the target, including ionization and external bremsstrahlung. It does not incorporate internal radiative effects. However, GENEV, the event generator, includes an optional internal radiative

effect implemented according to the "practical and reliable recipe" laid out by Mo and Tsai [36]. This GENEV option was used to determine a corrective multiplier for each kinematic bin i by simulating an equal number of events with (on) and without (off) radiative effects and taking the binned ratio R_i that appears in (1.10),

$$R_i = \frac{N_i^{off}}{N_i^{on}} \, . \tag{6.1}$$

Figure 6.2 illustrates the W dependence of R_i for representative Q^2 values from 1.25 to 5.25 GeV^2. The variation in multiplier for fixed W reflects that the radiative multiplier decreases more rapidly as Q^2 increases. However, the change is dominantly seen with changes in W. Specifically, near the exclusive channel's threshold of 1.72 GeV, the radiative effects can only diminish the cross section by migrating events to higher W. As W increases, the corresponding yields can be fueled by radiated events from lower W even while losing events to higher W bins. Thus, the corrective multiplier R_i will increase low-W cross sections and decrease high-W cross sections.

It is important to note that the radiative effect leads not only to bin migration in W and Q^2 but also to a radiative tail in the distribution of $MM_X(epX)$, from which ω events are identified. Figure 6.2 does not reflect the impact of losing ω events to the radiative tail; the acceptance corrections already account for it.

6.2 EMPIRICAL MOMENTUM CORRECTIONS

The CLAS detector is a composite, layered system of many sub-detectors and components (Chapter 2), and reconstructing its signals into physically meaningful quantities relies on our presumption of precise knowledge about the configuration of the detector as a whole – its collective components and magnetic fields (Chapter 3). As a practical matter, the systematic resolution and accuracy is not simply optimized as a consequence of optimizing its individual components and reconstruction algo-

73
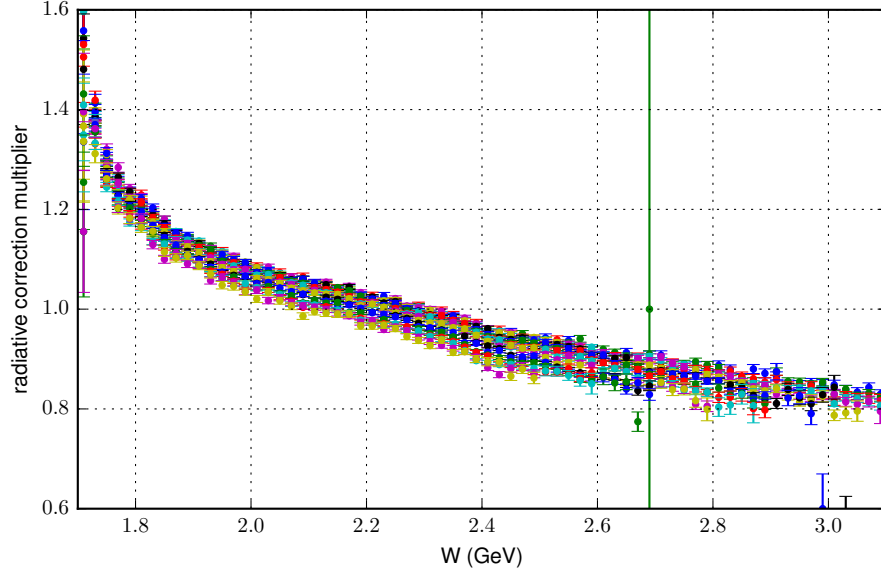
Figure 6.2   Radiative correction multipliers as a function of W for E1F at various Q^2 values plotted in different colors. The radiative correction multipliers fall with increasing W more rapidly for higher Q^2.

rithms. So, empirical corrections are made by optimizing higher level results to well known physical quantities. For momentum and energy corrections, invariant and missing mass peak positions can serve as benchmarks. Several methods have been employed to acquire momentum correction parameters for each sector and particle type [40, 41, 42, 43, 44]. All of the methods are capable of absorbing various known and unknown effects, but the most commonly stated issues that momentum corrections address are the ϕ-dependent inaccuracies that derive from DC misalignments and inadequate magnetic field knowledge.

Typically, momentum corrections amount to less than a few percent in the final cross sections. In the case of this analysis, standard momentum corrections were applied according to the methods of [44] for E1F and of [45] for E16. The impact of the corrections on the ω mass distribution, from the missing mass $MM_X(epX)$, is illustrated in Figure 6.3. It is notable that while neither method explicitly calibrates to the ω mass, both are effective in aligning the ω mass peaks from events

74
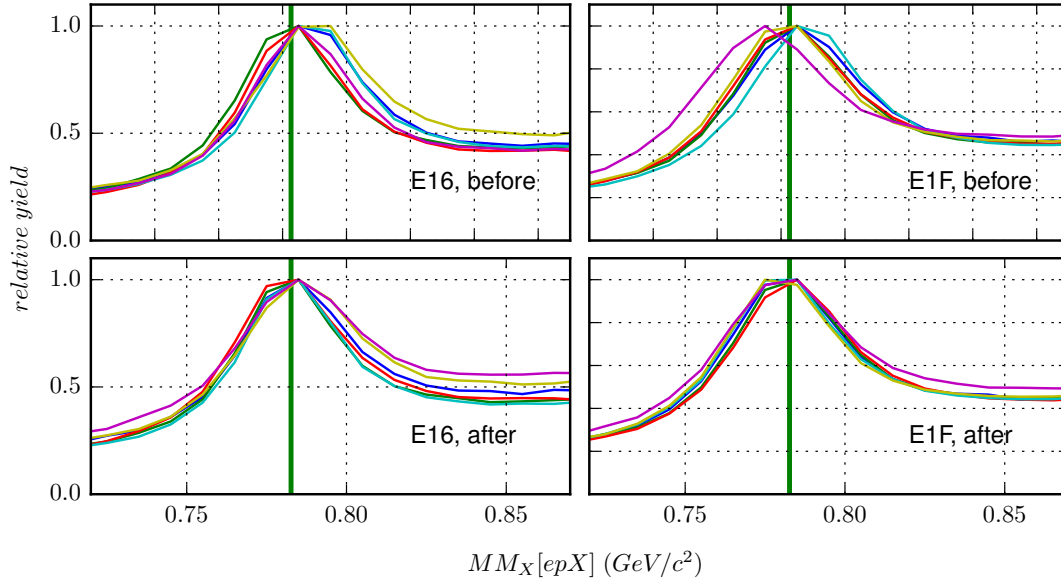
Figure 6.3 Empirical momentum corrections. The effect of the empirical momentum corrections on the spectrum of the missing mass of X in epX, $MM_X(epX)$, in the region of the ω mass is shown. Each panel displays six different mass curves – one for each sector in which the electrons was detected. The solid green line indicates the PDG mass of ω.

whose electrons were detected in different sectors. This fact is demonstrated by the convergence of peak positions when comparing top and bottom panels of Figure 6.3. The convergence of peak positions in the left panels is not as obvious, because E16 cooking parameters are thought to be very well calibrated in terms of the magnetic field map and drift chamber [45].

6.3 Energy Loss Corrections

No additional energy loss corrections were performed during this analysis: the common `eloss` package, implemented based on [46], were not applied. The `eloss` package is commonly applied to overcome a limitation of the reconstruction software with regards to the momentum determined from track curvatures. Specifically, the cooking procedure calculates an effective momentum over the full track rather than account-

75

ing for the incremental energy loss due to ionization along its path. The effect is more pronounced for very slow hadrons.

There are a few factors that mitigate the impact of these energy loss effects in the current analysis. First and foremost, the same effect is present in the simulation and, therefore, absorbed into the acceptance corrections. Second, the momentum distribution of the protons in the final event selection is primarily higher than the critical energy below which the energy loss effects become important. Hence, pions are more commonly affected although they are lighter; but this does not contribute to the ω reconstruction. The effect on pions will typically push more events into the selected events and manifest as background rather than migrating out of the selection. The event loss due to the latter migrations would be treated by the acceptance corrections, albeit with dependence on the thrown event model.

CHAPTER 7

RESULTS: EXTRACTION OF CROSS SECTIONS AND RESPONSE FUNCTIONS

Previous chapters addressed how particles are detected and how events are reconstructed. They described how ω production events are counted and how inefficiencies, inaccuracies, and known energy loss mechanisms affecting the measurements are corrected. The concepts, methods, and corrections that were introduced can now be applied to relate our binned experimental data to differential cross sections in more detail. From the differential cross sections, we can extract the unpolarized cross sections and interference terms of (1.6) and the response functions of (1.7).

7.1 DIFFERENTIAL CROSS SECTIONS

The connection between binned experimental data and differential cross sections encapsulated by (1.10) can now be elaborated with the developments of previous chapters and with more explicit bin labeling,

$$\left(\frac{d^2\sigma_h}{d\Omega^*}\right)_{ijkl} = \frac{1}{\epsilon^{ABS}} \cdot \frac{1}{B} \cdot \frac{1}{L} \cdot \frac{1}{\Gamma_{ij}} \cdot \frac{R_{ij}}{\eta_{ijkl}^{ACC} \langle \eta^{CC} \rangle_{ijkl} \langle \eta^{TR} \rangle_{ijkl}} \cdot \frac{1}{\Delta_i W \Delta_j Q^2} \cdot \frac{N_{ijkl}}{\Delta_{kl} \Omega^*} \cdot \quad (7.1)$$

The terms and notation of the expression are defined as follows.

- The position (superscript or subscript) of any index is a matter of convenience, not of meaning. This is the convention throughout the chapter unless otherwise stated.

77

- $ijkl$ identifies a cell in the four-dimensional kinematic space, with labels corresponding to ranges of the continuous parameters: $i \sim W$, $j \sim Q^2$, $k \sim \cos\theta^*$, and $l \sim \phi^*$. The linearized bin labeling of (1.10) can be decomposed into $ijkl$ because the bin edges in each dimension are independent of each other dimension. The decomposition will make it easier to move between expressions of continuous values and those of discrete, binned values – e.g.,

$$f_{ijl} = \sum_k F_{ijkl} \iff f(W, Q^2, \phi^*) = \int F(W, Q^2, \cos\theta^*, \phi^*) \, d(\cos\theta^*).$$

- The *averaging* that is intrinsic to moving between expressions of continuous values and those of binned values is left implicit. The *averaging* indicated by the angled brackets relates to factors that have direct dependencies in variables other than the four kinematic variables of the binning scheme and so require tracking a weighted average over the events in each kinematic bin. For example, the CC cut efficiencies are to be interpreted as

$$\left\langle \eta^{CC} \right\rangle_{ijkl} := \frac{\sum \eta^{CC}_{mn} \tilde{N}^{mn}_{ijkl}}{\tilde{N}_{ijkl}},$$

where m labels the sector, n labels the CC PMT number, and $\tilde{N}$ is the number of events before background subtraction.

- $\epsilon^{ABS} = 0.7$ for E1F; $\epsilon^{ABS} = 1$ for E16. ϵ^{ABS} is the systematic efficiency factor that compensates for the inequivalence between the reconstruction of experiment versus simulation, discussed in Section 5.5.

- $B = 0.892$. B is the branching ratio for the $\pi^+\pi^-\pi^0$ decay mode of ω.

- $L = 19.844 \, fb^{-1}$ for E1F; $L = 28.101 \, fb^{-1}$ for E16. L is the integrated luminosity,

$$L = \frac{Q_{tot} l \rho N_A}{q_e M_H},$$

where Q_{tot} is the integrated charge collected in the Faraday cup for luminosity blocks that survive the conditions of Section 3.2; $l = 5 \, cm$ is the target length;

$\rho = 0.0708 \, g/cm^3$ is the target density; $N_A = 6.022 \times 10^{23} \, mol^{-1}$ is Avogadro's number; $q_e = 1.602 \times 10^{-19} \, C$ is the elementary charge; and $M_H = 1.007 \, g/mol$ is the molar mass of hydrogen.

- Γ_{ij} is the virtual photon flux of (1.2).

- $\Delta_i W$ and $\Delta_j Q^2$ are the bin widths along W and Q^2 in the ith W bin and j^{th} Q^2 bin; $\Delta_{kl}\Omega^*$ is the hadronic CMS solid angle of the angular cells at the intersection of the kth $\cos\theta^*$ bin and l^{th} ϕ^* bin. Since the bin widths in each of the four dimensions do not depend on any other dimension, the subscripts are reduced from $ijkl$ to the independent indexes.

- R_{ij} is the radiative correction factor associated with one W-Q^2 bin, discussed in Section 6.1.

- η_{ijkl}^{ACC} is the acceptance factor of bin $ijkl$, discussed in Section 5.3. The previously discussed *holes* in acceptance are treated here as a special flavor of zero – one that leads to *nothing* when entering as the denominator. *Nothing* does not contribute as a point during any fitting procedure and must be *filled* in any integration procedure.

- $\left\langle \eta^{CC} \right\rangle_{ijkl}$ is the average CC cut efficiency factor in bin $ijkl$, discussed in Section 3.7.

- $\left\langle \eta^{TR} \right\rangle_{ijkl}$ is the average overall track reconstruction efficiency in bin $ijkl$, discussed in Section 5.4.

- N_{ijkl} is the background-subtracted yield of ω events in bin $ijkl$ as discussed in Chapter 4. The empirical momentum corrections of Section 6.2 and the fiducial cuts of Section 5.2 will have already been applied event-by-event, before entering into the event selection process.

Note that the angled-bracket notation to indicate averaging over events is a more specialized meaning than the same notation in (1.10). The corresponding event-averaged factors are capable of introducing some additional model dependence since the background events could, in principle, have different correlations to the extraneous variables that determine the event-level efficiency. This effect has not be investigated.

More than 60,000 differential cross-section data points were determined in accordance with the binning scheme of Table 7.1. It is impractical to tabulate all of

Table 7.1   Kinematic binning scheme. N_X is the number of bins in the parameter X. The angular binning covers the full 4π radians. W, $\cos\theta^*$, and ϕ^* have fixed bin widths of $20\,\mathrm{MeV}$, 0.2, and $\pi/9$ radians, respectively.

Q^2 (GeV^2)	W (GeV)	N_W	$N_{\cos\theta^*}$	N_{ϕ^*}
$[1.85, 2.20)$	$[1.71, 2.59)$	44	10	18
$[2.20, 2.50)$	$[1.71, 2.59)$	44	10	18
$[2.50, 2.90)$	$[1.71, 2.55)$	42	10	18
$[2.90, 3.35)$	$[1.71, 2.29)$	29	10	18
$[3.35, 3.85)$	$[1.71, 2.19)$	24	10	18
$[3.85, 4.65)$	$[1.71, 2.09)$	19	10	18
$[4.65, 5.15)$	$[1.71, 1.99)$	14	10	18

the differential cross-sections within this text, but a sample of E1F data for a single W and Q^2 cell appears in Appendix C. Figure 7.1 summarizes the differential cross section values and uncertainties for E1F and E16 separately.

In principle, the differential cross-sections of E1F and E16 cannot be directly compared, because the difference in beam energy propagates into a difference in polarization for a common kinematic bin. For each linearized bin number i, the relative difference is expressed as

$$\frac{\langle\epsilon\rangle_i^{E16} - \langle\epsilon\rangle_i^{E1F}}{\left(\langle\epsilon\rangle_i^{E16} + \langle\epsilon\rangle_i^{E1F}\right)/2},$$

which is illustrated as a bin frequency in the right panel of Figure 7.2. The left panel of the figure illustrates the relative difference bin frequency of the virtual photon
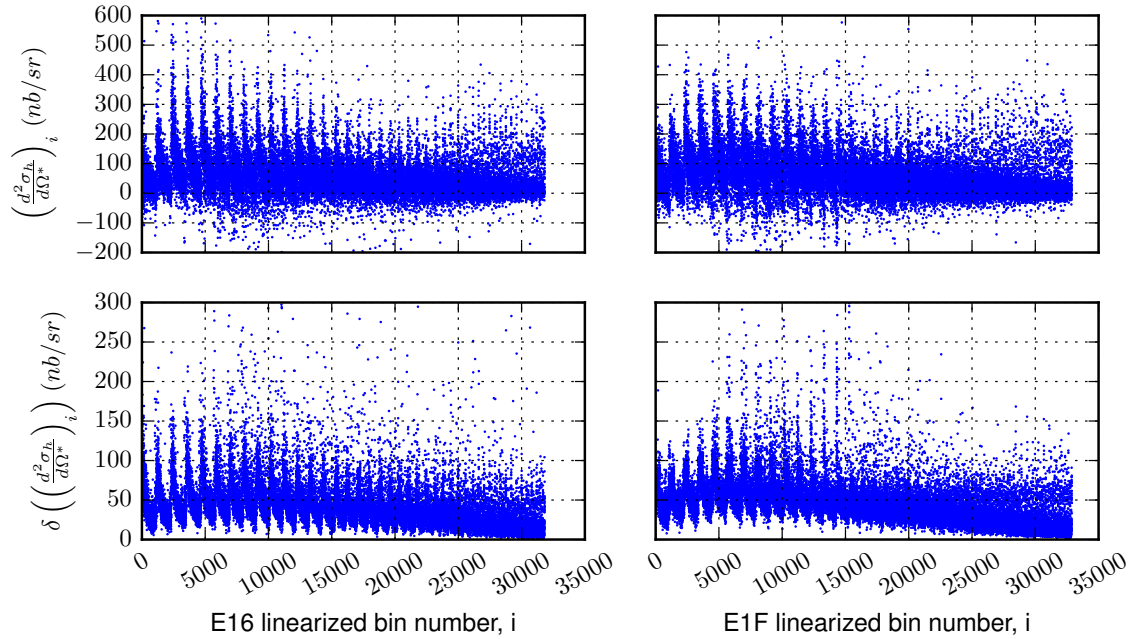
Figure 7.1   Summary of differential cross section values. More than 60,000 differential cross section values (top) and uncertainty values (bottom) are plotted. Each point represents one bin within the space of W, Q^2, $\cos\theta^*$, and ϕ^*. The bin numbers are serialized with lexicographical ordering in $\{W, Q^2, \cos\theta^*, \phi^*\}$.

flux. The effect of beam energy on the virtual photon flux is already fully accounted for in the differential cross section formula of (7.1); but the ϕ^* dependence of the cross sections enters through the polarization parameter ϵ, which differs substantially between common kinematic bins of E1F and E16, by between 2% and 18%. From the differential cross sections, we will extract values that account for the polarization differences and are, therefore, comparable. Furthermore, even though the unpolarized measurements (e.g., σ_o of (1.6) and $\mathscr{R}_T + \epsilon_L\mathscr{R}_L$ of (1.7)) are not *strictly* comparable between experiments, the longitudinal components are thought to be quite small [7], so they are *practically* comparable. Accordingly, combined results will be presented whenever possible, and variation between E1F and E16 is assumed to be driven primarily by systematic uncertainty.

81
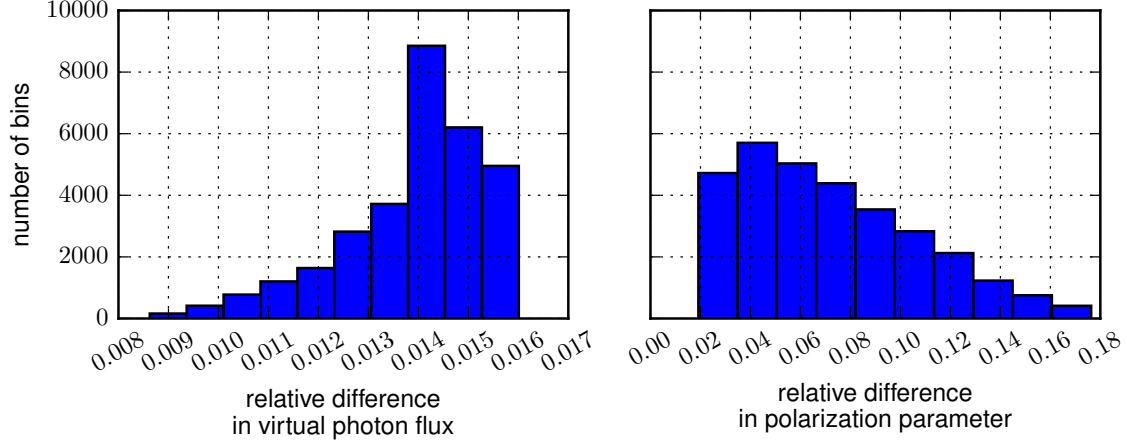
Figure 7.2   Differences in polarization and virtual photon flux due to beam energy differences between E1F and E16. The relative difference in virtual photon flux for common kinematic bins between E1F and E16 is illustrated in the left panel. Similarly, the relative difference in the polarization parameter is illustrated in the right panel. In principal, the difference in ϵ makes the unpolarized cross sections of E1F and E16 incomparable.

7.2   Unpolarized cross sections and interference terms

The equation of (1.6) laid out the explicit dependence of the measured unpolarized differential cross sections on the hadronic CMS azimuthal angle of the produced ω meson. It was presented to set up for direct comparison to results of [7], which looked at only the integrated quantities and did not differentiate between the polarization parameter ϵ and the longitudinal polarization ϵ_L:

$$\frac{d\sigma_h}{d\phi^*} = \frac{1}{2\pi}\left(\sigma_o + \epsilon\,\sigma_{TT}\,cos(2\phi^*) + \sqrt{2\epsilon(1+\epsilon)}\,\sigma_{LT}\,cos(\phi^*)\right). \qquad (1.6)$$

From the differential cross sections of this analysis, we can arrive at comparable results (σ_o, σ_{TT}, and σ_{LT}) by fitting (1.6) to the single-differential ϕ^* distribution of each W-Q^2 bin according to the following formulation that uses the conventions of

82

(7.1):

$$\left(\frac{d\sigma_h}{d\phi^*}\right)^{ij} = \frac{1}{2\pi}\left(\sigma_o + \epsilon^{ij}\,\sigma_{TT}\,cos(2\phi^*) + \sqrt{2\epsilon^{ij}(1+\epsilon^{ij})}\,\sigma_{LT}\,cos(\phi^*)\right) \qquad (7.2a)$$

$$= f^{ij}(\phi^*;\sigma_o,\sigma_{TT},\sigma_{LT}) \implies f^{ijl} = \sum_k \left(\frac{d^2\sigma_h}{d\Omega^*}\right)^\star_{ijkl} \Delta_k\left(\cos\theta^*\right), \qquad (7.2b)$$

where $\left(\frac{d^2\sigma_h}{d\Omega^*}\right)^\star_{ijkl}$ is the variant of the measured differential cross section that has its *acceptance holes* filled by linear interpolation with respect to its nearest neighbors in the same ijk bin. The artificial data point derives its statistical uncertainty from its neighbors in way that gives it less weight than a measured data point. The data points $\left(\phi^*_{ijl}, f^{ijl}\right)$ are fitted with the function $f^{ij}(\phi^*;\sigma_o,\sigma_{TT},\sigma_{LT})$, where each abscissa is equal to the central ϕ^* value of bin ijl and is implicated by the presence of the index l in the binned data expression of (7.2b).

Figure 7.3 illustrates the fits of $f^{ij}(\phi^*;\sigma_o,\sigma_{TT},\sigma_{LT})$ to the hole-filled, integrated data f^{ijl}. The solid green lines represent the optimized fit functions $f^{ij}(\phi^*;\sigma_o = \sigma_o^{ij}, \sigma_{TT} = \sigma_{TT}^{ij}, \sigma_{LT} = \sigma_{LT}^{ij})$; the shaded regions around the lines represent the effect of parametric optimization uncertainties for σ_{TT} and σ_{LT}. The open red circles represent the data without the effect of filling holes in the underlying differential cross sections. Each row shows the results of E16 (left) and E1F (right) for a common bin ij.

The unpolarized cross sections and interference terms that result from the fits in every bin ij are tabulated in Section D.1 for E16 and Section D.2 for E1F. The combined E16 and E1F unpolarized cross sections for six of the seven Q^2 bins, along with comparable data of [7], are illustrated in Figure 7.4. The interference terms σ_{LT} and σ_{TT} are similarly presented in Figure 7.5.

The consistency between the E1F and E16 unpolarized cross sections of the current analysis over the full Q^2 range is notable. Meanwhile, at high Q^2, there are strong deviations from the previously published E16 results (red markers in Figure 7.4) of [7] (Morand et al.). A possible explanation lies in the choice of kinematic binning. Specifically, the current analysis chose very fine binning that exposed many holes in

83

acceptance (Section 5.3), which could then be filled according to experimental data in the kinematic neighborhood. The much coarser binning of Morand trades the uncertainty of explicitly filling holes for amplified model-dependence in the acceptance corrections. Without modification, GENEV's model favors forward-angle scattering even at low-W where the $\cos\theta^*$ distribution is not significantly forward-peaked. Typically, there are more holes at higher W where the events *are* forward-peaked – i.e., where the model is a better match to reality; however, at high Q^2 values, holes set in at very low W where the model is inadequate. Consistent with this suggestion, the high-Q^2, low-W range is where the largest deviations between the current analysis and the work of Morand occur.

7.3 Response functions

Multipole decompositions, including the methods employed by the ANL-Osaka DCC analysis [3, 4], require information about how the strength of total cross sections and interferences depend on the polar angle in the hadron CMS. This information is carried in the response functions of (1.7), restated here for convenience.

$$\frac{d^2\sigma_h}{d\Omega^*} = \frac{|\vec{p}_\omega^*|}{k_\gamma^*} \left(\mathscr{R}_T + \epsilon_L \mathscr{R}_L + \epsilon \mathscr{R}_{TT} \cos(2\phi^*) + \sqrt{2\epsilon_L(1+\epsilon)} \, \mathscr{R}_{TL} \cos(\phi^*) \right) \quad (1.7)$$

$$k_\gamma^* = \frac{M_p}{W} k_\gamma = \frac{M_p}{W} \left(\frac{W^2 - M_p^2}{2M_p} \right) = \frac{W^2 - M_p^2}{2W} \quad (1.9)$$

$$|\vec{p}_\omega^*| = \frac{1}{2W} \sqrt{M_\omega^4 - 2M_\omega^2 M_p^2 - 2M_\omega^2 W^2 + M_p^4 - 2M_p^2 W^2 + W^4} \quad (1.8)$$

The response functions $\mathscr{R}_i(W, Q^2, \theta^*)$ directly link to components of the hadronic tensor [11], a connection derived in the context of extracting nucleon resonance parameters by Skorodumina et al. in [47]. They can be determined in analogy to the extraction of σ_o, σ_{TT}, and σ_{LT} in Section 7.2. The expected ϕ^* dependency will be leveraged to fit the ϕ^* distribution of differential cross sections in each bin ijk

according to

$$\left(\frac{d^2\sigma_h}{d\Omega^*}\right)_{ijk} = \frac{|\vec{p}_\omega^*|}{k_\gamma^*}\left(\mathscr{R}_o + \epsilon\,\mathscr{R}_{TT}\,cos(2\phi^*) + \sqrt{2\epsilon_L(1+\epsilon)}\,\mathscr{R}_{TL}\,cos(\phi^*)\right) \tag{7.4a}$$

$$= f^{ijk}(\phi^*; \mathscr{R}_o, \mathscr{R}_{TT}, \mathscr{R}_{LT}) \Longrightarrow f^{ijkl} = \left(\frac{d^2\sigma_h}{d\Omega^*}\right)_{ijkl}, \tag{7.4b}$$

where $\mathscr{R}_T + \epsilon_L\mathscr{R}_L$ is reduced to the directly measured $\mathscr{R}_o$, and the differential cross section is the unstarred version, which means that the fit ignores holes in the ϕ^* distribution of each bin ijk.

Figure 7.6 illustrates the fitting outcome for two different W-Q^2 bins – 10 fits related to (7.4b) span the full $cos\,\theta^*$ range for each W-Q^2 bin. Parameters were extracted separately for E16 and E1F and as a combined data set. The figure illustrates the results of the combined fitting procedure, which (a) accounted for the difference in polarization, (b) allowed $\mathscr{R}_T + \epsilon_L\mathscr{R}_L$ to vary independently for each experiment, but (c) required a simultaneous minimization of shared $\mathscr{R}_{TT}$ and $\mathscr{R}_{TL}$ parameters in each $cos\,\theta^*$ bin. The resulting response function for over 2,000 ijk bins that were populated in both E16 and E1F are tabulated in Appendix E.

Using the same sample bins of Figure 7.6, the θ^* dependence of the optimized parameters $\mathscr{R}_T + \epsilon_L\mathscr{R}_L$, $\mathscr{R}_{TT}$, and $\mathscr{R}_{TL}$ (top to bottom) is illustrated in Figure 7.7 for E16, E1F, and for the combined data set (left to right). $\mathscr{R}_T + \epsilon_L\mathscr{R}_L$ was fit with a second-order Legendre plus a forward-peaking exponential to naively model the effect of s-channel and t-channel processes, respectively. A backward-peaking exponential, suggestive of a u-channel process, was allowed, but it never improved the fit, so it optimized to zero. It is clear that the low-W sample (top 9 panels) has no significant exponential contribution while the high-W sample (bottom 9 panels) has a dominant forward peak. This trend is summarized by Figure 7.8. The low-order Legendre moments effectively describe the shape of $\mathscr{R}_T + \epsilon_L\mathscr{R}_L$ as a function of θ^* from low W to around $W = 2.1$ GeV, where the t-channel dominance sets in and necessitates a growing exponential contribution to describe the data.
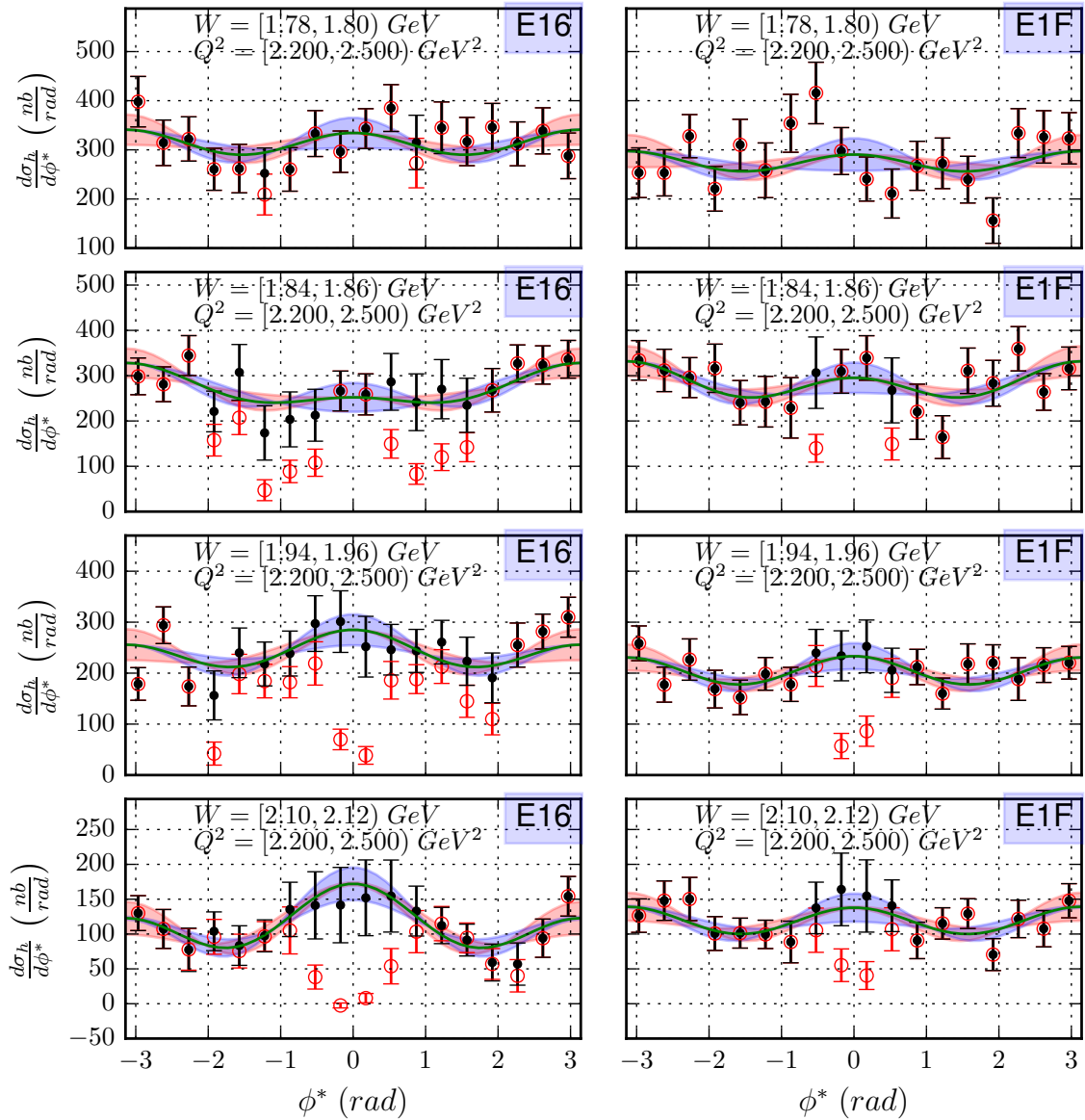
Figure 7.3   Sample fits of expected $\frac{d\sigma_h}{d\phi^*}$ to hole-filled, integrated data in four representative W bins for $Q^2 = [2.2, 2.5)$ GeV^2 of E16 (left) and E1F (right). The solid green line represents the optimized fit function; the red and blue shaded region around the function represents uncertainty in the parameters σ_{TT} and σ_{LT}. The black points represent the hole-filled differential cross-sections integrated over $\cos\theta^*$. The open red circles with error bars represent the same but without the correction for holes in acceptance. Error bars reflect statistical uncertainty from all sources.
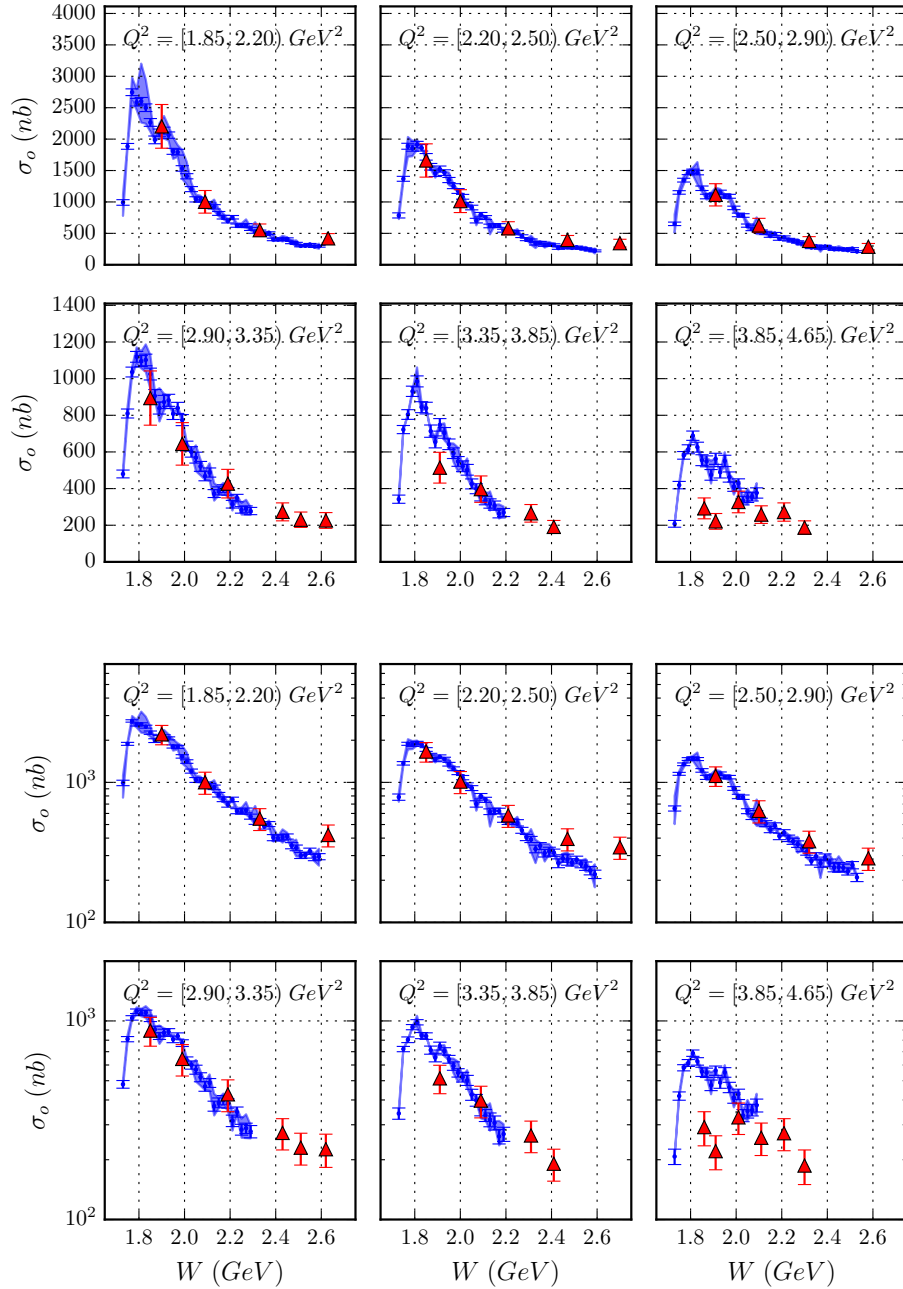
Figure 7.4   Unpolarized cross sections, E1F and E16 combined, for six ranges of Q^2 on linear (top 6 panels) and logarithmic (bottom 6 panels) scales. The blue circular points represent a weighted average of the E1F and E16 results with the weighted statistical uncertainty as error bars. The shaded blue region is bounded by the separate results of E1F and E16. The red triangular data points correspond to the published data with systematic plus statistical uncertainties of [7].
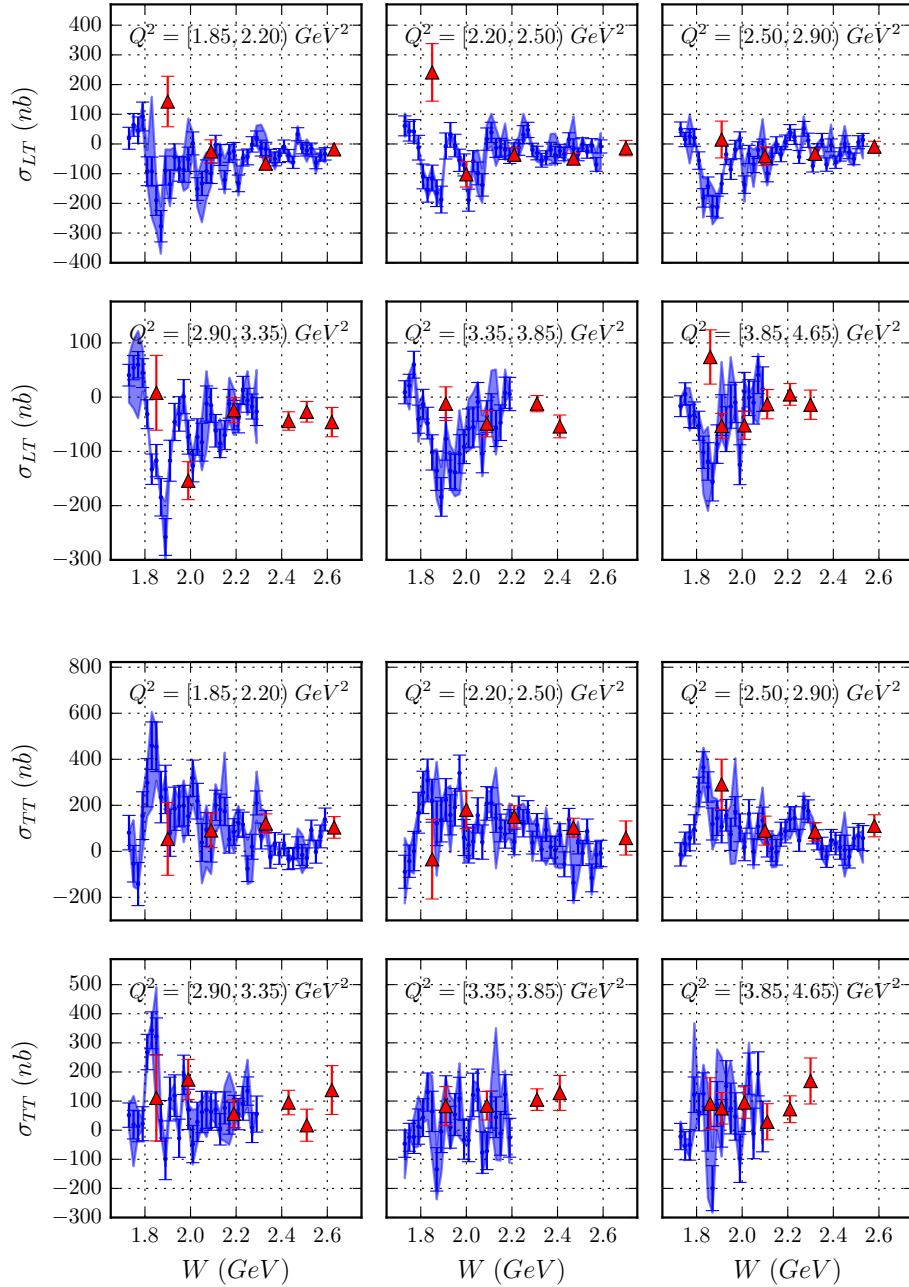
Figure 7.5 Longitudinal-transverse (top 6 panels) and transverse-transverse (bottom 6 panels) interference term, E1F and E16 combined. The blue circular points represent a weighted average of the E1F and E16 results with the weighted statistical uncertainty as error bars. The shaded blue region is bounded by the separate results of E1F and E16. The red triangular data points correspond to the published data with systematic plus statistical uncertainties of [7].
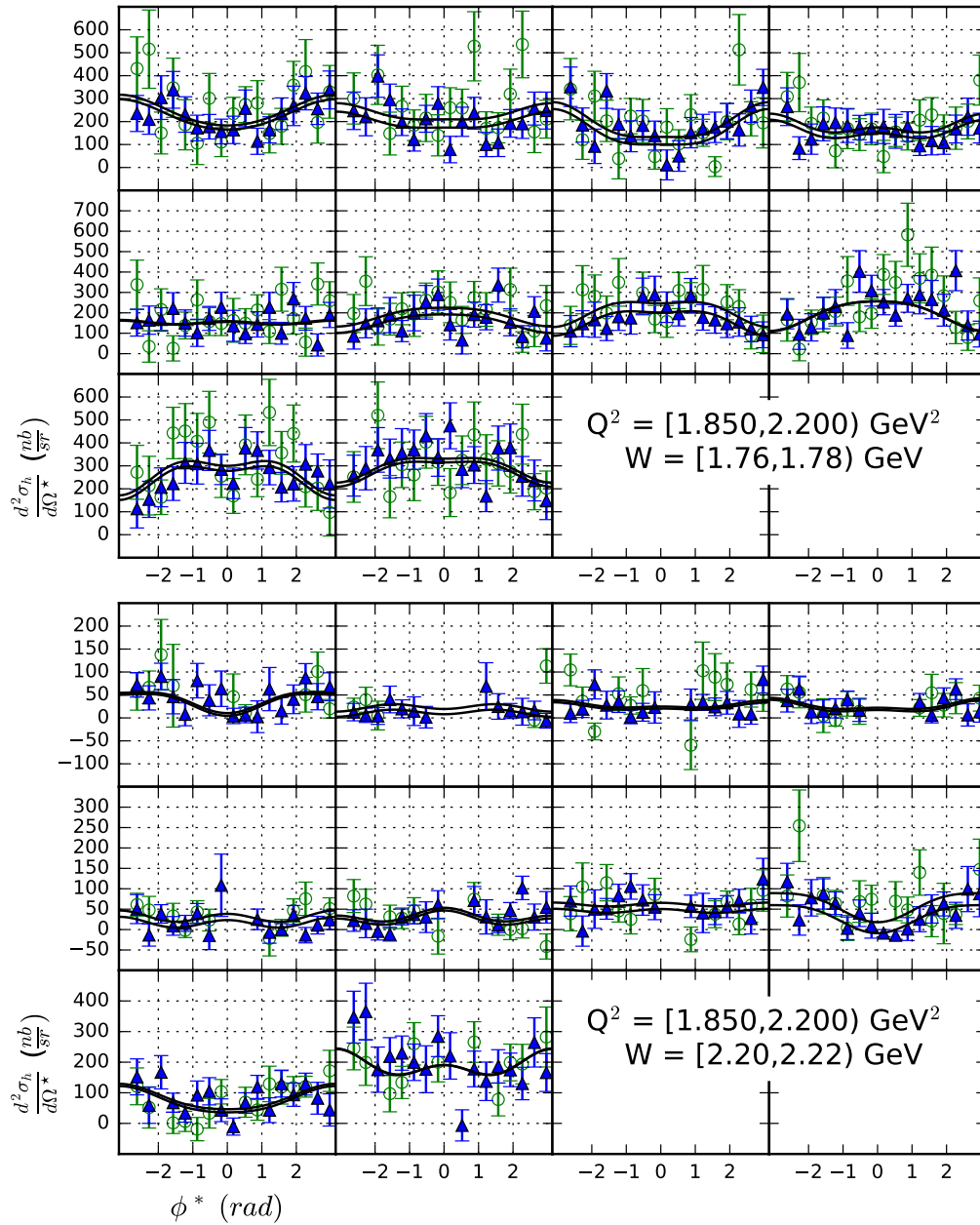
Figure 7.6 Sample fits of expected ϕ^* dependence of $\frac{d^2\sigma_h}{d\Omega^*}$ for E16 (open green circles) and E1F (blue solid triangles). The fitted functions resulted from a simultaneous optimization of both data sets using different polarizations and σ_o parameters but requiring the interference parameters σ_{TT} and σ_{TL} to be equal.
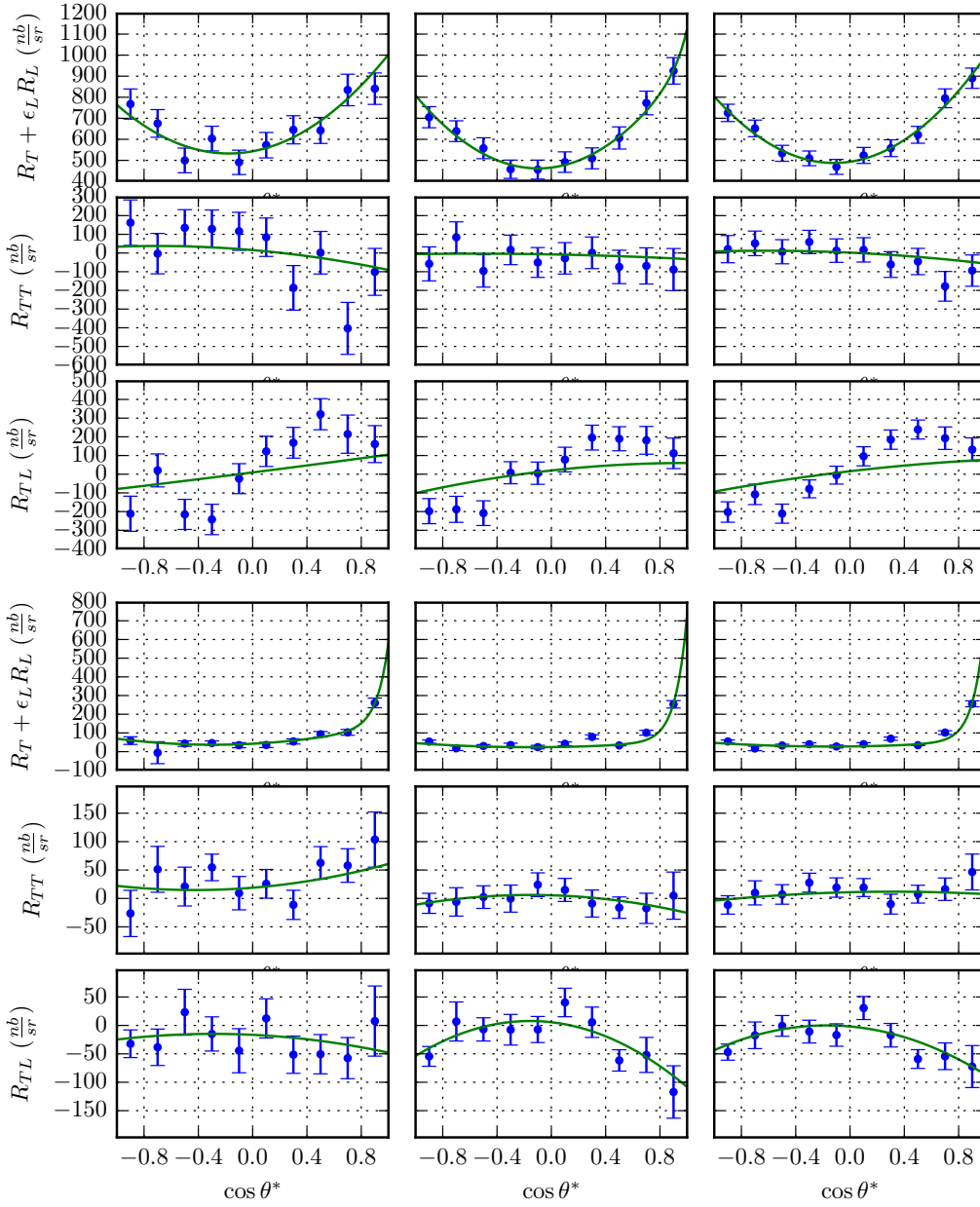
Figure 7.7 Sample Legendre and exponential fits to the $\cos\theta^*$ dependence of the response functions for $Q^2 = [1.85, 2.2)$ GeV^2, $W = [1.76, 1.78)$ GeV in the top 9 panels and for $Q^2 = [1.85, 2.2)$ GeV^2, $W = [2.2, 2.22)$ GeV in the bottom 9 panels. From left to right, each row contains data from E16, E1F, and both. At low W, $\mathscr{R}_T + \epsilon_L \mathscr{R}_L$ (top 3) is well described by second-order Legendre polynomials, suggestive of s-channel processes; at high W, the exponential dominates the fit, reflecting t-channel dominance.
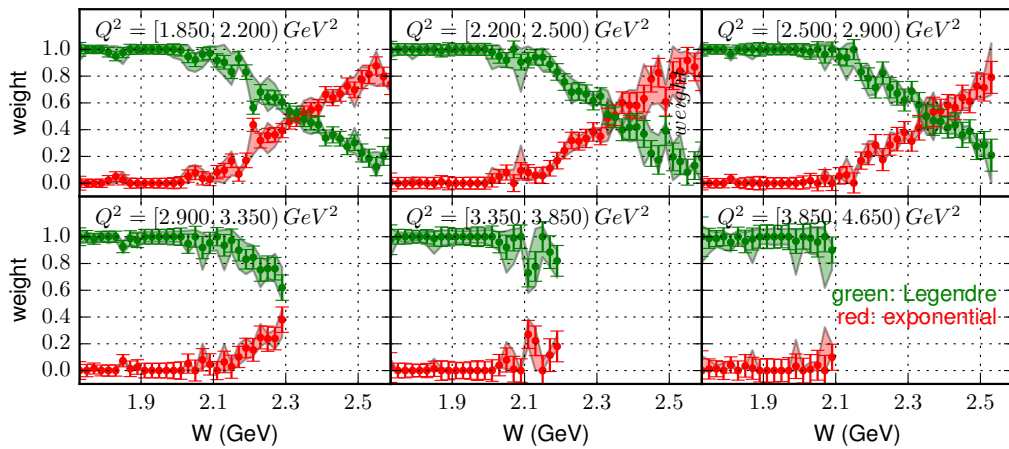
Figure 7.8 Relative Legendre and exponential weight factors evolve with W. These are the weight factors required to model $\mathscr{R}_T + \epsilon_L \mathscr{R}_L$ as a function of θ^*. At low-W, second-order Legendre polynomials match well with the response functions shape in θ^* (green points are close to 1). As W increases and t-channel processes become accessible, the exponential is required to strengthen weight to reflect the forward-peaking nature of t-channel processes (red points are increasing from 0).

CHAPTER 8

SUMMARY

A chief aim of this analysis was to provide access to sufficiently precise angular information to motivate the ω production channel's inclusion into broader coupled-channel analyses that rely on high sensitivity to W, precise angular production information, and some depth in virtuality. While the photoproduction work of Williams et al. [48, 49] offered excellent precision at the real-photon point, and Morand et al. [7] offered a high virtuality view above the resonance region where vector meson dominance applies, the extension of our view of the resonance region into the virtual photon domain has been lacking. By combining E16 and E1F data, the current work presents the largest set of results for the ω electroproduction channel in the resonance region to date. The differential cross sections and derived response functions represent a kinematic range of $Q^2 = [1.85, 5.15)$ GeV^2 and $W = [1.72, 2.6)$ GeV. The response functions $\mathscr{R}_T + \epsilon_L \mathscr{R}_L$, $\mathscr{R}_{TT}$, and $\mathscr{R}_{TL}$ are tabulated in Appendix E for all W, Q^2, and $\cos\theta^*$ shared by the events of E16 and E1F.

Bibliography

[1] I.G. Aznauryan et al., *Studies of Nucleon Resonance Structure in Exclusive Meson Electroproduction*, Int. J. Mod. Phys. **E22** (2013), 1330015.

[2] Ralf W. Gothe, *Experimental Challenges of the N* Program*, AIP Conf.Proc. **1432** (2012), 26–32.

[3] Hiroyuki Kamano, *Light-quark baryon spectroscopy from anl-osaka dynamical coupled-channels analysis.*

[4] Hiroyuki Kamano, *Light-quark baryon spectroscopy within anl-osaka dynamical coupled-channels approach*, Few-Body Systems **57** (2016), no. 10, 933–940.

[5] A. Matsuyama, T. Sato, and T.-S. H. Lee, *Dynamical coupled-channel model of meson production reactions in the nucleon resonance region*, Physics Reports **439** (2007), 193–253.

[6] *EBAC publications*, `http://ebac-theory.jlab.org/papers.htm`, 2012.

[7] L. Morand et al., *Deeply virtual and exclusive electroproduction of omega mesons*, Eur. Phys. J. **A24** (2005), 445–458.

[8] P.A.M. Dirac, *The quantum theory of the emission and absorption of radiation*, Proceedings of the Royal Society of London. Series A, Containing Papers of a Mathematical and Physical Character **114** (1927), no. 767, pp. 243–265 (English).

[9] K. Schilling and G. Wolf, *How to analyse vector-meson production in inelastic lepton scattering*, Nuclear Physics B **61** (1973), 381 – 413.

[10] C. W. Akerlof, W. W. Ash, K. Berkelman, C. A. Lichtenstein, A. Ramanauskas, and R. H. Siemann, *Measurement of the pion form factor*, Phys. Rev. **163** (1967), 1482–1497.

[11] D Dreschsel and L Tiator, *Threshold pion photoproduction on nucleons*, Journal of Physics G: Nuclear and Particle Physics **18** (1992), no. 3, 449.

[12] K.A. Olive et al., *Review of Particle Physics*, Chin. Phys. **C38** (2014), 090001.

[13] David Gross and Frank Wilczek, *A watershed: the emergence of qcd*, CERN Courier **53** (2013), no. 1, pp. 24–27.

[14] Henry W. Kendall, *Nobel lecture: Deep inelastic scattering: Experiments on the proton and the observation of scaling*, `http://www.nobelprize.org/nobel_prizes/physics/laureates/1990/kendall-lecture.html`, December 1990.

[15] H.A. Grunder et al., *The continuous electron beam accelerator facility*, Nuclear Physics A **478** (1988), no. 0, 831 – 846.

[16] Bernhard A Mecking et al., *The CEBAF large acceptance spectrometer (CLAS)*, Nuclear Instruments and Methods in Physics Research Section A: Accelerators, Spectrometers, Detectors and Associated Equipment **503** (2003), no. 3, 513–553.

[17] C.W. Leemann, D.R. Douglas, and G.A. Krafft, *The Continuous Electron Beam Accelerator Facility: CEBAF at the Jefferson Laboratory*, Ann. Rev. Nucl. Part. Sci. **51** (2001), 413–450.

[18] M. Poelker, J. Grames, J. Hansknecht, R. Kazimi, and J. Musson, *Generation of electron bunches at low repetition rates using a beat-frequency technique*, Phys. Rev. ST Accel. Beams **10** (2007), 053502.

[19] B. Povh, M. Lavelle, K. Rith, C. Scholz, and F. Zetsche, *Particles and nuclei: An introduction to the physical concepts*, Springer, 2008.

94

[20] J. O'Meara et al., *A superconducting toroidal magnet for the cebaf large accep-tance spectrometer*, Magnetics, IEEE Transactions on **25** (1989), no. 2, 1902–1905.

[21] M.D Mestayer et al., *The CLAS drift chamber system*, Nuclear Instruments and Methods in Physics Research Section A: Accelerators, Spectrometers, Detectors and Associated Equipment **449** (2000), no. 1-2, 81–111.

[22] D.S Carman et al., *CLAS-NOTE-1997-001: Hall B test run: Drift chamber studies*, 1997.

[23] E.S. Smith et al., *The time-of-flight system for CLAS*, Nuclear Instruments and Methods in Physics Research Section A: Accelerators, Spectrometers, Detectors and Associated Equipment **432** (1999), no. 2-3, 265 – 298.

[24] G. Adams, V. Burkert, R. Carl, T. Carstens, V. Frolov, L. Houghtlin, G. Jacobs, M. Kossov, M. Klusman, B. Kross, M. Onuk, J. Napolitano, J.W. Price, C. Riggs, Y. Sharabian, A. Stavinsky, L.C. Smith, W.A. Stephens, P. Stoler, W. Tuzel, K. Ullrich, A. Vlassov, A. Weisenberger, M. Witkowski, B. Wojtekhowski, P.F. Yergin, and C. Zorn, *The CLAS cherenkov detector*, Nuclear Instruments and Methods in Physics Research Section A: Accelerators, Spectrometers, Detectors and Associated Equipment **465** (2001), no. 2-3, 414 – 427.

[25] M. Amarian, G. Asryan, K. Beard, W. Brooks, V. Burkert, T. Carstens, A. Coleman, R. Demirchyan, Yu. Efremenko, H. Egiyan, K. Egiyan, H. Fun-sten, V. Gavrilov, K. Giovanetti, R.M. Marshall, B. Mecking, R.C. Minehart, H. Mkrtchan, M. Ohandjanyan, Yu. Sharabian, L.C. Smith, S. Stepanyan, W.A. Stephens, T.Y. Tung, and C. Zorn, *The CLAS forward electromagnetic calorime-ter*, Nuclear Instruments and Methods in Physics Research Section A: Acceler-

ators, Spectrometers, Detectors and Associated Equipment **460** (2001), no. 2-3, 239 – 265.

[26] J. J. Manak, E. S. Smith, S. McAleer, and S. Barrow, *CLAS-NOTE-1999-016: e1, g1, and g6 Data Processing Procedures*, 1999.

[27] Harut Avagyan, Mark Ito, Greg Riccardi, and Riad Suleiman, *CLAS-NOTE-2001-003: The CLAS Calibration Database*, 2003.

[28] V. Blobel, *The BOS System (manual)*, `http://www.desy.de/~blobel/bosman.pdf`, 2003.

[29] ———, *THE BOS SYSTEM. DYNAMIC MEMORY MANAGEMENT*, (1988).

[30] V Blobel, *Clas software group*, The BOS system for CLAS software (1995).

[31] Bogdan B. Niczyporuk, *CLAS-NOTE-1991-001: Track Fitting in an Inhomogeneous Magnetic Field*, 1991.

[32] Wesley P. Gohn, *Probing the proton's quark dynamics in semi-inclusive pion electroproduction*, Ph.D. thesis, University of Connecticut, 2012, p. 32.

[33] K. Egiyan, *CLAS-NOTE-1999-007: Determination of Electron Energy Cut Due to CLAS EC Thresholds*, 1999.

[34] *GSIM User's Guide*, `https://www.jlab.org/Hall-B/document/gsim/userguide.html`, 1996.

[35] R. Brun, R. Hagelberg, M. Hansroul, and J.C. Lassalle, *Geant: Simulation Program for Particle Physics Experiments. User Guide and Reference Manual*, (1978).

[36] L.W. Mo and Y.S. Tsai, *Radiative corrections to elastic and inelastic* ep *and* up *scattering*, Rev. Mod. Phys. **41** (1969), 205–235.

[37] D.S. Carman, K. Park, and B.A. Raue, *Separated Structure Functions for the Exclusive $K^+\Lambda$ and $K^+\Sigma^0$ Electroproduction at 5.5 GeV at CLAS*, `http://clasweb.jlab.org/rungroups/e1f/carman/e1f-note-v3.pdf`, 2012.

[38] D. S. Carman, K. Park, B. A. Raue, et al., *Separated structure functions for exclusive $K^+\Lambda$ and $K^+\Sigma^0$ electroproduction at 5.5 GeV measured with CLAS*, Phys. Rev. C **87** (2013), 025204.

[39] Younes Mejaddem, Dževad Belkić, Simo Hyödynmaa, and Anders Brahme, *Calculations of electron energy loss straggling*, Nuclear Instruments and Methods in Physics Research Section B: Beam Interactions with Materials and Atoms **173** (2001), no. 4, 397 – 410.

[40] Kijun Park, Volker Burkert, Latifa Elouadrhiri, and Wooyoung Kim, *CLAS-NOTE-2003-012: Kinematic Corrections for CLAS*, 2003.

[41] Daniel S. Carman, *Momentum Corrections for e1-6*, `https://userweb.jlab.org/~carman/6gev/pcorr.ps`, 2004.

[42] Mike Williams, Doug Applegate, and Curtis A. Meyer, *CLAS-NOTE-2004-017: Determining Momentum and Energy Corrections for g1c Using Kinematic Fitting*, 2004.

[43] Marianna Gabrielyan, *E1F Momentum Corrections*, `http://clasweb.jlab.org/rungroups/e1f/marianna/update_pcorr_post/Pcorr_final_results.pdf`, 2009.

[44] M. Mirazita, *Momentum Correction for e1f data*, `https://www.jlab.org/Hall-B/secure/e1f/mirazita/momcorr/`, 2010.

[45] Kijun Park, *Measurement of the polarized structure function $\sigma_{LT'}$ using the single pion electroproduction channel in the nucleon resonance region for the $1.7 \leq Q^2 \leq 4.5(GeV/c)^2$*, Ph.D. thesis, Kyungpook National University, 2006.

97

[46] E. Pasyuk, *CLAS-NOTE-2007-016: Energy loss corrections for charged particles in CLAS*, 2007.

[47] Iu. A. Skorodumina, V. D. Burkert, E. N. Golovach, R. W. Gothe, E. L. Isupov, B. S. Ishkhanov, V. I. Mokeev, and G. V. Fedotov, *Nucleon resonances in exclusive reactions of photo- and electroproduction of mesons*, Moscow University Physics Bulletin **70** (2015), no. 6, 429–447.

[48] M. Williams et al., *Differential cross sections and spin density matrix elements for the reaction $\gamma p \to p\omega$*, Phys. Rev. C **80** (2009), 065208.

[49] ⸺, *Partial wave analysis of the reaction $\gamma p \to p\omega$ and the search for nucleon resonances*, Phys. Rev. C **80** (2009), 065209.

Appendix A

BOS Banks

The BOS dynamic memory management system [30] specifies a scheme in which information can be identified with *data words* contained by *banks*. The BOS data used for the analysis of ωp electroproduction are tabulated below. This small subset of the available information was reproduced verbatim from the data definition (DDL) files[1] used to generate BOS input/out code. As a programming resource, the misspellings and capitalization inconsistencies are important to retain, especially in the *Data Word* column.

A.1   Banks

The banks used in this analysis follow.

Bank	Description
EVNT	reconstructed event and particle data; pointers to reconstructed track data
CCPB	CC hits for event
DCPB	DC tracks for event
ECPB	EC hits for event
SCPB	SC hits for event
ECHB	forward EC hit-based tracking results

---

[1]https://jlabsvn.jlab.org/svnroot/clas/trunk/io/bankdefs

A.2 DATA WORDS

Bank	Data Word	Description
HEVT	ESTATUS	Event Statuse after reconstruction
HEVT	NRUN	Run Number (monotonically increasing)
HEVT	NEVENT	Event Number in the run NRUN
HEVT	TYPE	Event Type (Data or MC)
HEVT	NPGP	Number of final reconstructed particles*100 + Number of geometrically reconstructed particles
HEVT	TRGPRS	Trigger type*10000 + Prescale factor for that trigger (Event Class)
HEVT	FC	Faraday Cup (K)
HEVT	FCG	Faraday Cup Gated (K)
HEVT	TG	Clock Gated
HEVT	STT	Event Start Time
HEVT	RF1	RF Time
HEVT	RF2	RF Time
HEVT	CON1	Control Rates
HEVT	CON2	Control Rates
HEVT	CON3	Control Rates
HEVT	PTIME	Event Processing Time (UNIX time = seconds)
EVNT	ID	Particle Data Group ID (from SEB)
EVNT	Pmom	momentum (from tracking)
EVNT	Mass	mass squared (from SEB =p**2(1.-betta**2)/beta**2)
EVNT	Charge	charge (from tracking)
EVNT	Betta	Particle velocity in the units of c (=R_trk/TOF/c)
EVNT	Cx	x dir cosine at track origin
EVNT	cy	y dir cosine at track origin
EVNT	cz	z dir cosine at track origin
EVNT	X	X coordinate of vertex (cm)
EVNT	Y	Y coordinate of vertex (cm)
EVNT	Z	Z coordinate of vertex (cm)
EVNT	DCstat	Pointer to DCPB bank (=0 if DC is not involved)
EVNT	CCstat	Pointer to CCPB bank (=0 if CC is not involved)
EVNT	SCstat	Pointer to SCPB bank (=0 if SC is not involved)
EVNT	ECstat	Pointer to ECPB bank (=0 if EC is not involved)
EVNT	LCstat	Pointer to LCPB bank (=0 if LAC is not involved)
EVNT	STstat	Pointer to STPB bank (=0 if ST is not involved)
EVNT	Status	Status word (=0 out of time particle)
DCPB	ScTr	100*sector+track_ID in *BTR

100

DCPB	x_SC	x coordinate of track intersection with SC plane
DCPB	y_SC	y coordinate of track intersection with SC plane
DCPB	z_SC	z coordinate of track intersection with SC plane
DCPB	CX_SC	X dir cosine at (x_SC,y_SC,z_SC)
DCPB	CY_SC	y dir cosine at (x_SC,y_SC,z_SC)
DCPB	CZ_SC	z dir cosine at (x_SC,y_SC,z_SC)
DCPB	X_v	vertex X after fiting to the beam position
DCPB	Y_v	vertex Y after fiting to the beam position
DCPB	Z_v	vertex Z after fiting to the beam position
DCPB	R_v	distance from production vertex to the bemam.
DCPB	Chi2	Chisquare of track fitting
DCPB	Status	Status word
CCPB	ScSgHt	100*sector + Cluster # in CCRC
CCPB	Nphe	Number of photo-electrons*10
CCPB	Time	Flight time relative to the evnt start time
CCPB	Path	Path lenght from target (from tracking)
CCPB	Chi2CC	Geometrical matching: angle between CC hit and nearest SC hit (in rad)
CCPB	Status	Status: 10*(CC seg. number)+1000*(1+phy_index). PHY_INDEX = -1: left PMT (1,3,5...35); PHY_INDEX = +1: right PMT (2,4,6...36); PHY_INDEX = 0: both left and right
ECPB	ScHt	100*sector+Whole_Hit_ID in ECHB
ECPB	Etot	Reconstructed total energy
ECPB	Ein	Inner energy
ECPB	Eout	Outer energy
ECPB	Time	Flight time relative to the evnt start time
ECPB	Path	Path lenght from target
ECPB	X	x coordinate of hit
ECPB	Y	y coordinate of hit
ECPB	Z	z coordinate of hit
ECPB	M2_hit	second moment of _hit pattern
ECPB	M3_hit	third moment of _hit pattern
ECPB	M4_hit	forth moment of _hit pattern
ECPB	InnStr	10000*UI+100*VI+WI
ECPB	OutStr	10000*UO+100*VO+WO
ECPB	Chi2EC	Quality measure of geometrical matching
ECPB	Status	Status word (not implemented yet)
SCPB	ScPdHt	10000*sector+100*SC_PD_ID+Hit_ID in SCR

101

SCPB	Edep	Deposited energy (dE/dX)
SCPB	Time	measured time
SCPB	Path	Path lenght from target
SCPB	Chi2SC	Quality measure of geometrical matching
SCPB	Status	Status word (not defined yet)
ECHB	Sect	Sector number & Layer number
ECHB	E___hit	energy found
ECHB	dE_hit	error on the energy found
ECHB	t_hit	time found
ECHB	dt_hi	error time found
ECHB	i_hit	sector rectangular coordinate
ECHB	j_hit	sector rectangular coordinate
ECHB	di_hit	sector rectangular coordinate error,
ECHB	dj_hit	sector rectangular coordinate error,
ECHB	x_hit	lab coordinate,
ECHB	y_hit	lab coordinate,
ECHB	z_hit	lab coordinate,
ECHB	dx_hit	lab coordinate error,
ECHB	dy_hit	lab coordinate error,
ECHB	dz_hit	lab coordinate error,
ECHB	u2_hit	second moment of u _hit pattern
ECHB	v2_hit	second moment of v _hit pattern
ECHB	w2_hit	second moment of w _hit pattern
ECHB	u3_hit	third moment of u _hit pattern
ECHB	v3_hit	third moment of v _hit pattern
ECHB	w3_hit	third moment of w _hit pattern
ECHB	u4_hit	forth moment of u _hit pattern
ECHB	v4_hit	forth moment of v _hit pattern
ECHB	w4_hit	forth moment of w _hit pattern
ECHB	centr_U	peak position on U axis
ECHB	centr_V	peak position on V axis
ECHB	centr_W	peak position on W axis
ECHB	path_U	path length from hit position to U axis
ECHB	path_V	path length from hit position to V axis
ECHB	path_W	path length from hit position to W axis
ECHB	Nstrp_U	Number of U strips in the hit
ECHB	Nstrp_V	Number of V strips in the hit
ECHB	Nstrp_W	Number of W strips in the hit
ECHB	MatchID1	Id of matched hit in the layer1

ECHB	CH21	Quality measure of matching with layer1
ECHB	MatchID2	Id of matched hit in the layer2
ECHB	CH22	Quality measure of matching with layer2
ECHB	istat	Number of hits & hit ID

Appendix B

GSIM Configurations

B.1 GSIM, E1F

```
c ----- threshold in detectors -----
CUTS   5.e-3 5.e-3 5.e-3 5.e-3 5.e-3
CCCUTS 1.e-3 1.e-3 1.e-3 1.e-3 1.e-3
DCCUTS 1.e-4 1.e-4 1.e-4 1.e-4 1.e-4
ECCUTS 1.e-4 1.e-4 1.e-4 1.e-4 1.e-4
SCCUTS 1.e-4 1.e-4 1.e-4 1.e-4 1.e-4

c -------- geometry ---------
RUNG   10
GEOM   'ALL '
NOGEOM 'PTG' 'ST' 'IC'
UPSTPOS 0.0 0.0 0.0

c ------- magnetic field -------
MAGTYPE  3
MAGSCALE 0.582902 0.75
FIELD    2

c --------- target ---------

TARGET  'e6a'

TGTP 1 1

TGPOS   0.0  0.0  -25.
TGUSER  5.0 0.97 0.012 4
c STZOFF  -25.0
c ---------- beam ----------
POSBEAM  0.0 0.0
SIGBEAM 0.00

c ----- don't save geant banks -----
c NOMCDATA 'ALL'
```

```
    KINE 1
    AUTO 1

    STOP


B.2   GSIM, E16

    c ----- threshold in detectors -----
    CUTS   5.e-3 5.e-3 5.e-3 5.e-3 5.e-3
    CCCUTS 1.e-3 1.e-3 1.e-3 1.e-3 1.e-3
    DCCUTS 1.e-4 1.e-4 1.e-4 1.e-4 1.e-4
    ECCUTS 1.e-4 1.e-4 1.e-4 1.e-4 1.e-4
    SCCUTS 1.e-4 1.e-4 1.e-4 1.e-4 1.e-4

    c -------- geometry ---------
    RUNG   10
    GEOM   'ALL '
    NOGEOM 'PTG' 'ST' 'IC'
    UPSTPOS 0.0 0.0 0.0

    c ------- magnetic field -------
    MAGTYPE  3
    MAGSCALE 0.874352 0.75
    FIELD    2

    c --------- target ---------
    CHAMBER 2
    TARGET  'e1-6'
    TGMATE  'HYDR'
    TGPOS   0.0 0.0 -4.0

    c ---------- beam ----------
    c POSBEAM 0.090 -0.345
    c SIGBEAM 0.00
    c ----- don't save geant banks -----
    NOMCDATA 'ALL'

    KINE 1
    AUTO 1

    STOP
```

Appendix C

Sample of raw differential cross section data

The following table contains raw differential cross section data for a single cell in W and Q^2 for E1F. With knowledge that the beam energy $E_0^{E1F} = 5.497\,GeV$, other variables can be calculated from what is given in the table. In particular, the polarization parameter ϵ and lab-frame energy ν would be required to look into the transverse and longitudinal interferences that give rise to explicit azimuthal dependence of the differential cross sections.

Q_i^2 (GeV^2)	Q_f^2 (GeV^2)	W_i (GeV)	W_f (GeV)	$\cos\theta_i^*$	$\cos\theta_f^*$	ϕ_i^* (rad)	ϕ_f^* (rad)	$\frac{d^2\sigma_h}{d\Omega^*}$ (nb/sr)	$\Delta\left(\frac{d^2\sigma_h}{d\Omega^*}\right)$ (nb/sr)
2.2	2.5	1.84	1.86	-1.0	-0.8	-3.14	-2.79	NaN	NaN
2.2	2.5	1.84	1.86	-1.0	-0.8	-2.79	-2.44	370	91
2.2	2.5	1.84	1.86	-1.0	-0.8	-2.44	-2.09	128	57
2.2	2.5	1.84	1.86	-1.0	-0.8	-2.09	-1.75	179	60
2.2	2.5	1.84	1.86	-1.0	-0.8	-1.75	-1.40	257	68
2.2	2.5	1.84	1.86	-1.0	-0.8	-1.40	-1.05	171	58
2.2	2.5	1.84	1.86	-1.0	-0.8	-1.05	-0.70	123	59
2.2	2.5	1.84	1.86	-1.0	-0.8	-0.70	-0.35	47	46
2.2	2.5	1.84	1.86	-1.0	-0.8	-0.35	-0.00	118	64
2.2	2.5	1.84	1.86	-1.0	-0.8	0.00	0.35	202	58
2.2	2.5	1.84	1.86	-1.0	-0.8	0.35	0.70	268	66
2.2	2.5	1.84	1.86	-1.0	-0.8	0.70	1.05	177	63
2.2	2.5	1.84	1.86	-1.0	-0.8	1.05	1.40	176	72
2.2	2.5	1.84	1.86	-1.0	-0.8	1.40	1.75	168	84
2.2	2.5	1.84	1.86	-1.0	-0.8	1.75	2.09	178	58
2.2	2.5	1.84	1.86	-1.0	-0.8	2.09	2.44	192	59
2.2	2.5	1.84	1.86	-1.0	-0.8	2.44	2.79	162	58
2.2	2.5	1.84	1.86	-1.0	-0.8	2.79	3.14	154	55
2.2	2.5	1.84	1.86	-0.8	-0.6	-3.14	-2.79	NaN	NaN
2.2	2.5	1.84	1.86	-0.8	-0.6	-2.79	-2.44	198	77
2.2	2.5	1.84	1.86	-0.8	-0.6	-2.44	-2.09	291	86
2.2	2.5	1.84	1.86	-0.8	-0.6	-2.09	-1.75	216	67
2.2	2.5	1.84	1.86	-0.8	-0.6	-1.75	-1.40	165	58
2.2	2.5	1.84	1.86	-0.8	-0.6	-1.40	-1.05	160	59
2.2	2.5	1.84	1.86	-0.8	-0.6	-1.05	-0.70	287	106

Continued on next page

Q_i^2	Q_f^2	W_i	W_f	$\cos\theta_i^*$	$\cos\theta_f^*$	ϕ_i^*	ϕ_f^*	$\frac{d^2\sigma_h}{d\Omega^*}$	$\Delta\left(\frac{d^2\sigma_h}{d\Omega^*}\right)$
(GeV^2)	(GeV^2)	(GeV)	(GeV)			(rad)	(rad)	(nb/sr)	(nb/sr)
2.2	2.5	1.84	1.86	-0.8	-0.6	-0.70	-0.35	106	57
2.2	2.5	1.84	1.86	-0.8	-0.6	-0.35	-0.00	115	58
2.2	2.5	1.84	1.86	-0.8	-0.6	0.00	0.35	136	43
2.2	2.5	1.84	1.86	-0.8	-0.6	0.35	0.70	158	50
2.2	2.5	1.84	1.86	-0.8	-0.6	0.70	1.05	163	59
2.2	2.5	1.84	1.86	-0.8	-0.6	1.05	1.40	118	57
2.2	2.5	1.84	1.86	-0.8	-0.6	1.40	1.75	90	83
2.2	2.5	1.84	1.86	-0.8	-0.6	1.75	2.09	113	71
2.2	2.5	1.84	1.86	-0.8	-0.6	2.09	2.44	70	48
2.2	2.5	1.84	1.86	-0.8	-0.6	2.44	2.79	127	47
2.2	2.5	1.84	1.86	-0.8	-0.6	2.79	3.14	182	66
2.2	2.5	1.84	1.86	-0.6	-0.4	-3.14	-2.79	NaN	NaN
2.2	2.5	1.84	1.86	-0.6	-0.4	-2.79	-2.44	226	67
2.2	2.5	1.84	1.86	-0.6	-0.4	-2.44	-2.09	166	77
2.2	2.5	1.84	1.86	-0.6	-0.4	-2.09	-1.75	168	67
2.2	2.5	1.84	1.86	-0.6	-0.4	-1.75	-1.40	48	61
2.2	2.5	1.84	1.86	-0.6	-0.4	-1.40	-1.05	293	106
2.2	2.5	1.84	1.86	-0.6	-0.4	-1.05	-0.70	213	146
2.2	2.5	1.84	1.86	-0.6	-0.4	-0.70	-0.35	75	66
2.2	2.5	1.84	1.86	-0.6	-0.4	-0.35	-0.00	119	59
2.2	2.5	1.84	1.86	-0.6	-0.4	0.00	0.35	72	45
2.2	2.5	1.84	1.86	-0.6	-0.4	0.35	0.70	124	60
2.2	2.5	1.84	1.86	-0.6	-0.4	0.70	1.05	91	57
2.2	2.5	1.84	1.86	-0.6	-0.4	1.05	1.40	134	66
2.2	2.5	1.84	1.86	-0.6	-0.4	1.40	1.75	125	97
2.2	2.5	1.84	1.86	-0.6	-0.4	1.75	2.09	87	64
2.2	2.5	1.84	1.86	-0.6	-0.4	2.09	2.44	203	65
2.2	2.5	1.84	1.86	-0.6	-0.4	2.44	2.79	201	66
2.2	2.5	1.84	1.86	-0.6	-0.4	2.79	3.14	108	61
2.2	2.5	1.84	1.86	-0.4	-0.2	-3.14	-2.79	NaN	NaN
2.2	2.5	1.84	1.86	-0.4	-0.2	-2.79	-2.44	133	58
2.2	2.5	1.84	1.86	-0.4	-0.2	-2.44	-2.09	243	80
2.2	2.5	1.84	1.86	-0.4	-0.2	-2.09	-1.75	88	46
2.2	2.5	1.84	1.86	-0.4	-0.2	-1.75	-1.40	18	52
2.2	2.5	1.84	1.86	-0.4	-0.2	-1.40	-1.05	94	60
2.2	2.5	1.84	1.86	-0.4	-0.2	-1.05	-0.70	-10	68
2.2	2.5	1.84	1.86	-0.4	-0.2	-0.70	-0.35	83	93
2.2	2.5	1.84	1.86	-0.4	-0.2	-0.35	-0.00	222	90
2.2	2.5	1.84	1.86	-0.4	-0.2	0.00	0.35	123	59
2.2	2.5	1.84	1.86	-0.4	-0.2	0.35	0.70	94	49
2.2	2.5	1.84	1.86	-0.4	-0.2	0.70	1.05	64	64
2.2	2.5	1.84	1.86	-0.4	-0.2	1.05	1.40	5	66
2.2	2.5	1.84	1.86	-0.4	-0.2	1.40	1.75	-42	46
2.2	2.5	1.84	1.86	-0.4	-0.2	1.75	2.09	178	74
2.2	2.5	1.84	1.86	-0.4	-0.2	2.09	2.44	141	78
2.2	2.5	1.84	1.86	-0.4	-0.2	2.44	2.79	131	67
2.2	2.5	1.84	1.86	-0.4	-0.2	2.79	3.14	48	50
2.2	2.5	1.84	1.86	-0.2	0.0	-3.14	-2.79	NaN	NaN
2.2	2.5	1.84	1.86	-0.2	0.0	-2.79	-2.44	111	59

Continued on next page

107

Q_i^2	Q_f^2	W_i	W_f	$\cos\theta_i^*$	$\cos\theta_f^*$	ϕ_i^*	ϕ_f^*	$\frac{d^2\sigma_h}{d\Omega^*}$	$\Delta\left(\frac{d^2\sigma_h}{d\Omega^*}\right)$
(GeV^2)	(GeV^2)	(GeV)	(GeV)			(rad)	(rad)	(nb/sr)	(nb/sr)
2.2	2.5	1.84	1.86	-0.2	0.0	-2.44	-2.09	121	64
2.2	2.5	1.84	1.86	-0.2	0.0	-2.09	-1.75	79	74
2.2	2.5	1.84	1.86	-0.2	0.0	-1.75	-1.40	71	72
2.2	2.5	1.84	1.86	-0.2	0.0	-1.40	-1.05	112	68
2.2	2.5	1.84	1.86	-0.2	0.0	-1.05	-0.70	2	62
2.2	2.5	1.84	1.86	-0.2	0.0	-0.70	-0.35	-38	97
2.2	2.5	1.84	1.86	-0.2	0.0	-0.35	-0.00	109	103
2.2	2.5	1.84	1.86	-0.2	0.0	0.00	0.35	171	80
2.2	2.5	1.84	1.86	-0.2	0.0	0.35	0.70	94	63
2.2	2.5	1.84	1.86	-0.2	0.0	0.70	1.05	16	95
2.2	2.5	1.84	1.86	-0.2	0.0	1.05	1.40	130	105
2.2	2.5	1.84	1.86	-0.2	0.0	1.40	1.75	15	62
2.2	2.5	1.84	1.86	-0.2	0.0	1.75	2.09	59	55
2.2	2.5	1.84	1.86	-0.2	0.0	2.09	2.44	163	80
2.2	2.5	1.84	1.86	-0.2	0.0	2.44	2.79	65	54
2.2	2.5	1.84	1.86	-0.2	0.0	2.79	3.14	77	55
2.2	2.5	1.84	1.86	0.0	0.2	-3.14	-2.79	NaN	NaN
2.2	2.5	1.84	1.86	0.0	0.2	-2.79	-2.44	96	55
2.2	2.5	1.84	1.86	0.0	0.2	-2.44	-2.09	74	78
2.2	2.5	1.84	1.86	0.0	0.2	-2.09	-1.75	174	79
2.2	2.5	1.84	1.86	0.0	0.2	-1.75	-1.40	223	123
2.2	2.5	1.84	1.86	0.0	0.2	-1.40	-1.05	-5	65
2.2	2.5	1.84	1.86	0.0	0.2	-1.05	-0.70	131	88
2.2	2.5	1.84	1.86	0.0	0.2	-0.70	-0.35	163	123
2.2	2.5	1.84	1.86	0.0	0.2	-0.35	-0.00	NaN	NaN
2.2	2.5	1.84	1.86	0.0	0.2	0.00	0.35	159	85
2.2	2.5	1.84	1.86	0.0	0.2	0.35	0.70	141	79
2.2	2.5	1.84	1.86	0.0	0.2	0.70	1.05	-89	156
2.2	2.5	1.84	1.86	0.0	0.2	1.05	1.40	75	90
2.2	2.5	1.84	1.86	0.0	0.2	1.40	1.75	161	94
2.2	2.5	1.84	1.86	0.0	0.2	1.75	2.09	131	84
2.2	2.5	1.84	1.86	0.0	0.2	2.09	2.44	102	78
2.2	2.5	1.84	1.86	0.0	0.2	2.44	2.79	37	53
2.2	2.5	1.84	1.86	0.0	0.2	2.79	3.14	35	50
2.2	2.5	1.84	1.86	0.2	0.4	-3.14	-2.79	NaN	NaN
2.2	2.5	1.84	1.86	0.2	0.4	-2.79	-2.44	59	45
2.2	2.5	1.84	1.86	0.2	0.4	-2.44	-2.09	63	56
2.2	2.5	1.84	1.86	0.2	0.4	-2.09	-1.75	98	64
2.2	2.5	1.84	1.86	0.2	0.4	-1.75	-1.40	19	71
2.2	2.5	1.84	1.86	0.2	0.4	-1.40	-1.05	89	62
2.2	2.5	1.84	1.86	0.2	0.4	-1.05	-0.70	124	68
2.2	2.5	1.84	1.86	0.2	0.4	-0.70	-0.35	434	192
2.2	2.5	1.84	1.86	0.2	0.4	-0.35	-0.00	NaN	NaN
2.2	2.5	1.84	1.86	0.2	0.4	0.00	0.35	109	108
2.2	2.5	1.84	1.86	0.2	0.4	0.35	0.70	219	109
2.2	2.5	1.84	1.86	0.2	0.4	0.70	1.05	NaN	NaN
2.2	2.5	1.84	1.86	0.2	0.4	1.05	1.40	168	111
2.2	2.5	1.84	1.86	0.2	0.4	1.40	1.75	126	72
2.2	2.5	1.84	1.86	0.2	0.4	1.75	2.09	53	80

Continued on next page

Q_i^2	Q_f^2	W_i	W_f	$\cos\theta_i^*$	$\cos\theta_f^*$	ϕ_i^*	ϕ_f^*	$\frac{d^2\sigma_h}{d\Omega^*}$	$\Delta\left(\frac{d^2\sigma_h}{d\Omega^*}\right)$
(GeV^2)	(GeV^2)	(GeV)	(GeV)			(rad)	(rad)	(nb/sr)	(nb/sr)
2.2	2.5	1.84	1.86	0.2	0.4	2.09	2.44	54	66
2.2	2.5	1.84	1.86	0.2	0.4	2.44	2.79	94	75
2.2	2.5	1.84	1.86	0.2	0.4	2.79	3.14	53	56
2.2	2.5	1.84	1.86	0.4	0.6	-3.14	-2.79	NaN	NaN
2.2	2.5	1.84	1.86	0.4	0.6	-2.79	-2.44	260	87
2.2	2.5	1.84	1.86	0.4	0.6	-2.44	-2.09	203	84
2.2	2.5	1.84	1.86	0.4	0.6	-2.09	-1.75	173	89
2.2	2.5	1.84	1.86	0.4	0.6	-1.75	-1.40	232	98
2.2	2.5	1.84	1.86	0.4	0.6	-1.40	-1.05	8	56
2.2	2.5	1.84	1.86	0.4	0.6	-1.05	-0.70	91	89
2.2	2.5	1.84	1.86	0.4	0.6	-0.70	-0.35	103	90
2.2	2.5	1.84	1.86	0.4	0.6	-0.35	-0.00	NaN	NaN
2.2	2.5	1.84	1.86	0.4	0.6	0.00	0.35	62	90
2.2	2.5	1.84	1.86	0.4	0.6	0.35	0.70	129	91
2.2	2.5	1.84	1.86	0.4	0.6	0.70	1.05	NaN	NaN
2.2	2.5	1.84	1.86	0.4	0.6	1.05	1.40	152	145
2.2	2.5	1.84	1.86	0.4	0.6	1.40	1.75	58	58
2.2	2.5	1.84	1.86	0.4	0.6	1.75	2.09	208	93
2.2	2.5	1.84	1.86	0.4	0.6	2.09	2.44	113	79
2.2	2.5	1.84	1.86	0.4	0.6	2.44	2.79	188	93
2.2	2.5	1.84	1.86	0.4	0.6	2.79	3.14	264	87
2.2	2.5	1.84	1.86	0.6	0.8	-3.14	-2.79	NaN	NaN
2.2	2.5	1.84	1.86	0.6	0.8	-2.79	-2.44	108	64
2.2	2.5	1.84	1.86	0.6	0.8	-2.44	-2.09	205	83
2.2	2.5	1.84	1.86	0.6	0.8	-2.09	-1.75	49	49
2.2	2.5	1.84	1.86	0.6	0.8	-1.75	-1.40	273	105
2.2	2.5	1.84	1.86	0.6	0.8	-1.40	-1.05	198	106
2.2	2.5	1.84	1.86	0.6	0.8	-1.05	-0.70	73	57
2.2	2.5	1.84	1.86	0.6	0.8	-0.70	-0.35	121	133
2.2	2.5	1.84	1.86	0.6	0.8	-0.35	-0.00	NaN	NaN
2.2	2.5	1.84	1.86	0.6	0.8	0.00	0.35	381	101
2.2	2.5	1.84	1.86	0.6	0.8	0.35	0.70	236	103
2.2	2.5	1.84	1.86	0.6	0.8	0.70	1.05	NaN	NaN
2.2	2.5	1.84	1.86	0.6	0.8	1.05	1.40	61	136
2.2	2.5	1.84	1.86	0.6	0.8	1.40	1.75	-30	53
2.2	2.5	1.84	1.86	0.6	0.8	1.75	2.09	287	98
2.2	2.5	1.84	1.86	0.6	0.8	2.09	2.44	168	120
2.2	2.5	1.84	1.86	0.6	0.8	2.44	2.79	431	123
2.2	2.5	1.84	1.86	0.6	0.8	2.79	3.14	180	78
2.2	2.5	1.84	1.86	0.8	1.0	-3.14	-2.79	NaN	NaN
2.2	2.5	1.84	1.86	0.8	1.0	-2.79	-2.44	104	67
2.2	2.5	1.84	1.86	0.8	1.0	-2.44	-2.09	59	62
2.2	2.5	1.84	1.86	0.8	1.0	-2.09	-1.75	250	84
2.2	2.5	1.84	1.86	0.8	1.0	-1.75	-1.40	270	98
2.2	2.5	1.84	1.86	0.8	1.0	-1.40	-1.05	78	103
2.2	2.5	1.84	1.86	0.8	1.0	-1.05	-0.70	174	96
2.2	2.5	1.84	1.86	0.8	1.0	-0.70	-0.35	48	68
2.2	2.5	1.84	1.86	0.8	1.0	-0.35	-0.00	123	63
2.2	2.5	1.84	1.86	0.8	1.0	0.00	0.35	129	58

Continued on next page

Q_i^2	Q_f^2	W_i	W_f	$\cos\theta_i^*$	$\cos\theta_f^*$	ϕ_i^*	ϕ_f^*	$\frac{d^2\sigma_h}{d\Omega^*}$	$\Delta\left(\frac{d^2\sigma_h}{d\Omega^*}\right)$
(GeV^2)	(GeV^2)	(GeV)	(GeV)			(rad)	(rad)	(nb/sr)	(nb/sr)
2.2	2.5	1.84	1.86	0.8	1.0	0.35	0.70	228	77
2.2	2.5	1.84	1.86	0.8	1.0	0.70	1.05	233	82
2.2	2.5	1.84	1.86	0.8	1.0	1.05	1.40	79	63
2.2	2.5	1.84	1.86	0.8	1.0	1.40	1.75	148	74
2.2	2.5	1.84	1.86	0.8	1.0	1.75	2.09	256	96
2.2	2.5	1.84	1.86	0.8	1.0	2.09	2.44	206	97
2.2	2.5	1.84	1.86	0.8	1.0	2.44	2.79	356	99
2.2	2.5	1.84	1.86	0.8	1.0	2.79	3.14	215	67

Appendix D

Tabulation of unpolarized cross sections and interference terms

Measured unpolarized cross sections, $\sigma_o \pm \Delta\sigma_o$, and interference terms, $\sigma_{TT} \pm \Delta\sigma_{TT}$ and $\sigma_{LT} \pm \Delta\sigma_{LT}$, are tabulated below for E1F and E16. The values were extracted according to the formulation of Equation 7.2.

D.1 E16

Q_i^2 (GeV^2)	Q_f^2 (GeV^2)	W_i (GeV)	W_f (GeV)	ϵ	σ_o (nb)	$\Delta\sigma_o$ (nb)	σ_{TT} (nb)	$\Delta\sigma_{TT}$ (nb)	σ_{LT} (nb)	$\Delta\sigma_{LT}$ (nb)
1.85	2.20	1.72	1.74	0.85	777	73	67	122	18	58
1.85	2.20	1.74	1.76	0.85	1938	78	136	135	59	66
1.85	2.20	1.76	1.78	0.84	2980	89	-103	154	29	73
1.85	2.20	1.78	1.80	0.84	2795	99	2	170	133	78
1.85	2.20	1.80	1.82	0.84	3202	101	152	174	-21	80
1.85	2.20	1.82	1.84	0.83	2948	101	184	175	159	79
1.85	2.20	1.84	1.86	0.82	2516	102	307	179	-293	80
1.85	2.20	1.86	1.88	0.82	2007	103	209	186	-370	82
1.85	2.20	1.88	1.90	0.81	2252	93	326	167	-18	74
1.85	2.20	1.90	1.92	0.81	2369	94	160	169	-19	76
1.85	2.20	1.92	1.94	0.80	2207	83	32	152	-90	69
1.85	2.20	1.94	1.96	0.80	2027	80	226	148	-66	68
1.85	2.20	1.96	1.98	0.79	1905	73	39	138	-158	65
1.85	2.20	1.98	2.00	0.78	1824	72	211	134	86	64
1.85	2.20	2.00	2.02	0.78	1636	68	206	128	39	61
1.85	2.20	2.02	2.04	0.77	1307	66	122	121	-214	59
1.85	2.20	2.04	2.06	0.76	1116	75	-139	147	-264	68
1.85	2.20	2.06	2.08	0.76	1100	63	-68	117	-187	60
1.85	2.20	2.08	2.10	0.75	1003	56	-99	105	-39	53
1.85	2.20	2.10	2.12	0.74	981	52	83	99	-3	49
1.85	2.20	2.12	2.14	0.73	1037	57	114	107	-98	56
1.85	2.20	2.14	2.16	0.72	891	50	429	95	-49	50
1.85	2.20	2.16	2.18	0.71	817	50	56	97	-10	50

Continued on next page

Q_i^2 (GeV²)	Q_f^2 (GeV²)	W_i (GeV)	W_f (GeV)	ϵ	σ_o (nb)	$\Delta\sigma_o$ (nb)	σ_{TT} (nb)	$\Delta\sigma_{TT}$ (nb)	σ_{LT} (nb)	$\Delta\sigma_{LT}$ (nb)
1.85	2.20	2.18	2.20	0.71	724	46	-3	89	-67	46
1.85	2.20	2.20	2.22	0.70	772	45	198	89	-174	43
1.85	2.20	2.22	2.24	0.69	659	42	125	86	-68	42
1.85	2.20	2.24	2.26	0.68	658	46	50	94	-52	45
1.85	2.20	2.26	2.28	0.67	723	45	-133	92	-4	44
1.85	2.20	2.28	2.30	0.66	603	40	347	87	62	41
1.85	2.20	2.30	2.32	0.65	679	61	187	132	65	58
1.85	2.20	2.32	2.34	0.64	549	32	79	69	-81	34
1.85	2.20	2.34	2.36	0.63	494	33	21	76	-51	36
1.85	2.20	2.36	2.38	0.61	535	34	35	78	-86	37
1.85	2.20	2.38	2.40	0.60	470	38	-5	85	-22	44
1.85	2.20	2.40	2.42	0.59	413	34	36	78	-17	39
1.85	2.20	2.42	2.44	0.58	462	29	-12	71	-60	31
1.85	2.20	2.44	2.46	0.57	438	27	-32	69	-52	30
1.85	2.20	2.46	2.48	0.55	378	31	100	75	60	38
1.85	2.20	2.48	2.50	0.54	296	22	-95	62	-7	25
1.85	2.20	2.50	2.52	0.53	309	22	2	61	16	26
1.85	2.20	2.52	2.54	0.51	306	22	75	62	-6	26
1.85	2.20	2.54	2.56	0.50	317	23	-2	67	-30	28
1.85	2.20	2.56	2.58	0.48	273	21	36	65	-31	27
1.85	2.20	2.58	2.60	0.47	336	21	149	66	-9	28
2.20	2.50	1.72	1.74	0.83	726	57	-227	100	24	46
2.20	2.50	1.74	1.76	0.82	1412	55	-84	96	44	46
2.20	2.50	1.76	1.78	0.82	2035	65	82	115	40	54
2.20	2.50	1.78	1.80	0.81	1972	68	183	121	-12	56
2.20	2.50	1.80	1.82	0.80	1990	71	322	129	-131	58
2.20	2.50	1.82	1.84	0.80	1865	72	366	129	-183	57
2.20	2.50	1.84	1.86	0.79	1665	73	202	130	-146	58
2.20	2.50	1.86	1.88	0.79	1519	78	389	143	-145	64
2.20	2.50	1.88	1.90	0.78	1550	78	208	142	-158	66
2.20	2.50	1.90	1.92	0.78	1509	72	274	134	-13	63
2.20	2.50	1.92	1.94	0.77	1485	68	-5	132	36	61
2.20	2.50	1.94	1.96	0.76	1468	64	192	125	12	57
2.20	2.50	1.96	1.98	0.76	1284	62	336	119	-34	58
2.20	2.50	1.98	2.00	0.75	1155	59	-46	119	-64	55
2.20	2.50	2.00	2.02	0.74	1123	57	-43	113	-176	52
2.20	2.50	2.02	2.04	0.73	955	53	-3	108	-85	50
2.20	2.50	2.04	2.06	0.73	959	57	150	116	-20	57
2.20	2.50	2.06	2.08	0.72	627	57	26	113	-199	55
2.20	2.50	2.08	2.10	0.71	823	57	263	112	65	57
2.20	2.50	2.10	2.12	0.70	760	49	260	97	102	52
2.20	2.50	2.12	2.14	0.69	483	42	-75	87	-74	44
2.20	2.50	2.14	2.16	0.68	619	44	141	91	-36	47
2.20	2.50	2.16	2.18	0.67	626	53	134	101	69	61
2.20	2.50	2.18	2.20	0.66	518	35	58	72	-48	37
2.20	2.50	2.20	2.22	0.65	569	41	131	87	4	44
2.20	2.50	2.22	2.24	0.64	514	35	174	76	-48	37
2.20	2.50	2.24	2.26	0.63	568	49	208	99	102	54
2.20	2.50	2.26	2.28	0.62	459	33	164	70	57	38

Continued on next page

Q_i^2 (GeV^2)	Q_f^2 (GeV^2)	W_i (GeV)	W_f (GeV)	ϵ	σ_o (nb)	$\Delta\sigma_o$ (nb)	σ_{TT} (nb)	$\Delta\sigma_{TT}$ (nb)	σ_{LT} (nb)	$\Delta\sigma_{LT}$ (nb)
2.20	2.50	2.28	2.30	0.61	408	30	119	70	-7	31
2.20	2.50	2.30	2.32	0.60	319	28	151	68	-6	31
2.20	2.50	2.32	2.34	0.59	265	32	-21	70	-66	32
2.20	2.50	2.34	2.36	0.58	336	27	190	63	-53	32
2.20	2.50	2.36	2.38	0.57	272	26	-12	61	-55	31
2.20	2.50	2.38	2.40	0.55	363	43	-69	94	35	49
2.20	2.50	2.40	2.42	0.54	308	23	127	58	-30	27
2.20	2.50	2.42	2.44	0.53	256	25	-70	69	-22	27
2.20	2.50	2.44	2.46	0.51	273	22	163	57	26	28
2.20	2.50	2.46	2.48	0.50	317	55	61	138	93	67
2.20	2.50	2.48	2.50	0.49	279	21	129	61	-31	27
2.20	2.50	2.50	2.52	0.47	283	23	-7	67	-14	28
2.20	2.50	2.52	2.54	0.46	252	21	103	65	-29	28
2.20	2.50	2.54	2.56	0.44	284	27	-36	87	10	34
2.20	2.50	2.56	2.58	0.43	237	22	-50	73	-94	29
2.20	2.50	2.58	2.60	0.41	260	21	34	75	38	28
2.50	2.90	1.72	1.74	0.79	503	39	15	68	57	34
2.50	2.90	1.74	1.76	0.79	1104	39	-11	71	8	33
2.50	2.90	1.76	1.78	0.78	1406	41	39	77	99	35
2.50	2.90	1.78	1.80	0.78	1501	47	93	88	27	40
2.50	2.90	1.80	1.82	0.77	1428	49	180	89	-70	41
2.50	2.90	1.82	1.84	0.76	1280	53	451	97	-248	44
2.50	2.90	1.84	1.86	0.76	1159	53	395	97	-169	44
2.50	2.90	1.86	1.88	0.75	1038	54	235	99	-143	49
2.50	2.90	1.88	1.90	0.74	1147	56	227	106	-175	52
2.50	2.90	1.90	1.92	0.74	993	49	110	97	-129	46
2.50	2.90	1.92	1.94	0.73	1075	54	159	102	-35	53
2.50	2.90	1.94	1.96	0.72	1064	49	199	98	-85	47
2.50	2.90	1.96	1.98	0.72	1039	48	405	91	0	47
2.50	2.90	1.98	2.00	0.71	840	39	106	83	-3	39
2.50	2.90	2.00	2.02	0.70	804	42	47	82	-76	42
2.50	2.90	2.02	2.04	0.69	770	40	153	84	-60	42
2.50	2.90	2.04	2.06	0.68	576	34	47	73	-19	35
2.50	2.90	2.06	2.08	0.68	543	34	72	76	-6	37
2.50	2.90	2.08	2.10	0.67	489	34	33	75	-75	37
2.50	2.90	2.10	2.12	0.66	485	34	32	75	-140	38
2.50	2.90	2.12	2.14	0.65	482	35	86	77	-9	41
2.50	2.90	2.14	2.16	0.64	497	37	55	77	12	41
2.50	2.90	2.16	2.18	0.63	466	31	101	68	-22	34
2.50	2.90	2.18	2.20	0.62	408	30	99	67	-10	33
2.50	2.90	2.20	2.22	0.61	426	30	192	68	30	36
2.50	2.90	2.22	2.24	0.60	424	30	173	65	33	35
2.50	2.90	2.24	2.26	0.59	366	24	37	59	-42	27
2.50	2.90	2.26	2.28	0.57	408	27	255	66	94	35
2.50	2.90	2.28	2.30	0.56	330	25	170	62	8	32
2.50	2.90	2.30	2.32	0.55	288	22	44	56	-83	26
2.50	2.90	2.32	2.34	0.54	277	22	60	54	-33	26
2.50	2.90	2.34	2.36	0.53	292	24	38	59	19	30
2.50	2.90	2.36	2.38	0.51	290	21	-7	55	-84	26

Continued on next page

Q_i^2 (GeV^2)	Q_f^2 (GeV^2)	W_i (GeV)	W_f (GeV)	ϵ	σ_o (nb)	$\Delta\sigma_o$ (nb)	σ_{TT} (nb)	$\Delta\sigma_{TT}$ (nb)	σ_{LT} (nb)	$\Delta\sigma_{LT}$ (nb)
2.50	2.90	2.38	2.40	0.50	289	20	43	57	-36	26
2.50	2.90	2.40	2.42	0.49	244	20	41	59	-58	25
2.50	2.90	2.42	2.44	0.47	266	25	-6	71	-10	32
2.50	2.90	2.44	2.46	0.46	297	38	170	102	61	49
2.50	2.90	2.46	2.48	0.44	232	19	-30	59	-13	25
2.50	2.90	2.48	2.50	0.43	220	16	64	54	-44	22
2.50	2.90	2.50	2.52	0.41	250	18	80	62	5	25
2.50	2.90	2.52	2.54	0.40	208	17	90	62	34	25
2.90	3.35	1.72	1.74	0.75	463	28	85	54	76	26
2.90	3.35	1.74	1.76	0.74	782	32	118	64	106	29
2.90	3.35	1.76	1.78	0.74	1016	35	-21	68	122	31
2.90	3.35	1.78	1.80	0.73	1080	39	37	76	11	35
2.90	3.35	1.80	1.82	0.72	1056	40	239	79	-26	35
2.90	3.35	1.82	1.84	0.72	1037	42	372	83	-138	37
2.90	3.35	1.84	1.86	0.71	945	43	491	82	-120	39
2.90	3.35	1.86	1.88	0.70	882	48	67	92	-182	46
2.90	3.35	1.88	1.90	0.70	766	43	-125	91	-298	43
2.90	3.35	1.90	1.92	0.69	827	51	131	100	-123	55
2.90	3.35	1.92	1.94	0.68	863	45	158	95	-43	47
2.90	3.35	1.94	1.96	0.67	808	43	-32	87	-9	44
2.90	3.35	1.96	1.98	0.66	837	40	224	87	10	40
2.90	3.35	1.98	2.00	0.66	785	40	88	89	-57	40
2.90	3.35	2.00	2.02	0.65	617	35	-119	81	-141	38
2.90	3.35	2.02	2.04	0.64	594	38	74	86	-86	44
2.90	3.35	2.04	2.06	0.63	636	41	106	96	-37	48
2.90	3.35	2.06	2.08	0.62	559	36	131	82	48	42
2.90	3.35	2.08	2.10	0.61	448	35	38	83	-11	41
2.90	3.35	2.10	2.12	0.60	445	34	104	80	-55	41
2.90	3.35	2.12	2.14	0.59	334	28	-30	68	-112	33
2.90	3.35	2.14	2.16	0.58	409	30	153	71	-66	36
2.90	3.35	2.16	2.18	0.57	377	28	-51	69	-44	34
2.90	3.35	2.18	2.20	0.56	354	29	3	73	-70	36
2.90	3.35	2.20	2.22	0.55	280	30	46	70	-25	38
2.90	3.35	2.22	2.24	0.53	337	27	46	76	15	33
2.90	3.35	2.24	2.26	0.52	258	23	78	60	-33	27
2.90	3.35	2.26	2.28	0.51	257	22	-20	64	-18	29
2.90	3.35	2.28	2.30	0.50	256	28	54	83	-85	34
3.35	3.85	1.72	1.74	0.70	334	27	4	56	5	26
3.35	3.85	1.74	1.76	0.69	723	27	-28	58	44	26
3.35	3.85	1.76	1.78	0.68	807	34	-61	71	65	32
3.35	3.85	1.78	1.80	0.68	939	37	-56	78	-10	34
3.35	3.85	1.80	1.82	0.67	932	39	26	82	4	35
3.35	3.85	1.82	1.84	0.66	824	40	196	85	-43	39
3.35	3.85	1.84	1.86	0.65	836	44	187	92	-99	45
3.35	3.85	1.86	1.88	0.64	713	46	-52	100	-96	48
3.35	3.85	1.88	1.90	0.64	631	43	79	91	-217	45
3.35	3.85	1.90	1.92	0.63	744	50	178	111	-107	56
3.35	3.85	1.92	1.94	0.62	663	39	-65	94	-169	43
3.35	3.85	1.94	1.96	0.61	636	40	96	97	-104	44

Continued on next page

114

Q_i^2 (GeV^2)	Q_f^2 (GeV^2)	W_i (GeV)	W_f (GeV)	ϵ	σ_o (nb)	$\Delta\sigma_o$ (nb)	σ_{TT} (nb)	$\Delta\sigma_{TT}$ (nb)	σ_{LT} (nb)	$\Delta\sigma_{LT}$ (nb)
3.35	3.85	1.96	1.98	0.60	646	42	230	99	-24	51
3.35	3.85	1.98	2.00	0.59	493	35	-47	84	-101	40
3.35	3.85	2.00	2.02	0.58	518	40	-53	94	-100	48
3.35	3.85	2.02	2.04	0.57	460	38	93	94	-91	46
3.35	3.85	2.04	2.06	0.56	408	38	120	96	-44	50
3.35	3.85	2.06	2.08	0.55	392	35	-149	89	-146	45
3.35	3.85	2.08	2.10	0.54	323	30	-64	78	-46	35
3.35	3.85	2.10	2.12	0.53	317	30	14	79	-62	37
3.35	3.85	2.12	2.14	0.52	280	32	-102	85	-106	40
3.35	3.85	2.14	2.16	0.51	303	34	-105	99	-45	43
3.35	3.85	2.16	2.18	0.50	236	27	83	83	-9	34
3.35	3.85	2.18	2.20	0.48	253	27	9	79	7	37
3.85	4.65	1.72	1.74	0.62	208	23	-47	55	-25	24
3.85	4.65	1.74	1.76	0.61	411	26	-66	60	-2	27
3.85	4.65	1.76	1.78	0.60	571	26	-30	64	-62	26
3.85	4.65	1.78	1.80	0.59	622	31	-6	75	-38	30
3.85	4.65	1.80	1.82	0.59	682	32	42	78	-64	33
3.85	4.65	1.82	1.84	0.58	622	34	71	89	-66	36
3.85	4.65	1.84	1.86	0.57	570	39	159	98	-55	45
3.85	4.65	1.86	1.88	0.56	568	39	-284	98	-161	44
3.85	4.65	1.88	1.90	0.55	427	37	-4	94	-103	44
3.85	4.65	1.90	1.92	0.54	561	38	-91	100	-76	45
3.85	4.65	1.92	1.94	0.53	489	43	182	114	-23	57
3.85	4.65	1.94	1.96	0.52	522	39	-3	106	-58	48
3.85	4.65	1.96	1.98	0.51	481	37	-5	103	-29	49
3.85	4.65	1.98	2.00	0.50	448	35	-139	111	-96	50
3.85	4.65	2.00	2.02	0.49	438	34	109	98	31	47
3.85	4.65	2.02	2.04	0.48	325	29	151	84	7	40
3.85	4.65	2.04	2.06	0.47	400	42	-64	118	22	58
3.85	4.65	2.06	2.08	0.45	359	29	206	89	80	41
3.85	4.65	2.08	2.10	0.44	336	37	41	106	17	52
4.65	5.15	1.72	1.74	0.53	179	51	-116	142	-67	59
4.65	5.15	1.74	1.76	0.52	318	35	-18	101	27	41
4.65	5.15	1.76	1.78	0.51	504	46	-177	125	-17	48
4.65	5.15	1.78	1.80	0.50	508	49	-10	153	-46	59
4.65	5.15	1.80	1.82	0.49	580	52	246	143	43	64
4.65	5.15	1.82	1.84	0.48	476	48	107	130	-100	59
4.65	5.15	1.84	1.86	0.47	403	66	-270	180	-177	84
4.65	5.15	1.86	1.88	0.46	513	77	-6	209	-51	115
4.65	5.15	1.88	1.90	0.45	511	68	131	178	128	98
4.65	5.15	1.90	1.92	0.44	317	72	-179	200	-131	107
4.65	5.15	1.92	1.94	0.43	328	53	97	181	-173	54
4.65	5.15	1.94	1.96	0.42	509	57	268	218	-9	85
4.65	5.15	1.96	1.98	0.41	421	44	158	165	-145	60
4.65	5.15	1.98	2.00	0.39	198	37	-313	143	-106	54

D.2   E1F

Q_i^2	Q_f^2	W_i	W_f	ϵ	σ_o	$\Delta\sigma_o$	σ_{TT}	$\Delta\sigma_{TT}$	σ_{LT}	$\Delta\sigma_{LT}$
(GeV^2)	(GeV^2)	(GeV)	(GeV)		(nb)	(nb)	(nb)	(nb)	(nb)	(nb)
1.85	2.20	1.72	1.74	0.84	1118	56	90	95	20	48
1.85	2.20	1.74	1.76	0.83	1856	57	-154	98	67	47
1.85	2.20	1.76	1.78	0.83	2614	67	-165	118	57	56
1.85	2.20	1.78	1.80	0.82	2464	76	246	131	67	62
1.85	2.20	1.80	1.82	0.82	2263	76	381	131	-133	61
1.85	2.20	1.82	1.84	0.81	2246	76	606	128	-248	62
1.85	2.20	1.84	1.86	0.81	2119	78	538	135	-122	65
1.85	2.20	1.86	1.88	0.80	1977	77	251	140	-211	69
1.85	2.20	1.88	1.90	0.79	2011	73	232	135	-145	65
1.85	2.20	1.90	1.92	0.79	2008	69	35	129	-210	61
1.85	2.20	1.92	1.94	0.78	1978	64	279	119	-12	57
1.85	2.20	1.94	1.96	0.77	1685	59	178	112	-94	53
1.85	2.20	1.96	1.98	0.77	1718	59	308	114	-34	56
1.85	2.20	1.98	2.00	0.76	1364	55	115	108	-146	53
1.85	2.20	2.00	2.02	0.75	1276	52	386	100	-23	50
1.85	2.20	2.02	2.04	0.74	1143	51	285	101	-107	50
1.85	2.20	2.04	2.06	0.74	1008	50	119	99	-59	51
1.85	2.20	2.06	2.08	0.73	998	48	200	94	-28	49
1.85	2.20	2.08	2.10	0.72	951	45	105	88	-142	45
1.85	2.20	2.10	2.12	0.71	927	44	292	88	-4	44
1.85	2.20	2.12	2.14	0.70	857	43	226	87	2	45
1.85	2.20	2.14	2.16	0.69	772	39	-8	80	-167	40
1.85	2.20	2.16	2.18	0.68	726	37	50	76	-44	38
1.85	2.20	2.18	2.20	0.67	675	37	147	76	5	38
1.85	2.20	2.20	2.22	0.66	747	35	71	74	-102	37
1.85	2.20	2.22	2.24	0.65	601	33	109	71	-33	35
1.85	2.20	2.24	2.26	0.64	601	31	-143	69	-39	33
1.85	2.20	2.26	2.28	0.63	590	30	101	67	0	32
1.85	2.20	2.28	2.30	0.62	552	29	134	65	-8	32
1.85	2.20	2.30	2.32	0.61	496	27	40	62	-35	30
1.85	2.20	2.32	2.34	0.60	519	27	174	63	33	30
1.85	2.20	2.34	2.36	0.58	479	26	-56	63	-34	29
1.85	2.20	2.36	2.38	0.57	486	26	31	63	-27	30
1.85	2.20	2.38	2.40	0.56	377	24	-10	58	-46	28
1.85	2.20	2.40	2.42	0.54	395	23	23	59	-5	27
1.85	2.20	2.42	2.44	0.53	371	23	-49	60	-23	27
1.85	2.20	2.44	2.46	0.52	391	23	-27	62	-70	28
1.85	2.20	2.46	2.48	0.50	341	22	-40	61	19	27
1.85	2.20	2.48	2.50	0.49	390	23	74	66	-24	29
1.85	2.20	2.50	2.52	0.47	294	20	-60	62	-60	26
1.85	2.20	2.52	2.54	0.46	300	20	109	61	-26	27
1.85	2.20	2.54	2.56	0.44	329	22	-3	71	-99	29
1.85	2.20	2.56	2.58	0.43	311	22	104	76	-46	31
1.85	2.20	2.58	2.60	0.41	254	21	125	75	-63	31
2.20	2.50	1.72	1.74	0.81	847	58	58	103	103	49
2.20	2.50	1.74	1.76	0.80	1323	56	5	103	42	48
2.20	2.50	1.76	1.78	0.79	1719	69	-97	127	45	59
2.20	2.50	1.78	1.80	0.79	1728	72	150	131	-13	62
2.20	2.50	1.80	1.82	0.78	1829	74	188	131	-86	60

Continued on next page

Q_i^2 (GeV^2)	Q_f^2 (GeV^2)	W_i (GeV)	W_f (GeV)	ϵ	σ_o (nb)	$\Delta\sigma_o$ (nb)	σ_{TT} (nb)	$\Delta\sigma_{TT}$ (nb)	σ_{LT} (nb)	$\Delta\sigma_{LT}$ (nb)
2.20	2.50	1.82	1.84	0.78	1858	73	245	134	-123	60
2.20	2.50	1.84	1.86	0.77	1774	75	239	134	-75	65
2.20	2.50	1.86	1.88	0.76	1594	71	-106	132	-186	63
2.20	2.50	1.88	1.90	0.76	1386	67	77	131	-213	62
2.20	2.50	1.90	1.92	0.75	1535	65	177	128	-1	61
2.20	2.50	1.92	1.94	0.74	1453	60	285	116	26	57
2.20	2.50	1.94	1.96	0.74	1267	53	191	107	-19	51
2.20	2.50	1.96	1.98	0.73	1229	51	343	104	-70	49
2.20	2.50	1.98	2.00	0.72	1189	51	141	104	-76	50
2.20	2.50	2.00	2.02	0.71	1049	51	90	107	-203	53
2.20	2.50	2.02	2.04	0.70	958	49	84	103	-30	51
2.20	2.50	2.04	2.06	0.69	877	48	161	102	-165	52
2.20	2.50	2.06	2.08	0.69	756	48	51	99	-83	52
2.20	2.50	2.08	2.10	0.68	781	45	168	96	-21	50
2.20	2.50	2.10	2.12	0.67	745	41	171	88	-8	45
2.20	2.50	2.12	2.14	0.66	740	40	363	87	53	46
2.20	2.50	2.14	2.16	0.65	631	36	71	80	6	39
2.20	2.50	2.16	2.18	0.64	624	35	41	76	-54	38
2.20	2.50	2.18	2.20	0.63	565	33	209	76	-31	37
2.20	2.50	2.20	2.22	0.62	499	32	-21	72	-41	35
2.20	2.50	2.22	2.24	0.60	531	32	199	75	24	37
2.20	2.50	2.24	2.26	0.59	492	32	74	74	-2	37
2.20	2.50	2.26	2.28	0.58	452	30	176	73	39	35
2.20	2.50	2.28	2.30	0.57	401	28	-43	70	-35	33
2.20	2.50	2.30	2.32	0.56	464	28	74	72	-60	34
2.20	2.50	2.32	2.34	0.54	389	28	40	72	-42	34
2.20	2.50	2.34	2.36	0.53	370	29	-60	79	-39	36
2.20	2.50	2.36	2.38	0.52	363	29	69	79	34	37
2.20	2.50	2.38	2.40	0.50	305	27	54	77	-73	35
2.20	2.50	2.40	2.42	0.49	329	32	-74	93	-9	41
2.20	2.50	2.42	2.44	0.48	278	30	-35	87	-61	40
2.20	2.50	2.44	2.46	0.46	310	29	79	89	-6	39
2.20	2.50	2.46	2.48	0.45	272	29	-226	93	-56	40
2.20	2.50	2.48	2.50	0.43	253	26	-124	81	-42	35
2.20	2.50	2.50	2.52	0.41	274	28	-6	95	23	41
2.20	2.50	2.52	2.54	0.40	277	26	53	94	-17	40
2.20	2.50	2.54	2.56	0.38	230	23	-189	84	-22	34
2.20	2.50	2.56	2.58	0.37	232	24	41	93	-26	38
2.20	2.50	2.58	2.60	0.35	178	22	-70	89	-85	36
2.50	2.90	1.72	1.74	0.77	800	39	-48	76	42	35
2.50	2.90	1.74	1.76	0.76	1201	40	80	75	23	35
2.50	2.90	1.76	1.78	0.76	1279	44	83	84	-66	39
2.50	2.90	1.78	1.80	0.75	1434	48	98	92	14	41
2.50	2.90	1.80	1.82	0.74	1547	49	343	93	-41	42
2.50	2.90	1.82	1.84	0.74	1635	50	282	95	-115	44
2.50	2.90	1.84	1.86	0.73	1266	48	180	90	-116	43
2.50	2.90	1.86	1.88	0.72	1126	49	7	97	-271	47
2.50	2.90	1.88	1.90	0.72	1048	52	61	106	-250	52
2.50	2.90	1.90	1.92	0.71	1227	49	104	102	-139	49

Continued on next page

117

Q_i^2 (GeV²)	Q_f^2 (GeV²)	W_i (GeV)	W_f (GeV)	ϵ	σ_o (nb)	$\Delta\sigma_o$ (nb)	σ_{TT} (nb)	$\Delta\sigma_{TT}$ (nb)	σ_{LT} (nb)	$\Delta\sigma_{LT}$ (nb)
2.50	2.90	1.92	1.94	0.70	1206	45	155	93	-35	45
2.50	2.90	1.94	1.96	0.69	1120	45	-56	100	-87	47
2.50	2.90	1.96	1.98	0.68	1127	41	-53	90	-33	41
2.50	2.90	1.98	2.00	0.68	973	40	98	88	30	42
2.50	2.90	2.00	2.02	0.67	785	39	-13	88	-195	41
2.50	2.90	2.02	2.04	0.66	799	41	174	92	-7	45
2.50	2.90	2.04	2.06	0.65	682	38	-75	89	-145	43
2.50	2.90	2.06	2.08	0.64	600	38	156	87	-40	43
2.50	2.90	2.08	2.10	0.63	755	39	278	89	84	46
2.50	2.90	2.10	2.12	0.62	582	37	32	86	-43	44
2.50	2.90	2.12	2.14	0.61	534	35	-70	82	-72	40
2.50	2.90	2.14	2.16	0.60	434	33	-68	80	-17	38
2.50	2.90	2.16	2.18	0.59	522	34	37	81	-50	39
2.50	2.90	2.18	2.20	0.57	416	32	72	79	25	37
2.50	2.90	2.20	2.22	0.56	451	34	54	87	49	41
2.50	2.90	2.22	2.24	0.55	374	30	102	78	14	37
2.50	2.90	2.24	2.26	0.54	403	31	68	81	-47	37
2.50	2.90	2.26	2.28	0.53	314	28	105	75	8	35
2.50	2.90	2.28	2.30	0.51	349	28	183	78	18	36
2.50	2.90	2.30	2.32	0.50	370	28	146	79	-55	36
2.50	2.90	2.32	2.34	0.49	269	26	31	74	3	34
2.50	2.90	2.34	2.36	0.47	303	27	-34	82	3	36
2.50	2.90	2.36	2.38	0.46	207	32	-65	90	-25	45
2.50	2.90	2.38	2.40	0.44	298	28	58	87	66	39
2.50	2.90	2.40	2.42	0.43	307	26	18	87	-69	37
2.50	2.90	2.42	2.44	0.41	231	22	46	77	-59	31
2.50	2.90	2.44	2.46	0.40	230	23	-110	85	-27	33
2.50	2.90	2.46	2.48	0.38	266	23	-9	88	-61	35
2.50	2.90	2.48	2.50	0.37	265	27	27	107	-74	43
2.50	2.90	2.50	2.52	0.35	274	29	11	120	9	46
2.50	2.90	2.52	2.54	0.33	214	26	-50	113	-49	44
2.90	3.35	1.72	1.74	0.72	503	33	2	66	-10	31
2.90	3.35	1.74	1.76	0.72	849	38	-124	77	-21	35
2.90	3.35	1.76	1.78	0.71	1065	42	67	85	-39	39
2.90	3.35	1.78	1.80	0.70	1171	45	1	91	90	41
2.90	3.35	1.80	1.82	0.69	1149	46	311	95	-39	41
2.90	3.35	1.82	1.84	0.69	1187	48	303	98	-126	43
2.90	3.35	1.84	1.86	0.68	1129	49	71	100	-113	46
2.90	3.35	1.86	1.88	0.67	933	52	-15	107	-188	52
2.90	3.35	1.88	1.90	0.66	948	52	-55	116	-192	55
2.90	3.35	1.90	1.92	0.65	918	51	76	114	-112	52
2.90	3.35	1.92	1.94	0.64	903	48	68	108	-49	50
2.90	3.35	1.94	1.96	0.64	807	43	-22	100	-55	46
2.90	3.35	1.96	1.98	0.63	845	46	139	107	-14	51
2.90	3.35	1.98	2.00	0.62	759	46	46	110	-100	50
2.90	3.35	2.00	2.02	0.61	654	43	70	104	-103	48
2.90	3.35	2.02	2.04	0.60	608	43	-44	109	-56	52
2.90	3.35	2.04	2.06	0.59	495	43	10	105	-135	51
2.90	3.35	2.06	2.08	0.58	472	41	-24	102	-100	51

Continued on next page

Q_i^2 (GeV^2)	Q_f^2 (GeV^2)	W_i (GeV)	W_f (GeV)	ϵ	σ_o (nb)	$\Delta\sigma_o$ (nb)	σ_{TT} (nb)	$\Delta\sigma_{TT}$ (nb)	σ_{LT} (nb)	$\Delta\sigma_{LT}$ (nb)
2.90	3.35	2.08	2.10	0.57	496	40	101	100	-21	49
2.90	3.35	2.10	2.12	0.55	538	37	24	95	-70	44
2.90	3.35	2.12	2.14	0.54	430	34	58	88	-40	43
2.90	3.35	2.14	2.16	0.53	363	32	-38	87	-75	40
2.90	3.35	2.16	2.18	0.52	431	33	198	90	36	42
2.90	3.35	2.18	2.20	0.51	420	31	147	85	15	41
2.90	3.35	2.20	2.22	0.50	347	29	68	83	-53	38
2.90	3.35	2.22	2.24	0.48	363	31	155	89	8	42
2.90	3.35	2.24	2.26	0.47	322	28	242	83	48	38
2.90	3.35	2.26	2.28	0.46	339	28	61	86	-16	38
2.90	3.35	2.28	2.30	0.44	299	28	57	93	50	39
3.35	3.85	1.72	1.74	0.66	360	40	-165	86	17	37
3.35	3.85	1.74	1.76	0.66	720	39	-17	85	-23	36
3.35	3.85	1.76	1.78	0.65	800	42	45	95	52	39
3.35	3.85	1.78	1.80	0.64	920	43	116	96	-83	40
3.35	3.85	1.80	1.82	0.63	1062	47	72	106	-40	44
3.35	3.85	1.82	1.84	0.62	870	45	35	103	-54	44
3.35	3.85	1.84	1.86	0.61	843	46	-95	105	-105	47
3.35	3.85	1.86	1.88	0.61	714	49	-238	112	-188	55
3.35	3.85	1.88	1.90	0.60	687	50	-151	121	-129	58
3.35	3.85	1.90	1.92	0.59	751	47	29	116	-48	55
3.35	3.85	1.92	1.94	0.58	756	44	117	112	-89	51
3.35	3.85	1.94	1.96	0.57	648	42	1	108	-183	50
3.35	3.85	1.96	1.98	0.56	545	40	-26	105	-179	49
3.35	3.85	1.98	2.00	0.55	624	41	-9	110	-76	50
3.35	3.85	2.00	2.02	0.54	526	43	-7	117	-4	54
3.35	3.85	2.02	2.04	0.53	565	46	169	123	8	61
3.35	3.85	2.04	2.06	0.51	444	39	161	108	28	51
3.35	3.85	2.06	2.08	0.50	410	43	55	120	-34	58
3.35	3.85	2.08	2.10	0.49	413	39	-87	111	-13	52
3.35	3.85	2.10	2.12	0.48	362	37	175	107	49	51
3.35	3.85	2.12	2.14	0.47	385	42	351	123	51	60
3.35	3.85	2.14	2.16	0.45	312	37	116	115	-50	51
3.35	3.85	2.16	2.18	0.44	314	38	205	120	51	54
3.35	3.85	2.18	2.20	0.43	302	38	-113	125	3	55
3.85	4.65	1.72	1.74	0.58	207	31	30	79	-2	32
3.85	4.65	1.74	1.76	0.57	431	32	-30	82	17	32
3.85	4.65	1.76	1.78	0.56	600	35	-92	91	17	36
3.85	4.65	1.78	1.80	0.55	602	40	368	104	-24	42
3.85	4.65	1.80	1.82	0.54	700	42	104	113	-31	46
3.85	4.65	1.82	1.84	0.53	633	45	225	121	-179	53
3.85	4.65	1.84	1.86	0.52	534	46	-235	122	-210	54
3.85	4.65	1.86	1.88	0.51	522	46	-61	125	-149	57
3.85	4.65	1.88	1.90	0.50	552	47	278	133	-56	60
3.85	4.65	1.90	1.92	0.49	565	50	251	141	65	68
3.85	4.65	1.92	1.94	0.48	489	45	109	135	-99	60
3.85	4.65	1.94	1.96	0.47	599	50	238	154	74	72
3.85	4.65	1.96	1.98	0.46	440	42	134	133	16	57
3.85	4.65	1.98	2.00	0.44	367	38	-44	124	-158	54

Continued on next page

119

Q_i^2 (GeV^2)	Q_f^2 (GeV^2)	W_i (GeV)	W_f (GeV)	ϵ	σ_o (nb)	$\Delta\sigma_o$ (nb)	σ_{TT} (nb)	$\Delta\sigma_{TT}$ (nb)	σ_{LT} (nb)	$\Delta\sigma_{LT}$ (nb)
3.85	4.65	2.00	2.02	0.43	414	39	10	132	-19	55
3.85	4.65	2.02	2.04	0.42	352	40	301	132	-18	59
3.85	4.65	2.04	2.06	0.41	315	37	51	128	-38	54
3.85	4.65	2.06	2.08	0.40	350	41	161	144	-49	62
3.85	4.65	2.08	2.10	0.38	430	43	-46	153	11	67
4.65	5.15	1.72	1.74	0.47	233	65	-254	197	47	73
4.65	5.15	1.74	1.76	0.46	438	59	44	179	119	70
4.65	5.15	1.76	1.78	0.45	579	62	133	198	52	77
4.65	5.15	1.78	1.80	0.44	655	81	235	249	258	106
4.65	5.15	1.80	1.82	0.43	532	94	148	287	-85	130
4.65	5.15	1.82	1.84	0.42	566	86	480	268	-68	121
4.65	5.15	1.84	1.86	0.41	599	91	431	293	64	131
4.65	5.15	1.86	1.88	0.40	683	98	-66	315	39	139
4.65	5.15	1.88	1.90	0.39	867	106	-565	364	194	153
4.65	5.15	1.90	1.92	0.38	794	111	427	389	55	163
4.65	5.15	1.92	1.94	0.37	927	121	-837	462	115	175
4.65	5.15	1.94	1.96	0.35	971	149	1015	570	590	228
4.65	5.15	1.96	1.98	0.34	88	145	-304	601	64	218
4.65	5.15	1.98	2.00	0.33	0	0	0	0	0	0

APPENDIX E

RESPONSE FUNCTIONS FROM COMBINED FIT OF E16 AND E1F

Measured response functions $\mathscr{R}_o = \mathscr{R}_T + \epsilon_L \mathscr{R}_L$, $\mathscr{R}_{TT}$, and $\mathscr{R}_{TL}$ are tabulated below. They were extracted according to the formulation of Equation 7.4 using a combined fit of E16 and E1F data.

Q_i^2 (GeV^2)	Q_f^2 (GeV^2)	W (GeV)	$\cos\theta^*$	$\mathscr{R}_o$ (nb/sr)	$\Delta\mathscr{R}_o$ (nb/sr)	$\mathscr{R}_{TT}$ (nb/sr)	$\Delta\mathscr{R}_{TT}$ (nb/sr)	$\mathscr{R}_{TL}$ (nb/sr)	$\Delta\mathscr{R}_{TL}$ (nb/sr)
1.85	2.20	1.73	-0.9	468	75	89	146	-32	117
1.85	2.20	1.73	-0.7	557	74	-45	164	-132	123
1.85	2.20	1.73	-0.5	409	75	-261	149	-245	110
1.85	2.20	1.73	-0.3	451	71	324	149	-100	123
1.85	2.20	1.73	-0.1	326	64	-19	131	51	98
1.85	2.20	1.73	0.1	304	66	35	137	189	109
1.85	2.20	1.73	0.3	436	69	122	140	118	114
1.85	2.20	1.73	0.5	521	77	-107	164	38	124
1.85	2.20	1.73	0.7	599	87	141	167	29	134
1.85	2.20	1.73	0.9	638	90	112	197	293	142
1.85	2.20	1.75	-0.9	644	45	-42	96	-93	71
1.85	2.20	1.75	-0.7	521	39	77	82	-88	72
1.85	2.20	1.75	-0.5	495	42	-33	93	-117	74
1.85	2.20	1.75	-0.3	309	34	-101	85	-69	59
1.85	2.20	1.75	-0.1	463	38	-103	84	57	64
1.85	2.20	1.75	0.1	420	38	-43	88	83	63
1.85	2.20	1.75	0.3	459	40	-106	83	206	61
1.85	2.20	1.75	0.5	561	44	46	102	138	76
1.85	2.20	1.75	0.7	720	50	104	104	178	85
1.85	2.20	1.75	0.9	719	50	-198	107	78	80
1.85	2.20	1.77	-0.9	725	41	-58	90	-197	67
1.85	2.20	1.77	-0.7	651	39	83	82	-188	69
1.85	2.20	1.77	-0.5	533	37	-95	86	-208	66
1.85	2.20	1.77	-0.3	509	34	16	79	7	59
1.85	2.20	1.77	-0.1	469	35	-50	79	5	59
1.85	2.20	1.77	0.1	523	37	-28	84	78	65
1.85	2.20	1.77	0.3	557	39	1	84	195	66
1.85	2.20	1.77	0.5	621	40	-74	89	189	64

Q_i^2 (GeV^2)	Q_f^2 (GeV^2)	W (GeV)	$\cos\theta^*$	$\mathscr{R}_o$ (nb/sr)	$\Delta\mathscr{R}_o$ (nb/sr)	$\mathscr{R}_{TT}$ (nb/sr)	$\Delta\mathscr{R}_{TT}$ (nb/sr)	$\mathscr{R}_{TL}$ (nb/sr)	$\Delta\mathscr{R}_{TL}$ (nb/sr)
1.85	2.20	1.77	0.7	794	44	-69	96	181	74
1.85	2.20	1.77	0.9	890	48	-88	112	111	81
1.85	2.20	1.79	-0.9	651	35	90	80	-62	62
1.85	2.20	1.79	-0.7	588	36	-81	79	-223	65
1.85	2.20	1.79	-0.5	526	35	-10	78	-206	62
1.85	2.20	1.79	-0.3	389	33	75	74	-75	58
1.85	2.20	1.79	-0.1	295	37	128	74	5	66
1.85	2.20	1.79	0.1	390	44	74	85	166	66
1.85	2.20	1.79	0.3	456	43	106	91	245	72
1.85	2.20	1.79	0.5	553	47	95	98	118	70
1.85	2.20	1.79	0.7	607	42	116	90	173	66
1.85	2.20	1.79	0.9	690	40	-28	90	84	67
1.85	2.20	1.81	-0.9	591	31	-21	68	-117	52
1.85	2.20	1.81	-0.7	596	31	-53	71	-224	54
1.85	2.20	1.81	-0.5	428	30	97	64	-170	50
1.85	2.20	1.81	-0.3	352	35	127	68	-17	56
1.85	2.20	1.81	-0.1	332	37	54	72	39	54
1.85	2.20	1.81	0.1	246	37	150	69	-11	58
1.85	2.20	1.81	0.3	288	39	144	76	37	61
1.85	2.20	1.81	0.5	441	45	205	88	102	70
1.85	2.20	1.81	0.7	535	42	39	91	-18	62
1.85	2.20	1.81	0.9	651	34	-3	80	-48	60
1.85	2.20	1.83	-0.9	556	27	-86	59	-92	49
1.85	2.20	1.83	-0.7	487	28	28	62	-204	51
1.85	2.20	1.83	-0.5	410	28	64	59	-157	47
1.85	2.20	1.83	-0.3	335	33	245	64	-114	55
1.85	2.20	1.83	-0.1	218	35	97	57	12	48
1.85	2.20	1.83	0.1	232	36	202	63	78	55
1.85	2.20	1.83	0.3	306	44	240	74	-50	66
1.85	2.20	1.83	0.5	278	46	94	75	-8	60
1.85	2.20	1.83	0.7	416	49	56	88	-66	67
1.85	2.20	1.83	0.9	581	31	45	72	-17	54
1.85	2.20	1.85	-0.9	442	24	-24	52	-87	43
1.85	2.20	1.85	-0.7	403	25	107	56	-173	43
1.85	2.20	1.85	-0.5	352	29	85	55	-137	45
1.85	2.20	1.85	-0.3	207	35	100	59	-46	46
1.85	2.20	1.85	-0.1	129	30	80	51	-106	43
1.85	2.20	1.85	0.1	255	41	79	70	130	67
1.85	2.20	1.85	0.3	338	45	280	79	108	75
1.85	2.20	1.85	0.5	440	49	129	85	201	76
1.85	2.20	1.85	0.7	301	42	115	75	-73	65
1.85	2.20	1.85	0.9	525	31	63	74	-151	55
1.85	2.20	1.87	-0.9	363	20	-3	45	3	37
1.85	2.20	1.87	-0.7	319	22	115	51	-120	40
1.85	2.20	1.87	-0.5	257	26	140	52	-17	42
1.85	2.20	1.87	-0.3	206	29	91	55	-96	52
1.85	2.20	1.87	-0.1	129	32	11	58	-43	50
1.85	2.20	1.87	0.1	198	43	78	92	120	86
1.85	2.20	1.87	0.3	176	34	-26	81	-29	70

Continued on next page

Q_i^2 (GeV^2)	Q_f^2 (GeV^2)	W (GeV)	$\cos\theta^*$	$\mathscr{R}_o$ (nb/sr)	$\Delta\mathscr{R}_o$ (nb/sr)	$\mathscr{R}_{TT}$ (nb/sr)	$\Delta\mathscr{R}_{TT}$ (nb/sr)	$\mathscr{R}_{TL}$ (nb/sr)	$\Delta\mathscr{R}_{TL}$ (nb/sr)
1.85	2.20	1.87	0.5	330	35	4	86	-28	78
1.85	2.20	1.87	0.7	396	43	66	85	-76	75
1.85	2.20	1.87	0.9	434	31	100	68	-123	54
1.85	2.20	1.89	-0.9	311	19	-18	43	-50	34
1.85	2.20	1.89	-0.7	299	21	-26	47	5	36
1.85	2.20	1.89	-0.5	261	27	179	52	-158	47
1.85	2.20	1.89	-0.3	200	30	72	55	-82	50
1.85	2.20	1.89	-0.1	156	36	55	63	-16	63
1.85	2.20	1.89	0.1	214	27	42	65	74	57
1.85	2.20	1.89	0.3	261	25	-67	63	114	53
1.85	2.20	1.89	0.5	428	30	34	76	50	64
1.85	2.20	1.89	0.7	426	32	53	83	-53	72
1.85	2.20	1.89	0.9	336	31	55	65	-137	50
1.85	2.20	1.91	-0.9	268	17	72	40	-6	32
1.85	2.20	1.91	-0.7	228	20	33	47	-119	37
1.85	2.20	1.91	-0.5	179	28	41	50	-100	39
1.85	2.20	1.91	-0.3	182	31	-87	62	-135	53
1.85	2.20	1.91	-0.1	225	31	44	62	-43	55
1.85	2.20	1.91	0.1	238	23	-14	57	63	48
1.85	2.20	1.91	0.3	270	21	-4	54	7	45
1.85	2.20	1.91	0.5	393	23	-15	61	51	50
1.85	2.20	1.91	0.7	443	27	99	72	24	60
1.85	2.20	1.91	0.9	318	31	-19	64	-161	52
1.85	2.20	1.93	-0.9	268	16	61	39	10	31
1.85	2.20	1.93	-0.7	205	19	17	42	-56	33
1.85	2.20	1.93	-0.5	171	26	71	46	-121	46
1.85	2.20	1.93	-0.3	225	37	106	71	119	74
1.85	2.20	1.93	-0.1	134	20	-48	49	9	43
1.85	2.20	1.93	0.1	201	18	23	49	71	40
1.85	2.20	1.93	0.3	298	20	66	53	77	46
1.85	2.20	1.93	0.5	360	21	55	58	103	49
1.85	2.20	1.93	0.7	438	24	180	63	2	58
1.85	2.20	1.93	0.9	288	28	-34	59	-115	52
1.85	2.20	1.95	-0.9	184	13	-17	33	-38	26
1.85	2.20	1.95	-0.7	141	18	35	40	-33	33
1.85	2.20	1.95	-0.5	109	24	55	41	-109	40
1.85	2.20	1.95	-0.3	172	28	-4	58	5	53
1.85	2.20	1.95	-0.1	154	18	-22	48	-11	41
1.85	2.20	1.95	0.1	196	16	5	41	69	37
1.85	2.20	1.95	0.3	235	17	87	45	75	41
1.85	2.20	1.95	0.5	284	20	-18	52	-45	46
1.85	2.20	1.95	0.7	373	21	118	53	-36	48
1.85	2.20	1.95	0.9	353	26	2	59	-103	50
1.85	2.20	1.97	-0.9	156	13	-44	30	7	25
1.85	2.20	1.97	-0.7	150	18	-55	40	-82	30
1.85	2.20	1.97	-0.5	119	22	24	46	-55	48
1.85	2.20	1.97	-0.3	157	19	40	47	72	47
1.85	2.20	1.97	-0.1	145	15	54	38	-13	37
1.85	2.20	1.97	0.1	166	16	37	42	72	38

Continued on next page

123

Q_i^2 (GeV^2)	Q_f^2 (GeV^2)	W (GeV)	$\cos\theta^*$	$\mathscr{R}_o$ (nb/sr)	$\Delta\mathscr{R}_o$ (nb/sr)	$\mathscr{R}_{TT}$ (nb/sr)	$\Delta\mathscr{R}_{TT}$ (nb/sr)	$\mathscr{R}_{TL}$ (nb/sr)	$\Delta\mathscr{R}_{TL}$ (nb/sr)
1.85	2.20	1.97	0.3	216	17	61	46	6	43
1.85	2.20	1.97	0.5	259	19	60	49	13	49
1.85	2.20	1.97	0.7	340	20	24	54	-63	49
1.85	2.20	1.97	0.9	339	22	228	59	-68	55
1.85	2.20	1.99	-0.9	135	12	10	27	-50	23
1.85	2.20	1.99	-0.7	91	16	-5	34	-101	27
1.85	2.20	1.99	-0.5	76	25	51	51	-71	56
1.85	2.20	1.99	-0.3	120	16	-100	39	-114	35
1.85	2.20	1.99	-0.1	119	13	53	37	48	33
1.85	2.20	1.99	0.1	149	16	-32	42	38	39
1.85	2.20	1.99	0.3	157	18	-11	44	21	43
1.85	2.20	1.99	0.5	221	22	-13	57	-38	58
1.85	2.20	1.99	0.7	276	21	69	56	-50	55
1.85	2.20	1.99	0.9	342	21	106	57	-28	51
1.85	2.20	2.01	-0.9	114	11	-20	26	-2	21
1.85	2.20	2.01	-0.7	77	14	0	27	-54	24
1.85	2.20	2.01	-0.5	82	21	-8	48	-56	46
1.85	2.20	2.01	-0.3	122	14	60	37	-25	34
1.85	2.20	2.01	-0.1	90	12	68	31	52	32
1.85	2.20	2.01	0.1	154	15	74	41	118	42
1.85	2.20	2.01	0.3	145	18	20	48	-12	49
1.85	2.20	2.01	0.5	241	21	118	58	82	65
1.85	2.20	2.01	0.7	236	21	88	58	20	62
1.85	2.20	2.01	0.9	332	20	185	57	0	53
1.85	2.20	2.03	-0.9	75	9	28	23	-9	21
1.85	2.20	2.03	-0.7	35	13	-38	29	-39	26
1.85	2.20	2.03	-0.5	106	21	27	47	-10	50
1.85	2.20	2.03	-0.3	113	12	-23	34	-18	31
1.85	2.20	2.03	-0.1	83	12	5	31	8	30
1.85	2.20	2.03	0.1	124	16	42	41	-41	42
1.85	2.20	2.03	0.3	141	19	19	53	-22	53
1.85	2.20	2.03	0.5	194	22	100	60	41	65
1.85	2.20	2.03	0.7	166	21	-12	56	-127	58
1.85	2.20	2.03	0.9	284	21	131	59	-8	56
1.85	2.20	2.05	-0.9	46	9	20	20	-29	19
1.85	2.20	2.05	-0.7	45	13	-15	26	-54	24
1.85	2.20	2.05	-0.5	60	17	56	37	5	39
1.85	2.20	2.05	-0.3	85	10	33	28	0	25
1.85	2.20	2.05	-0.1	80	11	-34	32	-28	32
1.85	2.20	2.05	0.1	104	16	68	43	63	50
1.85	2.20	2.05	0.3	146	20	47	52	52	61
1.85	2.20	2.05	0.5	111	18	-14	44	13	47
1.85	2.20	2.05	0.7	162	20	47	49	-54	55
1.85	2.20	2.05	0.9	236	19	106	55	58	57
1.85	2.20	2.07	-0.9	55	8	-11	21	-29	19
1.85	2.20	2.07	-0.7	45	13	4	25	-87	26
1.85	2.20	2.07	-0.5	49	12	12	31	-15	30
1.85	2.20	2.07	-0.3	56	10	48	25	-16	26
1.85	2.20	2.07	-0.1	67	12	42	30	12	32

Continued on next page

Q_i^2 (GeV^2)	Q_f^2 (GeV^2)	W (GeV)	$\cos\theta^*$	$\mathscr{R}_o$ (nb/sr)	$\Delta\mathscr{R}_o$ (nb/sr)	$\mathscr{R}_{TT}$ (nb/sr)	$\Delta\mathscr{R}_{TT}$ (nb/sr)	$\mathscr{R}_{TL}$ (nb/sr)	$\Delta\mathscr{R}_{TL}$ (nb/sr)
1.85	2.20	2.07	0.1	84	15	27	40	40	46
1.85	2.20	2.07	0.3	117	18	-25	51	-61	57
1.85	2.20	2.07	0.5	140	18	-13	41	43	44
1.85	2.20	2.07	0.7	194	19	41	43	-6	46
1.85	2.20	2.07	0.9	264	22	74	57	28	62
1.85	2.20	2.09	-0.9	30	8	15	18	-5	16
1.85	2.20	2.09	-0.7	46	12	25	22	-22	23
1.85	2.20	2.09	-0.5	47	9	-26	27	-79	23
1.85	2.20	2.09	-0.3	58	10	-47	26	-28	27
1.85	2.20	2.09	-0.1	69	9	-45	33	-70	33
1.85	2.20	2.09	0.1	65	14	-43	40	-44	47
1.85	2.20	2.09	0.3	105	14	10	34	-53	38
1.85	2.20	2.09	0.5	163	14	63	35	64	39
1.85	2.20	2.09	0.7	170	14	60	38	-83	41
1.85	2.20	2.09	0.9	224	20	75	54	-38	56
1.85	2.20	2.11	-0.9	65	9	16	22	14	20
1.85	2.20	2.11	-0.7	28	23	10	47	-22	70
1.85	2.20	2.11	-0.5	56	9	14	27	-23	24
1.85	2.20	2.11	-0.3	60	8	27	24	-33	24
1.85	2.20	2.11	-0.1	49	12	-10	31	18	37
1.85	2.20	2.11	0.1	95	11	80	24	130	35
1.85	2.20	2.11	0.3	103	15	10	32	47	35
1.85	2.20	2.11	0.5	117	12	10	30	-67	32
1.85	2.20	2.11	0.7	141	13	59	33	-15	35
1.85	2.20	2.11	0.9	247	20	97	53	-25	55
1.85	2.20	2.13	-0.9	57	8	-21	20	-7	17
1.85	2.20	2.13	-0.7	40	19	-19	44	-32	53
1.85	2.20	2.13	-0.5	48	8	48	22	-16	23
1.85	2.20	2.13	-0.3	41	8	-36	26	-61	26
1.85	2.20	2.13	-0.1	57	12	37	31	-5	36
1.85	2.20	2.13	0.1	59	13	47	31	-22	35
1.85	2.20	2.13	0.3	97	11	33	31	47	35
1.85	2.20	2.13	0.5	111	11	-3	27	-15	31
1.85	2.20	2.13	0.7	129	11	-1	28	-10	30
1.85	2.20	2.13	0.9	238	18	113	51	75	56
1.85	2.20	2.15	-0.9	31	7	-1	18	-29	17
1.85	2.20	2.15	-0.7	18	19	-26	41	-52	56
1.85	2.20	2.15	-0.5	34	7	24	21	-35	20
1.85	2.20	2.15	-0.3	39	8	-89	25	-60	25
1.85	2.20	2.15	-0.1	36	11	-16	29	-68	36
1.85	2.20	2.15	0.1	58	12	-6	29	-48	32
1.85	2.20	2.15	0.3	83	10	7	27	-41	30
1.85	2.20	2.15	0.5	107	11	34	28	-43	31
1.85	2.20	2.15	0.7	118	10	3	26	-32	29
1.85	2.20	2.15	0.9	255	18	66	49	-10	54
1.85	2.20	2.17	-0.9	44	8	-14	19	-12	19
1.85	2.20	2.17	-0.7	24	12	0	28	-12	34
1.85	2.20	2.17	-0.5	25	7	-8	20	-27	19
1.85	2.20	2.17	-0.3	38	8	-16	24	-41	26

Continued on next page

Q_i^2 (GeV^2)	Q_f^2 (GeV^2)	W (GeV)	$\cos\theta^*$	$\mathscr{R}_o$ (nb/sr)	$\Delta\mathscr{R}_o$ (nb/sr)	$\mathscr{R}_{TT}$ (nb/sr)	$\Delta\mathscr{R}_{TT}$ (nb/sr)	$\mathscr{R}_{TL}$ (nb/sr)	$\Delta\mathscr{R}_{TL}$ (nb/sr)
1.85	2.20	2.17	-0.1	36	10	14	26	-33	31
1.85	2.20	2.17	0.1	59	12	28	26	44	33
1.85	2.20	2.17	0.3	58	12	31	25	92	30
1.85	2.20	2.17	0.5	92	10	-11	25	-55	27
1.85	2.20	2.17	0.7	125	11	33	29	-82	33
1.85	2.20	2.17	0.9	195	15	-27	39	24	42
1.85	2.20	2.19	-0.9	44	7	21	17	3	17
1.85	2.20	2.19	-0.7	3	7	-38	22	-59	23
1.85	2.20	2.19	-0.5	34	7	19	19	24	23
1.85	2.20	2.19	-0.3	9	11	60	24	25	29
1.85	2.20	2.19	-0.1	8	9	-44	25	-13	32
1.85	2.20	2.19	0.1	43	9	21	23	9	27
1.85	2.20	2.19	0.3	62	9	54	25	36	29
1.85	2.20	2.19	0.5	93	9	48	24	-60	28
1.85	2.20	2.19	0.7	88	10	-13	27	16	30
1.85	2.20	2.19	0.9	233	16	35	45	59	50
1.85	2.20	2.21	-0.9	54	7	-8	17	-54	17
1.85	2.20	2.21	-0.7	17	12	-6	24	6	34
1.85	2.20	2.21	-0.5	32	6	2	19	-6	20
1.85	2.20	2.21	-0.3	39	7	0	23	-7	26
1.85	2.20	2.21	-0.1	27	7	24	20	-7	22
1.85	2.20	2.21	0.1	39	8	14	20	40	25
1.85	2.20	2.21	0.3	69	8	-8	23	5	26
1.85	2.20	2.21	0.5	34	2	-16	18	-61	18
1.85	2.20	2.21	0.7	101	9	-17	26	-51	30
1.85	2.20	2.21	0.9	255	15	4	41	-117	46
1.85	2.20	2.23	-0.9	22	6	5	15	-2	16
1.85	2.20	2.23	-0.7	17	11	-25	28	-46	37
1.85	2.20	2.23	-0.5	18	6	5	17	-6	19
1.85	2.20	2.23	-0.3	11	7	-1	21	-8	27
1.85	2.20	2.23	-0.1	25	7	0	18	-37	21
1.85	2.20	2.23	0.1	33	7	16	19	18	23
1.85	2.20	2.23	0.3	49	8	-7	22	19	24
1.85	2.20	2.23	0.5	60	7	47	21	-41	25
1.85	2.20	2.23	0.7	76	8	0	23	-81	28
1.85	2.20	2.23	0.9	241	15	-3	40	62	45
1.85	2.20	2.25	-0.9	28	5	-25	19	-65	15
1.85	2.20	2.25	-0.7	13	9	-14	24	8	31
1.85	2.20	2.25	-0.5	16	6	-1	20	-25	21
1.85	2.20	2.25	-0.3	12	6	-52	20	-51	23
1.85	2.20	2.25	-0.1	41	5	14	17	19	23
1.85	2.20	2.25	0.1	11	6	-19	16	10	19
1.85	2.20	2.25	0.3	56	7	20	18	3	22
1.85	2.20	2.25	0.5	50	6	2	17	-22	21
1.85	2.20	2.25	0.7	65	8	-6	21	2	25
1.85	2.20	2.25	0.9	249	14	-59	42	-36	47
1.85	2.20	2.27	-0.9	27	5	21	15	-42	16
1.85	2.20	2.27	-0.7	7	5	-4	15	-40	16
1.85	2.20	2.27	-0.5	15	6	1	19	26	24

Continued on next page

Q_i^2 (GeV^2)	Q_f^2 (GeV^2)	W (GeV)	$\cos\theta^*$	$\mathscr{R}_o$ (nb/sr)	$\Delta\mathscr{R}_o$ (nb/sr)	$\mathscr{R}_{TT}$ (nb/sr)	$\Delta\mathscr{R}_{TT}$ (nb/sr)	$\mathscr{R}_{TL}$ (nb/sr)	$\Delta\mathscr{R}_{TL}$ (nb/sr)
1.85	2.20	2.27	-0.3	24	7	4	20	30	30
1.85	2.20	2.27	-0.1	22	6	16	17	-52	21
1.85	2.20	2.27	0.1	33	6	27	15	55	21
1.85	2.20	2.27	0.3	38	5	-16	17	-15	19
1.85	2.20	2.27	0.5	41	6	-13	17	-8	20
1.85	2.20	2.27	0.7	78	8	21	24	-2	29
1.85	2.20	2.27	0.9	240	13	45	40	76	46
1.85	2.20	2.29	-0.9	30	7	24	16	-36	20
1.85	2.20	2.29	-0.7	11	6	-2	18	-22	25
1.85	2.20	2.29	-0.5	11	5	-23	18	-4	20
1.85	2.20	2.29	-0.3	8	5	-11	20	-52	25
1.85	2.20	2.29	-0.1	8	4	-7	13	-17	17
1.85	2.20	2.29	0.1	24	5	26	14	19	17
1.85	2.20	2.29	0.3	26	5	0	17	13	19
1.85	2.20	2.29	0.5	34	5	12	16	-43	21
1.85	2.20	2.29	0.7	78	7	20	20	-20	26
1.85	2.20	2.29	0.9	237	14	7	40	49	45
1.85	2.20	2.31	-0.9	33	6	-9	17	-36	14
1.85	2.20	2.31	-0.7	16	6	5	19	-15	26
1.85	2.20	2.31	-0.5	6	4	-6	12	7	16
1.85	2.20	2.31	-0.3	4	4	0	14	0	20
1.85	2.20	2.31	-0.1	9	4	2	11	-32	14
1.85	2.20	2.31	0.1	23	4	6	12	9	15
1.85	2.20	2.31	0.3	27	5	2	15	-1	18
1.85	2.20	2.31	0.5	34	5	-2	16	-22	20
1.85	2.20	2.31	0.7	54	7	-5	20	-30	26
1.85	2.20	2.31	0.9	253	13	23	40	-1	47
1.85	2.20	2.33	-0.9	24	7	9	19	-6	20
1.85	2.20	2.33	-0.7	12	4	39	18	16	26
1.85	2.20	2.33	-0.5	3	3	0	12	4	16
1.85	2.20	2.33	-0.3	22	5	8	14	4	17
1.85	2.20	2.33	-0.1	5	3	6	11	17	13
1.85	2.20	2.33	0.1	15	4	12	14	15	17
1.85	2.20	2.33	0.3	28	4	17	13	-17	16
1.85	2.20	2.33	0.5	29	5	31	15	-24	19
1.85	2.20	2.33	0.7	65	7	5	21	-9	27
1.85	2.20	2.33	0.9	250	12	9	38	65	44
1.85	2.20	2.35	-0.9	35	10	17	23	41	33
1.85	2.20	2.35	-0.7	10	5	13	13	-3	21
1.85	2.20	2.35	-0.5	6	3	-1	11	13	12
1.85	2.20	2.35	-0.3	-3	4	-16	11	-36	16
1.85	2.20	2.35	-0.1	0	3	-1	9	0	11
1.85	2.20	2.35	0.1	8	3	-6	11	0	13
1.85	2.20	2.35	0.3	13	4	0	14	-29	16
1.85	2.20	2.35	0.5	22	4	-21	15	-3	19
1.85	2.20	2.35	0.7	63	6	0	20	-54	26
1.85	2.20	2.35	0.9	244	12	-67	41	-3	45
1.85	2.20	2.37	-0.9	32	10	32	20	24	29
1.85	2.20	2.37	-0.7	6	4	5	15	-3	20

Continued on next page

Q_i^2 (GeV^2)	Q_f^2 (GeV^2)	W (GeV)	$\cos\theta^*$	$\mathscr{R}_o$ (nb/sr)	$\Delta\mathscr{R}_o$ (nb/sr)	$\mathscr{R}_{TT}$ (nb/sr)	$\Delta\mathscr{R}_{TT}$ (nb/sr)	$\mathscr{R}_{TL}$ (nb/sr)	$\Delta\mathscr{R}_{TL}$ (nb/sr)
1.85	2.20	2.37	-0.5	7	4	-3	11	22	18
1.85	2.20	2.37	-0.3	7	3	2	10	-19	13
1.85	2.20	2.37	-0.1	3	3	0	10	-17	13
1.85	2.20	2.37	0.1	12	2	3	12	12	15
1.85	2.20	2.37	0.3	19	3	-3	12	-22	14
1.85	2.20	2.37	0.5	39	6	-20	13	-23	17
1.85	2.20	2.37	0.7	52	6	-16	19	-6	25
1.85	2.20	2.37	0.9	271	13	-8	40	-27	49
1.85	2.20	2.39	-0.9	22	26	61	34	42	62
1.85	2.20	2.39	-0.7	3	3	16	11	-5	14
1.85	2.20	2.39	-0.5	4	4	-10	13	-15	18
1.85	2.20	2.39	-0.3	1	3	0	10	1	15
1.85	2.20	2.39	-0.1	3	2	-6	8	2	10
1.85	2.20	2.39	0.1	4	3	-5	10	19	11
1.85	2.20	2.39	0.3	14	3	3	13	4	17
1.85	2.20	2.39	0.5	20	4	-9	12	1	17
1.85	2.20	2.39	0.7	56	6	-29	19	-34	24
1.85	2.20	2.39	0.9	209	12	-32	37	-73	45
1.85	2.20	2.41	-0.9	9	20	24	33	16	67
1.85	2.20	2.41	-0.7	13	5	6	14	-2	22
1.85	2.20	2.41	-0.5	0	4	-17	11	-17	17
1.85	2.20	2.41	-0.3	8	2	6	7	14	10
1.85	2.20	2.41	-0.1	6	3	10	9	3	11
1.85	2.20	2.41	0.1	2	2	14	9	6	10
1.85	2.20	2.41	0.3	9	3	13	10	26	13
1.85	2.20	2.41	0.5	13	3	-8	12	-7	14
1.85	2.20	2.41	0.7	48	6	7	20	-6	26
1.85	2.20	2.41	0.9	228	12	-62	37	-43	44
1.85	2.20	2.43	-0.9	10	19	-17	27	-11	52
1.85	2.20	2.43	-0.7	8	3	6	11	-7	17
1.85	2.20	2.43	-0.5	11	5	9	14	1	23
1.85	2.20	2.43	-0.3	1	2	-1	7	-1	10
1.85	2.20	2.43	-0.1	0	1	-15	6	-9	7
1.85	2.20	2.43	0.1	3	2	1	9	1	11
1.85	2.20	2.43	0.3	9	3	7	10	-11	11
1.85	2.20	2.43	0.5	14	3	-27	12	15	15
1.85	2.20	2.43	0.7	48	5	0	19	-38	24
1.85	2.20	2.43	0.9	222	11	-17	38	-27	45
1.85	2.20	2.45	-0.9	-5	18	-23	23	-61	21
1.85	2.20	2.45	-0.7	5	3	2	14	8	19
1.85	2.20	2.45	-0.5	-4	6	-11	12	-23	22
1.85	2.20	2.45	-0.3	1	1	-3	5	-1	6
1.85	2.20	2.45	-0.1	0	2	-7	7	-19	9
1.85	2.20	2.45	0.1	0	2	-4	7	-13	9
1.85	2.20	2.45	0.3	9	2	-4	10	-6	11
1.85	2.20	2.45	0.5	18	3	-1	13	23	15
1.85	2.20	2.45	0.7	53	5	-11	20	-50	25
1.85	2.20	2.45	0.9	241	12	-22	42	-35	50
1.85	2.20	2.47	-0.9	2	17	7	51	-17	107

Continued on next page

128

Q_i^2 (GeV^2)	Q_f^2 (GeV^2)	W (GeV)	$\cos\theta^*$	$\mathscr{R}_o$ (nb/sr)	$\Delta\mathscr{R}_o$ (nb/sr)	$\mathscr{R}_{TT}$ (nb/sr)	$\Delta\mathscr{R}_{TT}$ (nb/sr)	$\mathscr{R}_{TL}$ (nb/sr)	$\Delta\mathscr{R}_{TL}$ (nb/sr)
1.85	2.20	2.47	-0.7	1	2	-10	12	-24	12
1.85	2.20	2.47	-0.5	0	3	-5	11	-8	18
1.85	2.20	2.47	-0.3	-2	1	-5	6	0	7
1.85	2.20	2.47	-0.1	1	1	0	6	-3	7
1.85	2.20	2.47	0.1	4	2	3	8	-13	10
1.85	2.20	2.47	0.3	0	2	-18	8	5	10
1.85	2.20	2.47	0.5	11	2	0	11	-17	14
1.85	2.20	2.47	0.7	48	5	4	19	34	25
1.85	2.20	2.47	0.9	184	10	-70	40	25	46
1.85	2.20	2.49	-0.9	13	15	20	23	30	42
1.85	2.20	2.49	-0.7	7	3	14	11	-16	15
1.85	2.20	2.49	-0.5	2	5	15	13	11	21
1.85	2.20	2.49	-0.3	0	1	1	8	21	10
1.85	2.20	2.49	-0.1	1	1	0	5	13	7
1.85	2.20	2.49	0.1	4	2	9	8	23	10
1.85	2.20	2.49	0.3	4	2	-13	8	3	10
1.85	2.20	2.49	0.5	8	2	8	11	-5	14
1.85	2.20	2.49	0.7	46	5	-14	19	-61	26
1.85	2.20	2.49	0.9	202	11	-2	43	-90	52
1.85	2.20	2.51	-0.9	7	13	-10	27	-50	43
1.85	2.20	2.51	-0.7	1	2	9	11	-1	13
1.85	2.20	2.51	-0.5	4	8	10	11	19	21
1.85	2.20	2.51	-0.3	-1	1	-7	5	2	6
1.85	2.20	2.51	-0.1	0	1	-3	5	-4	7
1.85	2.20	2.51	0.1	2	2	-8	7	11	8
1.85	2.20	2.51	0.3	2	2	-7	11	-8	12
1.85	2.20	2.51	0.5	8	2	-3	12	3	14
1.85	2.20	2.51	0.7	33	4	15	16	-36	23
1.85	2.20	2.51	0.9	178	10	-85	44	-94	50
1.85	2.20	2.53	-0.9	0	7	25	22	18	43
1.85	2.20	2.53	-0.7	-1	2	-9	9	-6	12
1.85	2.20	2.53	-0.5	2	2	2	10	-2	13
1.85	2.20	2.53	-0.3	0	1	1	5	-2	6
1.85	2.20	2.53	-0.1	0	1	12	6	-3	8
1.85	2.20	2.53	0.1	2	1	-12	6	-7	7
1.85	2.20	2.53	0.3	-1	1	-3	10	14	10
1.85	2.20	2.53	0.5	11	2	-33	10	7	13
1.85	2.20	2.53	0.7	32	4	12	19	2	25
1.85	2.20	2.53	0.9	184	10	91	46	-41	57
1.85	2.20	2.55	-0.9	0	5	9	18	-19	24
1.85	2.20	2.55	-0.7	0	4	7	13	-11	22
1.85	2.20	2.55	-0.5	2	3	7	16	17	25
1.85	2.20	2.55	-0.3	-1	1	-1	4	0	6
1.85	2.20	2.55	-0.1	0	1	-8	5	-3	6
1.85	2.20	2.55	0.1	2	1	1	6	18	9
1.85	2.20	2.55	0.3	2	2	-15	10	-6	11
1.85	2.20	2.55	0.5	6	2	-12	10	5	14
1.85	2.20	2.55	0.7	31	4	-38	22	5	28
1.85	2.20	2.55	0.9	211	11	15	50	-214	61

Continued on next page

129

Q_i^2 (GeV^2)	Q_f^2 (GeV^2)	W (GeV)	$\cos\theta^*$	$\mathscr{R}_o$ (nb/sr)	$\Delta\mathscr{R}_o$ (nb/sr)	$\mathscr{R}_{TT}$ (nb/sr)	$\Delta\mathscr{R}_{TT}$ (nb/sr)	$\mathscr{R}_{TL}$ (nb/sr)	$\Delta\mathscr{R}_{TL}$ (nb/sr)
1.85	2.20	2.57	-0.9	-7	7	-10	22	-29	41
1.85	2.20	2.57	-0.7	2	3	10	17	10	28
1.85	2.20	2.57	-0.5	-1	2	5	11	-7	18
1.85	2.20	2.57	-0.3	0	1	-1	5	4	6
1.85	2.20	2.57	-0.1	-2	1	-1	4	-3	5
1.85	2.20	2.57	0.1	-1	1	5	6	-2	7
1.85	2.20	2.57	0.3	1	1	0	10	9	11
1.85	2.20	2.57	0.5	12	3	-7	13	-25	17
1.85	2.20	2.57	0.7	32	4	-8	20	-41	29
1.85	2.20	2.57	0.9	188	11	87	56	-48	66
1.85	2.20	2.59	-0.9	-1	13	30	30	33	63
1.85	2.20	2.59	-0.7	10	10	27	7	14	13
1.85	2.20	2.59	-0.5	3	6	16	6	31	9
1.85	2.20	2.59	-0.3	2	1	0	8	-15	8
1.85	2.20	2.59	-0.1	-1	1	-4	4	1	5
1.85	2.20	2.59	0.1	1	1	-13	8	8	8
1.85	2.20	2.59	0.3	7	1	2	10	-20	11
1.85	2.20	2.59	0.5	11	2	-8	12	-19	16
1.85	2.20	2.59	0.7	24	4	-23	23	-4	28
1.85	2.20	2.59	0.9	178	10	79	52	-42	63
2.20	2.50	1.73	-0.9	344	57	-37	151	-38	112
2.20	2.50	1.73	-0.7	465	85	89	154	51	119
2.20	2.50	1.73	-0.5	330	56	234	160	36	122
2.20	2.50	1.73	-0.3	242	56	-73	132	-34	108
2.20	2.50	1.73	-0.1	233	60	-81	171	111	113
2.20	2.50	1.73	0.1	222	58	92	141	0	111
2.20	2.50	1.73	0.3	283	58	83	137	146	95
2.20	2.50	1.73	0.5	328	63	38	159	76	123
2.20	2.50	1.73	0.7	473	75	-8	205	212	157
2.20	2.50	1.73	0.9	451	71	-168	186	94	131
2.20	2.50	1.75	-0.9	456	39	87	113	-81	78
2.20	2.50	1.75	-0.7	374	36	82	84	-39	71
2.20	2.50	1.75	-0.5	294	32	-25	91	-36	65
2.20	2.50	1.75	-0.3	251	32	55	89	-5	71
2.20	2.50	1.75	-0.1	271	30	6	74	47	58
2.20	2.50	1.75	0.1	297	32	-11	78	114	64
2.20	2.50	1.75	0.3	339	33	-49	94	10	65
2.20	2.50	1.75	0.5	430	36	-12	97	150	72
2.20	2.50	1.75	0.7	478	38	72	95	86	74
2.20	2.50	1.75	0.9	609	45	-26	125	6	91
2.20	2.50	1.77	-0.9	555	35	-31	94	57	72
2.20	2.50	1.77	-0.7	474	35	42	89	-41	67
2.20	2.50	1.77	-0.5	376	31	-71	85	-148	66
2.20	2.50	1.77	-0.3	333	30	102	85	-98	68
2.20	2.50	1.77	-0.1	332	32	-108	89	-25	67
2.20	2.50	1.77	0.1	334	32	-9	98	165	66
2.20	2.50	1.77	0.3	304	32	-31	87	99	61
2.20	2.50	1.77	0.5	444	36	-164	96	222	71
2.20	2.50	1.77	0.7	507	37	-51	106	81	75

Continued on next page

Q_i^2 (GeV^2)	Q_f^2 (GeV^2)	W (GeV)	$\cos\theta^*$	$\mathscr{R}_o$ (nb/sr)	$\Delta\mathscr{R}_o$ (nb/sr)	$\mathscr{R}_{TT}$ (nb/sr)	$\Delta\mathscr{R}_{TT}$ (nb/sr)	$\mathscr{R}_{TL}$ (nb/sr)	$\Delta\mathscr{R}_{TL}$ (nb/sr)
2.20	2.50	1.77	0.9	578	39	88	101	-33	81
2.20	2.50	1.79	-0.9	464	30	25	78	17	62
2.20	2.50	1.79	-0.7	409	29	10	74	-31	58
2.20	2.50	1.79	-0.5	363	28	122	75	-158	60
2.20	2.50	1.79	-0.3	275	27	32	71	-143	57
2.20	2.50	1.79	-0.1	236	27	79	70	-16	57
2.20	2.50	1.79	0.1	287	30	64	81	111	67
2.20	2.50	1.79	0.3	302	32	-108	86	2	64
2.20	2.50	1.79	0.5	351	34	-39	96	80	70
2.20	2.50	1.79	0.7	432	32	42	91	75	68
2.20	2.50	1.79	0.9	512	35	-35	95	-3	68
2.20	2.50	1.81	-0.9	459	28	22	66	-81	56
2.20	2.50	1.81	-0.7	406	26	130	63	-206	55
2.20	2.50	1.81	-0.5	325	25	83	69	-65	52
2.20	2.50	1.81	-0.3	264	24	203	61	-66	50
2.20	2.50	1.81	-0.1	186	26	136	71	-20	53
2.20	2.50	1.81	0.1	215	31	69	74	40	51
2.20	2.50	1.81	0.3	233	33	-75	79	-11	55
2.20	2.50	1.81	0.5	366	35	-3	80	15	64
2.20	2.50	1.81	0.7	376	32	1	89	62	65
2.20	2.50	1.81	0.9	485	30	-112	83	5	57
2.20	2.50	1.83	-0.9	402	23	96	58	-55	51
2.20	2.50	1.83	-0.7	366	23	-29	64	-98	47
2.20	2.50	1.83	-0.5	294	23	15	63	-108	46
2.20	2.50	1.83	-0.3	186	24	17	56	-102	43
2.20	2.50	1.83	-0.1	163	25	110	61	-67	46
2.20	2.50	1.83	0.1	173	31	125	69	-38	54
2.20	2.50	1.83	0.3	186	30	-28	72	-5	51
2.20	2.50	1.83	0.5	266	43	38	76	58	60
2.20	2.50	1.83	0.7	403	36	152	85	44	68
2.20	2.50	1.83	0.9	423	27	123	76	-4	58
2.20	2.50	1.85	-0.9	369	21	30	54	-22	42
2.20	2.50	1.85	-0.7	295	20	74	58	-59	45
2.20	2.50	1.85	-0.5	264	23	25	62	-100	45
2.20	2.50	1.85	-0.3	180	23	114	53	-51	42
2.20	2.50	1.85	-0.1	166	27	76	59	-32	50
2.20	2.50	1.85	0.1	142	29	-21	66	83	57
2.20	2.50	1.85	0.3	199	40	22	69	161	71
2.20	2.50	1.85	0.5	234	34	87	72	-130	68
2.20	2.50	1.85	0.7	318	35	159	80	40	71
2.20	2.50	1.85	0.9	326	24	-15	71	-59	50
2.20	2.50	1.87	-0.9	272	17	-5	45	-26	36
2.20	2.50	1.87	-0.7	258	19	-68	53	7	36
2.20	2.50	1.87	-0.5	202	21	32	49	-99	39
2.20	2.50	1.87	-0.3	176	24	49	57	-120	44
2.20	2.50	1.87	-0.1	169	28	40	56	-16	49
2.20	2.50	1.87	0.1	102	24	-33	61	-11	60
2.20	2.50	1.87	0.3	195	29	-125	71	-53	60
2.20	2.50	1.87	0.5	209	30	68	70	-65	69

Continued on next page

Q_i^2 (GeV^2)	Q_f^2 (GeV^2)	W (GeV)	$\cos\theta^*$	$\mathscr{R}_o$ (nb/sr)	$\Delta\mathscr{R}_o$ (nb/sr)	$\mathscr{R}_{TT}$ (nb/sr)	$\Delta\mathscr{R}_{TT}$ (nb/sr)	$\mathscr{R}_{TL}$ (nb/sr)	$\Delta\mathscr{R}_{TL}$ (nb/sr)
2.20	2.50	1.87	0.7	284	32	-7	78	-12	61
2.20	2.50	1.87	0.9	327	24	37	64	30	52
2.20	2.50	1.89	-0.9	222	16	58	41	-54	32
2.20	2.50	1.89	-0.7	234	18	33	49	-76	36
2.20	2.50	1.89	-0.5	178	23	-14	49	-96	39
2.20	2.50	1.89	-0.3	188	26	29	56	-43	49
2.20	2.50	1.89	-0.1	59	22	27	51	-67	43
2.20	2.50	1.89	0.1	137	24	-14	61	-24	52
2.20	2.50	1.89	0.3	168	25	93	59	37	58
2.20	2.50	1.89	0.5	245	26	22	73	78	62
2.20	2.50	1.89	0.7	254	30	2	69	-165	62
2.20	2.50	1.89	0.9	271	24	25	64	-51	51
2.20	2.50	1.91	-0.9	209	15	5	41	42	30
2.20	2.50	1.91	-0.7	150	16	26	41	-48	32
2.20	2.50	1.91	-0.5	156	19	16	42	-75	34
2.20	2.50	1.91	-0.3	139	23	37	46	-192	45
2.20	2.50	1.91	-0.1	93	26	113	50	65	48
2.20	2.50	1.91	0.1	150	21	46	56	117	48
2.20	2.50	1.91	0.3	167	19	67	57	164	54
2.20	2.50	1.91	0.5	231	20	96	62	137	54
2.20	2.50	1.91	0.7	306	26	118	72	-60	61
2.20	2.50	1.91	0.9	237	23	34	67	-41	55
2.20	2.50	1.93	-0.9	173	13	-61	35	-57	26
2.20	2.50	1.93	-0.7	169	15	54	40	-12	31
2.20	2.50	1.93	-0.5	175	19	67	43	-81	36
2.20	2.50	1.93	-0.3	84	23	6	43	-41	39
2.20	2.50	1.93	-0.1	91	20	-1	51	28	45
2.20	2.50	1.93	0.1	155	17	54	51	51	45
2.20	2.50	1.93	0.3	185	17	72	49	85	43
2.20	2.50	1.93	0.5	242	17	106	51	72	43
2.20	2.50	1.93	0.7	259	19	126	59	100	53
2.20	2.50	1.93	0.9	265	22	-62	53	-72	45
2.20	2.50	1.95	-0.9	139	12	39	33	12	26
2.20	2.50	1.95	-0.7	150	15	56	35	-31	29
2.20	2.50	1.95	-0.5	101	18	-38	40	-112	36
2.20	2.50	1.95	-0.3	88	16	-23	39	-99	33
2.20	2.50	1.95	-0.1	112	17	-40	44	0	40
2.20	2.50	1.95	0.1	142	15	-16	42	56	35
2.20	2.50	1.95	0.3	133	15	83	47	59	39
2.20	2.50	1.95	0.5	259	17	109	51	64	47
2.20	2.50	1.95	0.7	249	17	20	55	5	46
2.20	2.50	1.95	0.9	193	19	-12	56	-63	50
2.20	2.50	1.97	-0.9	138	12	24	30	-60	25
2.20	2.50	1.97	-0.7	108	14	-32	34	-20	26
2.20	2.50	1.97	-0.5	102	18	79	40	-47	38
2.20	2.50	1.97	-0.3	87	16	51	38	-7	36
2.20	2.50	1.97	-0.1	95	15	58	42	4	36
2.20	2.50	1.97	0.1	125	14	25	43	-21	34
2.20	2.50	1.97	0.3	166	14	44	42	60	38

Continued on next page

Q_i^2	Q_f^2	W	$\cos\theta^*$	$\mathscr{R}_o$	$\Delta\mathscr{R}_o$	$\mathscr{R}_{TT}$	$\Delta\mathscr{R}_{TT}$	$\mathscr{R}_{TL}$	$\Delta\mathscr{R}_{TL}$
(GeV^2)	(GeV^2)	(GeV)		(nb/sr)	(nb/sr)	(nb/sr)	(nb/sr)	(nb/sr)	(nb/sr)
2.20	2.50	1.97	0.5	198	16	51	50	32	46
2.20	2.50	1.97	0.7	226	15	67	49	-24	43
2.20	2.50	1.97	0.9	197	18	86	50	-106	44
2.20	2.50	1.99	-0.9	117	11	16	29	-24	24
2.20	2.50	1.99	-0.7	104	14	26	36	3	29
2.20	2.50	1.99	-0.5	97	16	-50	34	11	33
2.20	2.50	1.99	-0.3	101	16	11	41	-16	39
2.20	2.50	1.99	-0.1	92	12	58	35	20	32
2.20	2.50	1.99	0.1	107	13	50	40	18	34
2.20	2.50	1.99	0.3	130	14	40	44	104	41
2.20	2.50	1.99	0.5	167	16	55	48	-35	46
2.20	2.50	1.99	0.7	196	16	29	48	-137	45
2.20	2.50	1.99	0.9	212	18	-1	51	-59	46
2.20	2.50	2.01	-0.9	77	10	0	27	-26	21
2.20	2.50	2.01	-0.7	60	13	-4	29	-65	27
2.20	2.50	2.01	-0.5	64	21	7	49	-99	49
2.20	2.50	2.01	-0.3	100	14	24	38	-20	33
2.20	2.50	2.01	-0.1	77	11	72	35	35	33
2.20	2.50	2.01	0.1	99	13	-81	42	9	37
2.20	2.50	2.01	0.3	115	14	41	42	-15	42
2.20	2.50	2.01	0.5	166	18	32	49	-21	49
2.20	2.50	2.01	0.7	164	16	32	49	-116	46
2.20	2.50	2.01	0.9	229	18	111	52	-32	48
2.20	2.50	2.03	-0.9	51	8	-5	22	-3	18
2.20	2.50	2.03	-0.7	65	11	5	24	-20	22
2.20	2.50	2.03	-0.5	54	14	52	42	-30	43
2.20	2.50	2.03	-0.3	67	10	-3	31	-13	28
2.20	2.50	2.03	-0.1	73	11	17	32	54	30
2.20	2.50	2.03	0.1	75	12	23	37	-9	38
2.20	2.50	2.03	0.3	93	16	11	44	5	46
2.20	2.50	2.03	0.5	153	17	131	57	83	61
2.20	2.50	2.03	0.7	152	18	-8	53	-78	54
2.20	2.50	2.03	0.9	217	17	-8	56	48	51
2.20	2.50	2.05	-0.9	53	8	14	21	-1	17
2.20	2.50	2.05	-0.7	31	11	-12	26	-49	24
2.20	2.50	2.05	-0.5	67	13	11	39	-2	42
2.20	2.50	2.05	-0.3	70	11	29	31	-4	28
2.20	2.50	2.05	-0.1	49	10	26	29	-55	29
2.20	2.50	2.05	0.1	76	14	-18	38	-20	37
2.20	2.50	2.05	0.3	97	15	63	49	60	55
2.20	2.50	2.05	0.5	131	16	4	43	-134	47
2.20	2.50	2.05	0.7	130	18	0	50	-79	54
2.20	2.50	2.05	0.9	227	18	125	57	-1	56
2.20	2.50	2.07	-0.9	48	7	6	21	-39	18
2.20	2.50	2.07	-0.7	37	11	34	21	-46	24
2.20	2.50	2.07	-0.5	36	11	-3	31	-14	30
2.20	2.50	2.07	-0.3	34	8	-18	27	-78	26
2.20	2.50	2.07	-0.1	58	10	49	28	49	28
2.20	2.50	2.07	0.1	75	12	-34	36	-22	39

Continued on next page

133

Q_i^2 (GeV^2)	Q_f^2 (GeV^2)	W (GeV)	$\cos\theta^*$	$\mathscr{R}_o$ (nb/sr)	$\Delta\mathscr{R}_o$ (nb/sr)	$\mathscr{R}_{TT}$ (nb/sr)	$\Delta\mathscr{R}_{TT}$ (nb/sr)	$\mathscr{R}_{TL}$ (nb/sr)	$\Delta\mathscr{R}_{TL}$ (nb/sr)
2.20	2.50	2.07	0.3	84	16	-15	44	0	48
2.20	2.50	2.07	0.5	102	14	51	35	-36	38
2.20	2.50	2.07	0.7	89	16	-22	42	-96	41
2.20	2.50	2.07	0.9	136	15	-70	48	-94	48
2.20	2.50	2.09	-0.9	36	7	-3	22	-34	18
2.20	2.50	2.09	-0.7	36	11	-49	23	-29	23
2.20	2.50	2.09	-0.5	47	11	37	27	-9	28
2.20	2.50	2.09	-0.3	58	9	21	26	-5	25
2.20	2.50	2.09	-0.1	39	10	-5	28	19	29
2.20	2.50	2.09	0.1	66	13	63	40	-17	45
2.20	2.50	2.09	0.3	77	14	25	37	3	42
2.20	2.50	2.09	0.5	119	15	20	37	-1	39
2.20	2.50	2.09	0.7	109	14	58	37	-37	39
2.20	2.50	2.09	0.9	191	18	8	55	-6	57
2.20	2.50	2.11	-0.9	23	6	-6	17	22	16
2.20	2.50	2.11	-0.7	54	12	-34	24	-6	23
2.20	2.50	2.11	-0.5	39	9	-11	22	-68	20
2.20	2.50	2.11	-0.3	30	7	11	24	-5	26
2.20	2.50	2.11	-0.1	49	10	37	28	47	28
2.20	2.50	2.11	0.1	90	36	83	38	61	46
2.20	2.50	2.11	0.3	81	12	-42	31	-68	34
2.20	2.50	2.11	0.5	102	11	88	32	9	35
2.20	2.50	2.11	0.7	110	11	1	34	32	34
2.20	2.50	2.11	0.9	167	18	79	53	12	56
2.20	2.50	2.13	-0.9	31	6	17	17	11	18
2.20	2.50	2.13	-0.7	46	19	53	44	4	57
2.20	2.50	2.13	-0.5	43	7	4	25	-28	24
2.20	2.50	2.13	-0.3	30	7	-5	18	-41	19
2.20	2.50	2.13	-0.1	36	9	56	29	43	35
2.20	2.50	2.13	0.1	54	11	18	31	42	36
2.20	2.50	2.13	0.3	83	12	103	31	14	36
2.20	2.50	2.13	0.5	80	10	3	28	3	30
2.20	2.50	2.13	0.7	96	11	45	34	-4	34
2.20	2.50	2.13	0.9	139	18	101	52	36	58
2.20	2.50	2.15	-0.9	18	5	-11	15	-25	14
2.20	2.50	2.15	-0.7	27	14	-8	31	4	40
2.20	2.50	2.15	-0.5	17	6	-11	17	-26	16
2.20	2.50	2.15	-0.3	34	7	-26	21	-57	20
2.20	2.50	2.15	-0.1	14	8	-26	29	34	34
2.20	2.50	2.15	0.1	48	10	30	26	49	30
2.20	2.50	2.15	0.3	75	12	11	28	21	29
2.20	2.50	2.15	0.5	85	9	58	27	-35	29
2.20	2.50	2.15	0.7	99	10	9	29	-7	31
2.20	2.50	2.15	0.9	154	14	64	47	67	50
2.20	2.50	2.17	-0.9	34	6	-35	17	-22	15
2.20	2.50	2.17	-0.7	28	35	50	21	68	20
2.20	2.50	2.17	-0.5	29	8	-24	22	-38	22
2.20	2.50	2.17	-0.3	24	5	-36	16	-26	16
2.20	2.50	2.17	-0.1	24	8	-45	29	-66	33

Continued on next page

Q_i^2 (GeV²)	Q_f^2 (GeV²)	W (GeV)	$\cos\theta^*$	$\mathcal{R}_o$ (nb/sr)	$\Delta\mathcal{R}_o$ (nb/sr)	$\mathcal{R}_{TT}$ (nb/sr)	$\Delta\mathcal{R}_{TT}$ (nb/sr)	$\mathcal{R}_{TL}$ (nb/sr)	$\Delta\mathcal{R}_{TL}$ (nb/sr)
2.20	2.50	2.17	0.1	44	11	33	25	-3	28
2.20	2.50	2.17	0.3	54	9	24	23	40	27
2.20	2.50	2.17	0.5	78	8	35	25	-21	27
2.20	2.50	2.17	0.7	91	9	79	29	-31	31
2.20	2.50	2.17	0.9	167	13	-40	39	-23	39
2.20	2.50	2.19	-0.9	26	5	0	17	-10	15
2.20	2.50	2.19	-0.7	34	30	39	19	68	19
2.20	2.50	2.19	-0.5	17	5	-7	20	-24	21
2.20	2.50	2.19	-0.3	20	6	-3	17	-28	18
2.20	2.50	2.19	-0.1	19	8	30	25	-45	30
2.20	2.50	2.19	0.1	24	7	22	22	15	23
2.20	2.50	2.19	0.3	47	7	29	23	16	25
2.20	2.50	2.19	0.5	51	7	45	24	-54	26
2.20	2.50	2.19	0.7	67	8	2	28	13	28
2.20	2.50	2.19	0.9	146	12	24	39	-13	41
2.20	2.50	2.21	-0.9	25	6	-13	18	-21	16
2.20	2.50	2.21	-0.7	14	10	-9	23	-3	29
2.20	2.50	2.21	-0.5	21	5	32	20	36	21
2.20	2.50	2.21	-0.3	26	7	28	23	18	28
2.20	2.50	2.21	-0.1	7	7	-23	23	-56	25
2.20	2.50	2.21	0.1	20	7	-1	20	-31	24
2.20	2.50	2.21	0.3	50	7	-14	21	35	22
2.20	2.50	2.21	0.5	37	6	-16	22	-36	24
2.20	2.50	2.21	0.7	64	7	-10	23	-22	26
2.20	2.50	2.21	0.9	155	12	-18	37	-22	40
2.20	2.50	2.23	-0.9	19	5	0	18	20	19
2.20	2.50	2.23	-0.7	21	21	7	22	42	35
2.20	2.50	2.23	-0.5	21	6	26	18	11	22
2.20	2.50	2.23	-0.3	26	8	20	22	17	26
2.20	2.50	2.23	-0.1	11	5	-9	15	-40	15
2.20	2.50	2.23	0.1	23	5	6	17	11	18
2.20	2.50	2.23	0.3	59	7	49	20	45	24
2.20	2.50	2.23	0.5	38	6	21	22	-10	25
2.20	2.50	2.23	0.7	60	7	14	25	-9	28
2.20	2.50	2.23	0.9	179	12	41	39	13	43
2.20	2.50	2.25	-0.9	21	5	-14	19	-13	18
2.20	2.50	2.25	-0.7	2	5	9	25	-29	30
2.20	2.50	2.25	-0.5	14	6	10	17	-5	20
2.20	2.50	2.25	-0.3	12	6	-8	19	8	24
2.20	2.50	2.25	-0.1	5	7	7	16	0	20
2.20	2.50	2.25	0.1	16	5	-12	15	-16	16
2.20	2.50	2.25	0.3	50	6	-1	21	-3	23
2.20	2.50	2.25	0.5	30	5	-16	21	-14	24
2.20	2.50	2.25	0.7	56	7	-17	23	-15	27
2.20	2.50	2.25	0.9	169	12	-18	37	-20	41
2.20	2.50	2.27	-0.9	15	4	9	15	-20	16
2.20	2.50	2.27	-0.7	15	6	10	17	14	23
2.20	2.50	2.27	-0.5	13	5	-22	16	-21	19
2.20	2.50	2.27	-0.3	13	5	20	18	-8	21

Continued on next page

Q_i^2 (GeV^2)	Q_f^2 (GeV^2)	W (GeV)	$\cos\theta^*$	$\mathscr{R}_o$ (nb/sr)	$\Delta\mathscr{R}_o$ (nb/sr)	$\mathscr{R}_{TT}$ (nb/sr)	$\Delta\mathscr{R}_{TT}$ (nb/sr)	$\mathscr{R}_{TL}$ (nb/sr)	$\Delta\mathscr{R}_{TL}$ (nb/sr)
2.20	2.50	2.27	-0.1	1	4	2	15	-3	19
2.20	2.50	2.27	0.1	27	5	0	16	23	19
2.20	2.50	2.27	0.3	20	5	-6	18	8	20
2.20	2.50	2.27	0.5	38	5	11	20	-3	21
2.20	2.50	2.27	0.7	54	6	20	23	-24	27
2.20	2.50	2.27	0.9	156	11	39	40	51	42
2.20	2.50	2.29	-0.9	13	6	-9	17	-19	18
2.20	2.50	2.29	-0.7	7	5	-33	18	-40	19
2.20	2.50	2.29	-0.5	14	4	36	15	3	17
2.20	2.50	2.29	-0.3	7	4	-3	16	-27	20
2.20	2.50	2.29	-0.1	1	3	1	14	-26	14
2.20	2.50	2.29	0.1	12	4	1	13	-8	15
2.20	2.50	2.29	0.3	25	4	15	18	39	21
2.20	2.50	2.29	0.5	27	5	2	18	12	21
2.20	2.50	2.29	0.7	53	6	16	22	-39	25
2.20	2.50	2.29	0.9	160	10	-101	38	-21	42
2.20	2.50	2.31	-0.9	32	7	9	21	-27	21
2.20	2.50	2.31	-0.7	3	4	2	13	-24	20
2.20	2.50	2.31	-0.5	0	6	18	10	43	11
2.20	2.50	2.31	-0.3	5	5	-18	20	-4	24
2.20	2.50	2.31	-0.1	4	4	3	13	-15	16
2.20	2.50	2.31	0.1	18	4	-2	15	1	17
2.20	2.50	2.31	0.3	14	3	1	17	-28	19
2.20	2.50	2.31	0.5	26	5	2	19	4	21
2.20	2.50	2.31	0.7	56	6	35	25	-28	28
2.20	2.50	2.31	0.9	157	10	8	42	-51	46
2.20	2.50	2.33	-0.9	20	7	13	18	-55	20
2.20	2.50	2.33	-0.7	-1	3	22	17	-6	21
2.20	2.50	2.33	-0.5	0	3	24	15	26	22
2.20	2.50	2.33	-0.3	5	6	29	15	6	21
2.20	2.50	2.33	-0.1	5	3	10	12	-16	15
2.20	2.50	2.33	0.1	7	3	17	12	33	15
2.20	2.50	2.33	0.3	7	3	-11	16	4	18
2.20	2.50	2.33	0.5	20	4	7	22	-9	24
2.20	2.50	2.33	0.7	52	6	41	24	-38	29
2.20	2.50	2.33	0.9	158	10	-76	40	29	45
2.20	2.50	2.35	-0.9	19	11	-8	27	9	37
2.20	2.50	2.35	-0.7	11	4	23	24	29	33
2.20	2.50	2.35	-0.5	3	3	5	13	-22	14
2.20	2.50	2.35	-0.3	12	5	11	13	14	19
2.20	2.50	2.35	-0.1	11	4	3	12	0	15
2.20	2.50	2.35	0.1	4	3	-2	13	2	12
2.20	2.50	2.35	0.3	13	3	-9	13	-16	15
2.20	2.50	2.35	0.5	14	4	-8	17	-26	19
2.20	2.50	2.35	0.7	45	6	-21	26	-40	33
2.20	2.50	2.35	0.9	160	10	-39	42	-24	47
2.20	2.50	2.37	-0.9	17	25	14	24	76	22
2.20	2.50	2.37	-0.7	-6	4	-10	12	-13	18
2.20	2.50	2.37	-0.5	-2	2	0	14	-6	21

Continued on next page

Q_i^2 (GeV^2)	Q_f^2 (GeV^2)	W (GeV)	$\cos\theta^*$	$\mathscr{R}_o$ (nb/sr)	$\Delta\mathscr{R}_o$ (nb/sr)	$\mathscr{R}_{TT}$ (nb/sr)	$\Delta\mathscr{R}_{TT}$ (nb/sr)	$\mathscr{R}_{TL}$ (nb/sr)	$\Delta\mathscr{R}_{TL}$ (nb/sr)
2.20	2.50	2.37	-0.3	7	4	20	12	7	15
2.20	2.50	2.37	-0.1	3	2	11	15	26	23
2.20	2.50	2.37	0.1	4	3	-1	10	9	10
2.20	2.50	2.37	0.3	8	3	-30	15	-8	16
2.20	2.50	2.37	0.5	18	4	33	18	-41	20
2.20	2.50	2.37	0.7	40	5	-46	23	-12	29
2.20	2.50	2.37	0.9	150	10	-7	45	3	55
2.20	2.50	2.39	-0.9	4	8	-26	24	-52	34
2.20	2.50	2.39	-0.7	-3	3	-12	16	-17	17
2.20	2.50	2.39	-0.5	0	2	26	7	28	10
2.20	2.50	2.39	-0.3	1	3	-1	10	-9	12
2.20	2.50	2.39	-0.1	-1	2	-6	7	4	10
2.20	2.50	2.39	0.1	3	2	-10	11	-4	13
2.20	2.50	2.39	0.3	8	2	-3	15	5	17
2.20	2.50	2.39	0.5	18	4	-3	20	-21	21
2.20	2.50	2.39	0.7	38	4	-12	24	-58	24
2.20	2.50	2.39	0.9	151	10	4	47	-30	56
2.20	2.50	2.41	-0.9	-3	18	59	34	100	31
2.20	2.50	2.41	-0.7	1	2	-3	16	-18	16
2.20	2.50	2.41	-0.5	4	4	0	21	8	28
2.20	2.50	2.41	-0.3	-2	3	-8	9	-9	14
2.20	2.50	2.41	-0.1	-1	2	-4	8	7	10
2.20	2.50	2.41	0.1	0	2	19	11	2	11
2.20	2.50	2.41	0.3	5	2	-3	12	-21	13
2.20	2.50	2.41	0.5	13	3	17	21	-7	22
2.20	2.50	2.41	0.7	46	5	-5	26	-54	34
2.20	2.50	2.41	0.9	152	11	-116	48	-53	59
2.20	2.50	2.43	-0.9	15	27	-9	28	-105	32
2.20	2.50	2.43	-0.7	2	3	-3	16	0	23
2.20	2.50	2.43	-0.5	-4	3	7	20	-5	34
2.20	2.50	2.43	-0.3	-1	2	-1	12	-1	17
2.20	2.50	2.43	-0.1	-2	2	-4	10	0	10
2.20	2.50	2.43	0.1	1	2	-5	11	-13	12
2.20	2.50	2.43	0.3	1	2	-6	13	-16	14
2.20	2.50	2.43	0.5	9	3	0	16	-2	20
2.20	2.50	2.43	0.7	35	5	-37	26	-11	32
2.20	2.50	2.43	0.9	122	11	-78	43	-152	54
2.20	2.50	2.45	-0.9	6	24	6	35	76	30
2.20	2.50	2.45	-0.7	0	4	-10	17	-10	18
2.20	2.50	2.45	-0.5	6	3	24	21	45	31
2.20	2.50	2.45	-0.3	0	3	-4	13	-8	20
2.20	2.50	2.45	-0.1	-1	2	-2	9	8	11
2.20	2.50	2.45	0.1	3	2	4	9	-17	11
2.20	2.50	2.45	0.3	0	2	20	18	-3	20
2.20	2.50	2.45	0.5	6	2	15	16	-9	19
2.20	2.50	2.45	0.7	26	5	26	32	-18	39
2.20	2.50	2.45	0.9	143	9	-82	48	-78	58
2.20	2.50	2.47	-0.9	-7	10	0	26	-26	47
2.20	2.50	2.47	-0.7	1	5	0	21	-12	24

Continued on next page

Q_i^2 (GeV^2)	Q_f^2 (GeV^2)	W (GeV)	$\cos\theta^*$	$\mathscr{R}_o$ (nb/sr)	$\Delta\mathscr{R}_o$ (nb/sr)	$\mathscr{R}_{TT}$ (nb/sr)	$\Delta\mathscr{R}_{TT}$ (nb/sr)	$\mathscr{R}_{TL}$ (nb/sr)	$\Delta\mathscr{R}_{TL}$ (nb/sr)
2.20	2.50	2.47	-0.5	0	4	3	15	-12	22
2.20	2.50	2.47	-0.3	-4	5	0	19	26	36
2.20	2.50	2.47	-0.1	0	1	-7	9	1	8
2.20	2.50	2.47	0.1	1	1	0	8	3	8
2.20	2.50	2.47	0.3	0	2	5	10	47	13
2.20	2.50	2.47	0.5	7	2	-22	18	-7	19
2.20	2.50	2.47	0.7	25	5	-22	23	-16	33
2.20	2.50	2.47	0.9	133	6	-182	60	-115	59
2.20	2.50	2.49	-0.9	6	22	-67	52	-125	49
2.20	2.50	2.49	-0.7	5	7	11	12	37	11
2.20	2.50	2.49	-0.5	0	2	20	5	5	13
2.20	2.50	2.49	-0.3	-1	3	7	14	4	19
2.20	2.50	2.49	-0.1	0	1	0	13	-5	10
2.20	2.50	2.49	0.1	-1	1	8	10	2	8
2.20	2.50	2.49	0.3	2	1	0	11	-13	15
2.20	2.50	2.49	0.5	14	3	-20	17	-3	21
2.20	2.50	2.49	0.7	32	4	-35	24	-12	30
2.20	2.50	2.49	0.9	137	9	-118	50	-94	60
2.20	2.50	2.51	-0.9	-5	6	-66	47	-105	55
2.20	2.50	2.51	-0.7	7	11	53	14	52	20
2.20	2.50	2.51	-0.5	-2	2	-1	14	-8	21
2.20	2.50	2.51	-0.3	0	2	-11	9	-3	9
2.20	2.50	2.51	-0.1	-1	1	-4	8	-4	9
2.20	2.50	2.51	0.1	0	1	-1	9	-3	11
2.20	2.50	2.51	0.3	1	2	-8	13	27	15
2.20	2.50	2.51	0.5	12	2	25	20	-27	21
2.20	2.50	2.51	0.7	26	4	-32	25	24	34
2.20	2.50	2.51	0.9	150	10	-38	57	-1	68
2.20	2.50	2.53	-0.9	-7	8	54	21	76	24
2.20	2.50	2.53	-0.7	11	11	44	12	42	16
2.20	2.50	2.53	-0.5	7	8	18	9	31	10
2.20	2.50	2.53	-0.3	-2	1	1	6	-3	7
2.20	2.50	2.53	-0.1	0	1	1	8	9	11
2.20	2.50	2.53	0.1	0	1	3	9	0	8
2.20	2.50	2.53	0.3	3	1	0	12	27	13
2.20	2.50	2.53	0.5	12	2	22	18	-50	20
2.20	2.50	2.53	0.7	17	4	-2	26	-66	37
2.20	2.50	2.53	0.9	144	10	-90	61	-17	71
2.20	2.50	2.55	-0.9	-5	8	25	39	16	59
2.20	2.50	2.55	-0.7	-1	6	20	40	49	73
2.20	2.50	2.55	-0.5	-4	2	-21	12	-23	16
2.20	2.50	2.55	-0.3	-2	1	3	8	-10	9
2.20	2.50	2.55	-0.1	0	1	5	7	-18	8
2.20	2.50	2.55	0.1	0	1	-11	6	-2	6
2.20	2.50	2.55	0.3	0	1	13	9	-21	14
2.20	2.50	2.55	0.5	9	2	-21	18	23	19
2.20	2.50	2.55	0.7	21	4	5	25	-20	35
2.20	2.50	2.55	0.9	134	9	-239	56	-20	61
2.20	2.50	2.57	-0.9	-13	16	-66	33	-100	31

Continued on next page

Q_i^2 (GeV^2)	Q_f^2 (GeV^2)	W (GeV)	$\cos\theta^*$	$\mathscr{R}_o$ (nb/sr)	$\Delta\mathscr{R}_o$ (nb/sr)	$\mathscr{R}_{TT}$ (nb/sr)	$\Delta\mathscr{R}_{TT}$ (nb/sr)	$\mathscr{R}_{TL}$ (nb/sr)	$\Delta\mathscr{R}_{TL}$ (nb/sr)
2.20	2.50	2.57	-0.7	4	5	-29	28	-43	47
2.20	2.50	2.57	-0.5	0	3	-13	4	-17	9
2.20	2.50	2.57	-0.3	-4	1	2	7	7	10
2.20	2.50	2.57	-0.1	0	1	-3	7	9	8
2.20	2.50	2.57	0.1	4	1	18	9	-1	12
2.20	2.50	2.57	0.3	5	1	25	9	-2	10
2.20	2.50	2.57	0.5	11	2	44	10	13	21
2.20	2.50	2.57	0.7	21	4	-47	25	-10	33
2.20	2.50	2.57	0.9	160	11	7	63	-27	74
2.20	2.50	2.59	-0.9	-1	9	-21	78	-70	95
2.20	2.50	2.59	-0.7	8	11	49	27	80	24
2.20	2.50	2.59	-0.5	-1	5	-16	5	-46	16
2.20	2.50	2.59	-0.3	1	4	1	13	7	26
2.20	2.50	2.59	-0.1	1	2	4	8	0	10
2.20	2.50	2.59	0.1	-1	1	-1	9	0	7
2.20	2.50	2.59	0.3	4	1	-7	13	4	14
2.20	2.50	2.59	0.5	3	2	0	13	-5	17
2.20	2.50	2.59	0.7	23	4	-36	25	-11	37
2.20	2.50	2.59	0.9	127	10	-33	61	-118	70
2.50	2.90	1.73	-0.9	334	43	59	121	-217	88
2.50	2.90	1.73	-0.7	293	41	180	111	-23	85
2.50	2.90	1.73	-0.5	128	31	-22	87	-69	64
2.50	2.90	1.73	-0.3	191	37	-81	101	-28	72
2.50	2.90	1.73	-0.1	279	40	-94	118	166	84
2.50	2.90	1.73	0.1	266	42	-158	117	70	84
2.50	2.90	1.73	0.3	260	41	-122	123	167	81
2.50	2.90	1.73	0.5	312	44	-71	122	282	90
2.50	2.90	1.73	0.7	369	51	151	152	-73	114
2.50	2.90	1.73	0.9	442	51	-258	139	115	96
2.50	2.90	1.75	-0.9	425	27	103	77	4	55
2.50	2.90	1.75	-0.7	289	24	124	65	-89	53
2.50	2.90	1.75	-0.5	277	24	-113	67	-48	45
2.50	2.90	1.75	-0.3	240	23	50	60	-45	48
2.50	2.90	1.75	-0.1	223	22	-91	72	-16	50
2.50	2.90	1.75	0.1	295	26	75	73	63	56
2.50	2.90	1.75	0.3	292	25	-82	69	29	50
2.50	2.90	1.75	0.5	337	26	118	70	190	53
2.50	2.90	1.75	0.7	446	30	92	80	99	64
2.50	2.90	1.75	0.9	444	31	21	83	-46	60
2.50	2.90	1.77	-0.9	447	24	-22	66	-84	49
2.50	2.90	1.77	-0.7	347	22	0	66	-88	49
2.50	2.90	1.77	-0.5	264	20	29	53	-14	43
2.50	2.90	1.77	-0.3	210	21	-33	55	-24	40
2.50	2.90	1.77	-0.1	203	19	75	55	-91	45
2.50	2.90	1.77	0.1	232	21	32	60	17	46
2.50	2.90	1.77	0.3	266	22	55	63	-17	50
2.50	2.90	1.77	0.5	298	23	135	69	50	51
2.50	2.90	1.77	0.7	350	22	-73	65	43	45
2.50	2.90	1.77	0.9	445	25	67	68	-40	54

Continued on next page

Q_i^2 (GeV^2)	Q_f^2 (GeV^2)	W (GeV)	$\cos\theta^*$	$\mathscr{R}_o$ (nb/sr)	$\Delta\mathscr{R}_o$ (nb/sr)	$\mathscr{R}_{TT}$ (nb/sr)	$\Delta\mathscr{R}_{TT}$ (nb/sr)	$\mathscr{R}_{TL}$ (nb/sr)	$\Delta\mathscr{R}_{TL}$ (nb/sr)
2.50	2.90	1.79	-0.9	410	21	-28	61	-80	43
2.50	2.90	1.79	-0.7	341	21	38	56	-33	42
2.50	2.90	1.79	-0.5	274	20	28	57	-54	42
2.50	2.90	1.79	-0.3	263	20	-32	52	-45	40
2.50	2.90	1.79	-0.1	227	20	52	56	-15	41
2.50	2.90	1.79	0.1	165	20	-10	55	89	39
2.50	2.90	1.79	0.3	235	22	68	60	69	43
2.50	2.90	1.79	0.5	283	23	32	66	101	47
2.50	2.90	1.79	0.7	343	24	90	68	87	50
2.50	2.90	1.79	0.9	350	22	35	59	-35	47
2.50	2.90	1.81	-0.9	368	18	58	48	-70	38
2.50	2.90	1.81	-0.7	313	18	8	49	-83	35
2.50	2.90	1.81	-0.5	278	18	99	50	-73	38
2.50	2.90	1.81	-0.3	183	17	88	48	-74	37
2.50	2.90	1.81	-0.1	163	17	-27	48	-3	36
2.50	2.90	1.81	0.1	161	19	145	51	57	40
2.50	2.90	1.81	0.3	223	21	175	57	76	43
2.50	2.90	1.81	0.5	212	22	78	58	-46	43
2.50	2.90	1.81	0.7	303	22	57	64	0	49
2.50	2.90	1.81	0.9	417	20	30	58	33	44
2.50	2.90	1.83	-0.9	364	17	-61	47	12	35
2.50	2.90	1.83	-0.7	311	17	12	51	-82	34
2.50	2.90	1.83	-0.5	243	17	59	48	0	34
2.50	2.90	1.83	-0.3	158	16	64	45	-98	33
2.50	2.90	1.83	-0.1	135	18	70	45	-23	36
2.50	2.90	1.83	0.1	143	18	28	45	16	34
2.50	2.90	1.83	0.3	184	21	70	51	-1	43
2.50	2.90	1.83	0.5	244	23	105	58	-43	48
2.50	2.90	1.83	0.7	275	22	96	59	-63	45
2.50	2.90	1.83	0.9	336	18	73	55	-62	42
2.50	2.90	1.85	-0.9	274	15	-28	41	-61	28
2.50	2.90	1.85	-0.7	216	14	79	41	-24	30
2.50	2.90	1.85	-0.5	171	15	38	40	-31	29
2.50	2.90	1.85	-0.3	130	15	80	40	-57	33
2.50	2.90	1.85	-0.1	110	17	72	41	-57	35
2.50	2.90	1.85	0.1	133	20	-24	44	-22	37
2.50	2.90	1.85	0.3	151	19	50	45	89	42
2.50	2.90	1.85	0.5	150	20	-7	47	-53	40
2.50	2.90	1.85	0.7	223	21	8	52	-53	42
2.50	2.90	1.85	0.9	273	16	43	48	-89	37
2.50	2.90	1.87	-0.9	222	13	0	37	-95	28
2.50	2.90	1.87	-0.7	196	13	9	39	-37	28
2.50	2.90	1.87	-0.5	154	14	25	39	-89	28
2.50	2.90	1.87	-0.3	114	15	54	39	-113	31
2.50	2.90	1.87	-0.1	93	18	55	39	-25	36
2.50	2.90	1.87	0.1	63	17	-71	47	-111	41
2.50	2.90	1.87	0.3	92	18	-57	50	-43	43
2.50	2.90	1.87	0.5	149	19	0	53	-52	49
2.50	2.90	1.87	0.7	199	20	-62	54	-27	44

Continued on next page

140

Q_i^2 (GeV^2)	Q_f^2 (GeV^2)	W (GeV)	$\cos\theta^*$	$\mathscr{R}_o$ (nb/sr)	$\Delta\mathscr{R}_o$ (nb/sr)	$\mathscr{R}_{TT}$ (nb/sr)	$\Delta\mathscr{R}_{TT}$ (nb/sr)	$\mathscr{R}_{TL}$ (nb/sr)	$\Delta\mathscr{R}_{TL}$ (nb/sr)
2.50	2.90	1.87	0.9	218	16	46	46	-113	36
2.50	2.90	1.89	-0.9	217	13	64	34	-22	27
2.50	2.90	1.89	-0.7	185	13	9	38	-15	28
2.50	2.90	1.89	-0.5	122	14	-22	38	-82	29
2.50	2.90	1.89	-0.3	111	17	11	41	-93	37
2.50	2.90	1.89	-0.1	62	16	16	43	-102	37
2.50	2.90	1.89	0.1	104	17	-16	50	-6	45
2.50	2.90	1.89	0.3	166	20	45	57	108	49
2.50	2.90	1.89	0.5	200	20	23	55	-59	48
2.50	2.90	1.89	0.7	164	21	9	55	-114	51
2.50	2.90	1.89	0.9	183	16	94	45	-98	36
2.50	2.90	1.91	-0.9	170	11	40	32	-61	26
2.50	2.90	1.91	-0.7	149	12	21	33	-64	25
2.50	2.90	1.91	-0.5	141	14	-3	35	-61	29
2.50	2.90	1.91	-0.3	82	13	-15	36	-76	30
2.50	2.90	1.91	-0.1	57	14	-19	44	-120	37
2.50	2.90	1.91	0.1	88	14	-59	47	-48	34
2.50	2.90	1.91	0.3	124	15	-53	46	48	38
2.50	2.90	1.91	0.5	185	16	50	50	21	43
2.50	2.90	1.91	0.7	226	20	11	60	48	56
2.50	2.90	1.91	0.9	193	15	79	45	-150	37
2.50	2.90	1.93	-0.9	122	10	57	27	-1	23
2.50	2.90	1.93	-0.7	142	11	46	31	50	25
2.50	2.90	1.93	-0.5	120	15	40	36	-74	30
2.50	2.90	1.93	-0.3	88	14	-9	33	-68	31
2.50	2.90	1.93	-0.1	101	14	98	42	73	39
2.50	2.90	1.93	0.1	122	14	-29	40	16	34
2.50	2.90	1.93	0.3	147	12	25	39	96	34
2.50	2.90	1.93	0.5	151	13	-15	45	-59	36
2.50	2.90	1.93	0.7	234	15	33	50	16	42
2.50	2.90	1.93	0.9	174	15	11	45	-121	39
2.50	2.90	1.95	-0.9	135	10	31	30	-2	23
2.50	2.90	1.95	-0.7	99	10	-14	30	-50	24
2.50	2.90	1.95	-0.5	78	12	-26	29	-76	23
2.50	2.90	1.95	-0.3	78	11	-19	42	-24	39
2.50	2.90	1.95	-0.1	103	13	-5	38	-60	32
2.50	2.90	1.95	0.1	96	11	-28	38	9	31
2.50	2.90	1.95	0.3	146	12	73	40	108	34
2.50	2.90	1.95	0.5	195	12	-2	45	-11	37
2.50	2.90	1.95	0.7	188	13	66	45	-19	38
2.50	2.90	1.95	0.9	182	15	-83	45	-69	36
2.50	2.90	1.97	-0.9	104	8	-8	25	-18	19
2.50	2.90	1.97	-0.7	97	10	-58	28	-48	21
2.50	2.90	1.97	-0.5	100	12	-34	31	-35	26
2.50	2.90	1.97	-0.3	87	13	-62	39	-52	34
2.50	2.90	1.97	-0.1	76	9	-5	30	-6	26
2.50	2.90	1.97	0.1	109	11	78	37	88	33
2.50	2.90	1.97	0.3	154	11	-37	38	2	33
2.50	2.90	1.97	0.5	168	12	75	41	111	39

Continued on next page

Q_i^2 (GeV^2)	Q_f^2 (GeV^2)	W (GeV)	$\cos\theta^*$	$\mathscr{R}_o$ (nb/sr)	$\Delta\mathscr{R}_o$ (nb/sr)	$\mathscr{R}_{TT}$ (nb/sr)	$\Delta\mathscr{R}_{TT}$ (nb/sr)	$\mathscr{R}_{TL}$ (nb/sr)	$\Delta\mathscr{R}_{TL}$ (nb/sr)
2.50	2.90	1.97	0.7	195	11	66	40	-1	34
2.50	2.90	1.97	0.9	171	13	0	45	-41	39
2.50	2.90	1.99	-0.9	80	8	-13	21	-15	19
2.50	2.90	1.99	-0.7	86	10	26	27	-43	23
2.50	2.90	1.99	-0.5	51	11	-55	29	-66	29
2.50	2.90	1.99	-0.3	71	11	0	36	-36	31
2.50	2.90	1.99	-0.1	94	10	11	33	46	29
2.50	2.90	1.99	0.1	75	9	26	33	44	29
2.50	2.90	1.99	0.3	88	10	-28	34	22	30
2.50	2.90	1.99	0.5	142	11	110	43	45	40
2.50	2.90	1.99	0.7	168	11	40	42	-6	37
2.50	2.90	1.99	0.9	141	12	-36	42	-9	35
2.50	2.90	2.01	-0.9	57	7	0	19	-69	17
2.50	2.90	2.01	-0.7	65	9	22	26	-30	20
2.50	2.90	2.01	-0.5	41	11	-10	33	-80	33
2.50	2.90	2.01	-0.3	54	9	40	29	-62	25
2.50	2.90	2.01	-0.1	66	8	-10	31	-14	26
2.50	2.90	2.01	0.1	63	8	-65	29	-24	25
2.50	2.90	2.01	0.3	79	10	-6	34	-9	33
2.50	2.90	2.01	0.5	113	11	-35	39	-71	37
2.50	2.90	2.01	0.7	140	11	10	45	-10	42
2.50	2.90	2.01	0.9	164	12	32	45	-69	37
2.50	2.90	2.03	-0.9	52	7	18	21	7	17
2.50	2.90	2.03	-0.7	38	8	18	22	-30	20
2.50	2.90	2.03	-0.5	58	9	47	39	39	42
2.50	2.90	2.03	-0.3	45	8	7	25	-5	22
2.50	2.90	2.03	-0.1	70	8	9	26	-12	24
2.50	2.90	2.03	0.1	74	9	35	33	87	31
2.50	2.90	2.03	0.3	63	10	56	39	10	38
2.50	2.90	2.03	0.5	109	12	20	41	-35	42
2.50	2.90	2.03	0.7	148	12	36	46	-34	46
2.50	2.90	2.03	0.9	177	12	60	46	4	41
2.50	2.90	2.05	-0.9	25	6	21	20	-8	16
2.50	2.90	2.05	-0.7	21	7	12	23	-28	22
2.50	2.90	2.05	-0.5	54	10	-17	31	-16	29
2.50	2.90	2.05	-0.3	48	7	11	26	-19	23
2.50	2.90	2.05	-0.1	40	7	-36	27	9	24
2.50	2.90	2.05	0.1	49	8	-65	31	-57	27
2.50	2.90	2.05	0.3	85	11	-44	38	-63	39
2.50	2.90	2.05	0.5	110	12	-2	42	-110	41
2.50	2.90	2.05	0.7	132	13	20	51	-53	51
2.50	2.90	2.05	0.9	130	11	14	42	11	39
2.50	2.90	2.07	-0.9	36	6	1	17	-12	14
2.50	2.90	2.07	-0.7	31	7	27	23	-43	22
2.50	2.90	2.07	-0.5	33	7	-9	26	-15	27
2.50	2.90	2.07	-0.3	33	6	-5	24	-4	21
2.50	2.90	2.07	-0.1	47	7	-6	27	-4	26
2.50	2.90	2.07	0.1	44	9	29	29	40	30
2.50	2.90	2.07	0.3	76	11	-28	41	-17	43

Continued on next page

Q_i^2 (GeV^2)	Q_f^2 (GeV^2)	W (GeV)	$\cos\theta^*$	$\mathscr{R}_o$ (nb/sr)	$\Delta\mathscr{R}_o$ (nb/sr)	$\mathscr{R}_{TT}$ (nb/sr)	$\Delta\mathscr{R}_{TT}$ (nb/sr)	$\mathscr{R}_{TL}$ (nb/sr)	$\Delta\mathscr{R}_{TL}$ (nb/sr)
2.50	2.90	2.07	0.5	83	12	57	39	25	39
2.50	2.90	2.07	0.7	82	12	8	39	-101	40
2.50	2.90	2.07	0.9	130	11	72	48	36	45
2.50	2.90	2.09	-0.9	32	6	-4	19	-2	16
2.50	2.90	2.09	-0.7	38	8	45	22	-2	26
2.50	2.90	2.09	-0.5	30	9	-11	30	16	30
2.50	2.90	2.09	-0.3	33	6	-34	21	-17	18
2.50	2.90	2.09	-0.1	23	6	-2	26	0	26
2.50	2.90	2.09	0.1	47	12	83	23	70	28
2.50	2.90	2.09	0.3	77	10	87	36	73	40
2.50	2.90	2.09	0.5	86	10	40	40	19	40
2.50	2.90	2.09	0.7	133	13	139	41	61	48
2.50	2.90	2.09	0.9	125	12	23	49	10	51
2.50	2.90	2.11	-0.9	29	5	-24	19	-9	16
2.50	2.90	2.11	-0.7	8	6	-56	20	-59	22
2.50	2.90	2.11	-0.5	34	8	18	25	10	25
2.50	2.90	2.11	-0.3	12	5	-5	20	-38	18
2.50	2.90	2.11	-0.1	37	7	35	27	7	27
2.50	2.90	2.11	0.1	39	9	9	37	17	43
2.50	2.90	2.11	0.3	60	9	-32	29	0	33
2.50	2.90	2.11	0.5	59	7	-1	27	-102	27
2.50	2.90	2.11	0.7	99	9	4	29	-51	30
2.50	2.90	2.11	0.9	146	12	74	50	92	50
2.50	2.90	2.13	-0.9	27	6	17	17	-24	16
2.50	2.90	2.13	-0.7	32	13	0	28	11	35
2.50	2.90	2.13	-0.5	17	5	-1	19	-32	16
2.50	2.90	2.13	-0.3	26	6	-43	23	-81	20
2.50	2.90	2.13	-0.1	28	7	-88	31	-32	32
2.50	2.90	2.13	0.1	39	10	-9	35	28	38
2.50	2.90	2.13	0.3	56	8	-12	30	-47	31
2.50	2.90	2.13	0.5	57	7	-53	28	23	27
2.50	2.90	2.13	0.7	68	8	57	30	-27	31
2.50	2.90	2.13	0.9	114	12	31	46	9	50
2.50	2.90	2.15	-0.9	19	5	-19	19	-39	15
2.50	2.90	2.15	-0.7	29	14	-56	35	7	46
2.50	2.90	2.15	-0.5	8	4	-22	18	-27	16
2.50	2.90	2.15	-0.3	19	4	32	20	-11	19
2.50	2.90	2.15	-0.1	5	6	-11	28	-27	29
2.50	2.90	2.15	0.1	46	8	18	28	16	30
2.50	2.90	2.15	0.3	52	8	-14	27	-63	26
2.50	2.90	2.15	0.5	50	7	-34	26	-21	25
2.50	2.90	2.15	0.7	64	7	-13	27	24	27
2.50	2.90	2.15	0.9	95	10	1	44	60	44
2.50	2.90	2.17	-0.9	17	4	-8	16	-29	13
2.50	2.90	2.17	-0.7	6	9	-18	25	-67	26
2.50	2.90	2.17	-0.5	23	5	-26	21	4	22
2.50	2.90	2.17	-0.3	24	4	64	22	-9	24
2.50	2.90	2.17	-0.1	28	7	8	28	2	32
2.50	2.90	2.17	0.1	24	8	-3	25	29	26

Continued on next page

143

Q_i^2 (GeV^2)	Q_f^2 (GeV^2)	W (GeV)	$\cos\theta^*$	$\mathscr{R}_o$ (nb/sr)	$\Delta\mathscr{R}_o$ (nb/sr)	$\mathscr{R}_{TT}$ (nb/sr)	$\Delta\mathscr{R}_{TT}$ (nb/sr)	$\mathscr{R}_{TL}$ (nb/sr)	$\Delta\mathscr{R}_{TL}$ (nb/sr)
2.50	2.90	2.17	0.3	41	7	28	24	31	26
2.50	2.90	2.17	0.5	63	6	36	27	-59	28
2.50	2.90	2.17	0.7	57	6	19	29	-36	29
2.50	2.90	2.17	0.9	133	11	-11	49	61	48
2.50	2.90	2.19	-0.9	19	4	34	18	-38	16
2.50	2.90	2.19	-0.7	-1	9	-21	28	-1	33
2.50	2.90	2.19	-0.5	15	4	10	20	10	19
2.50	2.90	2.19	-0.3	24	5	1	26	-7	26
2.50	2.90	2.19	-0.1	-5	9	-64	25	-28	30
2.50	2.90	2.19	0.1	25	6	9	23	16	23
2.50	2.90	2.19	0.3	40	7	13	23	36	23
2.50	2.90	2.19	0.5	45	6	26	24	-32	24
2.50	2.90	2.19	0.7	40	6	-4	28	-9	26
2.50	2.90	2.19	0.9	125	10	38	46	1	47
2.50	2.90	2.21	-0.9	17	4	-11	16	17	15
2.50	2.90	2.21	-0.7	25	11	12	31	20	40
2.50	2.90	2.21	-0.5	22	4	42	23	55	26
2.50	2.90	2.21	-0.3	13	5	-27	22	-18	23
2.50	2.90	2.21	-0.1	12	6	3	27	-40	32
2.50	2.90	2.21	0.1	13	6	-29	22	-19	25
2.50	2.90	2.21	0.3	29	6	5	23	22	24
2.50	2.90	2.21	0.5	40	5	30	28	-20	26
2.50	2.90	2.21	0.7	48	6	-55	31	6	28
2.50	2.90	2.21	0.9	125	11	-18	48	-50	46
2.50	2.90	2.23	-0.9	15	4	21	20	0	22
2.50	2.90	2.23	-0.7	17	10	43	27	24	39
2.50	2.90	2.23	-0.5	12	4	5	20	23	22
2.50	2.90	2.23	-0.3	5	5	15	21	18	20
2.50	2.90	2.23	-0.1	3	5	-2	16	-13	17
2.50	2.90	2.23	0.1	19	5	4	21	-24	22
2.50	2.90	2.23	0.3	44	5	27	22	-9	23
2.50	2.90	2.23	0.5	30	5	35	22	8	24
2.50	2.90	2.23	0.7	54	6	20	28	43	28
2.50	2.90	2.23	0.9	111	9	-12	42	-17	41
2.50	2.90	2.25	-0.9	11	4	-9	22	-2	17
2.50	2.90	2.25	-0.7	12	6	35	18	51	15
2.50	2.90	2.25	-0.5	7	4	32	19	12	20
2.50	2.90	2.25	-0.3	-1	4	-27	23	-19	25
2.50	2.90	2.25	-0.1	7	5	7	17	-2	20
2.50	2.90	2.25	0.1	12	4	24	17	2	21
2.50	2.90	2.25	0.3	24	5	-29	18	0	19
2.50	2.90	2.25	0.5	38	5	26	25	-37	25
2.50	2.90	2.25	0.7	46	6	47	28	-49	30
2.50	2.90	2.25	0.9	131	9	42	48	0	49
2.50	2.90	2.27	-0.9	3	4	-5	17	-27	15
2.50	2.90	2.27	-0.7	5	5	18	17	-12	20
2.50	2.90	2.27	-0.5	13	2	-14	20	-15	22
2.50	2.90	2.27	-0.3	7	4	-4	19	0	23
2.50	2.90	2.27	-0.1	2	6	-6	17	-31	20

Continued on next page

144

| Q_i^2 | Q_f^2 | W | $\cos\theta^*$ | $\mathscr{R}_o$ | $\Delta\mathscr{R}_o$ | $\mathscr{R}_{TT}$ | $\Delta\mathscr{R}_{TT}$ | $\mathscr{R}_{TL}$ | $\Delta\mathscr{R}_{TL}$ |
(GeV^2)	(GeV^2)	(GeV)		(nb/sr)	(nb/sr)	(nb/sr)	(nb/sr)	(nb/sr)	(nb/sr)
2.50	2.90	2.27	0.1	14	4	-14	19	12	21
2.50	2.90	2.27	0.3	28	4	17	21	39	22
2.50	2.90	2.27	0.5	33	4	44	23	-5	24
2.50	2.90	2.27	0.7	49	6	39	28	-14	29
2.50	2.90	2.27	0.9	130	10	26	42	1	44
2.50	2.90	2.29	-0.9	15	5	28	22	-22	24
2.50	2.90	2.29	-0.7	3	3	-9	14	-19	17
2.50	2.90	2.29	-0.5	11	5	21	18	-8	22
2.50	2.90	2.29	-0.3	0	4	-1	18	-3	24
2.50	2.90	2.29	-0.1	3	4	15	16	-7	19
2.50	2.90	2.29	0.1	10	4	23	16	7	18
2.50	2.90	2.29	0.3	21	4	20	17	-3	19
2.50	2.90	2.29	0.5	20	4	16	21	-5	23
2.50	2.90	2.29	0.7	44	6	1	27	-7	28
2.50	2.90	2.29	0.9	132	9	17	42	1	44
2.50	2.90	2.31	-0.9	17	5	14	23	9	26
2.50	2.90	2.31	-0.7	0	3	-8	15	-18	15
2.50	2.90	2.31	-0.5	2	3	-26	15	-24	14
2.50	2.90	2.31	-0.3	0	5	-25	15	-16	22
2.50	2.90	2.31	-0.1	0	3	-16	14	-16	15
2.50	2.90	2.31	0.1	13	3	11	16	0	15
2.50	2.90	2.31	0.3	17	3	32	17	-21	19
2.50	2.90	2.31	0.5	21	4	31	20	10	21
2.50	2.90	2.31	0.7	53	5	43	27	-24	29
2.50	2.90	2.31	0.9	125	9	41	46	-29	47
2.50	2.90	2.33	-0.9	6	4	7	19	-55	24
2.50	2.90	2.33	-0.7	1	4	45	15	49	16
2.50	2.90	2.33	-0.5	-4	3	-2	13	0	16
2.50	2.90	2.33	-0.3	5	6	12	20	11	25
2.50	2.90	2.33	-0.1	3	2	-22	14	13	15
2.50	2.90	2.33	0.1	11	3	10	15	9	16
2.50	2.90	2.33	0.3	15	3	21	15	-1	18
2.50	2.90	2.33	0.5	23	3	12	18	-16	20
2.50	2.90	2.33	0.7	46	5	41	26	-7	27
2.50	2.90	2.33	0.9	136	9	-67	44	20	46
2.50	2.90	2.35	-0.9	24	8	34	24	-9	26
2.50	2.90	2.35	-0.7	4	4	-15	21	-25	19
2.50	2.90	2.35	-0.5	-1	2	16	20	24	21
2.50	2.90	2.35	-0.3	-3	4	-20	15	-40	18
2.50	2.90	2.35	-0.1	0	2	-2	10	-23	12
2.50	2.90	2.35	0.1	2	2	-14	12	-7	14
2.50	2.90	2.35	0.3	7	3	-11	15	20	14
2.50	2.90	2.35	0.5	22	3	25	21	-24	22
2.50	2.90	2.35	0.7	27	5	-67	26	7	29
2.50	2.90	2.35	0.9	135	9	-41	50	59	49
2.50	2.90	2.37	-0.9	-10	19	-19	20	-70	21
2.50	2.90	2.37	-0.7	0	2	39	15	38	19
2.50	2.90	2.37	-0.5	-2	2	-6	10	4	13
2.50	2.90	2.37	-0.3	1	3	-5	12	2	13

Continued on next page

Q_i^2 (GeV^2)	Q_f^2 (GeV^2)	W (GeV)	$\cos\theta^*$	$\mathscr{R}_o$ (nb/sr)	$\Delta\mathscr{R}_o$ (nb/sr)	$\mathscr{R}_{TT}$ (nb/sr)	$\Delta\mathscr{R}_{TT}$ (nb/sr)	$\mathscr{R}_{TL}$ (nb/sr)	$\Delta\mathscr{R}_{TL}$ (nb/sr)
2.50	2.90	2.37	-0.1	1	2	-4	11	9	11
2.50	2.90	2.37	0.1	0	2	-5	9	11	10
2.50	2.90	2.37	0.3	10	2	4	16	6	16
2.50	2.90	2.37	0.5	16	3	7	21	4	21
2.50	2.90	2.37	0.7	32	4	6	23	3	25
2.50	2.90	2.37	0.9	118	8	-32	41	-27	42
2.50	2.90	2.39	-0.9	23	18	55	20	59	20
2.50	2.90	2.39	-0.7	3	2	28	14	30	19
2.50	2.90	2.39	-0.5	-2	2	-34	15	-38	21
2.50	2.90	2.39	-0.3	0	2	-26	12	-13	16
2.50	2.90	2.39	-0.1	-3	1	2	9	-2	10
2.50	2.90	2.39	0.1	2	2	2	12	22	12
2.50	2.90	2.39	0.3	10	2	4	13	14	13
2.50	2.90	2.39	0.5	17	3	-17	15	29	16
2.50	2.90	2.39	0.7	37	4	37	27	6	28
2.50	2.90	2.39	0.9	150	9	-45	50	-55	49
2.50	2.90	2.41	-0.9	5	13	-15	52	-15	88
2.50	2.90	2.41	-0.7	0	4	-15	23	-39	26
2.50	2.90	2.41	-0.5	3	2	19	15	7	21
2.50	2.90	2.41	-0.3	0	1	-1	7	-2	9
2.50	2.90	2.41	-0.1	0	1	-18	9	0	7
2.50	2.90	2.41	0.1	2	2	-3	11	15	12
2.50	2.90	2.41	0.3	5	2	16	14	-12	14
2.50	2.90	2.41	0.5	13	3	7	16	-30	18
2.50	2.90	2.41	0.7	38	4	-24	28	-5	30
2.50	2.90	2.41	0.9	141	9	-56	50	-88	51
2.50	2.90	2.43	-0.9	5	16	-9	27	-66	24
2.50	2.90	2.43	-0.7	0	2	-4	22	-9	27
2.50	2.90	2.43	-0.5	0	2	-20	15	-5	18
2.50	2.90	2.43	-0.3	0	2	-9	12	-9	17
2.50	2.90	2.43	-0.1	-1	1	0	9	7	14
2.50	2.90	2.43	0.1	0	1	-4	10	10	10
2.50	2.90	2.43	0.3	4	2	7	11	10	12
2.50	2.90	2.43	0.5	13	2	3	15	-5	16
2.50	2.90	2.43	0.7	39	4	48	29	-16	30
2.50	2.90	2.43	0.9	125	8	-78	45	-64	48
2.50	2.90	2.45	-0.9	15	16	39	21	61	18
2.50	2.90	2.45	-0.7	4	3	27	20	5	20
2.50	2.90	2.45	-0.5	1	4	15	15	24	21
2.50	2.90	2.45	-0.3	0	3	-15	12	-19	14
2.50	2.90	2.45	-0.1	3	1	0	10	-11	10
2.50	2.90	2.45	0.1	0	1	-13	9	12	9
2.50	2.90	2.45	0.3	0	1	14	11	3	12
2.50	2.90	2.45	0.5	10	2	11	17	3	18
2.50	2.90	2.45	0.7	34	4	-41	29	-23	29
2.50	2.90	2.45	0.9	127	8	-104	55	-33	53
2.50	2.90	2.47	-0.9	14	17	-62	104	-38	229
2.50	2.90	2.47	-0.7	13	11	36	22	10	31
2.50	2.90	2.47	-0.5	0	2	-3	24	-4	26

Continued on next page

Q_i^2 (GeV^2)	Q_f^2 (GeV^2)	W (GeV)	$\cos\theta^*$	$\mathscr{R}_o$ (nb/sr)	$\Delta\mathscr{R}_o$ (nb/sr)	$\mathscr{R}_{TT}$ (nb/sr)	$\Delta\mathscr{R}_{TT}$ (nb/sr)	$\mathscr{R}_{TL}$ (nb/sr)	$\Delta\mathscr{R}_{TL}$ (nb/sr)
2.50	2.90	2.47	-0.3	0	2	-7	12	5	14
2.50	2.90	2.47	-0.1	0	1	3	9	-2	9
2.50	2.90	2.47	0.1	0	1	-15	9	0	10
2.50	2.90	2.47	0.3	2	1	7	12	-20	12
2.50	2.90	2.47	0.5	10	2	53	18	-18	21
2.50	2.90	2.47	0.7	32	4	-26	30	17	30
2.50	2.90	2.47	0.9	123	9	-62	52	-111	55
2.50	2.90	2.49	-0.9	-10	18	-54	32	-91	30
2.50	2.90	2.49	-0.7	0	3	19	18	6	29
2.50	2.90	2.49	-0.5	1	8	-2	32	9	49
2.50	2.90	2.49	-0.3	1	2	13	13	5	16
2.50	2.90	2.49	-0.1	-2	2	-5	9	-8	10
2.50	2.90	2.49	0.1	-3	1	12	12	0	12
2.50	2.90	2.49	0.3	2	1	-21	12	-17	12
2.50	2.90	2.49	0.5	7	2	-6	17	10	17
2.50	2.90	2.49	0.7	28	4	7	31	-2	35
2.50	2.90	2.49	0.9	124	9	-88	65	-128	70
2.50	2.90	2.51	-0.9	11	19	9	195	-48	504
2.50	2.90	2.51	-0.7	0	4	-39	32	-41	38
2.50	2.90	2.51	-0.5	2	7	2	31	27	40
2.50	2.90	2.51	-0.3	1	1	20	15	10	15
2.50	2.90	2.51	-0.1	-2	0	-7	8	1	10
2.50	2.90	2.51	0.1	2	1	-1	10	15	11
2.50	2.90	2.51	0.3	6	1	-4	15	-4	15
2.50	2.90	2.51	0.5	6	2	22	19	30	21
2.50	2.90	2.51	0.7	29	4	53	34	-74	36
2.50	2.90	2.51	0.9	135	9	-123	73	-23	73
2.50	2.90	2.53	-0.9	0	19	0	49	-74	39
2.50	2.90	2.53	-0.7	0	5	-4	34	-9	45
2.50	2.90	2.53	-0.5	-2	8	-26	48	-17	84
2.50	2.90	2.53	-0.3	-3	1	-12	15	-9	20
2.50	2.90	2.53	-0.1	-2	1	-3	8	-6	9
2.50	2.90	2.53	0.1	0	1	2	8	-2	9
2.50	2.90	2.53	0.3	4	1	-22	14	12	16
2.50	2.90	2.53	0.5	7	2	-10	17	8	16
2.50	2.90	2.53	0.7	25	4	63	32	-24	38
2.50	2.90	2.53	0.9	119	9	-140	71	-110	86
2.90	3.35	1.73	-0.9	316	38	22	124	3	94
2.90	3.35	1.73	-0.7	198	31	0	104	-183	70
2.90	3.35	1.73	-0.5	99	27	85	92	-67	64
2.90	3.35	1.73	-0.3	177	31	183	94	85	71
2.90	3.35	1.73	-0.1	166	29	-197	92	-20	65
2.90	3.35	1.73	0.1	117	32	-67	104	-72	72
2.90	3.35	1.73	0.3	192	34	141	107	5	81
2.90	3.35	1.73	0.5	224	34	44	107	169	85
2.90	3.35	1.73	0.7	276	37	-63	116	-21	90
2.90	3.35	1.73	0.9	277	39	-66	121	-97	89
2.90	3.35	1.75	-0.9	313	24	-37	73	-29	55
2.90	3.35	1.75	-0.7	242	23	-78	70	-137	54

Continued on next page

Q_i^2 (GeV^2)	Q_f^2 (GeV^2)	W (GeV)	$\cos\theta^*$	$\mathscr{R}_o$ (nb/sr)	$\Delta\mathscr{R}_o$ (nb/sr)	$\mathscr{R}_{TT}$ (nb/sr)	$\Delta\mathscr{R}_{TT}$ (nb/sr)	$\mathscr{R}_{TL}$ (nb/sr)	$\Delta\mathscr{R}_{TL}$ (nb/sr)
2.90	3.35	1.75	-0.5	214	22	-69	68	24	48
2.90	3.35	1.75	-0.3	164	19	-3	64	-102	45
2.90	3.35	1.75	-0.1	145	19	55	57	-7	47
2.90	3.35	1.75	0.1	182	21	-91	66	66	46
2.90	3.35	1.75	0.3	189	22	9	67	-71	52
2.90	3.35	1.75	0.5	209	23	21	75	38	57
2.90	3.35	1.75	0.7	303	25	-187	79	96	58
2.90	3.35	1.75	0.9	295	27	76	78	53	57
2.90	3.35	1.77	-0.9	308	20	-63	67	48	48
2.90	3.35	1.77	-0.7	302	20	50	64	-1	47
2.90	3.35	1.77	-0.5	240	18	59	57	-75	41
2.90	3.35	1.77	-0.3	206	18	2	57	-110	42
2.90	3.35	1.77	-0.1	158	18	-9	55	0	39
2.90	3.35	1.77	0.1	184	19	29	63	41	46
2.90	3.35	1.77	0.3	182	19	-4	62	-8	46
2.90	3.35	1.77	0.5	224	21	107	70	23	53
2.90	3.35	1.77	0.7	248	21	38	67	-68	52
2.90	3.35	1.77	0.9	305	21	33	69	-27	51
2.90	3.35	1.79	-0.9	316	19	-30	59	-63	42
2.90	3.35	1.79	-0.7	265	18	-76	59	-37	41
2.90	3.35	1.79	-0.5	246	18	-6	57	-97	39
2.90	3.35	1.79	-0.3	186	16	90	46	47	37
2.90	3.35	1.79	-0.1	118	17	134	51	-16	38
2.90	3.35	1.79	0.1	120	17	-16	52	93	36
2.90	3.35	1.79	0.3	149	18	-5	59	98	44
2.90	3.35	1.79	0.5	197	20	25	66	99	48
2.90	3.35	1.79	0.7	278	20	12	60	47	48
2.90	3.35	1.79	0.9	312	19	-27	63	138	45
2.90	3.35	1.81	-0.9	332	18	102	56	-68	41
2.90	3.35	1.81	-0.7	236	16	14	50	-69	34
2.90	3.35	1.81	-0.5	216	16	3	56	-90	38
2.90	3.35	1.81	-0.3	117	15	-10	49	-47	34
2.90	3.35	1.81	-0.1	133	16	108	53	-13	36
2.90	3.35	1.81	0.1	96	16	107	47	1	38
2.90	3.35	1.81	0.3	118	18	150	59	21	43
2.90	3.35	1.81	0.5	174	19	82	57	-4	44
2.90	3.35	1.81	0.7	216	18	126	59	24	45
2.90	3.35	1.81	0.9	292	18	-79	63	28	44
2.90	3.35	1.83	-0.9	281	16	23	46	-74	35
2.90	3.35	1.83	-0.7	231	15	12	51	0	33
2.90	3.35	1.83	-0.5	164	14	94	50	-123	36
2.90	3.35	1.83	-0.3	118	14	106	45	7	34
2.90	3.35	1.83	-0.1	119	15	86	44	-106	34
2.90	3.35	1.83	0.1	97	16	61	48	-42	38
2.90	3.35	1.83	0.3	125	17	-39	50	-16	38
2.90	3.35	1.83	0.5	166	18	199	54	9	44
2.90	3.35	1.83	0.7	196	18	10	58	-40	43
2.90	3.35	1.83	0.9	225	16	53	55	-18	41
2.90	3.35	1.85	-0.9	195	13	-33	43	-23	31

Continued on next page

148

Q_i^2 (GeV^2)	Q_f^2 (GeV^2)	W (GeV)	$\cos\theta^*$	$\mathscr{R}_o$ (nb/sr)	$\Delta\mathscr{R}_o$ (nb/sr)	$\mathscr{R}_{TT}$ (nb/sr)	$\Delta\mathscr{R}_{TT}$ (nb/sr)	$\mathscr{R}_{TL}$ (nb/sr)	$\Delta\mathscr{R}_{TL}$ (nb/sr)
2.90	3.35	1.85	-0.7	203	14	44	46	-50	32
2.90	3.35	1.85	-0.5	165	14	-14	45	-101	31
2.90	3.35	1.85	-0.3	124	14	1	43	-26	36
2.90	3.35	1.85	-0.1	82	13	37	46	-4	37
2.90	3.35	1.85	0.1	97	14	22	48	-16	39
2.90	3.35	1.85	0.3	90	16	82	49	-78	41
2.90	3.35	1.85	0.5	124	18	1	48	-21	40
2.90	3.35	1.85	0.7	148	17	77	51	-25	43
2.90	3.35	1.85	0.9	225	15	-18	55	-27	42
2.90	3.35	1.87	-0.9	172	13	62	42	-39	32
2.90	3.35	1.87	-0.7	157	12	110	36	-11	32
2.90	3.35	1.87	-0.5	119	13	11	44	-72	32
2.90	3.35	1.87	-0.3	71	14	-7	45	-70	34
2.90	3.35	1.87	-0.1	91	16	34	44	-52	37
2.90	3.35	1.87	0.1	49	15	36	43	1	40
2.90	3.35	1.87	0.3	60	17	4	52	-103	49
2.90	3.35	1.87	0.5	151	19	-53	62	-7	60
2.90	3.35	1.87	0.7	132	17	36	55	-81	48
2.90	3.35	1.87	0.9	184	15	-76	51	-53	38
2.90	3.35	1.89	-0.9	168	12	78	38	12	30
2.90	3.35	1.89	-0.7	165	12	93	42	-71	30
2.90	3.35	1.89	-0.5	86	12	-2	38	-64	30
2.90	3.35	1.89	-0.3	91	13	13	43	-76	33
2.90	3.35	1.89	-0.1	45	14	7	47	-21	41
2.90	3.35	1.89	0.1	58	14	-57	54	-11	50
2.90	3.35	1.89	0.3	79	16	-46	64	40	56
2.90	3.35	1.89	0.5	127	18	-91	62	-102	52
2.90	3.35	1.89	0.7	89	17	-103	56	-185	50
2.90	3.35	1.89	0.9	160	14	55	51	-77	39
2.90	3.35	1.91	-0.9	137	11	-11	37	-31	29
2.90	3.35	1.91	-0.7	111	11	16	39	-31	30
2.90	3.35	1.91	-0.5	112	13	16	47	-15	35
2.90	3.35	1.91	-0.3	83	16	29	45	-31	41
2.90	3.35	1.91	-0.1	79	14	-15	64	-52	61
2.90	3.35	1.91	0.1	73	15	92	54	85	51
2.90	3.35	1.91	0.3	79	13	42	47	6	40
2.90	3.35	1.91	0.5	133	15	73	49	-1	43
2.90	3.35	1.91	0.7	127	19	-47	65	-133	55
2.90	3.35	1.91	0.9	110	14	92	49	-51	41
2.90	3.35	1.93	-0.9	111	10	25	33	-1	27
2.90	3.35	1.93	-0.7	89	10	-27	40	-58	27
2.90	3.35	1.93	-0.5	79	12	17	33	-61	30
2.90	3.35	1.93	-0.3	42	12	-28	35	-73	30
2.90	3.35	1.93	-0.1	72	18	74	48	19	39
2.90	3.35	1.93	0.1	68	12	38	46	24	37
2.90	3.35	1.93	0.3	108	13	0	48	27	43
2.90	3.35	1.93	0.5	116	12	20	42	-47	37
2.90	3.35	1.93	0.7	186	15	25	60	43	48
2.90	3.35	1.93	0.9	155	14	7	49	-20	43

Continued on next page

149

Q_i^2 (GeV^2)	Q_f^2 (GeV^2)	W (GeV)	$\cos\theta^*$	$\mathscr{R}_o$ (nb/sr)	$\Delta\mathscr{R}_o$ (nb/sr)	$\mathscr{R}_{TT}$ (nb/sr)	$\Delta\mathscr{R}_{TT}$ (nb/sr)	$\mathscr{R}_{TL}$ (nb/sr)	$\Delta\mathscr{R}_{TL}$ (nb/sr)
2.90	3.35	1.95	-0.9	91	9	6	30	18	24
2.90	3.35	1.95	-0.7	95	10	-3	30	-36	27
2.90	3.35	1.95	-0.5	58	11	-6	38	-92	30
2.90	3.35	1.95	-0.3	49	10	-15	52	-57	46
2.90	3.35	1.95	-0.1	63	12	27	37	16	34
2.90	3.35	1.95	0.1	92	12	32	44	48	39
2.90	3.35	1.95	0.3	95	11	-24	44	10	37
2.90	3.35	1.95	0.5	105	11	-29	47	4	38
2.90	3.35	1.95	0.7	141	12	2	50	49	43
2.90	3.35	1.95	0.9	113	12	-4	48	-79	43
2.90	3.35	1.97	-0.9	89	9	34	32	30	27
2.90	3.35	1.97	-0.7	65	10	-3	35	-35	26
2.90	3.35	1.97	-0.5	47	11	19	32	-55	31
2.90	3.35	1.97	-0.3	31	12	-23	44	-57	42
2.90	3.35	1.97	-0.1	63	9	-4	41	-27	32
2.90	3.35	1.97	0.1	96	11	6	42	-7	35
2.90	3.35	1.97	0.3	121	11	99	42	62	38
2.90	3.35	1.97	0.5	135	11	84	41	12	37
2.90	3.35	1.97	0.7	137	11	5	51	-31	43
2.90	3.35	1.97	0.9	114	13	13	52	56	46
2.90	3.35	1.99	-0.9	66	8	2	32	-13	24
2.90	3.35	1.99	-0.7	29	9	14	28	-33	25
2.90	3.35	1.99	-0.5	58	12	-2	44	10	45
2.90	3.35	1.99	-0.3	60	11	-5	44	-23	38
2.90	3.35	1.99	-0.1	60	9	-63	36	-7	29
2.90	3.35	1.99	0.1	84	10	68	45	-5	40
2.90	3.35	1.99	0.3	103	11	24	42	-8	36
2.90	3.35	1.99	0.5	100	10	44	51	4	42
2.90	3.35	1.99	0.7	137	11	21	55	-15	45
2.90	3.35	1.99	0.9	137	12	-14	53	-121	46
2.90	3.35	2.01	-0.9	50	7	16	27	-26	23
2.90	3.35	2.01	-0.7	54	9	31	35	-16	28
2.90	3.35	2.01	-0.5	24	9	40	43	-35	42
2.90	3.35	2.01	-0.3	39	11	-20	35	-69	33
2.90	3.35	2.01	-0.1	52	9	-28	41	34	33
2.90	3.35	2.01	0.1	42	8	34	36	12	33
2.90	3.35	2.01	0.3	70	9	70	39	14	37
2.90	3.35	2.01	0.5	95	11	15	47	-5	41
2.90	3.35	2.01	0.7	120	11	75	50	19	46
2.90	3.35	2.01	0.9	109	12	-70	55	-87	45
2.90	3.35	2.03	-0.9	31	7	-16	25	38	20
2.90	3.35	2.03	-0.7	21	8	-41	25	-26	18
2.90	3.35	2.03	-0.5	42	10	-41	39	-16	36
2.90	3.35	2.03	-0.3	46	8	12	37	-9	33
2.90	3.35	2.03	-0.1	37	7	-37	32	-74	29
2.90	3.35	2.03	0.1	44	8	-2	38	22	35
2.90	3.35	2.03	0.3	93	11	-24	46	-19	45
2.90	3.35	2.03	0.5	85	12	39	55	39	56
2.90	3.35	2.03	0.7	71	9	-53	48	-54	44

Continued on next page

Q_i^2 (GeV^2)	Q_f^2 (GeV^2)	W (GeV)	$\cos\theta^*$	$\mathscr{R}_o$ (nb/sr)	$\Delta\mathscr{R}_o$ (nb/sr)	$\mathscr{R}_{TT}$ (nb/sr)	$\Delta\mathscr{R}_{TT}$ (nb/sr)	$\mathscr{R}_{TL}$ (nb/sr)	$\Delta\mathscr{R}_{TL}$ (nb/sr)
2.90	3.35	2.03	0.9	122	12	77	53	-52	47
2.90	3.35	2.05	-0.9	37	7	-19	22	0	19
2.90	3.35	2.05	-0.7	27	7	49	26	-31	25
2.90	3.35	2.05	-0.5	20	15	-37	46	-79	48
2.90	3.35	2.05	-0.3	29	7	17	32	-1	26
2.90	3.35	2.05	-0.1	33	7	30	29	-27	23
2.90	3.35	2.05	0.1	47	10	123	26	37	29
2.90	3.35	2.05	0.3	64	12	0	49	-20	46
2.90	3.35	2.05	0.5	61	12	-61	46	-37	47
2.90	3.35	2.05	0.7	76	12	-20	58	-37	55
2.90	3.35	2.05	0.9	104	11	-66	53	-95	46
2.90	3.35	2.07	-0.9	21	5	5	21	-42	17
2.90	3.35	2.07	-0.7	21	7	49	22	-14	27
2.90	3.35	2.07	-0.5	51	10	28	37	-16	39
2.90	3.35	2.07	-0.3	41	7	-91	32	-50	26
2.90	3.35	2.07	-0.1	28	7	-43	27	-49	23
2.90	3.35	2.07	0.1	41	8	-20	39	-31	39
2.90	3.35	2.07	0.3	60	11	-13	45	9	45
2.90	3.35	2.07	0.5	56	11	-13	43	-24	41
2.90	3.35	2.07	0.7	55	12	-6	46	-83	47
2.90	3.35	2.07	0.9	89	11	-16	57	-80	50
2.90	3.35	2.09	-0.9	7	4	17	18	-3	15
2.90	3.35	2.09	-0.7	10	6	-8	19	-69	18
2.90	3.35	2.09	-0.5	15	7	-1	27	-44	26
2.90	3.35	2.09	-0.3	15	5	26	28	-4	26
2.90	3.35	2.09	-0.1	13	7	1	31	9	28
2.90	3.35	2.09	0.1	40	9	13	42	-25	41
2.90	3.35	2.09	0.3	51	11	-49	41	-46	40
2.90	3.35	2.09	0.5	58	11	75	41	21	44
2.90	3.35	2.09	0.7	81	12	72	45	70	46
2.90	3.35	2.09	0.9	113	12	-18	55	-28	53
2.90	3.35	2.11	-0.9	20	5	-9	21	0	17
2.90	3.35	2.11	-0.7	4	9	-4	26	-57	22
2.90	3.35	2.11	-0.5	17	5	-19	26	-46	23
2.90	3.35	2.11	-0.3	24	5	-13	27	-57	23
2.90	3.35	2.11	-0.1	16	6	7	26	-41	23
2.90	3.35	2.11	0.1	37	9	6	36	0	38
2.90	3.35	2.11	0.3	67	10	35	37	30	36
2.90	3.35	2.11	0.5	60	8	-49	37	-41	36
2.90	3.35	2.11	0.7	90	10	13	41	34	40
2.90	3.35	2.11	0.9	114	13	26	60	26	58
2.90	3.35	2.13	-0.9	11	4	22	16	-32	15
2.90	3.35	2.13	-0.7	33	16	49	42	0	52
2.90	3.35	2.13	-0.5	17	5	63	30	21	32
2.90	3.35	2.13	-0.3	17	5	24	25	10	26
2.90	3.35	2.13	-0.1	15	5	42	34	46	32
2.90	3.35	2.13	0.1	57	13	33	37	84	44
2.90	3.35	2.13	0.3	32	6	-52	29	-6	28
2.90	3.35	2.13	0.5	55	7	10	34	-42	33

Continued on next page

Q_i^2 (GeV^2)	Q_f^2 (GeV^2)	W (GeV)	$\cos\theta^*$	$\mathscr{R}_o$ (nb/sr)	$\Delta\mathscr{R}_o$ (nb/sr)	$\mathscr{R}_{TT}$ (nb/sr)	$\Delta\mathscr{R}_{TT}$ (nb/sr)	$\mathscr{R}_{TL}$ (nb/sr)	$\Delta\mathscr{R}_{TL}$ (nb/sr)
2.90	3.35	2.13	0.7	47	8	31	35	0	34
2.90	3.35	2.13	0.9	76	11	-64	50	-40	49
2.90	3.35	2.15	-0.9	12	4	-2	15	-13	13
2.90	3.35	2.15	-0.7	30	27	75	23	72	22
2.90	3.35	2.15	-0.5	16	4	-30	22	-27	17
2.90	3.35	2.15	-0.3	2	4	-20	24	-11	22
2.90	3.35	2.15	-0.1	19	6	10	28	4	30
2.90	3.35	2.15	0.1	29	8	11	29	21	29
2.90	3.35	2.15	0.3	44	7	-38	27	-31	25
2.90	3.35	2.15	0.5	63	7	21	31	-27	31
2.90	3.35	2.15	0.7	50	7	-16	29	-47	28
2.90	3.35	2.15	0.9	89	11	7	53	-45	51
2.90	3.35	2.17	-0.9	14	4	-14	19	-10	18
2.90	3.35	2.17	-0.7	26	8	-9	42	35	61
2.90	3.35	2.17	-0.5	16	5	8	28	-16	27
2.90	3.35	2.17	-0.3	7	3	2	17	-6	16
2.90	3.35	2.17	-0.1	17	7	41	28	61	28
2.90	3.35	2.17	0.1	37	10	24	29	1	29
2.90	3.35	2.17	0.3	29	7	-10	28	-13	28
2.90	3.35	2.17	0.5	44	7	24	27	4	26
2.90	3.35	2.17	0.7	52	6	42	30	11	28
2.90	3.35	2.17	0.9	88	10	80	52	-13	49
2.90	3.35	2.19	-0.9	15	5	20	17	1	21
2.90	3.35	2.19	-0.7	9	6	-57	27	-47	25
2.90	3.35	2.19	-0.5	19	5	10	23	44	25
2.90	3.35	2.19	-0.3	16	5	-2	21	8	23
2.90	3.35	2.19	-0.1	12	5	23	29	41	30
2.90	3.35	2.19	0.1	6	6	-3	26	-38	26
2.90	3.35	2.19	0.3	38	5	26	25	7	24
2.90	3.35	2.19	0.5	43	6	45	27	-11	25
2.90	3.35	2.19	0.7	56	6	44	30	9	29
2.90	3.35	2.19	0.9	113	9	38	42	-22	42
2.90	3.35	2.21	-0.9	6	3	8	20	-42	14
2.90	3.35	2.21	-0.7	11	4	19	25	0	27
2.90	3.35	2.21	-0.5	8	4	28	17	27	21
2.90	3.35	2.21	-0.3	5	5	-27	24	-35	28
2.90	3.35	2.21	-0.1	5	5	15	26	25	27
2.90	3.35	2.21	0.1	13	4	7	23	15	22
2.90	3.35	2.21	0.3	26	5	32	22	-24	23
2.90	3.35	2.21	0.5	44	6	39	24	-20	25
2.90	3.35	2.21	0.7	38	6	15	30	-6	29
2.90	3.35	2.21	0.9	83	9	-47	44	-63	43
2.90	3.35	2.23	-0.9	19	4	22	22	-11	21
2.90	3.35	2.23	-0.7	10	8	18	34	-8	42
2.90	3.35	2.23	-0.5	4	4	-9	22	-18	19
2.90	3.35	2.23	-0.3	4	4	-15	23	-38	24
2.90	3.35	2.23	-0.1	0	4	11	20	13	20
2.90	3.35	2.23	0.1	11	4	-8	21	44	23
2.90	3.35	2.23	0.3	23	4	-2	21	-14	22

Continued on next page

Q_i^2 (GeV^2)	Q_f^2 (GeV^2)	W (GeV)	$\cos\theta^*$	$\mathscr{R}_o$ (nb/sr)	$\Delta\mathscr{R}_o$ (nb/sr)	$\mathscr{R}_{TT}$ (nb/sr)	$\Delta\mathscr{R}_{TT}$ (nb/sr)	$\mathscr{R}_{TL}$ (nb/sr)	$\Delta\mathscr{R}_{TL}$ (nb/sr)
2.90	3.35	2.23	0.5	30	5	16	22	-30	23
2.90	3.35	2.23	0.7	39	5	55	25	0	26
2.90	3.35	2.23	0.9	115	11	70	49	33	48
2.90	3.35	2.25	-0.9	13	4	14	20	-6	17
2.90	3.35	2.25	-0.7	8	4	43	25	-29	24
2.90	3.35	2.25	-0.5	10	5	36	21	23	27
2.90	3.35	2.25	-0.3	5	7	-5	29	-19	31
2.90	3.35	2.25	-0.1	7	4	13	21	1	24
2.90	3.35	2.25	0.1	14	4	34	23	42	24
2.90	3.35	2.25	0.3	26	4	-12	22	8	21
2.90	3.35	2.25	0.5	19	4	36	24	25	21
2.90	3.35	2.25	0.7	35	5	35	25	28	26
2.90	3.35	2.25	0.9	87	9	59	44	-8	45
2.90	3.35	2.27	-0.9	13	6	15	25	19	28
2.90	3.35	2.27	-0.7	3	5	14	30	-16	30
2.90	3.35	2.27	-0.5	0	3	-19	18	-33	17
2.90	3.35	2.27	-0.3	1	4	-15	22	-29	23
2.90	3.35	2.27	-0.1	4	4	-15	19	-4	20
2.90	3.35	2.27	0.1	9	3	-28	19	-25	20
2.90	3.35	2.27	0.3	23	4	-6	22	-24	21
2.90	3.35	2.27	0.5	31	4	-6	23	-3	24
2.90	3.35	2.27	0.7	32	4	92	30	-4	29
2.90	3.35	2.27	0.9	94	8	-21	46	-39	43
2.90	3.35	2.29	-0.9	20	7	46	28	11	36
2.90	3.35	2.29	-0.7	3	5	-8	24	-42	24
2.90	3.35	2.29	-0.5	4	4	-15	18	14	20
2.90	3.35	2.29	-0.3	0	3	2	29	38	35
2.90	3.35	2.29	-0.1	6	3	24	17	-13	16
2.90	3.35	2.29	0.1	5	3	-12	17	12	16
2.90	3.35	2.29	0.3	18	4	42	21	-25	21
2.90	3.35	2.29	0.5	18	4	3	23	17	23
2.90	3.35	2.29	0.7	30	5	41	31	22	28
2.90	3.35	2.29	0.9	106	8	-29	51	44	50
3.35	3.85	1.73	-0.9	136	35	197	146	-3	94
3.35	3.85	1.73	-0.7	125	34	-86	130	-164	94
3.35	3.85	1.73	-0.5	63	27	173	132	-100	84
3.35	3.85	1.73	-0.3	127	31	36	105	47	76
3.35	3.85	1.73	-0.1	128	32	114	91	1	78
3.35	3.85	1.73	0.1	96	29	-177	121	2	81
3.35	3.85	1.73	0.3	110	32	-213	136	75	93
3.35	3.85	1.73	0.5	92	35	40	106	37	88
3.35	3.85	1.73	0.7	128	37	-98	119	-78	95
3.35	3.85	1.73	0.9	156	39	-180	132	1	89
3.35	3.85	1.75	-0.9	230	21	-53	84	14	57
3.35	3.85	1.75	-0.7	190	21	-103	81	-72	54
3.35	3.85	1.75	-0.5	152	18	-21	66	-65	48
3.35	3.85	1.75	-0.3	147	18	137	67	-57	47
3.35	3.85	1.75	-0.1	127	17	-62	69	80	37
3.35	3.85	1.75	0.1	99	17	56	54	15	40

Continued on next page

Q_i^2 (GeV^2)	Q_f^2 (GeV^2)	W (GeV)	$\cos\theta^*$	$\mathscr{R}_o$ (nb/sr)	$\Delta\mathscr{R}_o$ (nb/sr)	$\mathscr{R}_{TT}$ (nb/sr)	$\Delta\mathscr{R}_{TT}$ (nb/sr)	$\mathscr{R}_{TL}$ (nb/sr)	$\Delta\mathscr{R}_{TL}$ (nb/sr)
3.35	3.85	1.75	0.3	190	21	80	78	25	56
3.35	3.85	1.75	0.5	217	21	-136	86	66	54
3.35	3.85	1.75	0.7	266	24	103	88	4	66
3.35	3.85	1.75	0.9	306	24	68	101	30	70
3.35	3.85	1.77	-0.9	289	21	49	72	-55	50
3.35	3.85	1.77	-0.7	234	19	92	66	4	51
3.35	3.85	1.77	-0.5	158	17	-32	65	-55	42
3.35	3.85	1.77	-0.3	134	17	23	76	-20	45
3.35	3.85	1.77	-0.1	127	17	-82	59	4	35
3.35	3.85	1.77	0.1	130	17	115	63	51	45
3.35	3.85	1.77	0.3	157	19	-35	72	50	49
3.35	3.85	1.77	0.5	163	20	180	71	0	52
3.35	3.85	1.77	0.7	191	20	25	71	76	52
3.35	3.85	1.77	0.9	252	20	-23	81	97	58
3.35	3.85	1.79	-0.9	261	17	50	60	-86	47
3.35	3.85	1.79	-0.7	208	17	38	59	-44	43
3.35	3.85	1.79	-0.5	161	16	5	53	-120	36
3.35	3.85	1.79	-0.3	130	15	68	53	-66	37
3.35	3.85	1.79	-0.1	96	14	-17	55	-68	35
3.35	3.85	1.79	0.1	96	17	52	57	20	42
3.35	3.85	1.79	0.3	122	18	17	62	110	44
3.35	3.85	1.79	0.5	216	19	62	63	49	46
3.35	3.85	1.79	0.7	222	19	44	64	-80	46
3.35	3.85	1.79	0.9	247	18	48	67	16	51
3.35	3.85	1.81	-0.9	276	18	48	59	-70	44
3.35	3.85	1.81	-0.7	214	16	-26	56	-62	39
3.35	3.85	1.81	-0.5	160	15	37	56	-15	38
3.35	3.85	1.81	-0.3	116	14	108	53	-23	40
3.35	3.85	1.81	-0.1	108	15	-36	57	22	39
3.35	3.85	1.81	0.1	115	16	6	62	0	42
3.35	3.85	1.81	0.3	87	15	100	58	37	43
3.35	3.85	1.81	0.5	139	18	40	65	-64	47
3.35	3.85	1.81	0.7	221	18	-45	65	57	47
3.35	3.85	1.81	0.9	231	16	-51	66	0	47
3.35	3.85	1.83	-0.9	203	14	-14	46	58	35
3.35	3.85	1.83	-0.7	174	13	55	49	-30	35
3.35	3.85	1.83	-0.5	104	12	-22	52	-79	35
3.35	3.85	1.83	-0.3	98	13	-43	45	-64	30
3.35	3.85	1.83	-0.1	78	14	-14	50	-59	39
3.35	3.85	1.83	0.1	29	14	31	42	-92	33
3.35	3.85	1.83	0.3	98	16	-51	54	7	42
3.35	3.85	1.83	0.5	120	16	75	62	54	49
3.35	3.85	1.83	0.7	155	16	117	62	-90	45
3.35	3.85	1.83	0.9	199	15	-37	59	-7	41
3.35	3.85	1.85	-0.9	166	12	-47	44	69	32
3.35	3.85	1.85	-0.7	161	13	-28	53	-78	34
3.35	3.85	1.85	-0.5	150	13	11	45	-104	33
3.35	3.85	1.85	-0.3	54	12	26	42	-102	29
3.35	3.85	1.85	-0.1	74	13	-25	44	2	36

Continued on next page

154

Q_i^2 (GeV^2)	Q_f^2 (GeV^2)	W (GeV)	$\cos\theta^*$	$\mathscr{R}_o$ (nb/sr)	$\Delta\mathscr{R}_o$ (nb/sr)	$\mathscr{R}_{TT}$ (nb/sr)	$\Delta\mathscr{R}_{TT}$ (nb/sr)	$\mathscr{R}_{TL}$ (nb/sr)	$\Delta\mathscr{R}_{TL}$ (nb/sr)
3.35	3.85	1.85	0.1	37	14	-11	48	-35	40
3.35	3.85	1.85	0.3	85	16	-13	52	-135	43
3.35	3.85	1.85	0.5	107	17	29	60	-3	51
3.35	3.85	1.85	0.7	153	15	-20	56	-21	44
3.35	3.85	1.85	0.9	179	15	22	53	28	39
3.35	3.85	1.87	-0.9	161	12	-14	39	3	29
3.35	3.85	1.87	-0.7	123	12	-43	43	-34	32
3.35	3.85	1.87	-0.5	80	11	-40	43	-76	32
3.35	3.85	1.87	-0.3	74	13	-53	45	-119	35
3.35	3.85	1.87	-0.1	63	14	70	46	3	38
3.35	3.85	1.87	0.1	28	14	-29	48	-24	49
3.35	3.85	1.87	0.3	60	15	-49	54	-81	52
3.35	3.85	1.87	0.5	91	17	-50	62	-53	55
3.35	3.85	1.87	0.7	101	16	-4	58	-73	51
3.35	3.85	1.87	0.9	138	14	0	49	-17	36
3.35	3.85	1.89	-0.9	104	10	-20	38	29	29
3.35	3.85	1.89	-0.7	111	11	-62	41	-3	29
3.35	3.85	1.89	-0.5	101	12	-24	44	-48	33
3.35	3.85	1.89	-0.3	37	10	47	42	-94	32
3.35	3.85	1.89	-0.1	21	11	-78	44	-96	33
3.35	3.85	1.89	0.1	58	13	-66	56	-39	45
3.35	3.85	1.89	0.3	71	17	45	64	33	62
3.35	3.85	1.89	0.5	107	18	27	67	47	66
3.35	3.85	1.89	0.7	70	16	-24	57	-190	48
3.35	3.85	1.89	0.9	97	12	-30	49	8	38
3.35	3.85	1.91	-0.9	126	10	-18	39	-10	29
3.35	3.85	1.91	-0.7	107	13	32	41	48	33
3.35	3.85	1.91	-0.5	102	14	19	41	-56	32
3.35	3.85	1.91	-0.3	42	11	-6	46	-50	40
3.35	3.85	1.91	-0.1	22	12	31	59	-2	53
3.35	3.85	1.91	0.1	65	13	-27	50	39	46
3.35	3.85	1.91	0.3	69	13	93	49	1	42
3.35	3.85	1.91	0.5	98	14	-44	56	37	47
3.35	3.85	1.91	0.7	114	16	90	61	-42	54
3.35	3.85	1.91	0.9	121	14	-104	53	-39	40
3.35	3.85	1.93	-0.9	106	10	-83	37	2	26
3.35	3.85	1.93	-0.7	87	10	-3	35	-22	27
3.35	3.85	1.93	-0.5	63	11	80	38	-14	31
3.35	3.85	1.93	-0.3	27	10	-71	38	-67	33
3.35	3.85	1.93	-0.1	44	12	30	41	-47	34
3.35	3.85	1.93	0.1	70	10	-14	49	-4	38
3.35	3.85	1.93	0.3	67	10	31	45	0	35
3.35	3.85	1.93	0.5	85	11	27	51	-1	42
3.35	3.85	1.93	0.7	101	12	115	61	50	52
3.35	3.85	1.93	0.9	117	13	11	54	-87	44
3.35	3.85	1.95	-0.9	75	10	24	35	-62	27
3.35	3.85	1.95	-0.7	40	8	89	31	-21	28
3.35	3.85	1.95	-0.5	33	8	-36	33	-151	28
3.35	3.85	1.95	-0.3	61	13	-9	50	3	49

Continued on next page

Q_i^2 (GeV^2)	Q_f^2 (GeV^2)	W (GeV)	$\cos\theta^*$	$\mathscr{R}_o$ (nb/sr)	$\Delta\mathscr{R}_o$ (nb/sr)	$\mathscr{R}_{TT}$ (nb/sr)	$\Delta\mathscr{R}_{TT}$ (nb/sr)	$\mathscr{R}_{TL}$ (nb/sr)	$\Delta\mathscr{R}_{TL}$ (nb/sr)
3.35	3.85	1.95	-0.1	47	10	59	41	-36	33
3.35	3.85	1.95	0.1	56	10	-32	40	47	31
3.35	3.85	1.95	0.3	81	10	70	47	33	41
3.35	3.85	1.95	0.5	78	10	-59	43	-59	36
3.35	3.85	1.95	0.7	106	12	53	53	-80	45
3.35	3.85	1.95	0.9	82	12	-63	52	-78	43
3.35	3.85	1.97	-0.9	57	8	31	29	-17	23
3.35	3.85	1.97	-0.7	61	9	69	32	-72	29
3.35	3.85	1.97	-0.5	35	9	-56	30	-45	28
3.35	3.85	1.97	-0.3	11	12	-10	38	-45	29
3.35	3.85	1.97	-0.1	25	7	1	26	-43	21
3.35	3.85	1.97	0.1	45	8	-87	40	-54	33
3.35	3.85	1.97	0.3	46	8	32	40	-23	35
3.35	3.85	1.97	0.5	105	10	-34	47	-53	38
3.35	3.85	1.97	0.7	109	11	50	55	30	45
3.35	3.85	1.97	0.9	95	12	-2	52	-73	45
3.35	3.85	1.99	-0.9	39	7	-6	25	-37	20
3.35	3.85	1.99	-0.7	38	9	-33	36	-79	26
3.35	3.85	1.99	-0.5	38	9	-62	33	-78	30
3.35	3.85	1.99	-0.3	46	9	93	38	0	36
3.35	3.85	1.99	-0.1	13	5	7	36	24	31
3.35	3.85	1.99	0.1	46	8	21	43	45	34
3.35	3.85	1.99	0.3	68	9	-19	48	31	37
3.35	3.85	1.99	0.5	82	9	-42	47	-65	36
3.35	3.85	1.99	0.7	91	10	-7	54	58	42
3.35	3.85	1.99	0.9	88	11	62	52	-46	46
3.35	3.85	2.01	-0.9	35	8	16	28	2	23
3.35	3.85	2.01	-0.7	27	7	-11	27	-58	21
3.35	3.85	2.01	-0.5	15	9	0	58	8	62
3.35	3.85	2.01	-0.3	37	10	-56	47	-29	44
3.35	3.85	2.01	-0.1	40	9	11	43	53	37
3.35	3.85	2.01	0.1	35	8	-39	39	-20	32
3.35	3.85	2.01	0.3	77	10	88	46	-16	42
3.35	3.85	2.01	0.5	58	10	18	45	1	38
3.35	3.85	2.01	0.7	91	11	67	53	20	46
3.35	3.85	2.01	0.9	100	13	-44	61	108	52
3.35	3.85	2.03	-0.9	33	7	-8	28	-47	20
3.35	3.85	2.03	-0.7	35	8	12	30	-6	28
3.35	3.85	2.03	-0.5	33	10	49	53	23	63
3.35	3.85	2.03	-0.3	43	8	42	39	-26	33
3.35	3.85	2.03	-0.1	29	7	3	39	-24	37
3.35	3.85	2.03	0.1	33	7	42	40	6	33
3.35	3.85	2.03	0.3	34	8	-91	46	-48	42
3.35	3.85	2.03	0.5	59	11	12	57	23	56
3.35	3.85	2.03	0.7	86	11	86	58	51	55
3.35	3.85	2.03	0.9	99	12	64	54	25	46
3.35	3.85	2.05	-0.9	10	5	-8	21	-2	17
3.35	3.85	2.05	-0.7	19	6	33	35	37	34
3.35	3.85	2.05	-0.5	18	9	39	33	2	39

Continued on next page

Q_i^2 (GeV^2)	Q_f^2 (GeV^2)	W (GeV)	$\cos\theta^*$	$\mathscr{R}_o$ (nb/sr)	$\Delta\mathscr{R}_o$ (nb/sr)	$\mathscr{R}_{TT}$ (nb/sr)	$\Delta\mathscr{R}_{TT}$ (nb/sr)	$\mathscr{R}_{TL}$ (nb/sr)	$\Delta\mathscr{R}_{TL}$ (nb/sr)
3.35	3.85	2.05	-0.3	51	11	-4	36	-62	30
3.35	3.85	2.05	-0.1	35	7	30	39	-6	33
3.35	3.85	2.05	0.1	32	8	-9	39	-24	36
3.35	3.85	2.05	0.3	32	9	-20	56	28	54
3.35	3.85	2.05	0.5	36	12	-41	54	56	55
3.35	3.85	2.05	0.7	72	12	37	64	-75	61
3.35	3.85	2.05	0.9	75	11	101	63	115	59
3.35	3.85	2.07	-0.9	24	6	42	30	8	25
3.35	3.85	2.07	-0.7	2	29	26	58	52	88
3.35	3.85	2.07	-0.5	7	6	112	32	15	34
3.35	3.85	2.07	-0.3	27	7	-62	33	-88	24
3.35	3.85	2.07	-0.1	16	6	-17	41	-29	38
3.35	3.85	2.07	0.1	28	7	22	46	84	47
3.35	3.85	2.07	0.3	36	11	-19	57	0	55
3.35	3.85	2.07	0.5	56	12	12	50	66	51
3.35	3.85	2.07	0.7	57	12	-86	69	-178	64
3.35	3.85	2.07	0.9	93	12	15	63	48	59
3.35	3.85	2.09	-0.9	19	5	15	27	18	25
3.35	3.85	2.09	-0.7	-1	16	-3	45	-44	53
3.35	3.85	2.09	-0.5	17	8	39	36	42	35
3.35	3.85	2.09	-0.3	21	6	-75	34	-21	30
3.35	3.85	2.09	-0.1	9	5	-22	31	-7	33
3.35	3.85	2.09	0.1	15	12	77	48	82	47
3.35	3.85	2.09	0.3	23	10	-64	38	-41	38
3.35	3.85	2.09	0.5	67	11	36	49	31	46
3.35	3.85	2.09	0.7	73	11	8	53	-23	50
3.35	3.85	2.09	0.9	64	10	-66	59	-16	53
3.35	3.85	2.11	-0.9	0	4	1	23	-19	18
3.35	3.85	2.11	-0.7	14	18	96	25	72	26
3.35	3.85	2.11	-0.5	6	6	20	36	5	35
3.35	3.85	2.11	-0.3	32	7	30	39	27	36
3.35	3.85	2.11	-0.1	-3	5	9	28	-22	31
3.35	3.85	2.11	0.1	15	13	-5	43	-32	45
3.35	3.85	2.11	0.3	18	10	-39	35	-23	38
3.35	3.85	2.11	0.5	39	8	-48	38	-47	36
3.35	3.85	2.11	0.7	39	7	118	54	-19	53
3.35	3.85	2.11	0.9	78	13	110	76	152	78
3.35	3.85	2.13	-0.9	-2	4	63	28	30	23
3.35	3.85	2.13	-0.7	32	30	91	30	88	32
3.35	3.85	2.13	-0.5	17	7	56	37	44	38
3.35	3.85	2.13	-0.3	10	5	-23	30	-37	27
3.35	3.85	2.13	-0.1	6	7	-9	38	-13	35
3.35	3.85	2.13	0.1	28	7	83	26	66	25
3.35	3.85	2.13	0.3	25	8	45	39	-21	43
3.35	3.85	2.13	0.5	36	7	27	43	-27	42
3.35	3.85	2.13	0.7	32	7	79	45	14	41
3.35	3.85	2.13	0.9	66	13	-75	66	-64	58
3.35	3.85	2.15	-0.9	11	7	7	33	5	35
3.35	3.85	2.15	-0.7	16	14	-32	33	-49	47

Continued on next page

Q_i^2 (GeV^2)	Q_f^2 (GeV^2)	W (GeV)	$\cos\theta^*$	$\mathscr{R}_o$ (nb/sr)	$\Delta\mathscr{R}_o$ (nb/sr)	$\mathscr{R}_{TT}$ (nb/sr)	$\Delta\mathscr{R}_{TT}$ (nb/sr)	$\mathscr{R}_{TL}$ (nb/sr)	$\Delta\mathscr{R}_{TL}$ (nb/sr)
3.35	3.85	2.15	-0.5	1	3	13	41	12	38
3.35	3.85	2.15	-0.3	6	5	34	40	27	38
3.35	3.85	2.15	-0.1	9	6	-18	29	-37	27
3.35	3.85	2.15	0.1	3	6	-21	32	-9	26
3.35	3.85	2.15	0.3	30	8	92	49	82	49
3.35	3.85	2.15	0.5	38	7	-10	43	-51	40
3.35	3.85	2.15	0.7	36	8	17	50	7	43
3.35	3.85	2.15	0.9	56	12	-57	58	-55	51
3.35	3.85	2.17	-0.9	9	5	-34	38	-17	20
3.35	3.85	2.17	-0.7	0	9	38	20	58	18
3.35	3.85	2.17	-0.5	9	6	-4	36	-48	39
3.35	3.85	2.17	-0.3	19	8	39	38	52	38
3.35	3.85	2.17	-0.1	10	5	24	33	-1	35
3.35	3.85	2.17	0.1	18	8	32	40	8	40
3.35	3.85	2.17	0.3	21	6	26	41	37	38
3.35	3.85	2.17	0.5	30	7	22	38	42	37
3.35	3.85	2.17	0.7	37	7	78	42	-32	38
3.35	3.85	2.17	0.9	66	11	126	71	75	69
3.35	3.85	2.19	-0.9	0	4	12	30	-59	33
3.35	3.85	2.19	-0.7	5	9	41	32	24	41
3.35	3.85	2.19	-0.5	0	4	-17	21	-6	22
3.35	3.85	2.19	-0.3	14	5	8	32	19	30
3.35	3.85	2.19	-0.1	6	5	-41	38	-85	33
3.35	3.85	2.19	0.1	5	5	18	21	0	25
3.35	3.85	2.19	0.3	31	7	-12	37	-39	30
3.35	3.85	2.19	0.5	31	6	-41	40	48	30
3.35	3.85	2.19	0.7	27	6	-31	39	53	32
3.35	3.85	2.19	0.9	64	11	-68	75	-28	67
3.85	4.65	1.73	-0.9	70	26	90	104	-88	79
3.85	4.65	1.73	-0.7	93	27	12	92	-93	69
3.85	4.65	1.73	-0.5	35	22	134	105	-32	74
3.85	4.65	1.73	-0.3	23	25	-136	105	49	70
3.85	4.65	1.73	-0.1	6	23	-1	137	27	86
3.85	4.65	1.73	0.1	74	27	-8	109	-101	72
3.85	4.65	1.73	0.3	16	26	82	114	-76	89
3.85	4.65	1.73	0.5	85	28	-83	128	49	78
3.85	4.65	1.73	0.7	77	28	-22	107	-114	77
3.85	4.65	1.73	0.9	47	30	128	157	69	110
3.85	4.65	1.75	-0.9	128	16	-69	57	65	40
3.85	4.65	1.75	-0.7	101	16	124	64	-88	49
3.85	4.65	1.75	-0.5	113	16	140	66	4	53
3.85	4.65	1.75	-0.3	84	16	-92	72	-9	45
3.85	4.65	1.75	-0.1	79	16	-99	67	97	47
3.85	4.65	1.75	0.1	66	15	164	63	42	46
3.85	4.65	1.75	0.3	53	16	-68	62	35	38
3.85	4.65	1.75	0.5	93	18	2	87	-37	52
3.85	4.65	1.75	0.7	129	20	8	88	-31	58
3.85	4.65	1.75	0.9	138	20	-83	85	78	54
3.85	4.65	1.77	-0.9	192	16	-149	65	-52	42

Continued on next page

| Q_i^2 | Q_f^2 | W | $\cos\theta^*$ | $\mathscr{R}_o$ | $\Delta\mathscr{R}_o$ | $\mathscr{R}_{TT}$ | $\Delta\mathscr{R}_{TT}$ | $\mathscr{R}_{TL}$ | $\Delta\mathscr{R}_{TL}$ |
(GeV^2)	(GeV^2)	(GeV)		(nb/sr)	(nb/sr)	(nb/sr)	(nb/sr)	(nb/sr)	(nb/sr)
3.85	4.65	1.77	-0.7	115	14	-80	54	-38	37
3.85	4.65	1.77	-0.5	109	13	86	56	-12	42
3.85	4.65	1.77	-0.3	114	13	-82	58	39	37
3.85	4.65	1.77	-0.1	95	14	-23	66	-68	44
3.85	4.65	1.77	0.1	104	13	-7	61	-12	41
3.85	4.65	1.77	0.3	84	13	31	61	-14	40
3.85	4.65	1.77	0.5	99	15	-20	77	69	47
3.85	4.65	1.77	0.7	121	16	-8	71	18	47
3.85	4.65	1.77	0.9	167	16	-39	84	6	54
3.85	4.65	1.79	-0.9	171	16	92	66	-29	46
3.85	4.65	1.79	-0.7	152	15	38	59	-26	42
3.85	4.65	1.79	-0.5	109	12	46	59	16	42
3.85	4.65	1.79	-0.3	111	13	104	62	-14	44
3.85	4.65	1.79	-0.1	75	13	113	48	-20	39
3.85	4.65	1.79	0.1	83	14	149	63	-27	43
3.85	4.65	1.79	0.3	70	14	61	60	6	39
3.85	4.65	1.79	0.5	85	15	106	65	-45	42
3.85	4.65	1.79	0.7	150	16	0	74	-3	46
3.85	4.65	1.79	0.9	129	16	124	79	-60	55
3.85	4.65	1.81	-0.9	173	14	-4	57	19	39
3.85	4.65	1.81	-0.7	130	13	-3	57	-72	41
3.85	4.65	1.81	-0.5	134	13	-3	63	-64	44
3.85	4.65	1.81	-0.3	75	12	41	56	-66	35
3.85	4.65	1.81	-0.1	71	13	-1	53	16	35
3.85	4.65	1.81	0.1	74	13	53	57	8	49
3.85	4.65	1.81	0.3	75	14	1	73	35	55
3.85	4.65	1.81	0.5	83	13	9	60	17	38
3.85	4.65	1.81	0.7	115	15	-4	67	55	44
3.85	4.65	1.81	0.9	171	15	58	73	-89	49
3.85	4.65	1.83	-0.9	159	13	-9	55	-43	40
3.85	4.65	1.83	-0.7	117	12	37	55	-124	40
3.85	4.65	1.83	-0.5	100	12	76	58	-41	45
3.85	4.65	1.83	-0.3	50	10	32	49	-62	36
3.85	4.65	1.83	-0.1	50	11	16	54	-26	42
3.85	4.65	1.83	0.1	42	12	10	59	-6	51
3.85	4.65	1.83	0.3	61	14	-13	73	-92	63
3.85	4.65	1.83	0.5	65	13	-2	71	-128	44
3.85	4.65	1.83	0.7	87	14	120	58	-115	47
3.85	4.65	1.83	0.9	97	12	-1	56	-54	36
3.85	4.65	1.85	-0.9	108	11	-21	45	-21	33
3.85	4.65	1.85	-0.7	94	12	63	54	-45	42
3.85	4.65	1.85	-0.5	82	10	40	48	7	35
3.85	4.65	1.85	-0.3	38	11	-63	45	-55	30
3.85	4.65	1.85	-0.1	10	9	-10	40	-93	36
3.85	4.65	1.85	0.1	27	14	-106	55	-19	52
3.85	4.65	1.85	0.3	31	14	-37	69	-75	61
3.85	4.65	1.85	0.5	51	14	-81	75	-180	57
3.85	4.65	1.85	0.7	93	14	-70	69	-32	53
3.85	4.65	1.85	0.9	121	13	40	64	-16	45

Continued on next page

Q_i^2 (GeV^2)	Q_f^2 (GeV^2)	W (GeV)	$\cos\theta^*$	$\mathscr{R}_o$ (nb/sr)	$\Delta\mathscr{R}_o$ (nb/sr)	$\mathscr{R}_{TT}$ (nb/sr)	$\Delta\mathscr{R}_{TT}$ (nb/sr)	$\mathscr{R}_{TL}$ (nb/sr)	$\Delta\mathscr{R}_{TL}$ (nb/sr)
3.85	4.65	1.87	-0.9	115	11	35	49	-43	36
3.85	4.65	1.87	-0.7	64	15	-66	49	-61	32
3.85	4.65	1.87	-0.5	44	9	44	34	-70	32
3.85	4.65	1.87	-0.3	40	9	-36	35	-88	27
3.85	4.65	1.87	-0.1	27	10	-75	46	-41	41
3.85	4.65	1.87	0.1	8	10	-35	65	-71	63
3.85	4.65	1.87	0.3	40	13	-19	87	-10	90
3.85	4.65	1.87	0.5	41	14	39	110	-18	97
3.85	4.65	1.87	0.7	64	15	224	69	154	49
3.85	4.65	1.87	0.9	110	12	46	63	-123	43
3.85	4.65	1.89	-0.9	87	10	15	45	-31	33
3.85	4.65	1.89	-0.7	66	10	82	46	-101	36
3.85	4.65	1.89	-0.5	42	9	84	51	-28	43
3.85	4.65	1.89	-0.3	31	11	33	67	-33	63
3.85	4.65	1.89	-0.1	-11	11	-38	81	-45	66
3.85	4.65	1.89	0.1	37	12	154	59	73	54
3.85	4.65	1.89	0.3	58	16	-7	62	-137	50
3.85	4.65	1.89	0.5	105	18	97	89	184	78
3.85	4.65	1.89	0.7	99	21	123	102	95	98
3.85	4.65	1.89	0.9	45	11	68	55	-78	40
3.85	4.65	1.91	-0.9	66	9	107	39	-15	31
3.85	4.65	1.91	-0.7	62	10	-38	44	-6	31
3.85	4.65	1.91	-0.5	29	9	14	39	-74	39
3.85	4.65	1.91	-0.3	32	13	-84	73	-90	54
3.85	4.65	1.91	-0.1	14	11	9	70	-70	70
3.85	4.65	1.91	0.1	43	11	53	64	48	62
3.85	4.65	1.91	0.3	61	12	13	58	70	51
3.85	4.65	1.91	0.5	89	12	33	73	67	62
3.85	4.65	1.91	0.7	117	17	98	77	45	65
3.85	4.65	1.91	0.9	55	11	10	58	-37	42
3.85	4.65	1.93	-0.9	42	7	61	37	-48	30
3.85	4.65	1.93	-0.7	48	9	23	47	-97	32
3.85	4.65	1.93	-0.5	11	7	-36	42	-75	30
3.85	4.65	1.93	-0.3	38	13	39	68	-15	71
3.85	4.65	1.93	-0.1	32	14	-51	70	-30	68
3.85	4.65	1.93	0.1	37	11	18	45	-43	35
3.85	4.65	1.93	0.3	49	9	-1	64	-31	51
3.85	4.65	1.93	0.5	57	10	100	74	23	61
3.85	4.65	1.93	0.7	68	13	-29	56	-92	40
3.85	4.65	1.93	0.9	46	11	-20	60	-23	45
3.85	4.65	1.95	-0.9	47	7	-25	37	-9	28
3.85	4.65	1.95	-0.7	46	9	4	52	-16	38
3.85	4.65	1.95	-0.5	44	10	76	70	10	74
3.85	4.65	1.95	-0.3	20	8	65	53	-25	33
3.85	4.65	1.95	-0.1	44	9	-17	55	7	47
3.85	4.65	1.95	0.1	22	8	46	56	29	47
3.85	4.65	1.95	0.3	54	10	-20	60	12	49
3.85	4.65	1.95	0.5	62	11	77	76	30	61
3.85	4.65	1.95	0.7	99	13	53	74	0	60

Continued on next page

Q_i^2 (GeV^2)	Q_f^2 (GeV^2)	W (GeV)	$\cos \theta^*$	$\mathscr{R}_o$ (nb/sr)	$\Delta\mathscr{R}_o$ (nb/sr)	$\mathscr{R}_{TT}$ (nb/sr)	$\Delta\mathscr{R}_{TT}$ (nb/sr)	$\mathscr{R}_{TL}$ (nb/sr)	$\Delta\mathscr{R}_{TL}$ (nb/sr)
3.85	4.65	1.95	0.9	56	11	47	58	-61	47
3.85	4.65	1.97	-0.9	38	7	-36	39	-14	25
3.85	4.65	1.97	-0.7	23	11	-82	40	0	31
3.85	4.65	1.97	-0.5	39	15	83	72	44	72
3.85	4.65	1.97	-0.3	25	9	-64	58	-52	54
3.85	4.65	1.97	-0.1	19	6	86	43	95	42
3.85	4.65	1.97	0.1	31	9	53	58	26	48
3.85	4.65	1.97	0.3	55	9	68	55	33	47
3.85	4.65	1.97	0.5	60	9	57	61	7	53
3.85	4.65	1.97	0.7	69	10	155	62	48	48
3.85	4.65	1.97	0.9	66	11	-33	63	-92	45
3.85	4.65	1.99	-0.9	26	6	45	34	-44	25
3.85	4.65	1.99	-0.7	25	7	25	45	11	46
3.85	4.65	1.99	-0.5	16	8	-44	53	-60	43
3.85	4.65	1.99	-0.3	16	7	-3	44	-82	43
3.85	4.65	1.99	-0.1	20	6	-41	39	-23	32
3.85	4.65	1.99	0.1	14	6	-18	50	-61	43
3.85	4.65	1.99	0.3	25	8	-15	49	-42	43
3.85	4.65	1.99	0.5	70	11	31	65	54	59
3.85	4.65	1.99	0.7	67	10	-17	46	-81	37
3.85	4.65	1.99	0.9	95	12	-20	77	-39	63
3.85	4.65	2.01	-0.9	18	5	-58	35	-2	22
3.85	4.65	2.01	-0.7	25	6	23	36	-91	30
3.85	4.65	2.01	-0.5	-9	11	-74	43	-100	37
3.85	4.65	2.01	-0.3	6	7	47	44	65	43
3.85	4.65	2.01	-0.1	24	7	6	36	21	35
3.85	4.65	2.01	0.1	38	10	79	54	117	50
3.85	4.65	2.01	0.3	50	8	76	68	43	55
3.85	4.65	2.01	0.5	49	9	67	72	-53	60
3.85	4.65	2.01	0.7	48	9	-108	73	-46	57
3.85	4.65	2.01	0.9	67	11	-139	63	-92	42
3.85	4.65	2.03	-0.9	9	4	-33	30	-13	22
3.85	4.65	2.03	-0.7	6	7	-84	49	-119	38
3.85	4.65	2.03	-0.5	13	7	-23	45	-23	38
3.85	4.65	2.03	-0.3	10	8	99	34	98	30
3.85	4.65	2.03	-0.1	12	6	90	47	102	39
3.85	4.65	2.03	0.1	30	8	26	54	-9	47
3.85	4.65	2.03	0.3	31	8	68	71	10	56
3.85	4.65	2.03	0.5	54	11	-17	66	-80	55
3.85	4.65	2.03	0.7	46	10	62	73	-22	60
3.85	4.65	2.03	0.9	71	12	196	89	59	77
3.85	4.65	2.05	-0.9	2	5	37	26	-17	21
3.85	4.65	2.05	-0.7	6	27	-71	47	-109	33
3.85	4.65	2.05	-0.5	0	8	-107	57	-136	47
3.85	4.65	2.05	-0.3	15	8	35	52	16	47
3.85	4.65	2.05	-0.1	29	9	-20	51	6	51
3.85	4.65	2.05	0.1	60	10	73	65	125	61
3.85	4.65	2.05	0.3	25	9	2	55	-76	38
3.85	4.65	2.05	0.5	45	13	20	70	50	61

Continued on next page

Q_i^2 (GeV²)	Q_f^2 (GeV²)	W (GeV)	$\cos\theta^*$	$\mathscr{R}_o$ (nb/sr)	$\Delta\mathscr{R}_o$ (nb/sr)	$\mathscr{R}_{TT}$ (nb/sr)	$\Delta\mathscr{R}_{TT}$ (nb/sr)	$\mathscr{R}_{TL}$ (nb/sr)	$\Delta\mathscr{R}_{TL}$ (nb/sr)
3.85	4.65	2.05	0.7	35	12	49	75	1	72
3.85	4.65	2.05	0.9	66	10	97	86	153	72
3.85	4.65	2.07	-0.9	5	4	21	33	-21	22
3.85	4.65	2.07	-0.7	7	28	77	92	54	118
3.85	4.65	2.07	-0.5	8	6	0	53	-81	41
3.85	4.65	2.07	-0.3	6	4	12	43	-4	43
3.85	4.65	2.07	-0.1	16	7	64	53	26	48
3.85	4.65	2.07	0.1	20	14	27	57	-4	51
3.85	4.65	2.07	0.3	31	8	69	64	23	68
3.85	4.65	2.07	0.5	48	7	-145	59	-167	50
3.85	4.65	2.07	0.7	55	12	4	96	-78	88
3.85	4.65	2.07	0.9	72	13	121	109	101	100
3.85	4.65	2.09	-0.9	8	4	8	36	34	28
3.85	4.65	2.09	-0.7	3	20	23	122	-44	171
3.85	4.65	2.09	-0.5	26	9	79	61	76	68
3.85	4.65	2.09	-0.3	7	6	-50	56	-71	57
3.85	4.65	2.09	-0.1	12	8	-42	45	-62	29
3.85	4.65	2.09	0.1	23	10	72	83	-34	86
3.85	4.65	2.09	0.3	13	14	-92	62	47	64
3.85	4.65	2.09	0.5	28	10	-86	59	-62	56
3.85	4.65	2.09	0.7	71	17	75	66	2	59
3.85	4.65	2.09	0.9	62	12	-101	104	19	90
4.65	5.15	1.73	-0.9	-19	45	-182	208	3	124
4.65	5.15	1.73	-0.7	-10	36	-218	313	99	176
4.65	5.15	1.73	-0.5	86	59	-192	394	-21	186
4.65	5.15	1.73	-0.3	2	51	-362	376	185	245
4.65	5.15	1.73	-0.1	-14	46	413	275	-327	218
4.65	5.15	1.73	0.1	-66	55	-343	367	-45	203
4.65	5.15	1.73	0.3	-23	49	151	297	107	199
4.65	5.15	1.73	0.5	-2	43	67	258	70	178
4.65	5.15	1.73	0.7	-56	47	-30	280	-73	181
4.65	5.15	1.73	0.9	27	49	28	207	85	153
4.65	5.15	1.75	-0.9	69	19	244	116	152	88
4.65	5.15	1.75	-0.7	75	24	-170	130	6	87
4.65	5.15	1.75	-0.5	32	19	151	149	-112	97
4.65	5.15	1.75	-0.3	16	26	27	150	-53	109
4.65	5.15	1.75	-0.1	136	30	55	174	-24	112
4.65	5.15	1.75	0.1	-9	22	262	172	228	153
4.65	5.15	1.75	0.3	32	22	-257	212	41	115
4.65	5.15	1.75	0.5	18	24	198	243	169	144
4.65	5.15	1.75	0.7	66	25	-323	233	-56	116
4.65	5.15	1.75	0.9	29	19	-182	147	78	87
4.65	5.15	1.77	-0.9	117	20	131	105	-23	75
4.65	5.15	1.77	-0.7	104	21	35	119	-13	79
4.65	5.15	1.77	-0.5	97	20	8	132	15	87
4.65	5.15	1.77	-0.3	73	24	-57	157	-181	99
4.65	5.15	1.77	-0.1	33	18	17	91	-62	65
4.65	5.15	1.77	0.1	81	22	287	170	162	138
4.65	5.15	1.77	0.3	37	20	-361	186	-153	134

Continued on next page

Q_i^2 (GeV^2)	Q_f^2 (GeV^2)	W (GeV)	$\cos\theta^*$	$\mathscr{R}_o$ (nb/sr)	$\Delta\mathscr{R}_o$ (nb/sr)	$\mathscr{R}_{TT}$ (nb/sr)	$\Delta\mathscr{R}_{TT}$ (nb/sr)	$\mathscr{R}_{TL}$ (nb/sr)	$\Delta\mathscr{R}_{TL}$ (nb/sr)
4.65	5.15	1.77	0.5	92	21	308	164	206	136
4.65	5.15	1.77	0.7	86	21	-179	157	-88	99
4.65	5.15	1.77	0.9	114	24	-185	139	168	82
4.65	5.15	1.79	-0.9	94	18	-109	103	-88	60
4.65	5.15	1.79	-0.7	117	22	69	135	-5	102
4.65	5.15	1.79	-0.5	76	17	111	130	4	124
4.65	5.15	1.79	-0.3	36	19	25	158	-174	116
4.65	5.15	1.79	-0.1	44	15	344	139	113	116
4.65	5.15	1.79	0.1	43	23	25	152	139	132
4.65	5.15	1.79	0.3	79	22	161	236	392	142
4.65	5.15	1.79	0.5	70	23	153	144	-139	114
4.65	5.15	1.79	0.7	95	23	-86	141	140	106
4.65	5.15	1.79	0.9	88	19	-68	125	59	83
4.65	5.15	1.81	-0.9	113	17	93	110	47	87
4.65	5.15	1.81	-0.7	114	19	101	112	-33	81
4.65	5.15	1.81	-0.5	80	21	-153	142	-214	91
4.65	5.15	1.81	-0.3	64	22	92	137	71	123
4.65	5.15	1.81	-0.1	27	19	87	211	-84	178
4.65	5.15	1.81	0.1	48	19	340	215	71	213
4.65	5.15	1.81	0.3	23	16	230	166	-26	145
4.65	5.15	1.81	0.5	36	24	-92	221	5	248
4.65	5.15	1.81	0.7	59	21	117	167	-43	103
4.65	5.15	1.81	0.9	54	16	-92	133	-112	80
4.65	5.15	1.83	-0.9	60	13	159	91	-17	57
4.65	5.15	1.83	-0.7	84	17	221	135	1	101
4.65	5.15	1.83	-0.5	41	14	186	108	222	95
4.65	5.15	1.83	-0.3	34	14	73	134	-238	93
4.65	5.15	1.83	-0.1	60	22	54	171	-213	162
4.65	5.15	1.83	0.1	-4	15	-100	197	-256	174
4.65	5.15	1.83	0.3	7	18	-158	166	62	94
4.65	5.15	1.83	0.5	18	20	371	193	-5	167
4.65	5.15	1.83	0.7	16	13	124	134	-45	130
4.65	5.15	1.83	0.9	53	16	0	103	-73	83
4.65	5.15	1.85	-0.9	42	13	-1	104	97	70
4.65	5.15	1.85	-0.7	57	16	28	89	-148	73
4.65	5.15	1.85	-0.5	12	26	40	108	-38	67
4.65	5.15	1.85	-0.3	24	17	392	228	123	236
4.65	5.15	1.85	-0.1	-6	14	9	188	-240	220
4.65	5.15	1.85	0.1	0	20	-198	198	-320	180
4.65	5.15	1.85	0.3	-16	17	3	250	-186	260
4.65	5.15	1.85	0.5	111	89	367	144	335	100
4.65	5.15	1.85	0.7	19	24	192	239	433	154
4.65	5.15	1.85	0.9	14	15	82	106	-63	70
4.65	5.15	1.87	-0.9	66	23	-133	105	-206	57
4.65	5.15	1.87	-0.7	44	13	96	120	75	82
4.65	5.15	1.87	-0.5	50	17	151	160	-187	177
4.65	5.15	1.87	-0.3	0	13	-81	294	-8	365
4.65	5.15	1.87	-0.1	-36	40	-64	240	-92	217
4.65	5.15	1.87	0.1	40	42	97	144	164	168

Continued on next page

| Q_i^2 | Q_f^2 | W | $\cos\theta^*$ | $\mathscr{R}_o$ | $\Delta\mathscr{R}_o$ | $\mathscr{R}_{TT}$ | $\Delta\mathscr{R}_{TT}$ | $\mathscr{R}_{TL}$ | $\Delta\mathscr{R}_{TL}$ |
(GeV^2)	(GeV^2)	(GeV)		(nb/sr)	(nb/sr)	(nb/sr)	(nb/sr)	(nb/sr)	(nb/sr)
4.65	5.15	1.87	0.3	69	29	359	232	186	296
4.65	5.15	1.87	0.5	24	14	202	313	38	326
4.65	5.15	1.87	0.7	28	56	-107	264	137	283
4.65	5.15	1.87	0.9	62	17	17	150	186	105
4.65	5.15	1.89	-0.9	12	12	-334	171	-273	114
4.65	5.15	1.89	-0.7	35	11	-49	139	107	115
4.65	5.15	1.89	-0.5	26	14	-286	116	-39	91
4.65	5.15	1.89	-0.3	61	46	378	97	-21	154
4.65	5.15	1.89	-0.1	0	26	-72	266	132	299
4.65	5.15	1.89	0.1	45	37	109	203	48	168
4.65	5.15	1.89	0.3	15	18	-26	150	-27	106
4.65	5.15	1.89	0.5	59	28	-540	253	-196	209
4.65	5.15	1.89	0.7	72	33	242	243	5	209
4.65	5.15	1.89	0.9	49	18	138	162	47	132
4.65	5.15	1.91	-0.9	41	11	-54	100	-6	57
4.65	5.15	1.91	-0.7	18	11	318	187	227	218
4.65	5.15	1.91	-0.5	33	33	360	124	175	136
4.65	5.15	1.91	-0.3	58	38	-135	182	312	107
4.65	5.15	1.91	-0.1	36	18	455	201	325	101
4.65	5.15	1.91	0.1	-2	11	328	204	214	217
4.65	5.15	1.91	0.3	18	13	-82	232	-84	218
4.65	5.15	1.91	0.5	13	15	-38	163	-130	113
4.65	5.15	1.91	0.7	44	21	149	276	57	207
4.65	5.15	1.91	0.9	9	17	4	224	-79	217
4.65	5.15	1.93	-0.9	13	7	46	208	159	238
4.65	5.15	1.93	-0.7	-2	13	-104	469	306	242
4.65	5.15	1.93	-0.5	88	80	269	302	565	192
4.65	5.15	1.93	-0.3	0	23	-362	215	-179	162
4.65	5.15	1.93	-0.1	0	10	249	217	32	204
4.65	5.15	1.93	0.1	0	34	-545	259	-239	181
4.65	5.15	1.93	0.3	12	16	-3	184	128	174
4.65	5.15	1.93	0.5	25	15	377	198	64	165
4.65	5.15	1.93	0.7	46	17	-445	278	-341	234
4.65	5.15	1.93	0.9	-1	15	-696	447	-238	523
4.65	5.15	1.95	-0.9	26	27	472	299	332	281
4.65	5.15	1.95	-0.7	21	15	-3620	1486	-2345	1323
4.65	5.15	1.95	-0.5	42	58	-73	312	327	171
4.65	5.15	1.95	-0.3	-1	17	-8	192	312	113
4.65	5.15	1.95	-0.1	33	18	349	149	311	146
4.65	5.15	1.95	0.1	29	43	211	160	382	111
4.65	5.15	1.95	0.3	38	14	192	268	-137	206
4.65	5.15	1.95	0.5	27	13	643	323	403	295
4.65	5.15	1.95	0.7	120	85	326	256	510	157
4.65	5.15	1.95	0.9	19	18	137	752	-25	1057
4.65	5.15	1.97	-0.9	6	11	-1717	1561	-614	2176
4.65	5.15	1.97	-0.7	0	11	11	529	-344	297
4.65	5.15	1.97	-0.5	0	16	56	2881	-444	5156
4.65	5.15	1.97	-0.3	24	33	-163	3437	-450	7245
4.65	5.15	1.97	-0.1	41	22	44	1555	76	1162

Continued on next page

164

Q_i^2 (GeV^2)	Q_f^2 (GeV^2)	W (GeV)	$\cos\theta^*$	$\mathscr{R}_o$ (nb/sr)	$\Delta\mathscr{R}_o$ (nb/sr)	$\mathscr{R}_{TT}$ (nb/sr)	$\Delta\mathscr{R}_{TT}$ (nb/sr)	$\mathscr{R}_{TL}$ (nb/sr)	$\Delta\mathscr{R}_{TL}$ (nb/sr)
4.65	5.15	1.97	0.1	19	11	178	340	231	353
4.65	5.15	1.97	0.3	61	19	247	739	-675	576
4.65	5.15	1.97	0.5	44	14	-437	405	-243	457
4.65	5.15	1.97	0.7	65	17	-70	741	676	609
4.65	5.15	1.97	0.9	76	26	-111	7816	703	5064
4.65	5.15	1.99	-0.9	NaN	NaN	NaN	NaN	NaN	NaN
4.65	5.15	1.99	-0.7	NaN	NaN	NaN	NaN	NaN	NaN
4.65	5.15	1.99	-0.5	NaN	NaN	NaN	NaN	NaN	NaN
4.65	5.15	1.99	-0.3	NaN	NaN	NaN	NaN	NaN	NaN
4.65	5.15	1.99	-0.1	NaN	NaN	NaN	NaN	NaN	NaN
4.65	5.15	1.99	0.1	NaN	NaN	NaN	NaN	NaN	NaN
4.65	5.15	1.99	0.3	NaN	NaN	NaN	NaN	NaN	NaN
4.65	5.15	1.99	0.5	NaN	NaN	NaN	NaN	NaN	NaN
4.65	5.15	1.99	0.7	NaN	NaN	NaN	NaN	NaN	NaN
4.65	5.15	1.99	0.9	NaN	NaN	NaN	NaN	NaN	NaN